

**OPTIONS FOR TREATMENT OF LEGACY AND ADVANCED  
NUCLEAR FUELS**

A thesis submitted to the University of Manchester for the degree of  
in the Faculty of Engineering and Physical Sciences.

**2014**

**CHRIS MAHER**

**SCHOOL OF CHEMICAL ENGINEERING AND ANALYTICAL SCIENCE**



4.3. Experimental.....	79
4.3.1. Dissolution apparatus and methodology.....	79
4.3.2. Off-line analytical methods.....	85
4.3.2.1. Uranium dioxide experiments .....	85
4.3.2.2. MOx experiments .....	86
4.3.3. Characterisation of materials .....	86
4.3.3.1. Uranium dioxide powders .....	86
4.3.3.2. MOx powder .....	87
4.3.3.3. MOx pellets .....	88
4.4. The thermodynamics of actinide dioxide dissolution in nitric acid ...	88
4.4.1. Introduction .....	88
4.4.2. Methodology.....	89
4.4.3. Dissolution in nitric acid .....	90
4.4.3.1. Individual actinide dioxides .....	90
4.4.3.2. Mixed uranium plutonium dioxide.....	93
4.4.4. Enhanced dissolution with oxidising and reducing agents .....	95
4.4.5. Summary.....	100
4.5. The effect of stirring and sparging upon uranium dioxide dissolution in nitric acid.....	101
4.5.1. Introduction .....	101
4.5.2. Experimental.....	103
4.5.2.1. Materials.....	103
4.5.2.2. Apparatus and methodology .....	103
4.5.2.3. Analysis methods .....	104
4.5.3. Results and Discussion .....	105
4.5.4. Summary.....	110
4.6. The role of nitrous acid in the dissolution of uranium plutonium mixed oxide powder .....	110
4.6.1. Introduction .....	110
4.6.2. Experimental.....	112
4.6.2.1. Materials.....	112
4.6.2.2. Apparatus and methodology .....	112
4.6.2.3. Analysis methods .....	113
4.6.3. Results and Discussion .....	113
4.6.4. Summary.....	120
4.7. Dissolution kinetics of 5 % plutonium content mixed oxide pellets in nitric acid.....	121
4.7.1. Introduction .....	121
4.7.2. Experimental.....	122

4.7.2.1.	Materials.....	122
4.7.2.2.	Apparatus and methodology .....	122
4.7.2.3.	Analysis methods.....	123
4.7.2.4.	Dissolution rate interpretation .....	123
4.7.3.	Results and Discussion .....	124
4.7.3.1.	Multi-component UV-Vis calibration .....	124
4.7.3.2.	Effect of cell conditions .....	125
4.7.3.3.	Effect of nitric and nitrous acid concentration .....	127
4.7.3.4.	Effect of temperature .....	129
4.7.3.5.	Comparison of dissolution rates with previously published results .....	131
4.7.4.	Summary.....	132
4.8.	Summary of direct dissolution of oxides in nitric acid.....	133
<b>5.</b>	<b>APPLICATION OF MEDIATED ELECTROCHEMICAL OF SILVER(II) FOR FUEL DISSOLUTION.....</b>	<b>135</b>
5.1.	Summary of literature relating to mediated electrochemical dissolution .....	135
5.1.1.	Review of the development leading MEO dissolution processes for plutonium dioxide .....	135
5.1.1.1.	Silver(II) chemistry in nitric acid.....	138
5.1.2.	Electrochemical generation of silver(II).....	142
5.1.3.	Summary of silver(II) mediated electrochemical processes ..	145
5.2.	Aims and objectives .....	145
5.3.	Experimental.....	148
5.3.1.	Apparatus and methods.....	148
5.3.1.1.	Glassware .....	148
5.3.1.2.	Power supply and voltage meters.....	151
5.3.1.3.	Electrodes .....	153
5.3.1.4.	Redox potential measurements.....	154
5.3.1.5.	Temperature measurement .....	155
5.3.1.6.	Inline UV-Vis spectrometry.....	155
5.3.1.7.	Silver(II) by sampling.....	155
5.3.2.	Initial testing.....	156
5.3.3.	Linear Staircase Voltammetry.....	157
5.3.4.	Bulk electrolysis.....	159
5.3.5.	Dissolution apparatus and methodology.....	163
5.4.	Optimisation of a batch electrolysis cell for silver(II) generation to dissolve plutonium dioxide .....	166
5.4.1.	Introduction .....	166

5.4.2.	Experimental .....	167
5.4.3.	Results and discussion .....	170
5.4.3.1.	Linear Sweep Staircase Voltammetry .....	170
5.4.3.2.	Bulk Electrolysis .....	176
5.4.3.3.	Generation of silver(II) .....	177
5.4.3.4.	Dzcomposition of silver(II) and steady state silver(II) concentrations .....	180
5.4.3.5.	Plutonium dioxide dissolution .....	185
5.4.4.	Summary .....	187
5.5.	Summary mediated electrochemical oxidation experiments .....	188
<b>6.</b>	<b>CONCLUSIONS .....</b>	<b>190</b>
6.1.	Literature flowsheet studies .....	190
6.2.	Direct dissolution in nitric acid .....	191
6.3.	Optimisation of a 100 ml electrochemical silver(II) dissolver from plutonium dioxide .....	194
<b>7.</b>	<b>FURTHER WORK .....</b>	<b>196</b>
7.1.	Technology and flowsheet studies .....	196
7.2.	Direct dissolution in nitric acid .....	196
7.3.	Application of mediated electrochemical oxidation to dissolution ...	197
<b>8.</b>	<b>REFERENCES .....</b>	<b>200</b>
<b>9.</b>	<b>APPENDICES .....</b>	<b>214</b>
9.1.	Summary of direct dissolution analytical method calibrations.....	214
9.1.1.	UO <sub>2</sub> studies - UV-Vis Uranyl calibration studies .....	214
9.1.2.	UO <sub>2</sub> studies - Determination of HNO <sub>2</sub> by titration .....	215
9.1.3.	UO <sub>2</sub> studies – Determination of HNO <sub>2</sub> by colourimetry .....	216
9.1.4.	Uranium dioxide studies – Determination of HNO <sub>2</sub> by in-situ potentiometry.....	217
9.1.5.	Uranium dioxide powder studies - Determination of HNO <sub>2</sub> by direct UV-Vis .....	218
9.1.6.	MOx pellet studies – U and Pu UV-Vis-nIR calibration (Off line analysis) .....	220
<b>10.</b>	<b>SUPLIMENTARY PUBLISHED MATERIAL .....</b>	<b>223</b>
10.1.	Head-end processing .....	223
10.1.1.	Introduction .....	223
10.2.	1.4 Current practices.....	226
10.2.1.1.	Disassembly and Fuel Exposure .....	226
10.2.1.2.	Dissolution .....	228
10.2.2.	Potential additional process steps for a future reprocessing plants.....	229



## LIST OF TABLES

Table 1: Key product requirements.....	29
Table 2: Summary of future reactor and fuel concepts [10] .....	30
Table 3: Civil reprocessing plants currently operational .....	31
Table 4: Comparison of $^{14}\text{C}$ production for 30 GWd.tHM $^{-1}$ fuel of various types [71] .....	47
Table 5: Effect of voloxidation conditions upon noble gas and iodine-129 removal [97].....	52
Table 6: Nitric acid reduction mechanisms[22] .....	62
Table 7: Proposed indirect reaction mechanism[22].....	63
Table 8: Copper dissolution mechanism[26].....	69
Table 9: Variation of $x$ , Eq 41, with nitric acid concentration.....	73
Table 10: Summary of MOx pellet analysis details .....	88
Table 11: Calculated Gibbs free energy for major dissolution mechanisms of plutonium dioxide.....	90
Table 12: Calculated Gibbs free energies for dissolution of actinide dioxides by various nitric acid reactions .....	92
Table 13: Electropotentials required for dissolution by oxidation or reduction .....	96
Table 14: List of reducing agents with evidence for plutonium dioxide dissolution .....	97
Table 15: List of oxidising agents with evidence for neptunium or plutonium dioxide dissolution .....	98
Table 16: Molar extinction coefficients for uranium.....	104
Table 17: Membrane types tested for divided cell.....	150
Table 18: Measured potentials over rate of $[\text{Ce}^{3+}]/[\text{Ce}^{4+}]$ .....	172
Table 19: Results of HNO $_2$ titration method testing .....	215
Table 20: UK reprocessing plants.....	226
Table 21: Residual Contamination after UNF Clad Washing. ....	238
Table 22: Generation IV Reactor fuels, matrix and cladding description[265] .....	242
Table 23: Carbon-14 contents of different fuel types [71] .....	252

## LIST OF FIGURES

Figure 1: Schematic overview of water reactor, fast reactor and ADS nuclear fuel cycles including the mass flows of uranium(U), Transuranium (TRU) and high level waste (HLW) [2] .....	23
Figure 2: Radiotoxicity – time plots for 40 GWd.t <sup>-1</sup> , 40 MW.t <sup>-1</sup> , 4 % <sup>235</sup> U for direct disposal, recovery of (A) U,Pu and (B) U, Np, Pu , Am, Cm [7] .....	24
Figure 3: Position of head-end in the reprocessing plant.....	28
Figure 4: Overview of process steps in current generation oxide reprocessing plants .....	31
Figure 5: Illustration of Magnox decanning .....	32
Figure 6: Left - Illustration of the THORP hydrolytic shear; Right – example sheared cross-sections from an inactive dummy AGR fuel bundle .....	33
Figure 7: Schematic diagram of oxide a) batch kettle and b) continuous rotary wheel dissolver .....	35
Figure 8: Nitric acid reduction chemistry [18] .....	36
Figure 9: Multiple oxidation states of iodine in dissolver .....	40
Figure 10: Industrial centrifuge used for clarification of the dissolver product .....	42
Figure 11: Extent of MOx dissolution for various plutonium contents [53] .....	46
Figure 12: Two step process to (Pu <sub>0.8</sub> An <sub>0.2</sub> )O <sub>2</sub> -MgO and PuO <sub>2</sub> -Mo IMF .....	49
Figure 13: VHTR fuel 'grind-leach' process .....	50
Figure 14: Industrial plutonium dioxide dissolver [123] .....	56
Figure 15: Standard reduction potentials (V) for nitric acid and other nitrogen containing species[35] .....	61
Figure 16: Systematic diagram of nitrate reduction.....	63
Figure 17: Reduction of nitrite on platinum electrode, as observed by SEIRA[25] .....	65
Figure 18: Phase diagram of U-O system, left O/U ratio 1.2 to 2.2 and right O/U ratio 2.0 – 3.0 [133] .....	66
Figure 19: a) Photograph of custom glassware for reactor and other apparatus b) Schematic diagram of dissolution apparatus	81
Figure 20: Equipment installed in glovebox, A - Photograph of dissolution vessel, B - Systematic diagram of apparatus dissolution .....	82
Figure 21: Equipment installed in glovebox, A UV-Vis flow cell and pump, B – redox reference electrode cell.....	83
Figure 22: Dissolver pellet support stand .....	84
Figure 23: Particle size distributions for Uranium dioxide powder sieve fractions 75 – 106 μm and 250 – 450 μm .....	87
Figure 24: Standard electrochemical potentials (V <sub>NHE</sub> ) for redox conversions of nitric acid and other nitrogen-containing species [35].....	91
Figure 25: Thermodynamics of dissolution of mixed uranium plutonium dioxide by favourable nitric acid reduction reactions at 298 K, O NO <sub>3</sub> <sup>-</sup> /NO <sub>2</sub> , Δ HNO <sub>2</sub> /NO, .....	93

Figure 26: Percentage MOx dissolved for various Pu contents when O 5 mol.l <sup>-1</sup> or □ 10 mol.l <sup>-1</sup> is used under boiling conditions for 6 hours[53] .....	94
Figure 27: Surface and near-surface reactions autocatalytic dissolution .....	102
Figure 28: UV-Vis absorption spectra for the dissolution of 6.9 g UO <sub>2</sub> in 6 mol.l <sup>-1</sup> HNO <sub>3</sub> at 80 °C with 25 mmol.l <sup>-1</sup> NaNO <sub>2</sub> added, stirring at 500 rpm, 10, 20, 40, 60, 100 minutes.....	104
Figure 29: Dissolution of 6.9 g UO <sub>2</sub> in 6 mol.l <sup>-1</sup> HNO <sub>3</sub> at 80 °C with 25 mmol.l <sup>-1</sup> NaNO <sub>2</sub> added, 6x30 mm follower at 500 rpm, □ [HNO <sub>2</sub> ], ● radius, — core shrinkage dissolution rate.....	105
Figure 30: Effect of stirring (small follower) upon dissolution rate and plateau HNO <sub>2</sub> concentration, O dissolution rate (μmol.cm <sup>-2</sup> .min <sup>-1</sup> ) □ [HNO <sub>2</sub> ] (mol.l <sup>-1</sup> ) .....	106
Figure 31: The effect of plateau [HNO <sub>2</sub> ] (caused by stirring) upon dissolution rate, □ small follower at variable rpm.....	106
Figure 32: Effect of increasing [HNO <sub>2</sub> ] upon dissolution rate, under three stirring regimes, Δ small follower 500 rpm, □ large follower 250 rpm, O small follower 1500 rpm.....	107
Figure 33: Effect of nitric acid concentration under air sparge and stirring (1500 rpm small follower), O dissolution rate, □ nitrous acid concentration.....	108
Figure 34: Comparison of effect of nitric acid (air sparge, small follower, 1500 rpm) with Ikeda <i>et al.</i> published kinetic rate law.....	109
Figure 35: Comparison of effect of nitrous acid (small follower, 1500 rpm) with Ikeda <i>et al.</i> published kinetic rate law.....	109
Figure 36: Nitrous acid autocatalytic cycle .....	111
Figure 37: Dissolution of 1 g MOx powder in 5 mol.l <sup>-1</sup> HNO <sub>3</sub> at 70 °C without added NaNO <sub>2</sub> : ● radius determined by inline analysis and equation (1), Δ [HNO <sub>2</sub> ] .....	114
Figure 38: Effect of nitric and nitrous acid upon dissolution rate constant at 40 °C, ◇ 4 mol.l <sup>-1</sup> , □ 5 mol.l <sup>-1</sup> , Δ 6 mol.l <sup>-1</sup> , O 7 mol.l <sup>-1</sup> .....	115
Figure 39: Nitric acid and nitrate dissolution rate constants at 40 °C, Δ nitrous acid reaction (gradient), ◇ nitrate reaction (intercept) .....	115
Figure 40: Effect of added potassium nitrate upon dissolution rate constant at 40 °C, □ 5 mol.l <sup>-1</sup> HNO <sub>3</sub> , O 6 mol.l <sup>-1</sup> HNO <sub>3</sub> , Δ 5 mol.l <sup>-1</sup> HNO <sub>3</sub> -1 mol.l <sup>-1</sup> KNO <sub>3</sub> .....	116
Figure 41: Arrhenius plots without addition of sodium nitrite in 5 mol.l <sup>-1</sup> HNO <sub>3</sub> .....	117
Figure 42: Effect of temperature and nitrous acid upon the dissolution rate constant in 5 mol.l <sup>-1</sup> HNO <sub>3</sub> , × 27 °C , ◇ 40 °C, O 47 °C , Δ 55 °C, □ 70 °C .....	118
Figure 43: Arrhenius plots for nitrous acid and nitrate reactions in 5 mol.l <sup>-1</sup> HNO <sub>3</sub> , O nitrous acid reaction (slope), □ nitrate reaction (intercept) .....	119
Figure 44: Effect of nitric and nitrous acid upon calculated dissolution rate constant of uranium dioxide at 40 °C, ◇ 4 mol.l <sup>-1</sup> , □ 5 mol.l <sup>-1</sup> , Δ 6 mol.l <sup>-1</sup> , O 7 mol.l <sup>-1</sup> .....	119
Figure 45: Effect of temperature and nitrous acid upon the calculated dissolution rate constant of uranium dioxide in 5 mol.l <sup>-1</sup> HNO <sub>3</sub> , × 27 °C , ◇ 40 °C, O 47 °C ,Δ 55 °C, □ 70 °C .....	120

Figure 46: Nitrous acid auto-catalytic cycle.....	122
Figure 47: Baseline corrected absorption spectra for U+Pu solution for ---- 8 mol.l <sup>-1</sup> , --10 mol.l <sup>-1</sup> , - -12 mol.l <sup>-1</sup> , — — 14 mol.l <sup>-1</sup> HNO <sub>3</sub> .....	125
Figure 48: Beer Lambert plot for uranium in 6-12 mol.l <sup>-1</sup> HNO <sub>3</sub> .....	125
Figure 49: Effect of dissolver cell conditions, 10 mol.l <sup>-1</sup> HNO <sub>3</sub> 80 °C, □ unstirred no pellet stand (f = 1.00, λ = 83.6), ○ unstirred with pellet stand (f = 1.00, λ = 99.0), ◇ 200 rpm with pellet stand (f = 1.00, λ = 102), △ 200 rpm with pellet stand sparged 250 ml.min <sup>-1</sup> (f = 1.00, λ = 136), × 900 rpm with pellet stand (f = 1.00, λ = 273).....	126
Figure 50: Effect of cell conditions, ■ 80 °C, ■ 110 °C.....	127
Figure 51: Effect of dissolver cell conditions, 10 mol.l <sup>-1</sup> HNO <sub>3</sub> 110 °C, ◇ 200 rpm with pellet stand (f = 1.00, λ = 113), × 900 rpm with pellet stand (f = 1.00, λ = 113).....	127
Figure 52: Effect of HNO <sub>3</sub> concentration at 80 °C upon dissolution rate, ○ 14 mol.l <sup>-1</sup> (f = 1.00, λ = 60.5), □ 12 mol.l <sup>-1</sup> (f = 1.00, λ = 81.2), ◇ 10 mol.l <sup>-1</sup> (f = 1.00, λ = 95.9), △ 8 mol.l <sup>-1</sup> (f = 1.00, λ = 219) .....	128
Figure 53: Effect of HNO <sub>3</sub> concentration at different temperatures: △ 80 °C, □ 70 °C. ◇ 60 °C, outline - no NaNO <sub>2</sub> added, shaded - NaNO <sub>2</sub> added, .....	129
Figure 54: Effect of temperature for 10 mol.l <sup>-1</sup> HNO <sub>3</sub> , ○ 90 °C (f = 1.00, λ = 81.4), □ 100 °C (f = 1.00, λ = 81.0), ◇ 80 °C (f = 1.00, λ = 102), × 110 °C (f = 1.00, λ = 113), △ 70 °C (f = 1.00, λ = 211), + 60 °C (f = 1.00, λ = 902) .....	130
Figure 55: The effect of temperature for different HNO <sub>3</sub> concentrations, ○ 14 mol.l <sup>-1</sup> , △ 12 mol.l <sup>-1</sup> , □ 10 mol.l <sup>-1</sup> , ◇ 8 mol.l <sup>-1</sup> , (grey solid points with NaNO <sub>2</sub> added), .....	130
Figure 56: Effect of temperature in 10 mol.l <sup>-1</sup> HNO <sub>3</sub> with (solid filled) and without (outline) added sodium nitrite, ◆ 80 °C (f = 1.00, λ = 95.9), ■ 70 °C (f = 1.00, λ = 172), ● 80 °C (f = 1.00, λ = 560) .....	131
Figure 57: Effect of density upon dissolution rate, ○ Taylor UO <sub>2</sub> , ◇ Uriarte (ORNL) UO <sub>2</sub> , □ Uriarte (NUMEC) UO <sub>2</sub> , ■ Uriarte 5 % Pu/(U+PU) Mechanical blended MOx ▲ Uriarte 0.5 % and 5 % Pu/(U+PU) Co-precipitated MOx, ● This work 5 % Pu/(U+PU) 110 °C 10 mol.l <sup>-1</sup> HNO <sub>3</sub> .....	132
Figure 58: MEO re-circulating dissolver [213] .....	138
Figure 59: Potential diagrams for silver [35].....	139
Figure 60: Potential-pH equilibrium diagram for silver-water (non- complexing media) [216] .....	140
Figure 61: Photographs of assembled version 1 and 2 reaction vessel and platinum working electrode .....	149
Figure 62: Photographs and diagrams of membranes.....	151
Figure 63: Photograph of digital multi meters and Agilent DC power supply.....	152
Figure 64: Photograph of Keighley multimeter and switching card. 152	
Figure 65: Example schematic timeline for LSCV experiment measurements.....	153
Figure 66: Photograph of Titanium thermometer pocket with Pt-100 thermometer.....	155

Figure 67: Photograph of 1 <sup>st</sup> bulk electrolysis test.....	156
Figure 68: Schematic diagram of LSV setup (anode monitoring shown) .....	158
Figure 69: Photograph electrolysis testing, apparatus in fumehood only (experiment e83) .....	161
Figure 70: Schematic diagram of bulk electrolysis setup. ....	162
Figure 71: Systematic diagram of plutonium dioxide dissolution apparatus.....	165
Figure 72: Dissolution of plutonium dioxide with silver(II) .....	167
Figure 73: Schematic diagram of bulk electrolysis experiment .....	169
Figure 74: LSCV – Tafel plot, 4 mol.l <sup>-1</sup> with and without 0.1 mol.l <sup>-1</sup> AgNO <sub>3</sub> (E <sub>0</sub> =1.85 V <sub>NHE</sub> ) .....	171
Figure 75: LSCV – effect of [Ag] with exchange current density.....	171
Figure 76: LSCV – Effect of anode [AgNO <sub>3</sub> ] in 4 mol.l <sup>-1</sup> HNO <sub>3</sub> , 500 rpm stirring) .....	173
Figure 77: LSCV – Effect of [HNO <sub>3</sub> ] for 0.05 mol.l <sup>-1</sup> AgNO <sub>3</sub> , 1500 rpm stirring.....	173
Figure 78: LSCV – Effect of stirring rate for 0.05 mol.l <sup>-1</sup> AgNO <sub>3</sub> – 4 mol.l <sup>-1</sup> HNO <sub>3</sub> , 1500 rpm stirring .....	174
Figure 79: LSCV – Effect of membrane type, 0.05 mol.l <sup>-1</sup> AgNO <sub>3</sub> 4 mol.l <sup>-1</sup> HNO <sub>3</sub> , 500 rpm stirring.....	174
Figure 80: LSCV – Effect of cathode type (ACE thimble, 0.05 mol.l <sup>-1</sup> AgNO <sub>3</sub> 4 mol.l <sup>-1</sup> HNO <sub>3</sub> ).....	175
Figure 81: LSCV – Effect of cathode nitric acid concentration (shown in figure) upon cathode potential, Ta pigtail cathode.....	175
Figure 82: Bulk electrolysis – example UV-Vis spectra .....	176
Figure 83: Bulk electrolysis – Potential, voltage, current (4 A), [Ag <sup>2+</sup> ] time plots (0.05 mol.l <sup>-1</sup> AgNO <sub>3</sub> 4 mol.l <sup>-1</sup> HNO <sub>3</sub> , 25 °C) .....	177
Figure 84: Bulk electrolysis – Effect of stirrer rate upon Ag <sup>2+</sup> generation efficiency using ACE E membrane (0.05 mol.l <sup>-1</sup> AgNO <sub>3</sub> 4 mol.l <sup>-1</sup> HNO <sub>3</sub> , 25 °C).....	178
Figure 85: Bulk electrolysis – Effect of [AgNO <sub>3</sub> ] on Ag <sup>2+</sup> generation efficiency using bored ACE E membrane (0.05 mol.l <sup>-1</sup> AgNO <sub>3</sub> 4 mol.l <sup>-1</sup> HNO <sub>3</sub> , 25 °C).....	178
Figure 86: Bulk electrolysis – Effect of temperature upon Ag <sup>2+</sup> generation efficiency (4A, bored ACE E membrane, 0.05 mol.l <sup>-1</sup> AgNO <sub>3</sub> 4 mol.l <sup>-1</sup> HNO <sub>3</sub> , 25 °C) .....	179
Figure 87: Bulk electrolysis – Effect of membrane type upon Ag <sup>2+</sup> generation efficiency (0.05 mol.l <sup>-1</sup> AgNO <sub>3</sub> 4 mol.l <sup>-1</sup> HNO <sub>3</sub> , 25 °C).....	179
Figure 88: Bulk electrolysis – Comparison of determined and calculated k <sub>1</sub> .....	181
Figure 89: Bulk electrolysis – Comparison of determined and calculated k <sub>2</sub> .....	181
Figure 90: Bulk electrolysis – Effect of [HNO <sub>3</sub> ] (3-8 mol.l <sup>-1</sup> ) upon the steady state and decomposition of Ag <sup>2+</sup> (0.05 mol.l <sup>-1</sup> AgNO <sub>3</sub> + 30 °C with bored ACE E membrane) .....	183
Figure 91: Bulk electrolysis – Effect of [AgNO <sub>3</sub> ] upon the steady state and decomposition of Ag <sup>2+</sup> (4 mol.l <sup>-1</sup> HNO <sub>3</sub> ~30 °C with bored ACE E membrane) .....	183

Figure 92: Bulk electrolysis – Effect of temperature (30-70 °C) upon the steady state and decomposition of $\text{Ag}^{2+}$ ( $0.05 \text{ mol.l}^{-1}$ $\text{AgNO}_3$ – $4 \text{ mol.l}^{-1}$ $\text{HNO}_3$ with bored ACE E membrane) ....	184
Figure 93: Bulk electrolysis – Effect of temperature (20-70 °C) upon the steady state and decomposition of $\text{Ag}^{2+}$ ( $0.05 \text{ mol.l}^{-1}$ $\text{AgNO}_3$ – $4 \text{ mol.l}^{-1}$ $\text{HNO}_3$ with Coorstek membrane) .....	184
Figure 94: Bulk electrolysis – Effect of temperature of calculated steady state and decomposition of $\text{Ag}^{2+}$ (to be compared with Figure 93) .....	185
Figure 95: Bulk electrolysis – Effect on current (1, 2 and 8 A) upon the steady state and decomposition of $\text{Ag}^{2+}$ ( $0.05 \text{ mol.l}^{-1}$ $\text{AgNO}_3$ – $4 \text{ mol.l}^{-1}$ $\text{HNO}_3$ with Coorstek membrane) .....	185
Figure 96: Dissolution – example UV-Vis spectra.....	187
Figure 97: Dissolution – $[\text{Ag}^{2+}]$ time plots ( $11.4 \text{ g PuO}_2$ , $0.05 \text{ mol.l}^{-1}$ $\text{AgNO}_3$ $4 \text{ mol.l}^{-1}$ $\text{HNO}_3$ , $25 \text{ }^\circ\text{C}$ ).....	187
Figure 98: Beer Lambert plot for uranyl in $6 \text{ mol.l}^{-1}$ nitric acid .....	214
Figure 99: Batch titration - Uranyl nitrate – nitric acid UV-Vis spectra .....	214
Figure 100: Comparison of molar extinction coefficients for titration and batch experiments .....	215
Figure 101: Beer Lambert UV-Vis plots for $\text{HNO}_2$ colorimetric method a) 1 cm cuvette, b) 10cm cuvette .....	216
Figure 102: Comparison of colorimetric and titration $\text{HNO}_2$ concentrations.....	217
Figure 103: Comparison of off-line $\text{HNO}_2$ methods with potentiometry method, top linear – linear scale, bottom $\log_{10}$ - $\log_{10}$ scale .....	218
Figure 104: $\text{HNO}_2$ UV-Vis extinction coefficients (0.2 cm flowcell) .	219
Figure 105: Uranyl in $6 \text{ mol.l}^{-1}$ nitric acid UV-Vis extinction coefficients at $\text{HNO}_2$ absorption wavelengths (1 cm cell) .....	219
Figure 106: UV-Vis-nIR spectra of 1 ml U,Pu solutions in $6 - 14 \text{ mol.l}^{-1}$ nitric acid.....	220
Figure 107: UV-Vis-nIR difference spectra for U, Pu solutions.....	221
Figure 108: Uranium Beer Lambert plot.....	221
Figure 109: Plutonium Beer Lambert plot for different $\text{HNO}_3$ concentration.....	222
Figure 110: Dependence of Pu calibration coefficient with $\text{HNO}_3$ concentration.....	222
Figure 111: Radioactivity of 4 % $^{235}\text{U}$ – 40 GWd/tHM, under three scenarios .....	225
Figure 112. Westinghouse PWR fuel assembly. (ORNL Photo 3897-77).....	228
Figure 113: Standard voloxidation process with off-gas treatment.	230
Figure 114: Advanced head-end operations.....	232
Figure 115: Typical head-end operations where zirconium recovery may be integrated.....	237
Figure 116: Interfacing zirconium recovery from cladding with tubing manufacture. ....	239
Figure 117: Head-end's position in a reprocessing plant .....	240
Figure 118: Systematic diagram of a high-temperature pre-treatment process .....	245
Figure 119: Flowcharts for Triso head-end processes [1].....	246

**Figure 120: Outline of steps involved in current head-end plant .... 253**

## **LIST OF ABBREVIATIONS**

$\alpha$  - activity or electrode exchange constant

%TD – percentage of theoretical density

ACSEPT – actinide separation for transmutation

ADS – Accelerator driven systems

AGR – Advanced gas cooled reactor

AIROX – atomics international reduction oxidation process

BDD – boron doped diamond (electrode)

BE – bulk electrolysis

BET – Brunauer-Emmett-Taylor theory of gas absorption, used for SSA determination

BU – burn-up

BWR – Boiling Water reactor

c – Concentration

CEPOD – catalysed electrochemical plutonium oxide dissolution

CSP – chemical separation plant

CV – cyclic voltammetry

DEMS – Dynamic electrochemical mass-spectrometry

DepU – Depleted uranium

DSA – Dimensionally stable anode

DUPIC – direct use of PWR fuel in CANDU process

E – potential

EIS – electrochemical impedance spectroscopy

Fabr – Fabrication

FBR – Fast breeder reactor

FMI – Fluid Metering Inc.

Fp – Fission product

FRs – Fast Reactors

FTIR – Fourier Transformed infra red

$\gamma$  - Activity coefficient

GANEX – group actinide extraction

GC – gas chromatography

GCFR – Gas cooled fast reactor

GDF – Geological Disposal Facility

GenI – generation one  
GenII – generation two  
GenIII – generation three  
GenIV – generation four  
GFR - Gas Fast reactor  
HA – Highly active  
HBU – high burn-up  
HLW – High level waste  
IFCs – Interfacial cruds  
IFPs – insoluble fission products  
ILW – Intermediate level waste  
IMF – inert matrix fuel  
ISO - international standard operation  
J – current density ( $A.cm^{-2}$ )  
LFR - Lead cooled fast reactor  
LLW – low level waste  
LSCV – linear staircase voltammetry  
LSV – linear sweep voltammetry  
LWR – Light water reactor  
MA – medium active  
Ma – Minor actinides  
MEO – mediated electrochemical oxidation  
MIMAS – Micronized Masterblend  
M-I – metal ligand  
MOx – Mixed (uranium plutonium) oxide  
NNL – National Nuclear Laboratory  
NOx – nitrogen oxides  
OCOM – Optimised Co-milling  
OREOX - oxidation reduction oxidation process  
OSPAR – Convention for the protection of the marine environment of the north Atlantic  
P – Primary  
PFA –perfluoroalkoxy (polymer)  
PHWR – Pressurised heavy water reactor  
PWR – Pressurised water reactor

RDE – Rotating disc electrode  
rds – rate determining step  
RepU – Reprocessed uranium  
Rpm – revolutions per minute  
RRDE – Rotating ring disc electrode  
S – Secondary  
SANEX – selective actinide extraction  
SBR – short binderless route  
SCWR - Super critical water reactor  
SEIRA – surface enhanced infra red absorption  
SEM-EDX – scanning electron microscopy – energy dispersive x-ray analysis  
SFR - Sodium fast reactor  
SIMFUEL –simulated irradiated fuel (fabricated from the sintering of mixed transition, rare earth and uranium oxides)  
SIT – Specific ionic interaction theory  
SSA - specific surface area analysis  
THORP – Thermal oxide reprocessing plant (based at Sellafield)  
TRISO – designation for particle fuel coating consisting of layers of three types: a porous carbon layer, pyrolytic carbon and a silicon carbide layer  
TRU – Transuranium  
UK – United Kingdom  
UV-Vis – ultraviolet – visible (spectrophotometry)  
V – applied voltage or volts (V)  
VHTR - Very high temperature reactor  
Volox – Voloxidation or volatile oxidation process  
XRD – X-ray diffraction

## ABSTRACT

The treatment of advanced nuclear fuels is relevant to the stabilisation of legacy spent fuels or nuclear materials and fuels from future nuclear reactors. Historically, spent fuel reprocessing has been driven to recover uranium and plutonium for reuse. Future fuel cycles may also recover the minor actinides neptunium, americium and perhaps curium. These actinides would be fabricated into new reactor fuel to produce energy and for transmutation of the minor actinides. This has the potential to reduce the long lived radioactivity of the spent fuel and reprocessing high level waste, whilst also maximising energy production. To achieve these aims there are a range of materials that could be used as advanced nuclear fuels, these include metals, oxides, carbides, nitrides and composite materials, and these fuels may also be alloyed. These advanced fuels may need to be reprocessed, and as head end is the first chemical treatment step in a reprocessing plant, the issues caused by treating these advanced fuels are faced primarily by head end. Changes to the overall reprocessing specification, such as reduction in discharge authorisations for volatile radionuclides, will have the greatest impact upon head end. All these factors may lead to the introduction of pre-treatment technologies (e.g. Voloxidation) or enhanced dissolution technologies, e.g. mediated dissolution using silver(II).

Literature and experimental studies show that uranium dioxide and low plutonium content MOx dissolves in nitric acid via direct and indirect nitrate reduction. The indirect nitrous acid catalysed route is kinetically most significant. The kinetics for the dissolution of uranium dioxide and 5 % plutonium MOx have been derived experimentally. Studies of the dissolution of MOx pellets in concentrated nitric acid and near boiling conditions indicate that dissolution shows a degree of mass transfer limitation. Thermodynamic studies show that the pronounced reduction in the MOx dissolution extent at 30-40% plutonium is due to the thermodynamics of the key dissolution reactions.

One technology that could be used to dissolve plutonium-rich residues that are generated from the reprocessing of MOx fuels is mediated dissolution. Inactive studies using linear staircase voltammetry (LSCV) and constant current bulk electrolysis (BE) have been used to optimise a 100 ml dissolution cell. The generation of silver(II) is dependent upon silver concentration, agitation and the size of the separator membrane. Whilst the stability of silver(II) is defined by the kinetics of water oxidation, this is dependent upon a number of factors including nitric acid concentration, silver(I):(II) ratio, temperature and the rate of migration from the catholyte into the anolyte. LSCV experiments have shown that Tafel analysis confirms there is a good relationship between potential and anode current density assuming oxygen evolution and silver(I) oxidation. Kinetic modelling of the BE experiments can be used to model the silver(II) generation, steady state and decomposition due to reaction with water. The dissolution cell has been demonstrated to be capable of dissolving plutonium dioxide to 200 g.l<sup>-1</sup> in less than 2 hours with good faradaic efficiency.

The University of Manchester

Chris Maher

Doctor of Philosophy

Options for treatment of legacy and advanced nuclear fuels

May 2014

Word Count = 66,390

## DECLARATION

No portion of this work referred to in this thesis has been submitted in support of an application for another degree or qualification at this or any other university or institute of learning.

## COPYRIGHT STATEMENT

- i. The author of this thesis (including any appendices and/or schedules to this thesis) owns certain copyright or related rights in it (the "Copyright") and s/he has given The University of Manchester certain rights to use such Copyright, including for administrative purposes.
- ii. Copies of this thesis, either in full or in extracts and whether in hard or electronic copy, may be made **only** in accordance with the Copyright, Designs and Patents Act 1988 (as amended) and regulations issued under it or, where appropriate, in accordance with licensing agreements which the University has from time to time. This page must form part of any such copies made.
- iii. The ownership of certain Copyright, patents, designs, trade marks and other intellectual property (the "Intellectual Property") and any reproductions of copyright works in the thesis, for example graphs and tables ("Reproductions"), which may be described in the thesis, may not be owned by the author and may be owned by third parties. Such Intellectual Property and Reproductions cannot and must not be made available for use without the prior written permission of the owner(s) of the relevant Intellectual Property and/or Reproductions.
- iv. Further information on the conditions under which disclosure, publication and commercialisation of this thesis, the Copyright and any Intellectual Property and/or Reproductions described in it may take place is available in the University IP Policy (see <http://documents.manchester.ac.uk/DocuInfo.aspx?DocID=487>), in any relevant Thesis restriction declarations deposited in the University Library, The University Library's regulations (see <http://www.manchester.ac.uk/library/aboutus/regulations>) and in The University's policy on Presentation of Theses.

## THE AUTHOR

Chris Maher carried out a MChem in Chemistry with a year in Europe between 1998 and 2002 at the University of York (1998-2001) and University of Helsinki (2001-2002). The EURAMAS exchange to the Radiochemistry department at the University of Helsinki provided a academic and practical foundation in the understanding of radioactivity measurement. During this period summer vacation jobs at the Geoffrey Schoffield Laboratory (routine radioanalytical analysis) and BNFL research and technology (engineering project) provided further experience in practical experiments.

Chris joined BNFL R&T process chemistry team in autumn 2002 as a technical support assistant. Chris has continued working in the same team and now holds the position of Technology Manager for head-end and dissolution in the Radiochemistry team at the UK's National Nuclear Laboratory, based at the Central Laboratory. During the past eleven years a large portion of his time has been spent planning and carrying out practical studies with the actinides. Due to the radioactive nature of the actinides, fumehoods (uranium, trace neptunium, plutonium, and americium) and gloveboxes (higher alpha activities) are used. Early work included the development of an analytical capability for process chemistry studies and carrying out experiments to support Sellafield operations. Chris has helped deliver projects that have lead to improvements in Sellafield operational plants and help support operational issues.

Between 2008 and 2012 Chris has worked part-time at the NNL and University of Manchester on the studies contained within this thesis. Since 2012 Chris has been writing this thesis in his spare time. The plutonium dissolutions studies were some of the first work in the Central Laboratories new Ivan Owens plutonium and minor actinide (PuMA) laboratory and as such formed part of the Active Safety Commissioning helping take the laboratory from milligram plutonium quantities to the operational limit.

Since working on the ACSEPT project, Chris has been helping underpin the chemistry for the treatment of plutonium containing aqueous waste in the new Sellafield Ltd alpha recovery process (ARP), investigating the disposal of plutonium contaminated organic wastes, planning a series of spent AGR leach tests to support the potential disposal to a UK geological disposal facility (GDF) and helping prepare for uranium carbide dissolution studies as part of the EU FPVII ASGARD project.

## ACKNOWLEDGEMENTS

This thesis would not have been possible without the funding from Sellafield Ltd, the UK Nuclear Decommissioning Authority (NDA) and the EU FPVII ACSEPT (project contract number 2007-211267). The silver(II) plutonium dioxide experiments reported here were carried out as part of a project to demonstrate the feasibility of producing high purity americium-241 from aged civil plutonium dioxide. This is of interest for the use as thermal sources for radioactive thermoelectric generator (RTG) by the European Space Agency (ESA).

This project would not have been possible without support from a large number of people. Dr. Danny Fox (now at the NDA) for negotiating the inclusion of this project into the ACSEPT project. Dr. Robin Taylor, Mr. Chris Mason and particularly Dr. Mike Carrott (NNL) for helping discuss this work, support me through the many piles of safety paperwork need to carry out experiments for the first time in a plutonium facility, supervising my very full glovebox experiments for lunch breaks, support me through the many woes of practical work and thus enabling me to ultimately present and publish the work contained within this thesis. I would also like to thank Prof. Sven Schroeder and Prof. Francis Livens to their time to discuss plans for experiments, results and review manuscripts.

Other people who have help greatly are Dr. Mark Sarsfield, Dr. Guy Whilock and particularly Dr. Bob Lewin for helpful electrochemistry discussions. The many other members of NNL who have help move equipment/material and manage the active laboratories. I'd also like to thank Roy Logsden and Dr. Rob Stephens. Roy organised the preparation of the uranium dioxide powder and analysis at the NNL uranium-active laboratories (Preston). Rob at the time worked for Sellafield Ltd, MOx Technical department and was instrumental in providing the MOx powders/pellets and spent time finding and discussing the material characterisation. There are also many other workers in Sellafield Ltd who have help in the packaging and movement of materials.

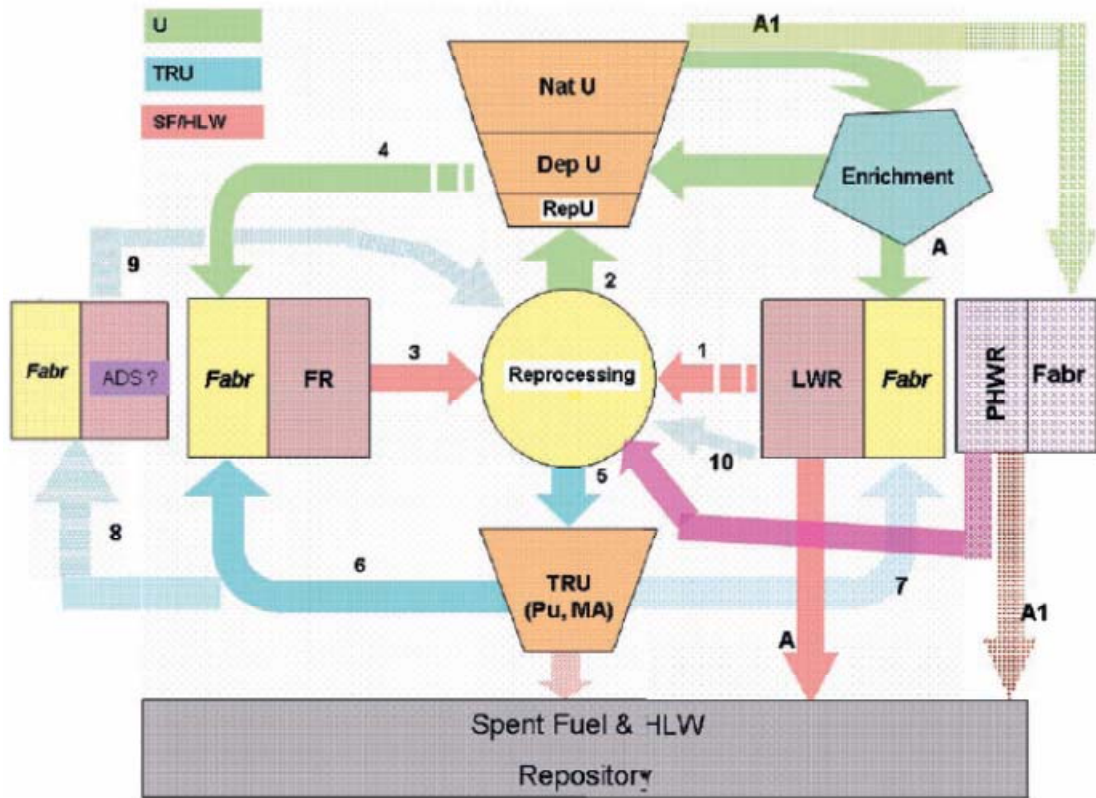
The write up of this thesis has at times seemed as challenging as the practical work. The write up would not have been possible without the continued support and encouragement of my Mum, Dad, Dr. Mike Carrott, Prof. Sven Schroeder and particularly my wife Zoë. These people have put up with (or perhaps enjoyed) the many hours where I have shut myself in a room full of too many books, reports, journal articles and a computer. I promise to tidy up!

I dedicate this thesis to Zoë, who has been very patient and is dearly loved.

## 1. Introduction

Nuclear fuel cycles in different nations have adopted various spent fuel management approaches. The main approaches are storage for eventual geological disposal or reprocessing to recover the uranium and plutonium for fabrication into new fuel. With increased national focus on the design, acceptability and construction of geological disposal facilities (GDF) many nations are revisiting reprocessing as a spent fuel management option. The increasing global rate of construction of nuclear reactors also places increased demands for further GDF capacity. Increased demand for uranium will also increase the price and ultimately the available natural resources may be reduced. For these reasons the management of spent fuel and the resulting actinides has in recent years led to the reconsideration of fast reactors (FRs) as 'burners', to generate and transmute actinides in equal amounts rather than breeding fissile material. To manage the radioactive inventory of further repositories the recovery of the minor actinides (Ma), neptunium, americium and curium, for transmutation in FRs or sub-critical accelerator driven systems (ADS) is gaining acceptance as a feasible option. The management of materials from thermal reactor, fast reactor and ADS is shown with material flows in Figure 1. These topics are considered in detail in many lengthy reports by international organisations [1-4].

The primary assumption of this thesis is that spent fuel is reprocessed. This thesis aims to highlight some of the important aspects relevant to the back-end of the nuclear fuel cycle (spent fuel management – reprocessing – fuel re-fabrication) for current commercial fuels (LWR uranium dioxide and mixed uranium plutonium oxide, MOx) and the various GenIV concept fuel types. In this discussion it will be seen that the requirements for further reprocessing for many of the different fuel concepts have the greatest impact on the first chemical treatment step, called head end. However, many of the requirements indicate considerable developments may also be necessary in reprocessing and fuel fabrication stages.



Fabr – fabrication, DepU – depleted uranium, RepU – reprocessed uranium

**Figure 1: Schematic overview of water reactor, fast reactor and ADS nuclear fuel cycles including the mass flows of uranium (U), Transuranium (TRU) and high level waste (HLW) [2]**

The aim of the current generation of spent fuel reprocessing plants is to recover uranium and plutonium for reuse as MOx fuel. The plans for future plants is to recover uranium, neptunium, plutonium, americium and perhaps curium for recycle as fuels and targets. This will reduce the radioactivity content of waste destined for ultimate disposal in a geological disposal facility (GDF). A major activity of the ACSEPT project is investigating the Group ActiNide EXtraction (GANEX) process [5]. This aims to co-recover americium and curium with plutonium and neptunium, which allows the production of a proliferation resistant mixed product that can be converted directly into solid material for reactor use. Alternative processes for minor actinide / lanthanide separation are the SANEX and Talspeak processes. Further aims for separation may include the separation of americium and curium, as reactor performance is increased without recycle of curium.

Whatever the aims of the separation process, any reprocessing plant will need a head end where reactor fuel is converted into solution form. Additionally, head end is the only part of the process where, as the conversion is carried out, recovery of the volatile and semi-volatile fission products can occur, the

radionuclides include tritium, carbon-14, krypton-85, and iodine-129 [6]. Furthermore, if a poor recovery is achieved (for example in head-end), then this reduces the overall process recovery efficiency. The radiotoxicity – time plots for material consigned to the GDF for U, Pu and U, Np, Pu, Am, Cm recovery are shown in Figure 2. It is clear that for U, Pu it is desirable to achieve >99 % recovery, whilst for U, Np, Pu, Am, Cm it is advantageous to achieve a recovery of >99.99 % [7]. This has clear implications for the efficiency of the entire nuclear fuel cycle and particularly for head-end where recovery is generally only 99.5-99.95 %.

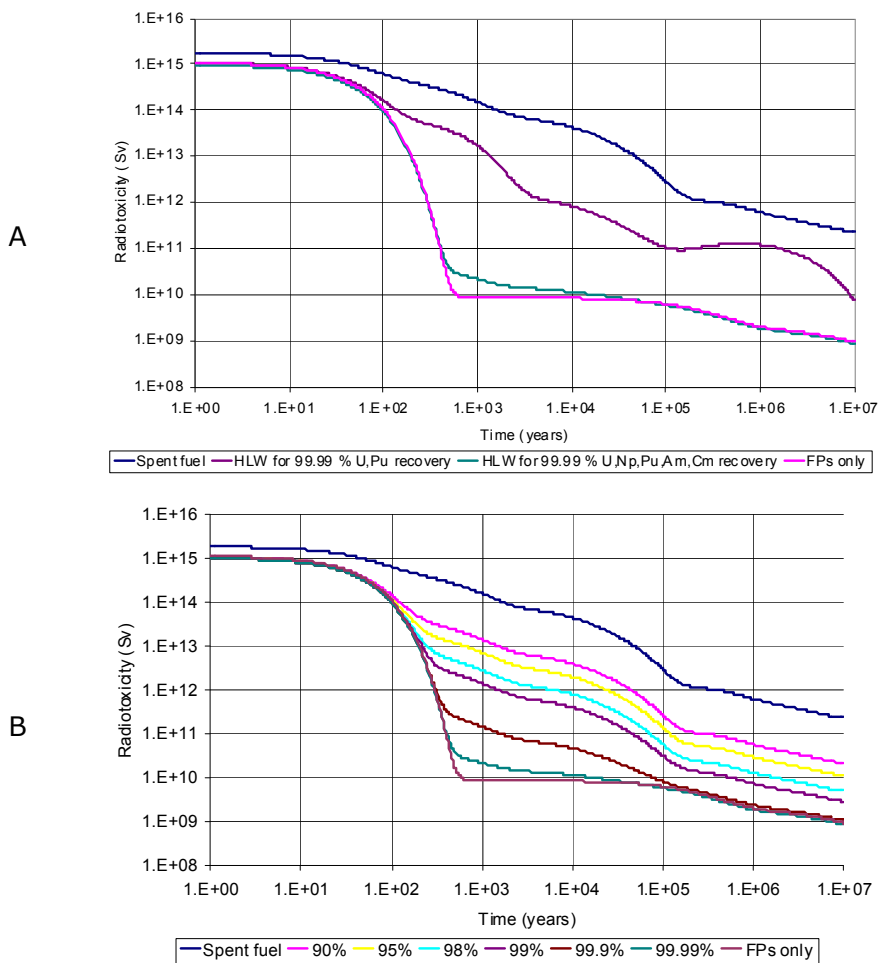


**Figure 2: Radiotoxicity – time plots for 40 GWd.t<sup>-1</sup>, 40 MW.t<sup>-1</sup>, 4 % <sup>235</sup>U for direct disposal, recovery of (A) U,Pu and (B) U, Np, Pu, Am, Cm [7]**

An inevitable part of head-end is dissolution to allow conversion from a solid to a solution. However, the direct dissolution does not allow the recovery of tritium as tritiated water is mixed with the dissolution liquor making separation difficult. Direct dissolution also makes recovery of other semi-volatile radionuclides, carbon-14 and iodine-129, more difficult. For these reasons it may be desirable to add process step(s) before dissolution to allow

efficient recovery. This would produce a gaseous stream concentrated in these radionuclides to simplify abatement.

A large amount of work has been carried out in dissolution techniques; these can be broken down into three parts, nitric acid only, nitric acid with additives and electrolytic techniques. The aim of these techniques is to allow complete dissolution of the fuel, which is often difficult as plutonium rich particles often do not dissolve in nitric acid. Dissolution in nitric acid with additives is disadvantageous as the addition of salts to head-end increases the HLW volumes and these mixtures, *e.g.* nitric acid – hydrofluoric acid, are highly corrosive to the typical plant materials (austenitic stainless steel), complicate separation and waste treatment processes. Electrolysis techniques include direct contact and mediated dissolutions, *e.g.* using electrochemically generated cerium(IV) or silver(II). They have advantages over nitric acid with additives as dissolution can be carried out in highly oxidative conditions requiring refractory construction materials. Then the corrosion can be reduced by conversion of the oxidising species to the reduced form prior to the separation and waste treatment processes, allowing the more typical construction materials to be used in downstream plant. Electrolysis processes also often only use low catalytic concentrations of reagents or catalysts can be recovered, therefore add less to HLW volumes.

Currently the most widely used plutonium containing commercial reactor fuel is MOx. This is largely produced by dry mixing processes where plutonium dioxide and uranium dioxide are milled and sintered with an aim of producing a 'homogenous' solid state solution. These processes produce material that has sufficient uranium plutonium diffusion to allow the bulk material to be dissolved in nitric acid without additives. However, small heterogeneities result in plutonium rich grains that do not dissolve in nitric acid. For this reason the dissolution of MOx produced via a dry route can be considered in two parts, dissolution of the bulk material and dissolution of plutonium rich residues. The industrial dissolution of spent light water reactor (LWR) MOx fuel currently uses direct dissolution in nitric acid that results in small losses of plutonium[8, 9]. To reduce the losses of plutonium in head-end the use of an alternative technology may be considered, whilst in the long term the use of truly homogenous MOx (U-Pu mixed at a atomic scale) may be considered, such as gel/co-precipitation methods, *e.g.* sol-gel processes under development in the ACSEPT project[5]. This report considers the dissolution of the bulk MOx material by studying the dissolution of unirradiated material. Later work will include consideration of the recovery of plutonium rich residues.

## 2. OVERALL OBJECTIVES

- Section 3: Carry out a thorough literature review of head-end technology; compare benefits of technology with issues caused by legacy and future advanced fuel types. Highlight areas where developments are required.
- Section 4: Carry out literature and experimental studies to develop the knowledge of the dissolution of uranium dioxide and mixed uranium plutonium dioxide in nitric acid.
- Section 0: Carry out literature and experimental studies on an 'enhanced' dissolution technology. This technology should be capable of dissolving plutonium dioxide and irradiated MOx dissolver residues. The selected technology is electrochemically generated silver(II).

### **3. TECHNOLOGY FOR THE HEAD-END TREATMENT OF LEGACY, CURRENT AND FUEL ADVANCED NUCLEAR FUELS**

#### ***3.1. Aims and objectives***

##### Aims

- Develop outline head-end flowsheets for legacy, current and future fuels.

##### Objectives

- Review historic, current and future nuclear reactor fuels. These are the feed to the head-end reprocessing plant
- Review factors that may influence the design of a future head-end process
- Review dissolution chemistry of these fuel types. To understand any issues with direct dissolution for these fuel types.
- Review other head-end technologies that could need to be used to achieve the process objectives.
- Highlight issues or knowledge gaps with current technologies and highlight any technology gaps

#### ***3.2. Science and technology of Head-End and influence of potential future challenges***

Here follows a chapter written for a book titled 'Reprocessing and recycling of spent nuclear fuel', edited by Dr. Robin J. Taylor, National Nuclear Laboratory, and is planned to be published by Woodhead publishing\* in March 2015.

---

\* <http://www.woodheadpublishing.com/en/book.aspx?bookID=3225>

### 3.2.1. Introduction

A key part of any reprocessing plant is the head-end area; this is where spent fuel is received and a dissolved product solution of standard composition is produced. The head-end currently produces three feeds for other parts of the reprocessing plant: the dissolver product, off-gases and solid wastes. The position of head-end with the feeds and products are highlighted in Figure 3. As solid spent fuel is transformed into an aqueous solution, solids such as cladding and undissolved residues must be removed and dispatched to a waste treatment plant. During head-end processing, gaseous and a portion of semi-volatile fission products are evolved into the process ventilation system, which is decontaminated in a separate process step, the off-gas treatment plant.

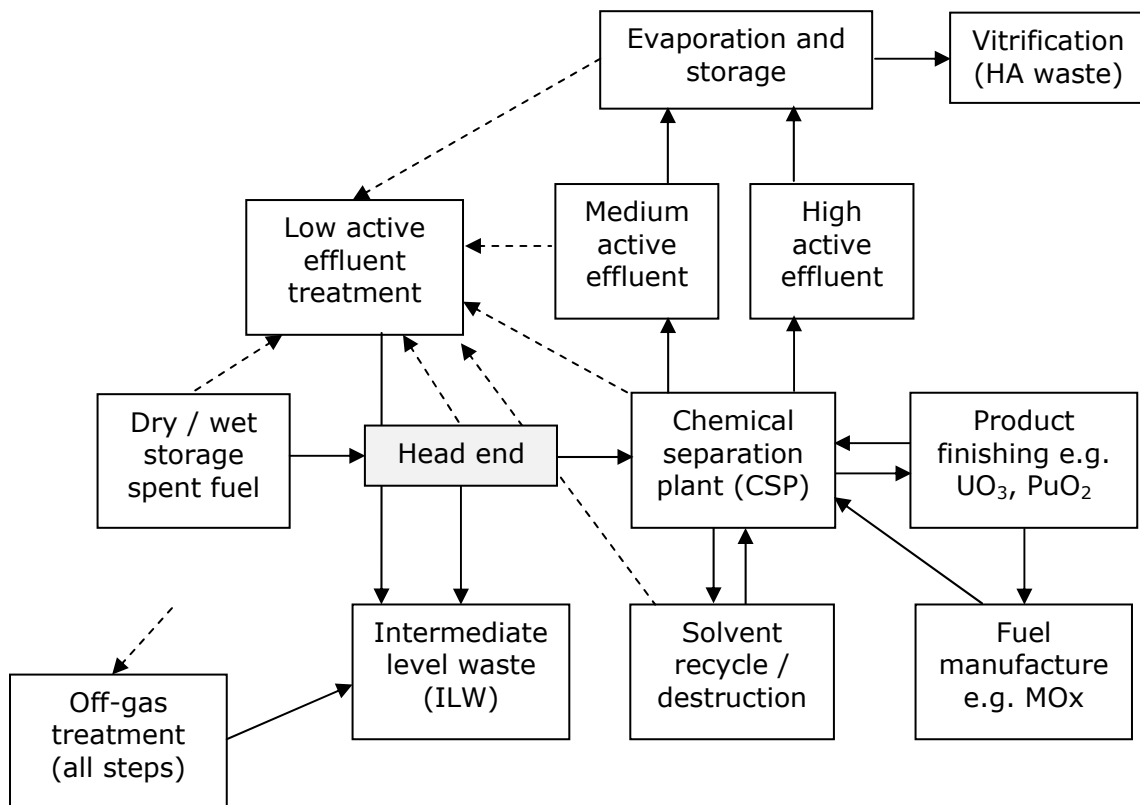


Figure 3: Position of head-end in the reprocessing plant

The reprocessing plant will have an overall process aim or specification, this can be used to define the requirements for each part of a reprocessing plant. As head-end does not produce any final products it must meet the requirements for the next process stage. Head-end must provide feeds that allow the chemical separation plant, off-gas and solid treatment plants to meet their objectives. An example of this is shown in Table 1. It is logical that any changes to the overall process aims could affect some or all of the final products. This in turn will affect the feed requirements to each process step. As the overall process aims for future reprocessing plants are continuously evolving as technology and regulatory constraints develop, the designs of future head-end processes must adapt to these requirements.

**Table 1: Key product requirements**

Products	Requirements
Dissolver product	3-4 mol.l <sup>-1</sup> nitric acid Free from settling particulates Minimal organic species Minimal halides present
Off-gases	Minimal suspended spent fuel particulates Minimal quantities of nitric acid / nitrogen oxides
Solid wastes	Minimal undissolved spent fuel Minimal quantity of nitric acid

A fundamental difference between head-end and any other part of the reprocessing plant is that spent fuel is received. Changes in fuel type or form can have a significant effect on the process steps needed to achieve the requirements for feeds to downstream processes. It is, therefore, highly important for developments in fuel and reactor technology to be linked to head-end development studies. For this reason the concept future reactor and fuel types are summarized in Table 2 [10]. The consequences of changes to fuel form or type will be the focus of discussion later in this chapter.

**Table 2: Summary of future reactor and fuel concepts [10]**

Reactor	Fuel				Fuel description	Cladding	Spectrum, Outlet temperature (°C)
	Oxide	Metal	Nitride	Carbide			
Gas Fast reactor (GFR)			S	P	(U,Pu)C-SiC	Ceramic	Fast 850
Sodium fast reactor (SFR)		P			U-Pu-Zr	Steel	Fast 550
	P				(U,Pu)O <sub>2</sub>	Steel	Fast 550
Lead cooled fast reactor (LFR)		S	P		(U,Pu)N	Steel, Ceramic or refractory alloy	Fast 550, Fast 800
Super critical water reactor (SCWR)	P				UO <sub>2</sub>	Steel	Fast 550
					(U,Pu)O <sub>2</sub> dispersion	Steel	Thermal 550
Very high temperature reactor (VHTR)	P				TRISO U(OC) in Graphite Compacts; ZrC coating	ZrC coating and surrounding graphite	Thermal 1000

P -Primary, S - Secondary option

There are three other changes that may change the aims of a future reprocessing plant and that could greatly affect the process steps required in head-end. These are:

- An increase in the percentage of transuranic actinides that need to be recovered;
- Reduction in environmental discharge limits and;
- Requirements to recover non-fuel components.

It is common that a small percentage of actinides, typically 0.05-0.5 wt%, is lost to the solid waste stream [11, 12]. If there is a future requirement to recovery >99.9 or >99.99 % of the actinides, clearly improvements in chemical methods or engineering techniques will be needed. Another example is tritium (<sup>3</sup>H), this is currently distributed between the off-gas, solid waste and dissolver product streams [11]. If a future requirement to abate or recover tritium is needed then a significant change to the process steps is needed. Similarly, if there are components of the fuel that are valuable and these need to be recovered for reuse; head-end processes must produce a

product that is consistent with the recovery process. Examples of non-fuel components that may need to be recovered from the fuel are; zirconium from cladding, nitrogen-15 from nitride fuel matrix, molybdenum from alloy or inert matrix fuel.

### 3.2.2. Current practice

The head-end plants that are currently operating use an engineering method of exposing the fuel prior to sending it to the dissolver to aid dissolution. For oxide fuel, following dissolution, hulls and insoluble fission products are removed from the dissolver liquor and then the liquor conditioned to remove iodine and to convert plutonium to plutonium(IV). Accountancy and buffer storage tanks are also used. This layout is summarized for thermal oxide fuel reprocessing in Figure 4. Table 3 lists reprocessing plants that are currently operational.

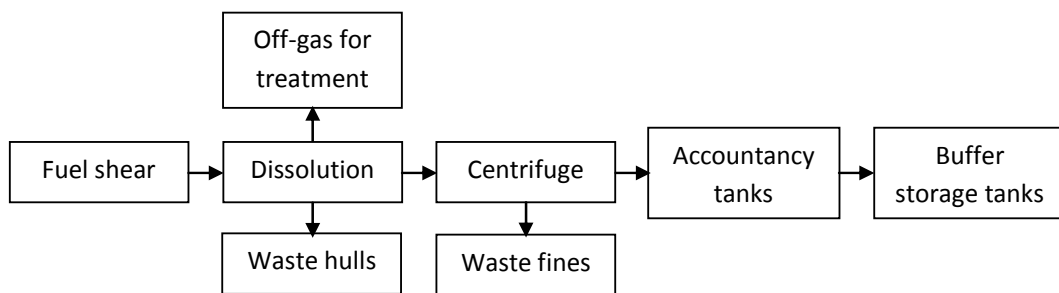


**Figure 4: Overview of process steps in current generation oxide reprocessing plants**

**Table 3: Civil reprocessing plants currently operational**

Country	Site, Name,	Commissioning date	Throughput (tHM/yr)	Fuel type
UK	Sellafield, Magnox	1964	1500	Magnox
	Sellafield, THORP	1994	1000	LWR+AGR
France	La Hague, UP2-800	1990	800	LWR
	La Hague, UP3	1990	800	LWR
Russian	Mayak, BB, RT-1	1976	400	LWR
Japan	Rokkasho	2005	800	LWR
India	Tarapur	1982	100	PHWR
	Kalpakkam	1998	100	PHWR+FBR
	Tarapur	2011	100	PHWR

AGR, advanced gas cooled reactor, LWR, light water reactor, PHWR, pressurized heavy water reactor, FBR, fast breeder reactor

### **3.2.2.1. Fuel conditioning**

It is current practice to de-clad Magnox (uranium metal) fuel or shear (chop up) oxide fuel assemblies prior to dissolution. These operations remove or breach the cladding to allow good access of nitric acid for dissolution. Magnesium alloy is removed from Magnox fuel as it would dissolve in the dissolution step and this would increase the quantity of dissolved salts and so increase the amount of high active (HA) vitrified glass waste product. As oxide fuel cladding is zircaloy or stainless steel these materials dissolve to a minimal extent so that they can be chopped up (sheared) and added to the dissolver without contributing significantly to the HA product volume. Fuel conditioning and addition of fuel to the dissolver is the most mechanically engineered part of the reprocessing plant.

Magnox fuel is de-canned by feeding the element through a die where the outer heat sink fins are removed. At the start and end of this process the fuel end-caps are cropped with a rotating blade. In the second stage, cutter wheels slit the Magnox cladding along its length and the metal fuel rod is forced through a die allowing the cladding to be peeled away from the metal rod. The bare metal rod is then transferred into a container for movement to the dissolver. This process is illustrated in Figure 5 below.

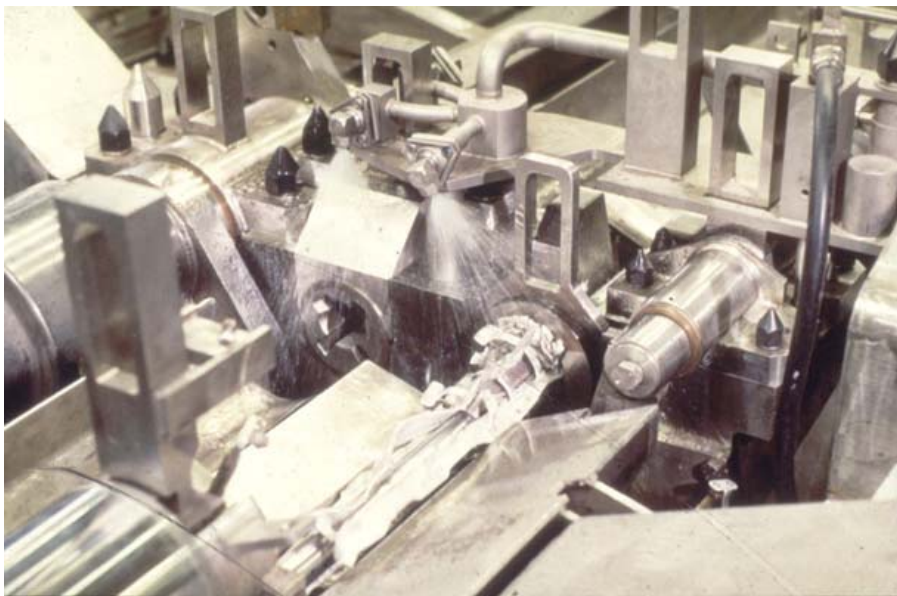


**Figure 5: Illustration of Magnox de-canning**

Oxide reprocessing plants are more modern compared to the Magnox reprocessing plant. This has led to an improvement in efficiency by integrating fuel conditioning and dissolution hence reducing building and operating costs, thereby improving process efficiency. In THORP and other oxide reprocessing

plants (e.g. UP2-800, UP3) fuel conditioning and addition of the fuel to the dissolver is carried out in a single step. This is achieved by chopping the fuel with a large hydrolytic shear, the cut fuel falls down a chute directly into the dissolver. Hydrolytic shears use a hydrolytic gag to hold the fuel securely and a hydrolytic cutting blade to shear the fuel [13]. Cuts at intervals of 5-10 cm are typical, which is suitable for leaching of the fuel from the hulls. Some reprocessing plants add the assembly end-plates to the dissolver or alternatively they can be disposed of via a separate chute. This process is illustrated in Figure 6 .

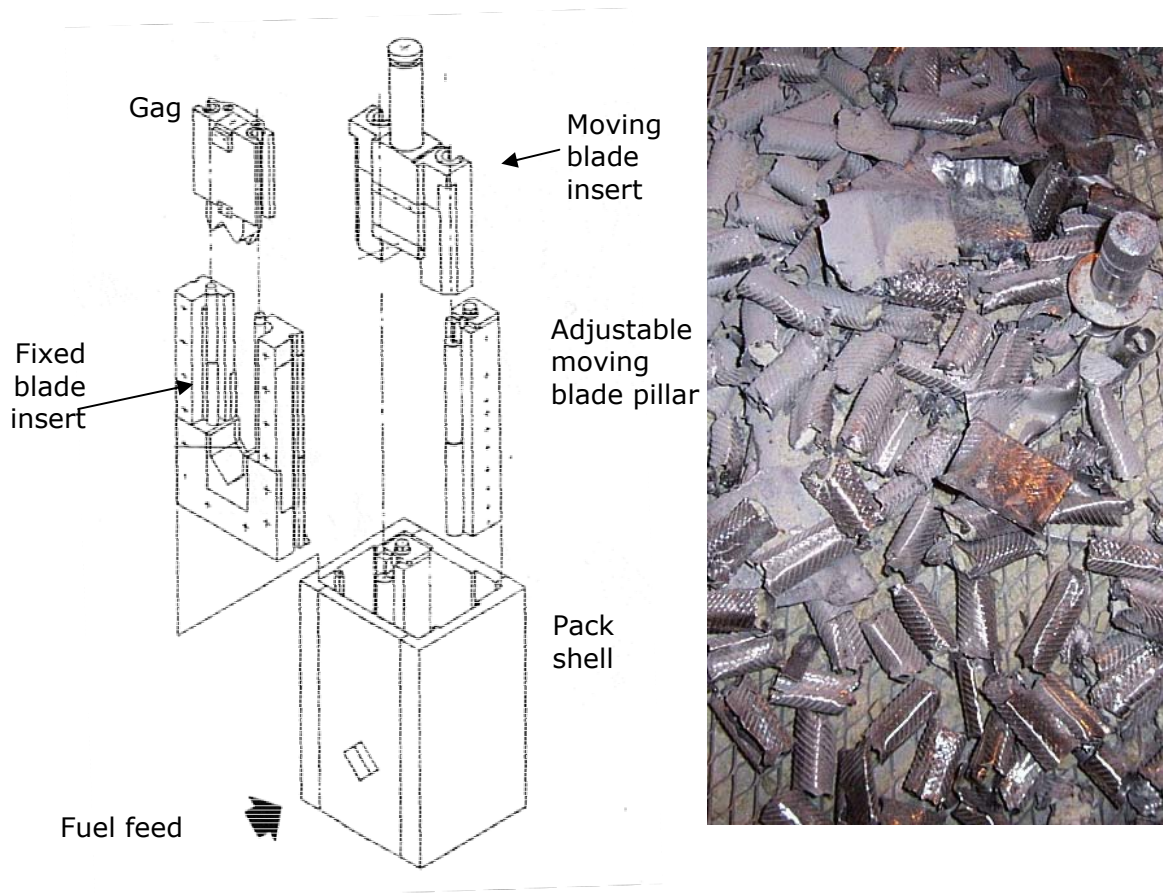


**Figure 6: Left - Illustration of the THORP hydrolytic shear; Right – example sheared cross-sections from an inactive dummy AGR fuel bundle**

### **3.2.2.2. Dissolution**

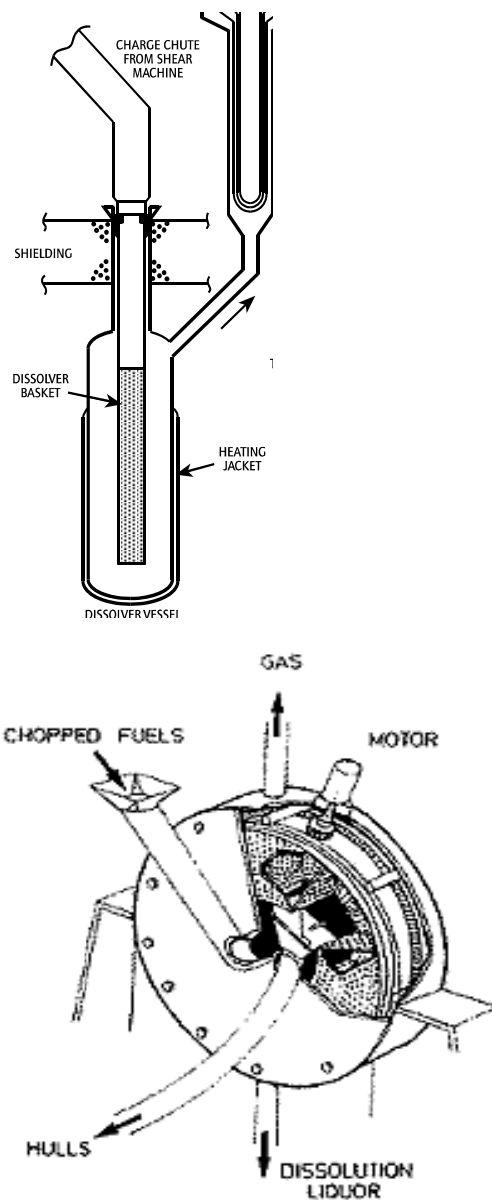
The dissolution of spent fuel is the first chemical step in current reprocessing plants. Spent fuel is dissolved in nitric acid as this is the medium of choice for solvent extraction chemistry; nitric acid reduction chemistry also allows dissolution. Dissolution is carried out either in batch or continuous dissolvers.

Dissolvers for oxide fuel use a basket to contain the cropped fuel and cladding pieces, which allows removal of the leached cladding hulls post-dissolution. Dissolvers for bare metal rods do not need a basket, as there are not any insoluble cladding components that need to be removed.

#### *3.2.2.2.1. Dissolvers*

The Magnox reprocessing plant uses a continuous 'kettle' dissolver, where fuel is dissolved in  $\sim 3 \text{ mol.l}^{-1}$  nitric acid to give a final solution containing  $300 \text{ g.l}^{-1}$  uranyl nitrate. The rate of addition of new fuel and top up nitric acid is controlled to prevent accumulation of fuel in the dissolver, these control the rate of liquor take off.

The THORP reprocessing plant uses three 'kettle' batch dissolvers. Sheared fuel falls via a movable chute into one of the three dissolvers, which each contain a basket [14]. This is illustrated in Figure 7a. The dissolvers are used in sequence to allow continuous fuel shearing. This sequence allows one dissolver to have the fuel added, the second is leaching fuel and conditioning the liquor and the third is being emptied. The fuel is added to the dissolver initially containing  $\sim 8 \text{ mol.l}^{-1}$  nitric acid. The rate of addition of fuel is controlled to allow the vigorous dissolution of the finer crushed fuel to dissolve before the next addition. The dissolution consumes nitric acid resulting in a final solution composition of  $\sim 3 \text{ mol.l}^{-1}$  nitric acid and  $250 \text{ g.l}^{-1}$  uranyl nitrate. Due to the relatively large amount of low enriched fuel in the THORP dissolver; a neutron poison, gadolinium nitrate, is added to ensure criticality safety is maintained [15].



- a) Batch 'kettle' dissolver                      b) Continuous rotary wheel dissolver

**Figure 7: Schematic diagram of oxide a) batch kettle and b) continuous rotary wheel dissolver**

The French reprocessing plants UP2-800 and UP3 operate a continuous rotary wheel dissolver, Figure 7b. These dissolvers have a rotating basket system that receives sheared fuel via a chute, allows dissolution and empties the baskets in a single rotation of the wheel [16, 17]. A schematic diagram of the dissolver design is shown in Figure 7b. The continuous nature of the dissolver means fuel is dissolved in  $\sim 3 \text{ mol.l}^{-1}$  nitric acid to  $250 \text{ g.l}^{-1}$  uranyl nitrate. The dimensions and relatively small amount of fuel in the dissolver means that a neutron poison is not required to maintain criticality safety.

### 3.2.2.2.2. Factors controlling dissolution

It is key to understand the dissolution chemistry in nitric acid and therefore some background is provided. Nitric acid can be reduced to form a number of different species, Figure 8 [18]. Nitrogen dioxide, monoxide and dinitrogen oxide are gaseous and so have limited solubilities in nitric acid. Nitrous acid has a limited vapour pressure but decomposes over time to nitrogen monoxide [19]. The rate of decomposition of nitrous acid is determined by the liquor surface area and gaseous nitrogen oxide mass transfer [20]. The decomposition rate can, therefore, be greatly reduced by gas purges flowing over the liquor or sparges through the liquor. The concentration of nitric acid [19], decomposition of nitrous acid and reaction kinetics [21] affect the ratio of the nitrogen oxides evolved during dissolution. There is a large variant of different fundamental [22-25] and applied chemistry studies [26-29] that suggest that nitrous acid and other nitric acid reduction products are the reactive species in dissolution [17].

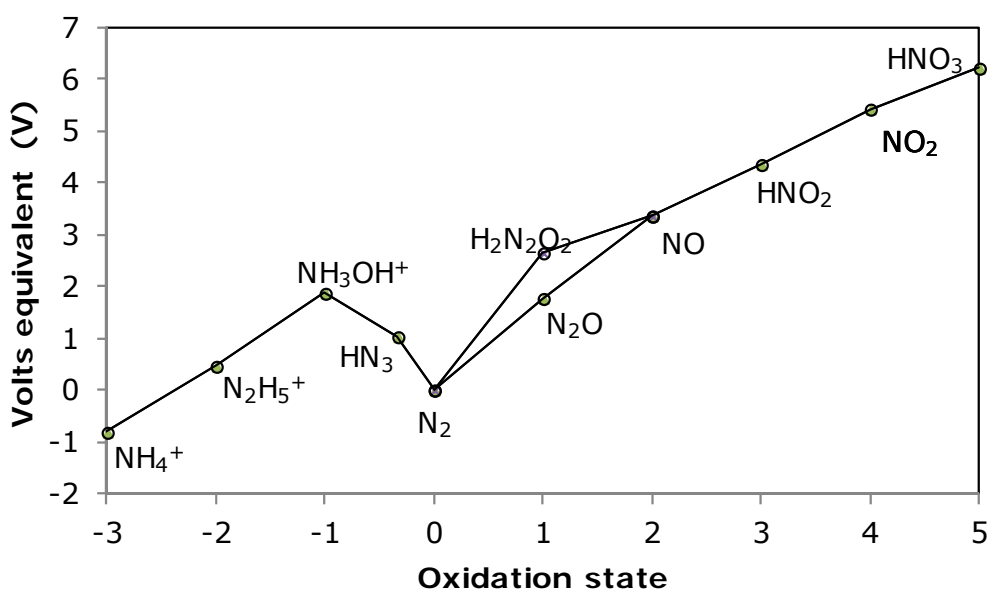


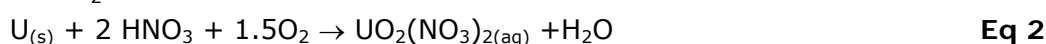
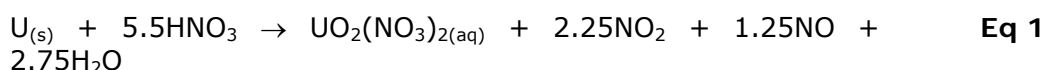
**Figure 8: Nitric acid reduction chemistry [18]**

A second key factor in understanding dissolution is surface area. This is because dissolution is a heterogeneous reaction. There are several good examples of this. First, during the dissolution of pellets the changes in surface area follow an 'S-shape' due to initial roughing of the pellets, which leads to an increase in surface area until a maximum is reached, followed by a decrease due to accelerating dissolution [30, 31]. Second, during irradiation macroscopic cracking occurs and microscopic porosity develops [17], again

increasing the surface area available for dissolution. During the shearing of oxide fuel, pellets are crushed [32], which increases their surface area. Another significant factor that affects the leaching of fuel is the hulls, which lead to decreased rates of dissolution [33, 34] for example in a packed bed of the crushed material and can result in incomplete dissolution for crimped 'end caps' due to gas locking.

### 3.2.2.2.3. Dissolution of uranium metal fuel

Uranium metal is a highly electropositive metal, with  $E_0(U^{4+}/U) = -1.38 V_{NHE}$  [35]. Therefore, thermodynamically, dissolution can produce hydrogen; however, hydrogen is often not the kinetically favoured reaction product under industrial dissolution conditions [36]. Strong exotherms can occur, which can result in large dissolvers requiring little heating or cooling to control the dissolver temperature. Industrially, dissolvers are often run to produce nitrogen oxides following Eq 1 below. The nitrogen oxides can be recovered either in the dissolver and condenser or in an acid recombination column to produce 'fumeless' dissolution [37] according to Eq 2. Industrial dissolvers often utilize 'fumeless' dissolution technology to varying degrees to minimise the nitrogen oxide burden upon the off-gas treatment plant and facilitate the efficient use of nitric acid.

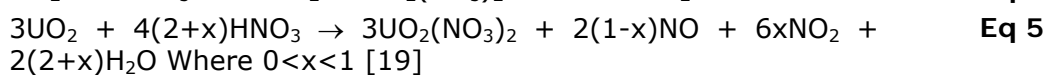
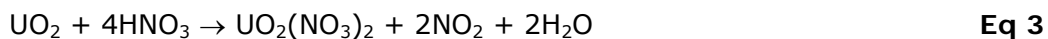


There have been numerous studies of dissolution of uranium metal in nitric acid, showing that surface area, nitric acid concentration, temperature and the type of alloy are key factors in controlling the dissolution rate [38-42]. Again, these experiments often observe an 'S-shaped' dissolution profile, which is believed to be associated with an autocatalytic mechanism, where an initial slow reaction (with nitric acid) results in a product (nitrite or nitrous acid) that reacts with the oxide fuel and generates more of itself, thereby accelerating both its own formation at the liquid/solid interface and interfacial dissolution simultaneously. This fits with general studies of nitric acid reduction chemistry where nitrate reduction is slow but nitric acid reduction products are more rapid oxidants [22]. Other workers have studied the sparging of solutions, or adding nitrous acid scavenging agents, which greatly slow the dissolution rate as only the nitrate reduction reaction can take place is working.

#### 3.2.2.2.4. Dissolution of uranium-based oxide fuel

Two types of thermal oxide fuel are currently used in commercial reactors: low enriched uranium oxide fuel and mixed uranium plutonium oxide (MOx) fuel. Current mixed uranium plutonium oxide fuels are manufactured by mechanical milling uranium dioxide and plutonium dioxide together [12]; this leads to a heterogeneous mix that contains a range of different plutonium contents [43].

The dissolution of uranium dioxide in nitric acid is known to be greatly affected by nitric acid concentration, temperature and surface area [34]. Like uranium metal, uranium dioxide dissolves via an autocatalytic mechanism and experiments lead to rate expressions that separate the nitrate and nitrous acid reaction rates [44]. Other process parameters, for example varying the ratio between dissolver liquor surface area and volume, sparging, and stirring have been shown to decrease the rate by depleting the nitrous acid concentration near the interface local to the dissolving solid and bulk solution concentration [34, 45, 46]. Results from this type of reaction make it possible to mathematically optimize the dissolution time for different dissolution conditions [47-49]. Dissolution is, however, complicated by the presence of hulls, which can lead to a reduction to the dissolution rate by gas-locking or mass-transfer limitations [33], which means industrial dissolvers are often optimized using more applied chemical engineering approaches. Dissolution experiments have led to expressions describing the rate in terms of nitrogen dioxide and monoxide concentration [19], as expressed in Eq 5. However, it is known that dinitrogen oxide is also produced [50]. It must also be recognized that the proportion of nitrogen monoxide is dependent upon the amount of nitrous acid decomposition [20, 49] and the amount that is oxidized by oxygen to nitrogen dioxide [18].



The dissolution of MOx occurs via the same mechanism [44], which is reasonable, but small plutonium-rich regions [43] lead to incomplete dissolution [51]. This is expected, as the reaction between plutonium dioxide and nitric acid (or its reduction products) is thermodynamically much less favourable than the reaction of  $\text{UO}_2$  [52]. The decrease in solubility of MOx at 20-40 wt% plutonium has been demonstrated experimentally [17, 53].

The presence of plutonium-rich particulates resulting from the industrial dissolution of MOx fuel is a criticality hazard that requires careful management. A great deal of work is necessary to justify the routing and control of these plutonium rich particulates before industrial reprocessing is possible, as for example justified and demonstrated in the French reprocessing plants at La Hague [8, 9].

#### *3.2.2.2.5. The formation and control of solids and precipitates in head-end*

During the irradiation of oxide fuel, refractory-noble metal alloys form inclusions at grain boundaries; these are called  $\epsilon$ -phase and contain molybdenum, technetium, rhenium, ruthenium and palladium metals [54]. During dissolution these particulates dissolve slowly and do not dissolve completely. The resulting particulate residues are termed insoluble fission products (IFPs).

As the burn-up of fuel increases the concentration of a large variety of fission product elements also increases. This leads to the formation of precipitates during dissolution, such as noble metal iodides or iodates [55] or zirconium molybdate [56-58]. At even higher burn-ups it is reasonable to expect that other precipitates will also form.

The formation of noble metal iodides and iodates is less of an issue, as smaller quantities of solids form. The solids are fine in nature and do not form on surfaces. During dissolver cycles the extent of formation is minimised, as iodine is removed from the dissolver solution, see below for further details.

Optimization of processing conditions in industrial dissolvers with the aim to achieve tolerable levels of zirconium molybdate formation are important as zirconium molybdate forms on surfaces in the dissolver, leading to the development of so-called 'cow pats'. The effects of temperature, nitric acid, molybdate and zirconium concentration are known to be key factors in the formation rate of zirconium molybdate [56-58]. For industrial dissolvers the preferred adjustable process parameter is temperature. In industrial dissolver cycles the peak temperature is therefore often minimised to slow the formation rate of zirconium molybdate. At La Hague parts of the reprocessing plant are leached with sodium carbonate to dissolve the zirconium molybdate and prevent chromic build-up [59]; a similar approach is employed in THORP, but using salt free reagents [60].

IFPs, together with fragments of cladding, precipitates (e.g. silver, palladium iodide, zirconium molybdate) and undissolved fuel (e.g. plutonium-rich particulates from MOx dissolution) form the dissolver insolubles.

### 3.2.2.3. Dissolver liquor conditioning

Current oxide reprocessing plants focus on three tasks during fuel conditioning, namely (i) removal of the majority of the iodine, (ii) conditioning plutonium to the tetravalent state and (iii) removal of particulates. These three tasks are explained in the following three sections.

#### 3.2.2.3.1. Iodine

Iodine is evolved into the off-gases in head-end to minimise accumulation in the organic phase in the solvent extraction plant and to minimise aerial discharges through the reprocessing plant. It is typical that Magnox and thermal oxide fuel is cooled for a number of years prior to reprocessing and this has the advantage that iodine-131 ( $t_{1/2} = 8$  days), which has a high radiotoxicity, has decayed sufficiently to leave only the long-lived iodine-129 isotope ( $t_{1/2} = 1.57 \times 10^7$  years).

During dissolution in nitric acid iodine is capable of existing in multiple oxidation states in equilibrium with each other, see Figure 9, [55, 61-64]. As elemental iodine has an appreciable vapour pressure it is evolved into the process off-gases; these act as a driving force to adjust the equilibrium to force the majority of the iodine to the off-gas system where it can be trapped or scrubbed from the gas stream. Solid silver or palladium iodides or iodates can form and are kinetically slow to dissolve as the solids 'age' [55]. Iodates can also be kinetically slow to equilibrate to iodine. The presence of iodine-containing solids or iodates can reduce the efficiency of iodine removal, resulting in a few percent iodine remaining in the dissolver solution.

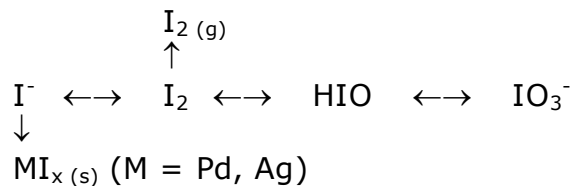


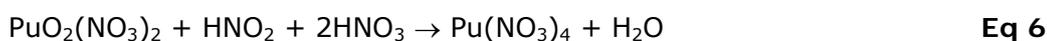
**Figure 9: Multiple oxidation states of iodine in dissolver**

THORP batch dissolvers and the continuous dissolvers at La Hague employ different methods for maximizing the removal of iodine. The batch dissolvers

can simply apply a sparge towards the end of the dissolver cycle, after dissolution is complete, removing the remaining fraction. For continuous dissolvers, the use of a sparge is not desirable as the dissolution rate is too slow to sequester the iodine that is produced. To achieve removal from continuous dissolver liquors a separate process step is used. The liquor flows through a column with an air counter-current, transferring the majority of the iodine into the process off-gas stream [65].

#### *3.2.2.3.2. Plutonium(IV) conditioning*

Plutonium can exist as a mixture of tetravalent and hexavalent oxidation states after dissolution. Continuous dissolution tends to produce a tetravalent product, whereas during the later stages of batch dissolution, when there is a low nitrous acid concentration, plutonium is partially oxidized to the hexavalent state [65]. As tetravalent plutonium is preferred for solvent extraction processes, towards the end of the THORP batch dissolver cycle a mixture of air and nitrogen dioxide is sparged through the dissolver solution. This reduces the plutonium to the tetravalent state, Eq 6 [66, 67]. Radiolytic reduction [68] can also take place.



#### *3.2.2.3.3. Removal of particulates*

The removal of dissolver insolubles is carried out to minimize the accumulation of solids in downstream plants [65]. This is important as the solids are heat-generating due to their intense radioactivity. Also, irradiated MOx insolubles contain plutonium-rich particulates [9], which need to be removed and routed to a single location with high efficiency. Another important reason for removal of particulates is to minimise the formation of interfacial cruds (IFCs) in the first solvent extraction cycle, which can lead to a reduction in solvent extraction performance. The dissolver insolubles are removed by centrifugation. An example of an industrial centrifuge is shown in Figure 10 [65]. After a defined amount of liquor has been processed through the centrifuge the bowls are washed and slurried solids are transferred to the waste plants for encapsulation.

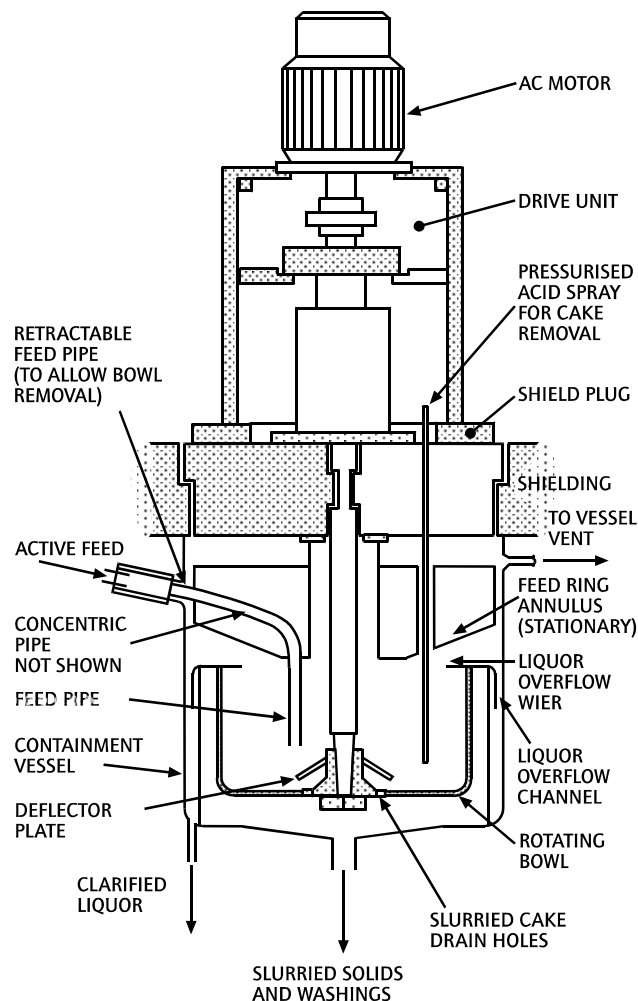


**Figure 10: Industrial centrifuge used for clarification of the dissolver product**

#### **3.2.2.4. Accountancy and buffer storage**

Clarified dissolver product liquor is collected in tanks to allow accountancy checks by weighing the liquor and sending samples for analysis. This is the first point in a reprocessing plant where fuel accountancy can be implemented. Monitoring mass balances through the reprocessing plant is important to demonstrate control to regulators and international safeguards. Plant operators and international safeguards analyse samples to ensure that material is not diverted for other uses. The accountancy tanks or other separate tanks also act as buffer storage between head-end and chemical separation plants to ensure efficient continuous operation of the entire reprocessing plant.

### 3.2.3. *Potential developments to meet future challenges*

Future reprocessing plants may be required to process advanced fuels with very high burn-ups. It may be necessary to achieve improved actinide recoveries [44] and the recovery of other valuable materials, such as zirconium based cladding. This may also need to be achieved against a much lower, near zero discharge authorization limit [69].

The detailed justification of overall reprocessing plant specification is an often emotive subject, which needs to be studied and debated in depth in future years. Potential improvements are easy to discern:

- An improvement in fuel recovery towards 99.99 %
- Recovery of other valuable materials for reuse
- Reduction of radioactive discharges to 'near zero'
- Enhanced safety – improved management of conventional, radiological and criticality risks.

The improvement in actinide recovery could be of interest in reducing the long-lived radioactivity to high level waste. This is of increased interest as development of solvent extraction processes to recover uranium, neptunium, plutonium, americium and curium reduces the radiotoxicity by more than five orders of magnitude in approximately five hundred years [44]. The answer to requirements for readily dissolvable fuels may well lie in improved process engineering, but for harder to dissolve materials such as MOx improved dissolution technologies will be needed.

The recovery of fuel materials has the advantage to potentially reduce the volume and amount of waste, which will ultimately be stored in a geological disposal facility, and may make the material available for reuse. Examples of potential materials for recovery include zirconium from cladding or inert matrix materials, molybdenum from inert matrix or alloying, and nitrogen-15. Zirconium is an expensive metal that is considered a strategic resource [70]. Isotopically purified molybdenum may be used to minimise the production of long lived technetium-99. As the isotopic purification of the molybdenum is likely to be expensive, recovery and reuse of molybdenum is potentially required. The use of nitrogen-15 is important for nitride fuels, where it minimizes the quantities of carbon-14 produced [71]; again recovery processes could be warranted as well.

In Europe the introduction of OSPAR, the convention for the protection of the marine environment of the north-east Atlantic, will require near zero discharges of radioactive elements [69]. Current and future discharges of

radionuclides into the environment will need to be set against the continued use of fossil fuels for energy production. The issue at the centre of this evaluation is the definition of acceptable levels of radioactive discharges. A fundamental requirement will be that the risk due to radioactivity both locally and globally from nuclear fuel cycle operations is low. From these discussions it can be envisaged that there are several options to consider, these include;

- Reduce risk of substantial failure
- Refine existing processes
- Abate tritium
- Abate noble gases

Existing abatement processes are discussed elsewhere. Notably carbon-14 (in the UK) [65] and iodine-129 (in France) [17] abatement. Improvements in abatement of these isotopes remain a possibility. This may be particularly warranted for short cooled fuels, which contain iodine-131. The abatement of tritium is a potential future requirement along with other low energy and radiotoxic isotopes. As tritium is currently distributed between dissolver liquor, off-gases and solid waste streams this will require the use of technology before dissolution. There are currently no industrially viable processes for the abatement of krypton-85 and other noble gases, due to the inherently low radiotoxicity of noble gases and the difficulties associated with handling gases, also in passively safe storage. Infinite dispersal has therefore been considered the best practical method [72]. If, in the future, noble gas abatement will be considered desirable, technology development will be necessary.

The implementation of new technologies is always subject to weighing the benefits against disadvantages, which includes financial and risk analysis. Recent global events will lead to increased and more detailed analysis of hazards, greater scrutiny of facilities and processes, and expectations for improved safety in future sustainable nuclear fuel cycles.

### ***3.2.3.1. Dissolution chemistry of alternative fuel types***

#### *3.2.3.1.1. Oxide fuels*

Mixed uranium plutonium oxides are currently used in thermal reactors. Due to the maturity of mechanical oxide fabrication technology it is likely that MOx for future thermal and fast reactors will continue to be produced in this way

for some time. The current MOx manufacture technologies use milling techniques to intimately mix the uranium and plutonium. This, however, does not provide perfect homogenisation at atomic length scales and plutonium-rich heterogeneities remain [43]. These heterogeneities lead to plutonium residues after dissolution [51]. The percentage of residues is dependent on the quality of the manufacturing process, but typical residues post-irradiation of thermal fuels (~5 wt% Pu) are 0.1-0.3% [11]. Depending upon the manufacturing and reactor conditions fast reactor fuels can have lower solubilities [71]. For example, with 0.5 wt% plutonium residues for 20 wt% MOx one kg of plutonium would be destined for waste per tonne heavy metal reprocessed. This is clearly unacceptable, from the perspectives of waste minimisation, plant criticality control and fissile material utilization. Future developments in dry manufacturing techniques could result in incremental improvements; however, it is expected that residues will continue to be an issue. The use of chemical precipitation techniques for manufacture of MOx could result in more homogeneous material that can wholly dissolve in nitric acid without leaving plutonium rich residues [73, 74]. However, the dry manufacturing techniques are currently in use, and thus produced fuels will need to be dissolved for reprocessing.

If future fuel cycles include recycle of minor actinides (neptunium, americium and curium) then the consequences of fuels containing elevated levels of these elements during dissolution will need to be assessed as well. However, there is significant opposition to recycling curium. Currently the recycle of americium-containing MOx seems a more likely development [75].

The dissolution rate of MOx decreases with increasing plutonium content [17, 53, 76], due to the unfavourable thermodynamics of plutonium dioxide dissolution [see also sections 3.2.2.2.4 above and 4.7.1 below], which has also been empirically explained in terms of kinetics [74]. Dissolution is slowed and ultimately halted by reducing the rates of initiation and of the rapid autocatalytic nitrous acid dissolution cycle. Figure 11 illustrates this phenomenon through an example of by 8 h leaching experiments on MOx with increasing plutonium content, under otherwise identical conditions, in 5 and 10 mol.l<sup>-1</sup> nitric acid [53].

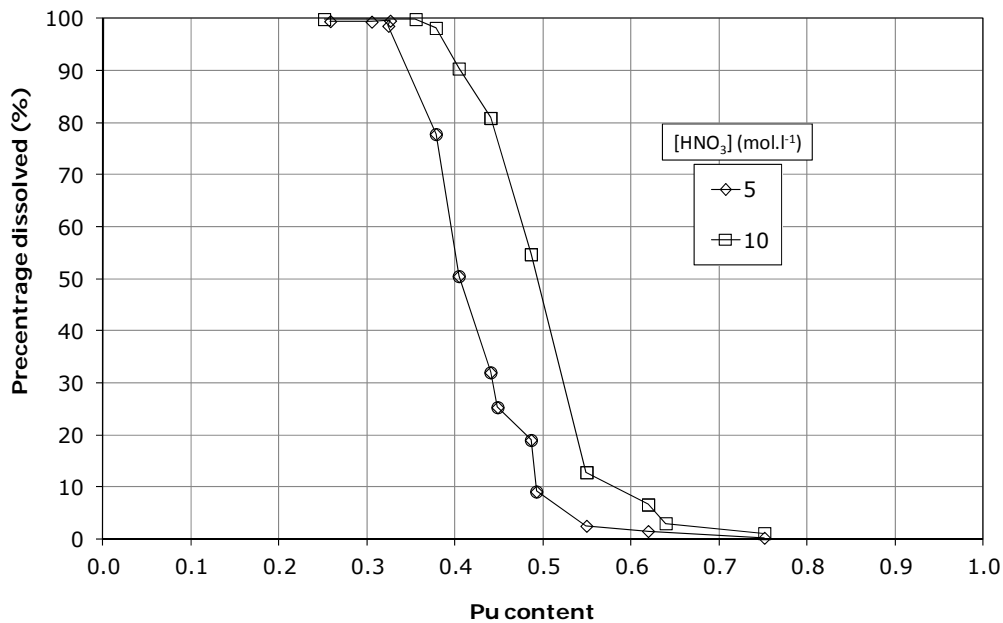


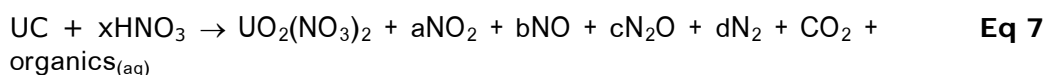
**Figure 11: Extent of MOx dissolution for various plutonium contents [53]**

### 3.2.3.1.2. Carbide

Enriched uranium monocarbide and mixed uranium plutonium monocarbide have been trialled as fast reactor fuels. Mixed uranium plutonium and minor actinide fuels are candidate fuels of the future [10, 71, 75, 77]. Carbide fuels have potential benefits over oxide fuels, for example, better neutron physics properties, which allow improved transmutation or breeding efficiency [71, 75]. Actinide carbides react more energetically with many oxidants compared with oxides, placing a requirement to work in anaerobic conditions for finely divided material [78, 79]. This has implications for fuel shearing.

The primary issue for the reprocessing of carbide fuels is the dissolution in nitric acid, where a fraction of the carbon remains in solution as organic acids [80-83] according to Eq 7. These organic acids are highly substituted with alcohol and carboxylic acid groups and include oxalic and mellitic acids [84]. These compounds decrease the extraction, backwashing and phase settling properties in solvent extraction processes and, therefore, the soluble organic content must be destroyed. Dissolution followed by destruction is indeed an option. The dissolution rate of actinide carbides increases with surface area, nitric acid concentration and temperature [83]. Recent studies have also demonstrated the role of nitrous acid in the dissolution mechanism [85, 86].

Although not demonstrated, it is reasonable to assume that an autocatalytic mechanism initiated by nitrate reduction occurs. Experiments studying the off-gases during dissolution have shown that dinitrogen oxide is present to a larger extent during carbide than oxide fuel dissolution [87]. This suggests that nitrogen monoxide reduction plays a more significant role and probably reflects the more electronegative nature of carbides.



The nitric acid consumption is much higher compared to oxides as the carbon is at least partially oxidised. Like oxides, the dissolution rate is dependent upon nitric acid concentration, with reaction product stoichiometry increasing from 4 to 10 as the initial nitric acid concentration is increased from 2 to 15.8 mol.l<sup>-1</sup> [88].

### 3.2.3.1.3. Nitride

Like actinide carbides, nitrides are under consideration due to their potential improvements in reactor performance [71, 75]. Nitrides are more reactive towards oxidation compared to oxide.

A key issue for the viability of nitrides is that natural nitrogen nitride fuels generate large quantities of carbon-14. This is illustrated in Table 4 [71]. For this reason nitrogen-15 is more likely to be used in the future, although the high cost of nitrogen-15 will mean that recovery for reuse may be necessary.

**Table 4: Comparison of <sup>14</sup>C production for 30 GWd.tHM<sup>-1</sup> fuel of various types [71]**

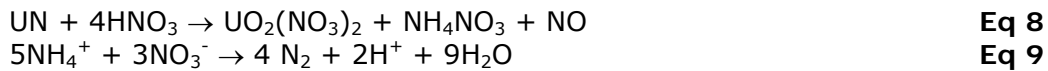
	MO <sub>2</sub>	MC	M <sup>14</sup> N	M <sup>15</sup> N
<sup>14</sup> C produced (GBq.tHM <sup>-1</sup> at ~30 GWd.tHM <sup>-1</sup> ) <sup>†</sup>	5.9	340	19000	190

Studies of the dissolution of uranium nitride in nitric acid show rapid dissolution rates under nitric acid concentrations of industrial interest [89, 90]. The dissolution results in oxidation to uranyl and ammonium ions,

---

<sup>†</sup> Dependent upon neutron specimen, MO<sub>2</sub> based on 20 ppm C and 20 ppm N (natural isotopic composition), MC based on 1000 ppm N (natural isotopic composition), M<sup>15</sup>N assumes 99 % <sup>15</sup>N

according to Eq 8. The ammonium can then be oxidised further, as in Eq 9. The dissolution results in larger amounts of dinitrogen oxide (N<sub>2</sub>O) and nitrogen (N<sub>2</sub>) gases compared to oxide fuel, due to the oxidation of ammonium. The fact that ammonium is produced and oxidized by nitric acid means that its reduction products lead to the isotopic dilution of nitrogen-15, thereby complicating and reducing the viability of nitrogen-15 recovery [91]. For this reason the direct dissolution of nitrogen-15 nitrides in nitric acid is unlikely to be the first chemical treatment step for their reprocessing.



#### 3.2.3.1.4. Alloys, composite materials and inert matrix fuels

Alloyed, composite and inert matrix (IMF) fuels have been grouped together as they differ considerably from the materials described so far. These materials contain a substantial quantity of other elements with low neutron absorption properties, i.e. they are 'inert'. These fuels include actinide-zirconium metal alloy fuel (SFR), silicon-actinide carbide composite ((U<sub>0.8</sub>Pu<sub>0.2</sub>)C-SiC, GCFR), 'Triso' type fuel (VHTR), plutonium-zirconium nitride ((Pu,Zr)<sup>15</sup>N, IMF), actinide oxide – molybdenum metal composite (e.g. (Pu<sub>0.8</sub>Am<sub>0.2</sub>)O<sub>2</sub>-Mo, IMF) and actinide oxide – magnesium oxide (PuO<sub>2</sub>-MgO, IMF). They are either used as the major reactor fuel in reactors or as targets for transmutation to reduce the actinide content.

These fuel types are more problematic to reprocess as they either do not dissolve in nitric acid or dissolve to produce a product that contains additional metals that need to be recovered or cause concerns to head-end or solvent extraction process chemistry. Some examples of these difficulties are described below:

- Actinide – zirconium metal alloy fuel does not readily dissolve in pure nitric acid [40, 41] and if dissolution is possible zirconium-rich residues are an explosive hazard [92].
- GCFR and VHTR fuels are composites that include silicon carbide or carbon and refractory coatings making fuel recovery difficult without intensive milling techniques prior to dissolution, e.g. [93].
- Plutonium zirconium nitride IMF requires nitrogen-15 recovery. A two step dissolution process has been proposed and is currently under testing. This involves hydrolysis to a hydrous oxide that allows recovery of the nitrogen-15 and then a second step to dissolve

plutonium-rich oxides using aggressive reagents capable of doing this [77].

- A similar approach for actinide oxide – magnesia or molybdenum metal composite materials has been proposed and is undergoing testing [77]. The first step is to dissolve the magnesia or molybdenum metal under cool dilute nitric acid. This is followed by the dissolution of the plutonium-rich oxides in a second more aggressive step. It is hoped that this will allow the dissolved magnesium to be diverted away from the high level wastes minimizing waste volumes. It is also hoped that the separate dissolution of molybdenum will allow the recovery of the isotopically enriched molybdenum for reuse [94]. This procedure also offers the potential to avoid the formation of solid molybdates, which are known to form when solutions are rich in actinides and molybdenum, e.g.[95]. These processes are shown schematically in Figure 12.

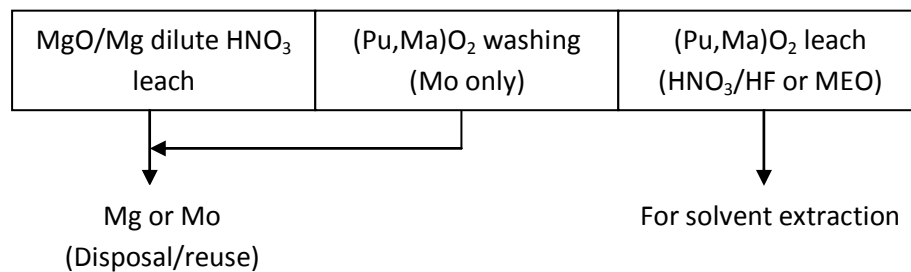


**Figure 12: Two step process to  $(\text{Pu}_{0.8}\text{An}_{0.2})\text{O}_2\text{-MgO}$  and  $\text{PuO}_2\text{-Mo}$  IMF**

### 3.2.3.2. Fuel conditioning - potential benefits of fuel pre-treatment

There a number of reasons why future head-end processes may deviate from the simple declad-leach and shear-leach process used today. These include:

- Mechanical processes that may be necessary to allow exposure of the fuel for dissolution.
- Chemical processes that may be necessary to prepare fuel before conditioning, e.g. metal coolant debonding.
- Improved control for volatile fission products, e.g. to allow tritium abatement.
- Simplification of dissolution process by pre-converting material, e.g. carbide to oxide.
- Recovery of fuel or cladding materials for reuse, e.g. nitrogen-15 or molybdenum.

### 3.2.3.2.1. Mechanical fuel preparation processes

It is probable that fuels that are similar in design, such as GCFR actinide carbide with silicon carbide cladding, could be dismantled and sheared as a fuel preparation step. However, reactor fuels that are radically different from a rod or pellet in cladding are likely to require alternative techniques to prepare the fuel. Depending upon the design of the fuel these processes could be very different from the current cladding stripping (Magnox metal fuel) and shearing (oxide fuel). Examples of fuels that are substantially different from conventional fuel types are [10]:

- GCFR actinide carbide – silicon carbide composition fuel
- VHTR fuel, which is a fuel microsphere surrounded by pyrolytic carbon and ceramic shells compacted into a rod or pebble

Concepts to treat these fuels, including crushing and milling to breach the refractory components and allow access to the fuel for dissolution, have been developed [93]. Attempts to recover fuel from VHTR Triso type fuels using the 'grind-leach' process have shown a degree of success, with recoveries of 99.6 % uranium. An example of this type of process is shown in Figure 13.

Currently, little work has been published about how to recover fuel from GCFR composite fuels. If the fuel is carbide pellets in silicon carbide cladding recovery could be readily achievable; however, if actinide-silicon carbide, alloy or composite are used recovery could be more of a challenge to an aqueous head-end.

The drive for process intensification to achieve higher throughputs in smaller plants or achieve improved fuel recoveries may also lead to consideration of replacing the shearing process with new innovative fuel preparation techniques [96].

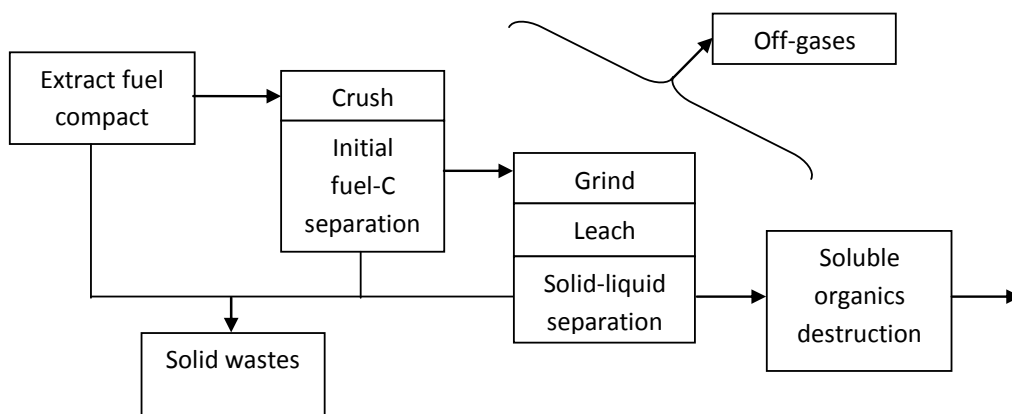


Figure 13: VHTR fuel 'grind-leach' process

### 3.2.3.2.2. Fuel pre-treatment using high and low temperature processes

#### Oxides

High temperature pre-treatments that oxidise uranium dioxide to higher oxides have been under development for decades but not deployed in large scale industrial reprocessing plants. These processes have been developed with different end purposes in mind;

- Volox – voloxidation, a method of removing volatile fission products from fuel to allow abatement and simplify the dissolution cycle [97].
- OREOX – oxidation reduction oxidation process is a development of the Volox process that uses alternate oxidation reduction processes to achieve higher efficiency of fission product removal [98].
- AIROX – atomics international reduction oxidation process is an OREOX process to allow pulverization of fuel in fuel rods with holes punched in them. This allows fuel and cladding separation before dissolution [99].
- DUPIC – direct use of PWR fuel in CANDU process is not strictly a head-end to reprocessing; it is a pyrochemical method for fuel reprocessing. The concept allows the removal of some fission products prior to refabrication into fuel [100].

These processes essentially use the same chemistry, the oxidation of uranium dioxide to higher oxides, Eq 10, with the accompanying decrease in density ( $\sim 11$  to  $8.4 \text{ g.cm}^{-3}$ ) thus allowing fuel pulverization. During this process, depending upon the process conditions, various amounts of tritium, carbon-14, iodine-129, krypton-85 and semi-volatiles, including caesium and ruthenium, are evolved. The fuel expansion process can also be used to break open cladding that has been punctured (AIROX process), thereby avoiding the need for a shear process, or the process could be carried out upon sheared fuel.



From experiments with unirradiated and irradiated materials, it is known that the presence of elements that cannot be oxidized in the solid state affects the process chemistry. Examples include the presence of plutonium [101], thorium [102], (MOx) or alkaline and rare-earth elements (SIMFUEL or irradiated fuels) [103] with uranium. These reduce the material reactivity as there is a smaller percentage of uranium to provide the driving force for pulverization and release of fission products. The presence of high contents of these dopant elements can stabilize intermediate phases, increase temperature or oxidant conditions to achieve oxidation and ultimately at high contents prevent oxidation [104, 105].

Experiments oxidizing SIMFUEL with varying portions of simulated fission products show that the presence of >7 % fission products (equivalent to ~70 GWd.tHM<sup>-1</sup>) greatly stabilizes the (U,Fp)<sub>4</sub>O<sub>9</sub> phase<sup>‡</sup> at 400 °C [106]. To achieve oxidation an increase in temperature to 800 °C is needed.

During the oxidation of mixed uranium plutonium oxide the material oxidizes to a plutonium-rich dioxide phase and a uranium-rich higher oxide phase, Eq 11 [101]. During this type of oxidation test the solubility of plutonium in the M<sub>3</sub>O<sub>8</sub> phase has been observed to be ~3 %Pu.HM<sup>-1</sup>, which means that oxidation of most MOx will result in the formation of plutonium-rich oxide particulates. This reduces the proportion of the plutonium dissolved in nitric acid [107]. However, at higher plutonium contents oxidation does not occur and experiments up to 900 °C have shown that unirradiated 20-25 %Pu.HM<sup>-1</sup> MOx does not result in pulverization. Similar segregation is also observed for the oxidation of mixed uranium thorium oxide and, as thorium oxide does not dissolve readily in nitric acid [102, 108], results in an increase in difficult to dissolve thorium oxide residues.



The oxidation of spent thermal and fast reactor fuels have been studied at the laboratory scale. These experiments have studied the effect of temperature, feed flow rate and oxygen concentration upon the extent of fission product removal e.g. [97]. This type of experiment has shown that near complete tritium removal is possible at moderate temperatures (480 °C) [109]. Less complete removal of the noble gases and iodine-129 has been achieved, Table 5.

**Table 5: Effect of voloxidation conditions upon noble gas and iodine-129 removal [97]**

T (°C)	[O <sub>2</sub> ] (%)	Gas Flow (cfh)	Volatilised (%)	
			<sup>85</sup> Kr- <sup>133</sup> Xe	<sup>131</sup> I
450	75	0.2	19	~ 8
750	75	1.0	69	~ 99
450	25	0.2	73	~85
750	75	1.0	42	~90
450	75	1.0	36	~33
750	75	0.2	76	~95
450	25	1.0	11	~38
750	25	0.2	~ 99	~92

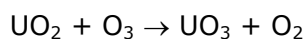
---

<sup>‡</sup> Fp and M are used as chemical symbols to represent fission products (largely alkaline and rare earth elements) and general metals respectively.

Oxidation of fuel at higher temperatures, e.g. greater than 700 °C increases the amount of the so-called semi-volatile elements that are released [97]. Examples of fission products that are evolved in significant quantities are caesium-137, ruthenium-106, antimony-125 and niobium-105. Experiments underpinning the DUPIC cycle development show that oxidation at higher temperatures quantitatively increases the release and number of semi-volatile elements [110]. These experiments also observe that control of the oxidation conditions can suppress the distillation of caesium and other elements by formation of less volatile oxides. Oxidation of spent fuel and distillation of fission product elements under high temperature conditions can be compared with studies of fuel distillation under severe reactor failure, such as Kundsén cell mass-spectrometry studies [111].

The oxidation of irradiated fast reactor 20 %Pu.HM<sup>-1</sup> MOx has also been demonstrated [97]. These experiments have shown that despite the difficulties in the oxidation of unirradiated 20 %Pu.HM<sup>-1</sup> MOx [101], the oxidation of irradiated MOx is achievable. Removal efficiencies of noble gases of up to 98 % at 750 °C has been demonstrated, which is excellent considering a portion of the noble gases are likely to be trapped in plutonium-rich oxides and not released. Comparing these results with irradiated uranium oxide experiments suggests good removal efficiencies of tritium, carbon-14 and iodine-129 will also be possible. This type of tests clearly shows oxidation of 20 % Pu.HM<sup>-1</sup> MOx is possible.

More recent advanced voloxidation studies have focused on the use of strong oxidants such as nitrogen dioxide and ozone [112]. These oxidants are capable of oxidizing uranium dioxide to trioxide, e.g. Eq 12, and show promise that near quantitative removal of tritium, carbon-14, noble gases and iodine-129 are possible at temperatures lower than air or oxygen.



**Eq 12**

### Carbides and nitrides

The conversion of carbides and nitrides to oxides could be an important step to allow:

- Carbides – removal of carbon that prevents the generation of organics during dissolution
- Nitrides – evolution of nitrogen-15 pre-dissolution for recovery.
- Carbides and nitrides - the removal of fission products for abatement.

These processes can be carried out with a variety of oxidants and temperatures. The conditions necessary tend to be more moderate compared

to oxide due to the reactivity of the materials. However, the reactivity also leads to concerns over pyrophorosity of the materials, which means careful control to prevent ignition is a key consideration.

The oxidation of uranium carbide and nitrides with oxygen or air leads to the formation of triuranium octoxide. The accompanying density change is even greater than that for uranium dioxide oxidation, so although these reactions have not been studied in as much detail as the oxidation of uranium dioxide, the uranium dioxide oxidation literature can be used as a starting point. This leads to two conclusions:

- Efficient removal of volatile fission products should be achievable.
- Segregation of uranium and plutonium phases will lead to incomplete plutonium recovery during dissolution in nitric acid. The extreme case for carbide is illustrated in Eq 13.



However, there is a significant density change in the conversion of carbides or nitrides to dioxides, 13.6 or 14.3 to 11.0 g.cm<sup>-3</sup> respectively. This density change is sufficient to cause pulverization of pellets. This could be used to as a pretreatment process to convert mixed uranium plutonium carbides or nitrides to oxides, with high plutonium solubility. This type of process has been demonstrated for unirradiated mixed uranium plutonium carbides using carbon dioxide [113] and steam [114]. These processes proceed with two steps, oxidation to the dioxide and carbon followed by reaction of carbon. Of the two reactants carbon dioxide is often preferred as water is prone to leave residual carbon and produces hydrogen as a product. However, the use of carbon dioxide or water as an oxidant for irradiated carbons would result in the abatement of very large quantities of carbon dioxide or water during the abatement of carbon-14 and tritium.

The conversion of mixed uranium plutonium nitride to solid state mixed dioxide may provide a method of removing nitrogen-15 without reducing the plutonium solubility.

### ***3.2.3.3. Developments in dissolution chemistry and technology***

Whether or not pre-treatment processes are used as a fuel preparation technology prior to dissolution it is likely that developments beyond the direct dissolution in nitric acid will need to be used. Examples of this include destruction of organics from direct dissolution of carbides and the dissolution

of plutonium oxide (from IMF) or plutonium-rich oxides (MO<sub>x</sub> or voloxidised fuel). The dissolution of thorium oxide or thorium containing fuels may also fall into this category. There is also likely to be interest in the multi-cycle leaching processes for composite fuels.

As the recovery of plutonium-rich oxide is likely to drive the development and use of enhanced dissolution technologies, the dissolution chemistry of pure plutonium oxide is a good starting place for any developments. It is widely reported there are three methods for the dissolution of plutonium dioxide:

- Use of strong complexants, the classic method is fluoride [115]
- Oxidative dissolution using cerium(IV) or silver(II) [116]
- Reductive dissolution using chromium(II) [116] or uranium(IV) [117]

Large disadvantages of the use of mineral acids, such as hydrofluoric acid, are dissolver and downstream corrosion issues and addition of salts leading to increased HLW volumes. This will favour the use of catalytic processes, the most widely developed is the catalyzed dissolution of plutonium using cerium or silver as a mediator [118]. These processes use electrochemical or ozonolysis to regenerate the oxidant (mediator) making the processes low in salt content, or, if the mediator is recovered, salt-free. These oxidative processes are also relevant to the destruction of organics from the direct dissolution of carbides. Reductive dissolution using uranium(IV) would also be an elegant solution to the dissolution of MO<sub>x</sub> as uranium is already present; however, there has been little work on this topic.

The oxidative dissolution of plutonium dioxide is known to be possible at above  $\sim 1.2 V_{\text{NHE}}$  [119] and with the use of cerium(IV) ( $E_0 \approx 1.4 V_{\text{NHE}}$ ) in hot nitric acid [116] or silver(II) ( $E_0 \approx 2.0 V_{\text{NHE}}$ ) at ambient temperatures [120] dissolutions are known to proceed rapidly. Silver is often preferred due to the high oxidation potential, rapid electron transfer rate [121] and surprising stability against water oxidation due to nitrate complexation [122]. This type of process has been termed catalysed electrochemical plутonium oxide dissolution (CEPOD) or more generally a mediated electrochemical oxidation (MEO) process. This process generates the mediator, for example silver(II) at an anode, Eq 14, and nitric acid is reduced at a cathode, Eq 15. The silver(II) dissolves the plutonium dioxide, Eq 16. The anode and cathode compartments are separated by a membrane that allows proton transfer and minimises mixing of the anolyte and catholyte, which would cause reduction of the silver(II) by nitric acid reduction products. A schematic diagram of an industrial dissolver is shown in Figure 14. This process is known to be very rapid and little silver(II) is observed until bulk plutonium dioxide dissolution is

achieved [123][Section 0]. For this reason, dissolution is highly dependent upon the generation rate of silver(II), which is dependent upon electrochemical mass transfer limits. Dissolution of plutonium dioxide with ozone with silver mediation is also limited by mass transfer of ozone [124].

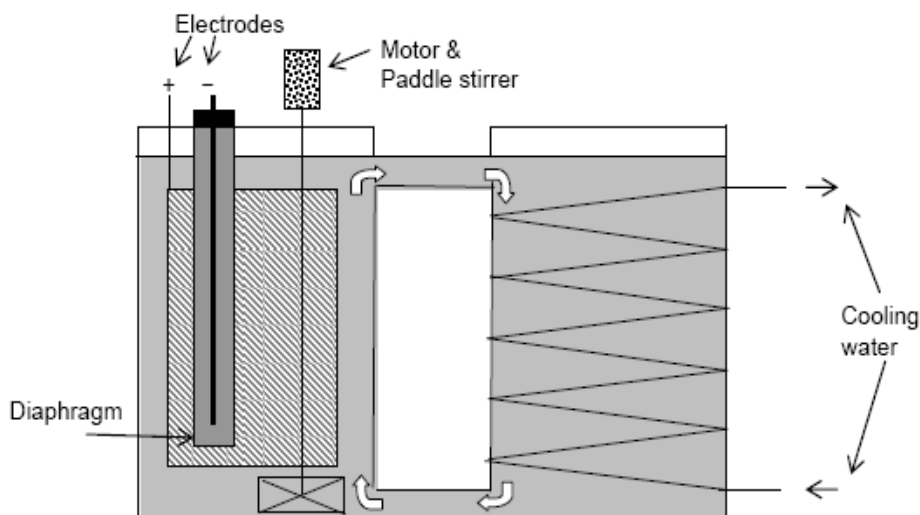
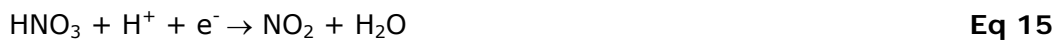


**Figure 14: Industrial plutonium dioxide dissolver [123]**

MEO type processing using cerium or silver can be used to dissolve plutonium-rich oxides in dissolved spent MOx [120] or for the dissolution and organics destruction of spent carbides [125]. The presence of a multitude of polyvalent metals leads to the oxidation of elements to high oxidation states. This can lead to side reactions or in extreme cases the catalytic consumption of the mediator [120]. An example of this is ruthenium, which is oxidized to the volatile tetroxide and is distilled [126]. As a result, due to the quantity and radiotoxicity of ruthenium-106, suitably efficient abatement precautions must be made.

The application of mediated dissolution processes are likely to be used after direct nitric acid dissolution due to the ease and speed of direct dissolution. Mediated dissolution would ideally be used in the same dissolver so as to minimize the potential for accumulation of solids, by avoiding the movement of plutonium-rich solids. However, this approach leads to batch dissolver cycles. Multi-leach dissolver cycles continue to be in vogue despite their inherent disadvantages, e.g. recent work with the select dissolution of inert

matrices from IMF fuels [77]. Another similar example is the dissolution of thorium oxide containing fuels using nitric acid with organic complexants, followed by the destruction of the organic complexants. Innovations to integrate and simplify the process chemistry and engineering will be advantageous for efficient head-end operations. An example may be the continuous dissolution of voloxidation product powder under cool conditions followed by continuous dissolution of plutonium-rich residues in a second dissolver or second part of the same dissolver. These developments will need to be mindful of the increasingly cautious nature of safety cases, for example over the management of the accumulation of plutonium-rich particulates.

#### *3.2.4. Summary and future developments*

Head-end is the first chemical treatment step in the reprocessing of spent nuclear fuel. Current practices use mechanical decladding and shearing followed by the direct dissolution of metal and oxide fuels in nitric acid. Changes to environmental discharge limits or the introduction of new fuel materials may require the introduction of additional process steps. Developments in fuel preparation, pre-treatment and dissolution technologies are expected. The significance of each part will depend upon evolution of reactor and fuel design for energy and actinide management (transmutation).

Radical changes in fuel design concepts from the rod or pellet in cladding could make exposure of fuel more difficult. Examples are adoption of Triso compacts or pebbles or actinide – silicon carbide composites, the refractory nature may require the use of intensive fuel preparation, such as grinding.

Fuel pre-treatment as a method overcoming difficulties of direct dissolution in nitric acid may become attractive if environmental discharge limits are tightened, particularly if tritium abatement is required or if advanced fuels, such as carbides or nitrides, are to be reprocessed. These pre-treatment processes could allow the abatement of tritium, which cannot be abated when it is isotopically mixed with the dissolver liquor. The evolution of carbon-14, noble gases and iodine-129 could also be achieved, giving other options for abatement and defining the dissolution and dissolver liquor conditioning required. Pre-treatment could also be a method to overcome the problem of dissolved organics from carbide fuels by conversion to an oxide and allow recovery of nitrogen-15 from nitride fuels for reuse.

The adaptation of new dissolution processing and technologies may also be required to receive pre-treated fuel, new fuel types, achieve high plutonium recoveries or condition dissolved carbide fuel to remove organics generated from dissolution. These new processes could involve multi-leaching approaches, for example to selectively dissolve inert matrices. The use of enhanced dissolution techniques using organic complexants or no or low salt mediated oxidative or reductive dissolution techniques could also be used to dissolve difficult materials or condition liquors.

Head-end chemistry, engineering and technology is expected to continue to be a demanding area of future reprocessing plants. As reactor fuel concepts develop and the required performance criteria for reprocessing plants become more clearly defined, the head-end processes will be driven to become more innovative. It is after all the role of head-end to provide standardised dissolver product suitable for downstream separations processes, regardless of the different reactors and fuel types from which it originates.

### ***3.3. Summary of key issues in the development of flowsheets for processing legacy, current and future advanced fuels***

A key part of developing any process is the specification of the process requirements are. The review sections above make it clear that a large amount of work has been carried out, including the development of many technologies that have not been used industrially, for example voloxidation for tritium abatement. At the centre of any development program must be:

- A process specification that details specific parameters or a range options for all aspects of the waste fuel management, reprocessing and fuel refabrication ('back-end'). As part of any future programme, the development of baseline process specifications for the advanced reprocessing plant is needed. From these specifications key technology gaps can be highlighted and incorporated into the development programmes. Any specifications that are drawn up will become out-dated as further detail and policy develops, and therefore a regular (*e.g.* biannual) review would be necessary. Without the clarity offered from a specification, key technological steps may be missed and technologies may be developed that are misaligned or inadequate.

Specific recommendations for future development of advanced actinide recycling processes include:

1. An analysis of national and international strategic aims for and constraints on the advanced nuclear fuel cycle globally,
2. The production of detailed specifications for the back-end of the nuclear fuel cycle. This will allow key technological gaps to be highlighted and incorporated into the development programmes.
3. Regular reviewing to ensure specifications remain relevant as further detail and policy develops.

## 4. DIRECT DISSOLUTION OF OXIDE IN NITRIC ACID

### 4.1. Summary of literature relevant to the direct dissolution of uranium, plutonium and mixed uranium plutonium oxides in nitric acid

#### 4.1.1. Background chemistry

##### 4.1.1.1. Nitric acid

Nitric acid is a strong acid with a dissociation constant,  $pK_a$ , of greater than 10. However, deviations from ideality, resulting from ionic and molecular interactions, lead to a decrease in the observed degree of deprotonation. This has led to the use of activities,  $\alpha$ , in place of concentrations,  $c$ , which are related by the activity coefficient,  $\gamma$  (Eq 18). Many studies have been undertaken to develop models to calculate activity coefficients. These have included the Gibbs-Duran equations, the Davis equation, SIT and Pitzer methods. As dissolution experiments are often carried out in concentrated solutions it will be necessary to consider the activity of species in solutions to gain the full insight into the dissolution reaction mechanism. The calculation method used will need to include the effects of any species that have been produced during the dissolution of the uranium oxide, such as uranyl ions and nitrous acid.



$$\alpha = \gamma c \quad \text{Eq 18}$$

$$K_a = \frac{\alpha_{\text{H}_3\text{O}^+} \alpha_{\text{NO}_3^-}}{\alpha_{\text{HNO}_3} \alpha_{\text{H}_2\text{O}}} \quad \text{Eq 19}$$

Another fundamental property of nitric acid chemistry is that it can be reduced to produce a range of other species (typically nitrogen oxides). These in turn can be reduced or oxidized leading to complicated aqueous redox chemistry. This work is largely concerned with those species on the left-hand side of Figure 15, although other species are known. In nitric acid appreciable concentrations of nitrous acid ( $\text{HNO}_2$ ) and lower concentrations of nitrogen oxides (particular  $\text{NO}$ ,  $\text{NO}_2$ ,  $\text{N}_2\text{O}_3$  and  $\text{N}_2\text{O}_4$ ) are known to be present. The concentration of nitrous acid and nitrogen oxides in solution are dependent upon the solution conditions, as nitrogen oxides have an appreciable vapour pressure [127] Eq 20-Eq 32. For example, the effect of sparging a solution or

use of a high surface area vessel causes higher losses of nitrogen oxides and reduces the concentration of  $\text{HNO}_2$  present in solution.

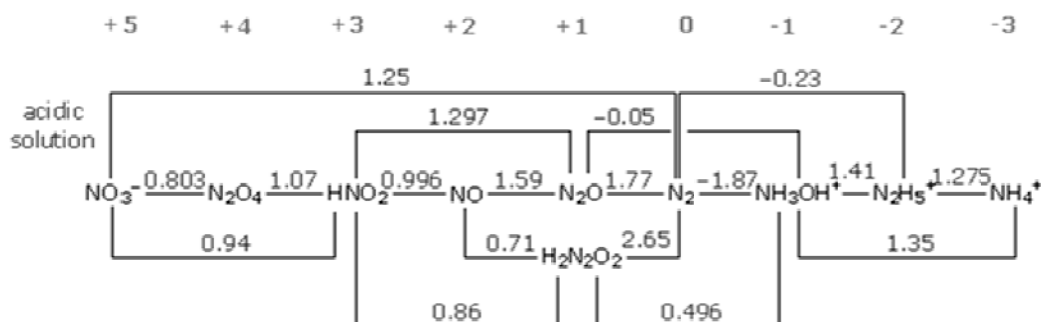


**Figure 15: Standard reduction potentials (V) for nitric acid and other nitrogen containing species[35]**

#### Solution phase equilibria



#### Solution-gas phase equilibria



A great deal of work has been carried out studying the corrosion of austenitic (Cr rich) stainless steels in nitric acid solutions; these studies focus on understanding the chemistry to allow conditions to be manipulated to reduce corrosion or allow development of improved materials. This is relevant as there are similarities in the chemistry of corrosion and dissolution. The species with the largest concentrations in nitric acid are nitrate and  $\text{HNO}_2$ , so their relative concentrations largely define the solution electropotential [20, 128, 129], Eq 33 and Eq 34. At low nitrous acid concentrations, the nitric acid solution is a long way from equilibrium, this leads to an elevated thermodynamic state (electropotential); which can increase the corrosion rate

of austenitic steels. Although nitrate and HNO<sub>2</sub> can act directly as oxidizing agents, the corrosion kinetics have been observed to greatly increase with the addition of other redox active species [130-132]. For example, addition of small equilibrium concentrations of dichromate (Eq 35) can react quickly with the steel and because nitric acid can reoxidise the chromium(III) to dichromate this leads to a catalytic acceleration in corrosion rate [131].



$$E = E_0 + \frac{RT}{2F} \left( \frac{\alpha_{\text{HNO}_3}}{\alpha_{\text{HNO}_2}} \right) \quad \text{Eq 34}$$



Nitric acid reduction chemistry has been widely studied on platinum using electrochemical methods. It is reported that nitric acid reduction proceeds via two mechanisms, direct and indirect reduction [22]:

- Direct reduction proceeds in all concentrations of nitric acid with a 0.5 V over-potential above the standard potential of 0.95 V (0.75 V vs. Ag/AgCl) and is selective for ammonia. At higher nitrate concentrations small amounts of nitrogen and nitrogen oxides (NO<sub>x</sub>) can be observed.
- Indirect reduction has been studied at 100 °C in the presence of nitrous acid. Under these conditions only a small over-potential is required and reduction is selective towards nitrous acid, nitrogen monoxide and nitrogen dioxide.

The reactions are summarised Table 6 [22].

**Table 6: Nitric acid reduction mechanisms[22]**

<u>Direct reduction</u>	<u>Indirect reduction</u>
$\text{NO}_3^- \rightleftharpoons \text{NO}_3^-_{(\text{ads})}$	$2\text{HNO}_{3(\text{g})} \rightleftharpoons 2\text{NO}_{(\text{g})} + 1.5\text{O}_{2(\text{g})} + \text{N}_2\text{O}_{(\text{g})}$
$\text{NO}_3^-_{(\text{ads})} + 2\text{H}^+ + 2\text{e}^- \rightleftharpoons \text{NO}_2^-_{(\text{ads})} + \text{H}_2\text{O}$ (rds <sup>d</sup> )	$2\text{HNO}_{3(\text{g})} \rightleftharpoons \text{N}_2\text{O}_{4(\text{g})} + 0.5\text{O}_{2(\text{g})} + \text{H}_2\text{O}_{(\text{g})}$
$\text{NO}_2^-_{(\text{ads})} + 2\text{H}^+ + \text{e}^- \rightleftharpoons \text{NO}_{(\text{ads})} + \text{H}_2\text{O}$ (fast)	$\text{N}_2\text{O}_4 \rightleftharpoons 2\text{NO}_2$
$\text{NO}_{\text{ads}} + 4\text{H}^+ + 3\text{e}^- \rightleftharpoons \text{NH}_3\text{OH}^+$ (fast)	$\text{N}_2\text{O}_4 + \text{H}_2\text{O} \rightleftharpoons \text{NO}_3^- + \text{H}^+ + \text{HNO}_2$
$\text{NO}_{\text{ads}} + 6\text{H}^+ + 5\text{e}^- \rightleftharpoons \text{NH}_4^+ + \text{H}_2\text{O}$ (fast)	$\text{NO}_2 + \text{NO} + \text{H}_2\text{O} \rightleftharpoons 2\text{HNO}_2$
	$\text{N}_2\text{O}_3 \rightleftharpoons \text{NO}_2 + \text{NO}$
	$2\text{HNO}_2 \rightleftharpoons \text{N}_2\text{O}_3 + \text{H}_2\text{O}$

The direct nitrate reduction (or thermal decomposition) reaction produces products that are electro-active species and these are involved in the indirect

<sup>d</sup> rds – rate determining step

mechanism. The direct reduction mechanism initiates the indirect mechanism, Figure 16. As the reduction products of the indirect mechanism are rapidly oxidised to produce further indirect electro-active species the indirect mechanism can be described as autocatalytic.

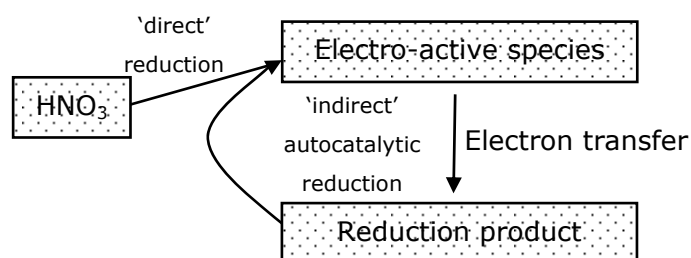


**Figure 16: Systematic diagram of nitrate reduction**

There are two proposed indirect reduction mechanisms, the debate is over which species is responsible for the electron transfer (the electro-active species)[22].

- Vetter’s mechanism requires that two molecules of nitrogen dioxide are generated for every one molecule of nitrous acid that is reduced. Nitrogen dioxide is the electro-active species.
- Schmid’s mechanism requires that for every two nitrogen monoxide molecules generated, three new nitrous acid molecules are produced. Electro-active species is  $\text{NO}^+$ .

The rival reaction mechanisms are shown in below:

**Table 7: Proposed indirect reaction mechanism[22]**

	Vetter	Schmid
Electron transfer	$\text{NO}_2 + \text{e}^- \rightarrow \text{NO}_2^-$	$\text{NO}^+ + \text{e}^- \rightarrow \text{NO}$
Intermediate step	$\text{NO}_2^- + \text{H}^+ \rightarrow \text{HNO}_2$	$\text{HNO}_2 + \text{H}^+ \rightleftharpoons \text{NO}^+ + \text{H}_2\text{O}$
Regeneration of electro-active species	$\text{HNO}_2 + \text{HNO}_3 \rightarrow \text{N}_2\text{O}_4 + \text{H}_2\text{O}$ $\text{N}_2\text{O}_4 \rightleftharpoons 2\text{NO}_2$	$\text{HNO}_3 + \text{HNO}_2 \rightarrow \text{N}_2\text{O}_4 + \text{H}_2\text{O}$ $\text{N}_2\text{O}_4 + 2\text{NO} + 2\text{H}_2\text{O} \rightleftharpoons 4\text{HNO}_2$

De Groot uses differential electrochemical mass spectrometry (DEMS) and rotating disc electrode (RDE) experiments to support Schmid’s mechanism [22]. DEMS allows the measurement of gaseous species generated during a voltammetry sweep. The head space is under vacuum and gaseous reaction products are rapidly stripped from the solution for mass spectrometer measurements. As the voltammetry is carried out the amount and mass of gaseous species generated is determined. DEMS shows that nitrogen monoxide is the dominant reaction product. Experiments with sodium nitrate and nitrite and mixtures in sulphuric acid and/or perchloric acid have shown

that both nitrate and nitrous acid are needed for the rapid indirect reduction to occur. It is argued that the dominant gaseous product is nitrogen monoxide because of the high platinum surface coverage. DEMS experiments, where an argon sparge was stopped and the cyclic voltammograms compared with DEMS experiments, clearly show the reaction occurs more rapidly in unstirred solutions, supporting the autocatalytic nature of the reaction.

Experiments using both electrochemical and infrared (Fourier Transformed InfraRed, FTIR) surface studies provide a powerful combination to study this reaction, as FTIR allows observation of the surface *in situ* during electrochemical experiments. The problem with observation of surfaces is that the concentration of adsorbed species is low, so Surface-Enhanced InfraRed Absorption spectroscopy (SEIRA) is used. SEIRA has been used to study the reduction of nitrogen monoxide [24], adsorption of nitrate [23] and the formation and reduction of nitrite [25] on platinum in perchloric acid. The experiments used a platinum film both as the SEIRA substrate and the working electrode. The results from the experiments are briefly described below:

- Experiments observing the reduction of nitrogen monoxide (on platinum) show that several nitrogen monoxide species (on-top and bridged) are present [24]. The relative amounts vary with applied potential. The reduction of on-top nitrogen monoxide is more rapid than bridged nitrogen monoxide and the rates of reduction both increase with more negative applied potentials (0 to -0.2 V vs. Ag/AgCl electrode).
- Experiments observing the bidentate chelating of nitrate to platinum [23] show desorption of nitrate on a timescale similar to nitrogen monoxide reduction (1-4 s).
- Experiments observed nitrite adsorption by the symmetric nitrogen dioxide stretch of the nitro form [25]. In 0.1 mol.l<sup>-1</sup> perchloric acid at -0.2 to ca. 0.6 V (vs. Ag/AgCl) nitrogen monoxide (on-top, bridged and at defect sites) are the dominant species adsorbed to the platinum, nitrogen monoxide is formed by the disproportionation of nitrous acid. Whereas at ca. 0.6 to 1.0 V (vs. Ag/AgCl) nitrite is the dominant adsorbed species. The reduction of nitrite is suggested to occur as shown in Figure 17.

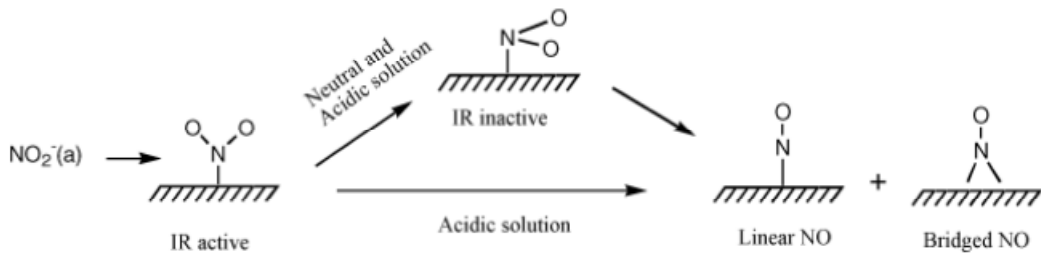


**Figure 17: Reduction of nitrite on platinum electrode, as observed by SEIRA[25]**

#### 4.1.1.2. Chemistry of uranium oxide

The uranium-oxygen phase diagram is complex, with many non-stoichiometric oxides, Figure 18 [133]. Many of these oxides also have a number of hydrates. The discussion of data in this thesis will be limited to the three main oxides, although more detailed consideration should ultimately be undertaken as irradiation forms  $(\text{U},\text{Fp})\text{O}_{2+x}^e$ , and voloxidation can produce a variety of products depending upon the process conditions. The three predominant forms to be considered in this thesis are:

- $\text{UO}_2$  – Used in nuclear reactors
- $\text{U}_3\text{O}_8$  – Produced from oxidation of the dioxide, for example, during voloxidation treatment processes
- $\text{UO}_3$  – Product material of some uranium finishing plants, for example, by thermal denitration

As most industrial interest is with the dissolution of dioxides, most work will focus on the dioxide.

---

<sup>e</sup> Fp = fission or activation product metal.

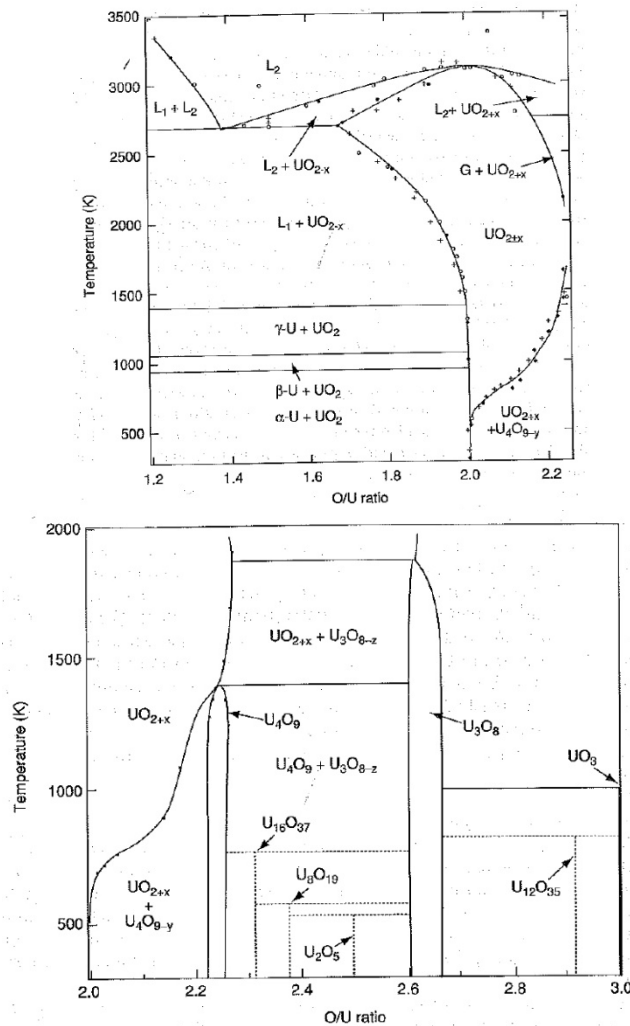


**Figure 18: Phase diagram of U-O system, left O/U ratio 1.2 to 2.2 and right O/U ratio 2.0 – 3.0 [133]**

Uranium oxide surfaces can have a number of different stoichiometries depending upon the atmosphere above the material and other conditions (such as temperature). When the oxide is added to water the surfaces are more likely to be hydrated and, depending on whether the solution is acid or alkaline, the solution will exchange  $H^+$  or  $OH^-$  and so the surface will become charged. A measure of this is the point of zero charge (pzc), which has been determined for  $UO_2$  and  $UO_3$  to be at a pH 5-5.5[134] and 7.3[135] respectively. Above or below this the surface will become charged and allow ion-exchange, Eq 36 and Eq 37. For example, at low pH,  $H^+$  exchange (Eq 37) increases the anion exchange capacity (e.g. fluoride). This has led to (hydr)oxides being described as amphoteric. As nitric acid dissolution is commonly carried out in  $>1 \text{ mol.l}^{-1}$  nitric acid (pH  $<0$ ), this should mean that all surface sites will be protonated, for example as  $UO_2-OH_2^+$ . However, the tests to determine pzc [134, 135] do not show whether there are different surface areas that are not protonated, for example, it may be that oxide sites

are not protonated. The rate of conversion of oxide sites to hydroxide sites is a topic for further investigation.



Ligand or metal exchange with surface (hydr)oxide has been implicated in many redox reactions where ligand-metal electron transfer processes occur. According to Stumm [136] the strength of solution and surface complexation can be linearly correlated, so the spectrochemical series, Eq 38, can be used as a guide to the order of ligand complex strengths. The ability of ligands to form surface complexes is one of the key steps to surface chemistry, including dissolution.



#### **4.1.1.3. Chemistry of plutonium oxide**

The plutonium oxide phase diagram is less complex than that of uranium oxide, exhibiting compounds from  $\text{Pu}_2\text{O}_3$  through  $\text{PuO}_{2-x}$  and  $\text{PuO}_2$  to the controversial hyper-stoichiometric  $\text{PuO}_{2+x}$  [133]. The discussion in this thesis will be limited to plutonium dioxide ( $\text{PuO}_2$ ), which is the only industrially relevant plutonium oxide. The industrial preparation of plutonium dioxide is dominated by the oxalate precipitation [137], calcination and sintering processes. The sintering conditions, notably increasing temperature, cause a decrease in surface area [138]. The finely divided nature of  $\text{PuO}_2$  means absorption of water and other gases is common.

#### **4.1.1.4. Chemistry of mixed uranium plutonium oxides**

Mixed uranium plutonium dioxide (MOx) is an important reactor fuel as it allows reuse of separated plutonium generated from the reprocessing of GenI (*e.g.* UK Magnox) and GenII (*e.g.* LWR) fuels in a closed nuclear fuel cycle. MOx is ideally a solid state solution of uranium – plutonium dioxides, to allow good reactor performance as well as complete dissolution in recycling. There are two distinct MOx manufacturing routes: dry and wet techniques. Dry routes start with uranium and plutonium oxides and use milling and sintering conditions to cause intimate mixing. Wet processes start with uranium and

plutonium liquors and aim to cause homogeneous mixtures by co-precipitation. Both routes can produce solid state solutions to a degree, but wet techniques offer the potential to produce mixing at atomic length scales. Dry processes are prone to producing some degree of inhomogeneity, resulting in grains of varying uranium and plutonium concentrations. Both types of processes have been used industrially for fabrication of thermal (typically 2-8 wt% plutonium) and fast (typically 15 – 35 wt% plutonium) fuels. However, the dry routes are historically and currently most prevalent. Work on wet co-precipitation processes continues, as they have potential benefits and are particularly relevant to future minor actinide bearing fuels.

Until recently there have been two operational thermal MOx fabrication processes, the French MIMAS process and the British SBR processes (closure announced August 2011 [139]). Both processes mix UO<sub>2</sub> and PuO<sub>2</sub> powders to produce thermal MOx pellets. The SBR process used a single high intensity milling step, whereas the MIMAS process uses a two step milling approach, first producing 30 wt% Pu granules and then a second milling step dilutes the MOx to the desired Pu content [140].

Pu content distributions in unirradiated MOx pellets have been determined by x-ray diffraction (XRD) [53], autoradiography [141] and scanning electron microscopy coupled to energy dispersive X-ray analysis (SEM-EDX) mapping techniques [43, 142]. Similar techniques can also be used for irradiated pellets.

#### ***4.1.2. Dissolution chemistry***

##### ***4.1.2.1. Dissolution chemistry of metals***

The dissolution of copper and other metals in nitric acid has been studied widely using batch and flow dissolution experiments as well as electrochemical techniques. El-Cheikh carried out batch dissolution studies determining the free acidity, copper and HNO<sub>2</sub> concentrations over time [26]. A slow induction period followed by a more rapid dissolution was observed, see Table 8. A linear (first order) dependence between log dissolution rate and nitrous acid concentration was observed, indicating one molecule of nitrous acid is involved in the rate determining step. Redox potentials over time show a rapid increase in oxidation potential followed by a slower increase, the slopes are greater for higher nitric acid concentrations. The redox potential

measurements had a value around the Cu|Cu<sup>2+</sup> couple value. The two parts to the redox measurements were explained by the two dissolution processes, HNO<sub>3</sub>|HNO<sub>2</sub> and HNO<sub>2</sub>|NO. Galvanostatic polarisation experiments showed cathodic polarisation potentials were higher than anodic, which suggests cathodic reactions limit the dissolution process, *i.e.* reductive reaction. Experiments varying the nitric acid concentration (0.1 to 0.7 mol.l<sup>-1</sup>) showed variation with log<sub>10</sub> current at t=0 suggesting the slow induction period is a first order process with respect to nitric acid concentration. The explicit kinetics were then derived based on the reactions shown in Table 8.

**Table 8: Copper dissolution mechanism[26]**

<u>Slow initial reaction</u>	<u>More rapid, catalytic reaction</u>
HNO <sub>3</sub> + Cu ⇌ HNO <sub>3</sub> :Cu	HNO <sub>2</sub> + Cu + H <sup>+</sup> → Cu <sup>+</sup> + NO + H <sub>2</sub> O    slow
HNO <sub>3</sub> :Cu + 2H <sup>+</sup> → Cu <sup>2+</sup> + HNO <sub>2</sub> + H <sub>2</sub> O    slow	HNO <sub>2</sub> + Cu <sup>+</sup> → Cu <sup>2+</sup> + NO + H <sub>2</sub> O    fast
	2NO + HNO <sub>3</sub> + H <sub>2</sub> O ⇌ 3 HNO <sub>2</sub> fast

Open circuit potential (redox) linear sweep voltammetry and electrochemical impedance spectroscopy (EIS) experiments have been used to examine the dissolution mechanism proposed by El-Cheikh at pH 2 in 0.1 to 2.0 mol.l<sup>-1</sup> nitrate [27]. These experiments support El-Cheikh's nitrous acid mechanism. Tafel<sup>f</sup> slopes of 37 mV/decade were found, indicating a single electrode transfer is involved in the rate determining step. The data were interpreted as the rate determining step was the second electron transfer, Cu<sup>+</sup>|Cu<sup>2+</sup>. Charge transfer resistance was observed to increase, suggesting a diffusion controlled reaction due to passive oxide film formation; at higher potentials no oxide film formation was observed.

The dissolution of zinc in nitric acid has been studied using batch dissolution experiments [28] using a similar approach to El-Cheikh's copper experiments. These studies also found dissolution to proceed via two reaction pathways, nitrate and HNO<sub>2</sub>.

The dissolution of cobalt in nitric acid has been studied using a thermometric (temperature increase over time) technique [29]. The maximum rise in temperature was observed to occur at 6 mol.l<sup>-1</sup> nitric acid, this was interpreted that at lower nitric acid concentrations dissolution occurs

---

<sup>f</sup> Tafel's law relates current density to the electrochemical potential (or overpotential).

according to an autocatalytic mechanism. It was also stated that concentrations greater than 6 mol.l<sup>-1</sup> nitric acid allows the accumulation of nitrous acid. This acts as a cathodic depolariser raising the anodic current density at the cobalt surface and causing growth of an oxide film, limiting the rate of dissolution.

Experiments have been carried out using a millifluidic device by Delwandle and Magnaldo [143, 144]. These experiments observed the dissolution of a copper metal sphere optically using a confocal microscope. The observation that bubbles formed on the copper surface during dissolution offered a plausible explanation of how the autocatalytic dissolution mechanism is maintained. The use of fluorophores, chemicals that have characteristic optical emissions depending upon the chemical conditions, was described. Mathematical image analysis allows comparison and profiling of images. Two fluorophores were described, one sensitive to pH changes and the second not. In 3 mol.l<sup>-1</sup> nitric acid these showed a factor of 2-3 depletion in acidity in the diffusion layer and the area behind the bubbles. CuO and Cu<sub>2</sub>O surface oxides were also identified from partially dissolved spheres, it was highlighted that these oxide layers should not exist at pH <3. Plans for further experiments to determine the chemical nature of species involved using new sensors were described.

#### **4.1.2.2. Chemistry of oxide dissolution**

Oxide surfaces can adsorb and ion-exchange metals and ligands on (hydr)oxide surfaces. Generally, the formation of a surface complex can make the metal ion entering the solution favourable. Stumm described these steps as fast surface adsorption, Eq 39, and a slow reaction followed by metal detachment, Eq 40. The first reaction step is essentially an equilibrium process. Although the structure of the surface sites and species has not been determined the reaction rate of Eq 40 is defined by the concentration (mol.kg<sup>-1</sup>) of the surface species.

Surface sites + reactants (H<sup>+</sup>, <sup>-</sup>OH, or ligands) ←fast→ surface species **Eq 39**

Surface species —slow, detachment of metal ion→ metal<sub>(aq)</sub> + surface sites **Eq 40**

This simplified reaction scheme can be used to describe the two general types of dissolution processes, reduction-oxidation process and ligand-promoted process. Both of these processes initially start with the formation of a surface

complex. For the redox process the next step is that the metal centre is reduced or oxidized, which leads to a weakening of the metal – bulk phase bonds. For the ligand-promoted process, the strength of the metal-ligand (M-L) bond leads to a weakening of the metal – bulk phase bonds. Ultimately this leads to the detachment of the metal into solution. In both cases the metal may be drawn into solution in an M-L complex, however, once there, the M-L complex is subject to the solution phase M-L equilibrium. For the redox process, after the electron transfer process has taken place, ligand exchange may then occur before the metal ion detaches.

Stumm's simplified reaction mechanism allows consideration of the factors that affect reaction rate. The two key factors that affect the rate for a specific sample (for a given number of surface sites) are:

- The concentration of surface species, which is dependent upon reactant concentrations.
- Acceleration of the rate-limiting step, that is the detachment of metal ions. A factor that may affect the rate of detachment is the thermodynamic stability of the solution complex, for example. Dissolution will then be slow when the solubility limit is reached.

#### ***4.1.2.3. Uranium oxide dissolution in nitric acid***

A great deal of work has been carried out studying the dissolution of unirradiated and irradiated  $\text{UO}_2$  in nitric acid [34, 45, 46, 145-147] because of the industrial importance of the process. Fewer studies have been carried out on other uranium oxides such as  $\text{U}_3\text{O}_8$  [148-150] and  $\text{UO}_3$  [48]. The dissolution behaviour of uranium dioxide is generally much slower than triuranium octoxide and uranium trioxide.

Many different uranium dioxide dissolution mechanisms have been proposed over the years, however, a key piece of evidence was provided in an oxygen-17 labelling study [151]. This showed that during dissolution of  $\text{U}^{17}\text{O}_2$  the labelled oxygen remained with the uranyl ion ( $\text{U}^{17}\text{O}_2^{2+}$ ), thereby confirming that dissolution proceeds by the oxidation of the surface sites and the detachment of the uranyl ion from the surface.

The majority of other studies considered the effect of nitric acid, nitrate, temperature [34, 45-47, 152-154], nitrous acid [34, 48, 49], nitrogen oxide off-gases [20, 87, 155] and material properties [145, 154]. Many of these

factors are interlinked. The dependence of each of these variables will be discussed in turn.

Many studies have investigated the effect of nitric acid and nitrate and all have found that the dissolution rate is proportional to the nitrate concentration raised to the power of 2 to 3 [34, 45, 46, 48, 49, 153, 154]. The actual order varies from study to study and with temperature. Several workers have also shown that the nitrate reaction order can fall to first order at high dissolution rates; this was attributed to diffusion control. There is also a great deal of evidence that the reaction is catalysed by nitrous acid. This evidence includes:

- A yellow 'corona' has been observed around pellets and when solutions are stirred the dissolution rate reduces. This can be explained by a locally high concentration of a catalyst that is being dispersed when stirred.
- During the dissolution of pellets in static solution a higher degree of pitting has been observed on the upper part of pellets, which is consistent with the tendency of over-saturated NO<sub>x</sub> to rise. This in turn increases the concentration of nitrous acid.
- When the solution is sparged or boiled the dissolution rate reduces due to decomposition of the catalyst. These tests have also shown a reduction in the concentration of nitrous acid (and dissolved NO<sub>x</sub>) due to an increase in the rate of decomposition of nitrous acid and increased rate of NO<sub>x</sub> removal from solution.
- In less aggressive conditions induction periods are observed. These induction periods are a classic sign of autocatalytic mechanisms.
- A first order dependence on uranium dioxide dissolution rate has been shown for nitrous acid [49] and different activation energies from nitrous acid and nitrate oxidation have been determined.

Many workers have concluded that the dissolution of uranium dioxide is autocatalytic and that the most probable catalyst is nitrous acid. However, Fukasawa [30] disputes this as, whilst studying uranium dioxide dissolution under a silicon oil film, it was observed that, as the uranyl concentration increased, the uranyl and nitrous acid concentrations remained the same throughout pellet dissolutions. This indicates that nitrous acid is produced but does not decompose or react with uranium dioxide. However, these results do not appear to have been taken into account or explained by later workers and Ikeda and others [49, 156] have carried out experiments supporting the involvement of nitrous acid in the uranium dioxide dissolution mechanism.

Initially, it was thought that the nitrogen monoxide and nitrogen dioxide evolved from solution could be used as evidence of the relative reaction rates of nitrate and nitrous acid reduction [49]. However, studies reacting nitrogen monoxide or nitrogen dioxide with nitric acid showed that the NO:NO<sub>2</sub> ratio that is evolved from nitric acid is largely an equilibrium ratio determined by solution factors, such as nitric acid concentration and temperature. These studies also showed that bubbling nitrogen dioxide through is less likely to produce equilibrium NO:NO<sub>2</sub> due to the slower reaction rates of nitrogen dioxide compared to nitrogen monoxide. These results generally showed an increase in nitrogen dioxide produced with increasing nitric acid concentration, Eq 41 and Table 9. Another interesting observation is that the presence of uranyl nitrate decreases the rate of evolution of nitrogen dioxide from a solution, which suggests that nitrogen dioxide is bound to the uranyl ion. However, no information about UO<sub>2</sub><sup>2+</sup>-NO<sub>2</sub> complexation can be found.

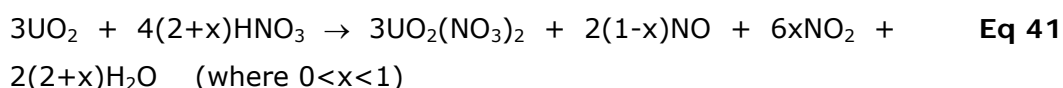


**Table 9: Variation of x, Eq 41, with nitric acid concentration**

[HNO <sub>3</sub> ] (mol.l <sup>-1</sup> )	3.4	4.5	6.7	8.1	12.5
x	0.05	0.06	0.10	0.30	0.70

The influence of temperature has been commonly studied as well, although its influence is complex, due to a number of competing effects. Whilst the dissolution rate increases with temperature, at high dissolution rates the activation energy decreases due to diffusion control. Also, at near boiling and boiling conditions the rate is observed to drop, and this is now understood to be due to a decrease in the HNO<sub>2</sub> concentration. The most recent dissolution studies have published separate rate constants for nitrate and nitrous acid dissolution. Several of the rate laws have been published, for example Eq 42 and Eq 43. The dissolution rate dependence of nitrate has been reported generally to be between second and third order ( $x = 2$  to  $3$ ) with activation energies ( $E_{a1}$ ) up to 67 kJ.mol<sup>-1</sup>. When the nitrate and nitrous acid reactions were studied together, Eq 43, the nitrate activation was observed to be higher at *ca.* 80 kJ.mol<sup>-1</sup> and nitrous acid reaction *ca.* 37 kJ.mol<sup>-1</sup> [34, 45, 48]. The more rapid dissolution of UO<sub>2</sub> by HNO<sub>2</sub> is reflected in the smaller activation energy for nitrous acid ( $A_2[\text{HNO}_2]$ ) compared to the nitrate reaction ( $A_1$ ).

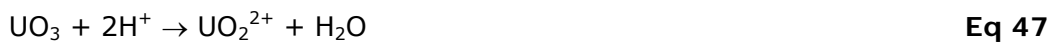
$$\frac{dU}{dt} \propto [NO_3^-]^x e^{\frac{-E_{a1}}{RT}} \quad \text{Eq 42 [34, 45]}$$

$$\frac{dU}{dt} \propto [NO_3^-]^{2.3} \left( A_1 e^{\frac{-79500}{RT}} + A_2 [HNO_2] e^{\frac{-36800}{RT}} \right) \quad \text{Eq 43 [48, 49]}$$

Another important aspect of uranium dioxide dissolution is the material properties. It is known that dissolution is dependent upon the concentration of active surface sites, which to the first approximation is dictated by the specific surface area. So it can be expected that powders will dissolve much faster than pellets. Indeed, the linear core shrinkage model [157] has been successfully applied to powders [48]. The dissolution of uranium dioxide pellets produces an S-shape curve as the surface area initially increases, until *ca.* 20 % dissolution, then the surface area decreases until pellet dissolution is complete [20, 30, 31].

Two other interesting and related material factors are porosity and density (%Theoretical Density (%TD)). High density materials have a low porosity and so dissolution is limited to the surface area. Whereas in lower density, higher porosity materials the solvent can penetrate the material and more rapid dissolution can occur. There are many other materials factors that also influence the dissolution rate such as grain size, manufacturing route, sintering time and temperature.

The dissolution behaviour of three uranium oxides powders, uranium dioxide, triuranium octoxide and uranium trioxide have been reported in nitric acid. The dissolution behaviour of uranium dioxide and triuranium octoxide is affected by similar variables, indicating similar mechanisms, whereas uranium trioxide has been reported to be simply related to the acid concentration [48], Eq 46. The similarities and differences are reasonable considering the reactions, Eq 44 to Eq 46.



#### **4.1.2.4. Plutonium oxide dissolution in nitric acid**

Plutonium dioxide is insoluble in nitric acid when sintered at temperatures greater than  $\sim 450^{\circ}\text{C}$  [138, 158]. Sintering to higher temperatures reduces the powder porosity and increases crystallinity [138]. Even plutonium dioxide sintered at lower temperatures dissolves slowly in concentrated nitric acid, particularly when compared to  $\text{UO}_2$ . The difference in dissolution rate is due to the unfavourable thermodynamics of dissolution in nitric acid. The  $\text{PuO}_2$  dissolution kinetics depends on the 4<sup>th</sup> power of the nitrate concentrations,  $[\text{NO}_3^-]^4$ , compared to  $[\text{NO}_3^-]^{2.7}$  for uranium dioxide. As a result,  $\text{PuO}_2$  is considered insoluble in  $<4 \text{ mol.l}^{-1}$  nitric acid [159]. The use of strong complexants, such as fluoride, has proved useful to accelerate the rate of dissolution [74, 159]. Similar to neptunium dioxide oxidative dissolution may be employed to accelerate the rate of dissolution, with silver(II) or cerium(IV) being commonly employed [160]. Unlike neptunium dioxide, the rate of plutonium dioxide dissolution can be enhanced using reductive dissolution due to the higher stability of plutonium(III) [161]. However, this process is less effective than oxidative dissolution as it requires cleavage of the Pu bonds, which is mechanistically more complicated than the single electron transfer required for oxidative dissolution [52].

#### **4.1.2.5. Mixed uranium plutonium dioxide dissolution in nitric acid**

MOx has been used as fuel in both fast and thermal reactors. Commercial thermal MOx usage is expected to increase over the next decades particularly with the introduction of the GenIII reactors. A large advantage of mixed oxide production is that plutonium present in a solid state solution with uranium at less than  $\sim 35\text{-}40 \text{ wt}\%$  plutonium is soluble in  $5\text{-}10 \text{ mol.l}^{-1}$  nitric acid [53]. Poor solubility was commonly experienced with early mechanically blended MOx due to poor homogeneity that resulted in plutonium rich grains [162]. Pu inhomogeneity and the proportion of insoluble plutonium residues are known to increase with increasing wt% Pu [53]. This was a significant factor for fast reactor fuel development, which had much higher fissile contents than thermal MOx fuels. Improvements in manufacturing methods have led to the production of modern MOx fuels, such as German OCOM, French MIMAS and British SBR. These fuels exhibit such an improved homogeneity that the pre-irradiation solubility for Pu is  $>99.5 \%$ , and often  $>99.9 \%$  post irradiation to

40 GWd/teHM [8]. High Pu solubility is a key factor for reprocessing as the uncontrolled accumulation of plutonium rich residues presents a criticality hazard. Any losses also reduce the efficiency of the fuel cycle and add to the burden upon the repository.

During MOx manufacture there are several factors that significantly affect the solubility and dissolution rate of MOx, these include homogeneity and porosity. Analytical techniques have been developed that allow the plutonium content of a sample to be mapped; this allows plutonium distribution plots to be produced. These plots give an indicator of the amount of high plutonium content grains and so can explain the low solubilities obtained for some materials. Another significant factor for unirradiated material is low porosity, which leads to low dissolution rates due to low reaction surface area and slow solvent penetration rates. This is predominantly an issue for low porosity unirradiated material, where skeletal residues have been observed after dissolution. However, such residues are an exception rather than the norm and manufacturing solubility tests have been designed to dissolve these skeletal residues and determine the true insolubility. The tests are carried out as part of the MOx manufacture QA procedure to provide evidence of pre-irradiation solubility. The tests are not designed to replicate a reprocessing dissolver cycle as irradiation increases the rate and extent of dissolution. The thermal MOx manufacturing solubility test gained international standard operation (ISO) status and involves dissolution in 10 mol.l<sup>-1</sup> nitric acid for 18 hours [163]. However, care must be taken to prevent fluoride contamination, which can give a misleadingly high solubility.

Irradiation of thermal MOx fuels, which typically contain ~5 wt% plutonium, has been observed to reduce the amount of insoluble plutonium residues in the dissolver compared to unirradiated material. plutonium rich regions or grains undergo locally higher burn-ups that cause an increase in local lattice damage and a larger reduction in local plutonium concentration [164]. In addition, plutonium redistribution occurs through local increases in the plutonium concentration of plutonium lean (uranium rich) regions. These combine to improve homogeneity and increase porosity, which leads to an increase in both the rate and extent of dissolution.

Earlier generations of fast reactor fuel types are more varied. They had an inner and outer core, which had a composition of ~15 and ~32 wt% plutonium respectively, and blanket fuel (depleted uranium) around the core. The blanket fuel tends to breed Pu whereas the core may either breed or burn plutonium. The burn-up of the core is typically much higher than thermal

reactors, >20 % burn-up compared with 4-6 % burn-up for thermal reactors. The thermal rating of the fuel has also been much higher, which has resulted in increased fuel restructuring. Dissolution tests in 8M nitric acid for inner core fuel have shown that typical residues are <1 % plutonium pre-irradiation and <0.5 % plutonium post-irradiation (20 % burn-up) [165, 166]. It has been found that irradiation at high ratings (e.g.  $W.g^{-1}$  or  $W.cm^{-1}$ ) increase diffusion of plutonium within the fuel pellet. At high ratings a void can develop at pellet cores and plutonium and noble metal alloys accumulate around this void [167]. The presence of plutonium rich regions with concentrations of up to 45 wt% plutonium have been observed [53]. Such local increases in plutonium concentration cause a decrease in solubility. These phases have been observed to be present in central voids at high linear ratings [54]. These effects decrease plutonium solubility. However, more moderate irradiation ratings can cause an increase in the plutonium solubility [168]. The increase in solubility is highly dependent upon the irradiation and manufacturing factors.

During unirradiated MOx and spent MOx fuel dissolution studies dissolution reagents other than nitric acid have been used. The dissolution of the unirradiated Plutonium rich residues is commonly carried out using methods that are known to dissolve plutonium dioxide. Methods such as nitric acid – hydrofluoric acid and silver(II) oxidation have been successfully employed for unirradiated materials. Nitric acid – hydrofluoric acid have also been applied to spent MOx fuel dissolver residues and do dissolve more plutonium, however, often residues still remain and material and process compatibility issues have prevented industrial application.

#### ***4.1.3. Summary of dissolution literature***

The review of nitric acid reduction chemistry, general oxide dissolution chemistry, metal, uranium oxide and plutonium oxide chemistry has highlighted the complex nature of the study of heterogeneous dissolution reactions in nitric acid solutions. The conditions that are required for uranium dioxide and plutonium dioxide dissolution are at the extremes of nitric acid chemistry; uranium dioxide requires high nitrous acid concentrations for optimal dissolution rates and plutonium dioxide requires very low nitrous acid concentrations and the presence of highly oxidising or reduced metals. To dissolve MOx, which contains a mixture of bulk material at the average Pu

content and small amounts of plutonium rich residues, may require very different conditions. The dissolution of uranium dioxide and MOx is likely to proceed via a slow nitrate reduction step, which initiates a more rapid nitrous acid reduction. So, the direction of these studies is to improve understanding on the relative roles of nitrate and nitrous acid.

#### **4.2. Aims and objectives**

As current commercial reactor fuel is large uranium or mixed uranium-plutonium oxide fuel, MOx is likely to be a future FR fuel. This is because MOx is the most mature technology and it will be required to act driver charges. However the details of how to optimise MOx fuel reprocessing have not been published in detail. As current MOx fuels are manufactured by milling uranium and plutonium oxides together these fuels are heterogeneous in nature and as such they contain plutonium rich regions. There are two key parts to the question of how to design dissolver cycles for MOx fuel.

1. How to optimise bulk-phase MOx dissolution?
2. How to optimise plutonium rich residues from direct nitric acid dissolution?

It was initially planned to obtain samples of MOx fuel with different plutonium contents. The studies could then be aimed at studying the effect of plutonium content upon dissolution rate and as higher plutonium content MOx will have increased plutonium rich residues these would provide some residues for further studies. However, the samples of MOx at up to 40 % plutonium MOx could not be obtained with the resources and timescales of this project.

MOx produced at the then operating Sellafield MOx plant (SMP) could be obtained with relative ease. An experimental programme designed around studying the role of nitrous acid, a key reactant for uranium dioxide dissolution, has been carried out. These include:

- Section 4.4: Study the effect of nitrous acid upon dissolution rate of uranium dioxide powder aimed at confirming literature observations.
- Section 4.6: Confirming the role of nitrous acid for the dissolution of MOx powders, as plutonium could interact with the dissolution auto-catalytic cycles. These experiments used fine MOx powders to allow dissolution experiments to be carried out under lower temperatures and nitric acid concentrations.

- Section 4.6.1: Investigate the role of nitrous acid, under high temperature and higher nitric acid concentrations, relevant to industrially and laboratory dissolutions. These experiments used pellets, which have low surface area to mass ratio, so could exhibit induction periods where nitrous acid concentration builds. However, the higher nitric acid concentration and temperature could also cause mass transfer limitations.
- Section 4.7.1: As experiments studying the effect of plutonium content are not possible within this work. A thermodynamic assessment for the effect of plutonium content upon the known dissolution chemistry of MO<sub>x</sub> in nitric acid has been carried out.

### ***4.3. Experimental***

#### ***4.3.1. Dissolution apparatus and methodology***

To study the dissolution of uranium dioxide or MO<sub>x</sub> there are a number of requirements that need to be considered for the design of the experimental equipment and methodology:

- Temperature control and monitoring.
- A gas inlet tube for solution sparging with air or inert gas (nitrogen or argon – only possible for fumehood experiments)
- Stirring of the solution.
- Support for pellets to allow stirring during pellet dissolution experiments.
- A method of adding the powder or pellets without opening the reactor (e.g. to prevent air ingress for inert experiments).
- A scale that is manageably small, yet large enough so that the removal of samples does not adversely affect the volume.
- Condenser to prevent excessive water and nitrogen oxides losses and provision of caustic traps to scrub the off-gas to prevent nitrogen oxides discharge to fumehood or glovebox ventilation system.
- Sampling system so that samples can be removed without allowing the ingress of air. This was carried out using 1/32" ID PFA (perfluoroalkoxy) tubing and syringe.
- A method of determining uranium and nitrous acid in-line, using a 0.5 cm flow cuvette with FMI piston pump (uranium dioxide studies) and Masterflex peristaltic pump (MO<sub>x</sub> studies). In-situ potentiometric

measurements were measured between a platinum wire and double junction Ag/AgCl reference electrode (Russell electrodes or Sentek Ltd), this allow qualitative comparison to the in-cell redox conditions. The results of these measurements are not discussed in this thesis.

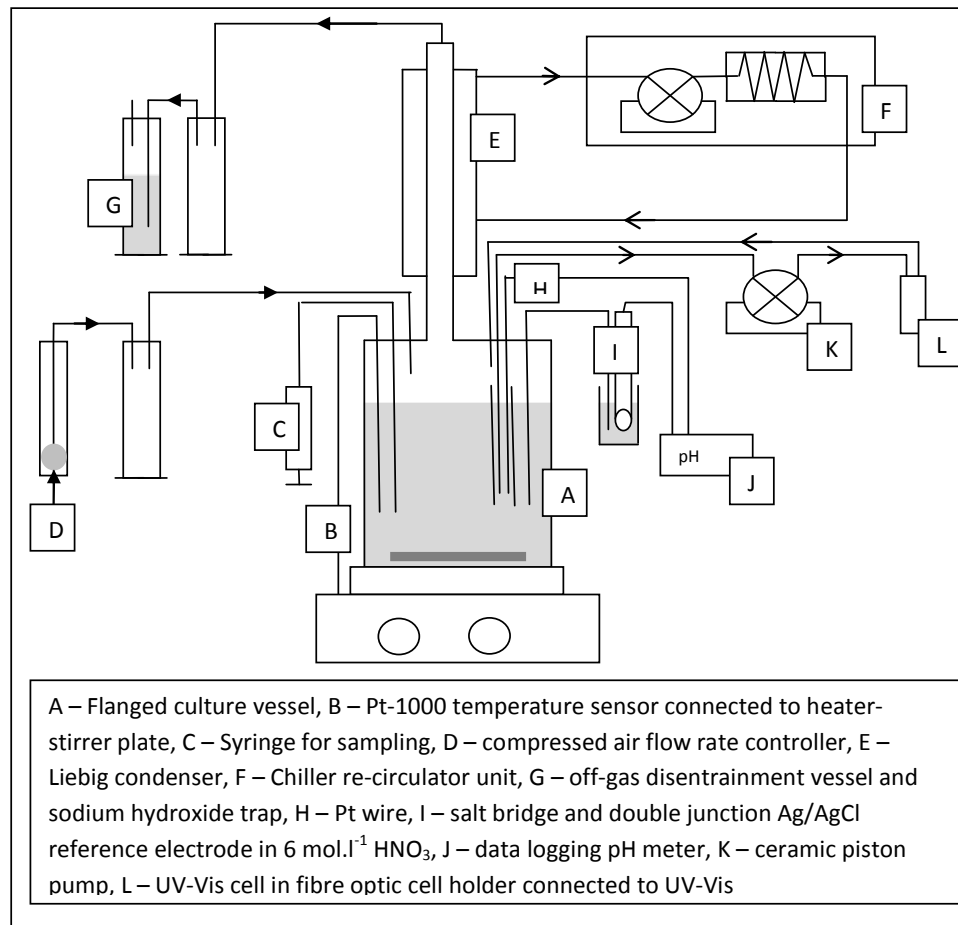
The reactor is based around a 500 ml glass vessel with a flanged lid. A custom reactor was made by Scott Glass (Stirling, UK) to allow the insertion of a support for pellets and the addition of larger ground glass joints on the lid, Figure 19a. The pellet support allows a magnetic follower to be used to stir the solution without bumping the pellets. A custom pellet/powder delivery arm was also made. A schematic diagram of the experimental apparatus is shown in Figure 19b.

During the uranium dioxide dissolution experiments the 'flat quickfit' glass flange leaked, so a second version of the dissolution apparatus was designed and purchased (Scott Glass Ltd, Stirling, UK). This used a 'Schott grooved flange with gasket', the experimental apparatus and systematic diagram are shown in Figure 20. As some caking of uranium dioxide powder was observed during the uranium dioxide powder experiments, the addition of MO<sub>x</sub> powder was carried out by partially removing a glass stopper and pouring the powder in using a glass weigh boat or dropping in the MO<sub>x</sub> pellet from a bottle. A photograph of the UV-Vis flow loop set up in the glovebox is shown in Figure 21A. The cell for potentiometric measurements is shown in Figure 21B. Pellet stand used in MO<sub>x</sub> pellet dissolution experiments is shown in Figure 22.

The methodology for all batch dissolution experiments involved the thermostatic of a defined concentration of nitric acid or nitric acid – potassium nitrate solution. The experiments were initiated with the addition of an aliquot of sodium nitrite (if used, to adjust the sodium nitrite concentration) and the powder or pellet. In-line or in-situ analysis was carried out and samples were taken periodically to allow the determination of uranium or uranium and plutonium concentrations and nitrous acid over time. All nitrous acid analysis of samples was carried out immediately (at line), to minimise nitrous acid decomposition.

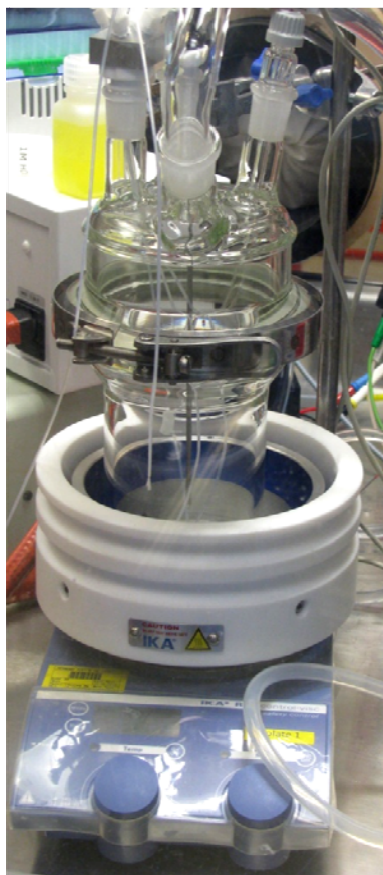


**A**

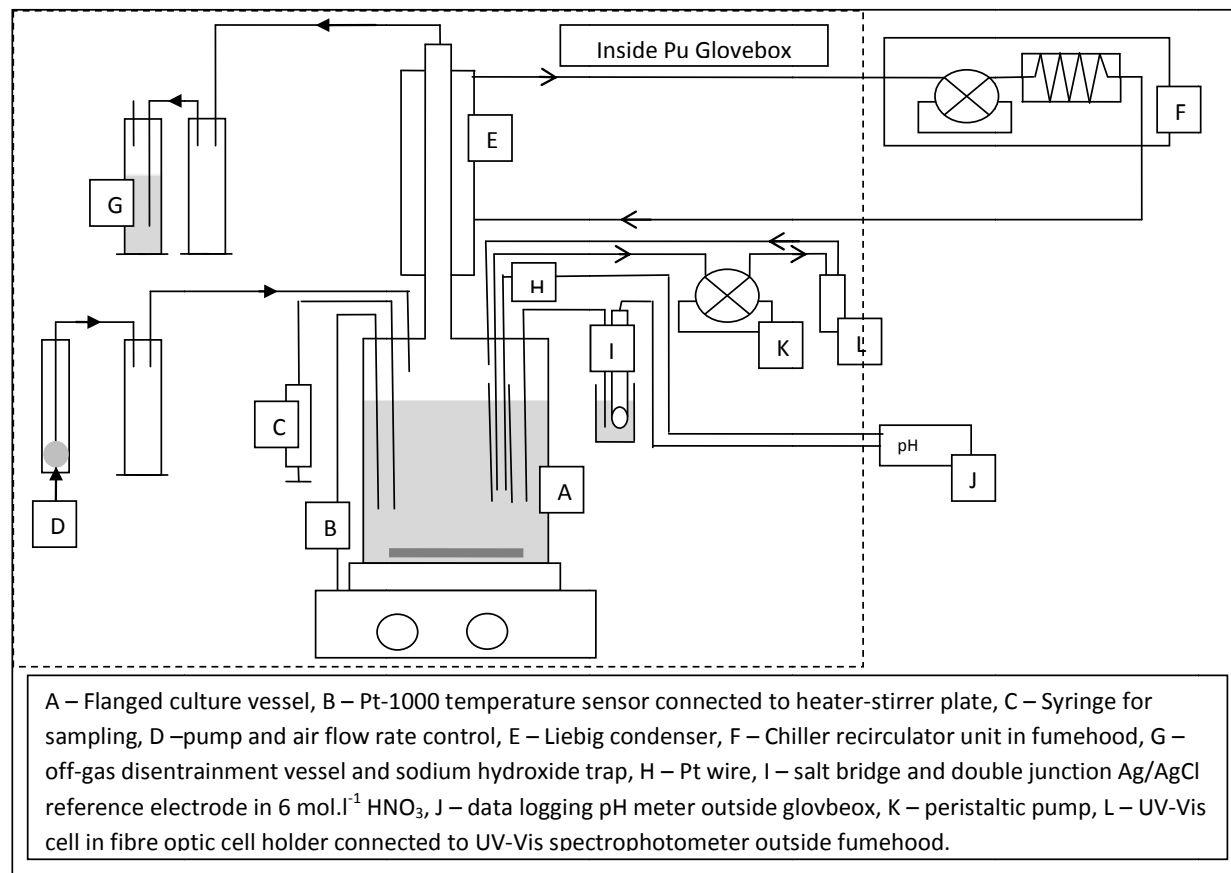


**B**

**Figure 19: a) Photograph of custom glassware for reactor and other apparatus b) Schematic diagram of dissolution apparatus**

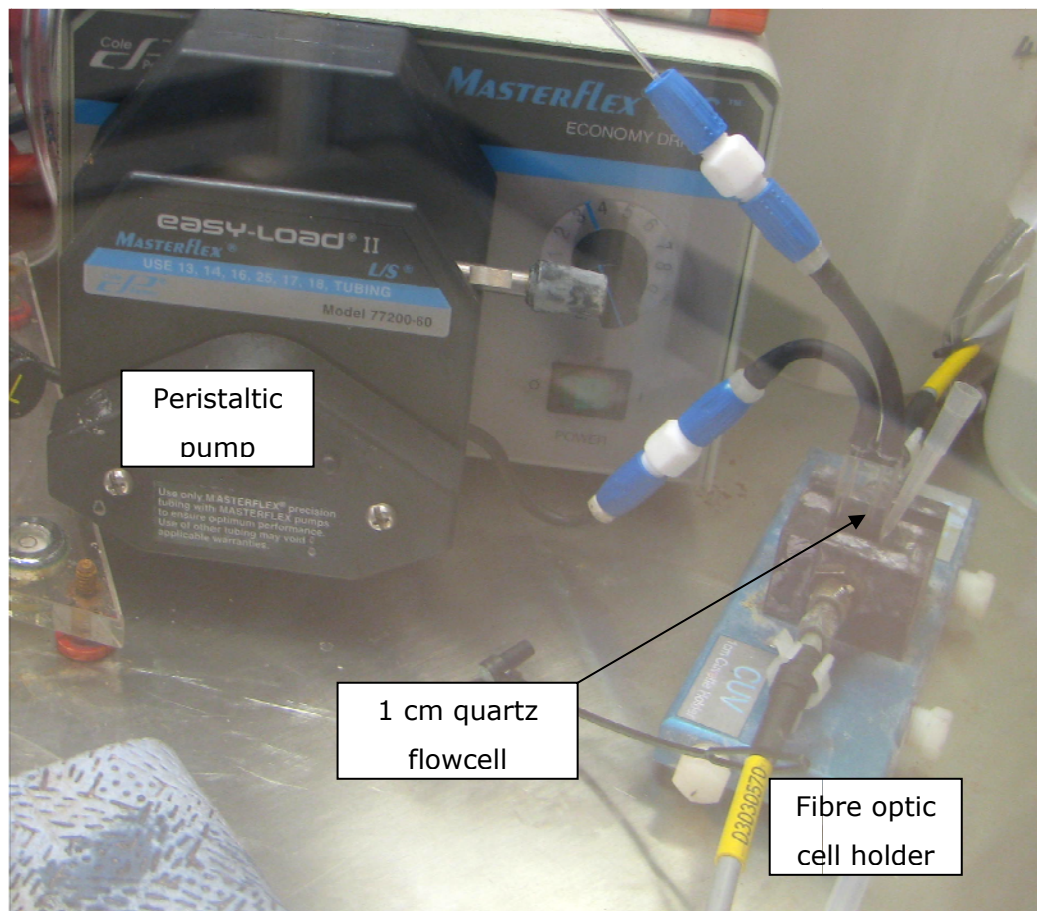


A

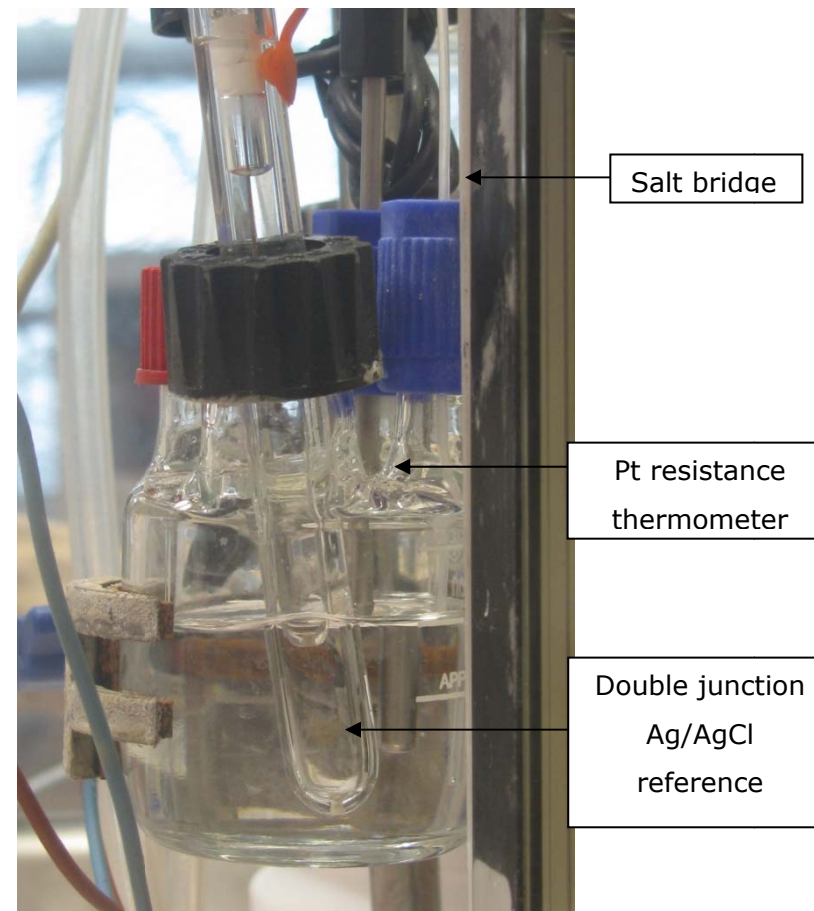


B

Figure 20: Equipment installed in glovebox, A - Photograph of dissolution vessel, B - Systematic diagram of apparatus dissolution



A



B

Figure 21: Equipment installed in glovebox, A UV-Vis flow cell and pump, B – redox reference electrode cell

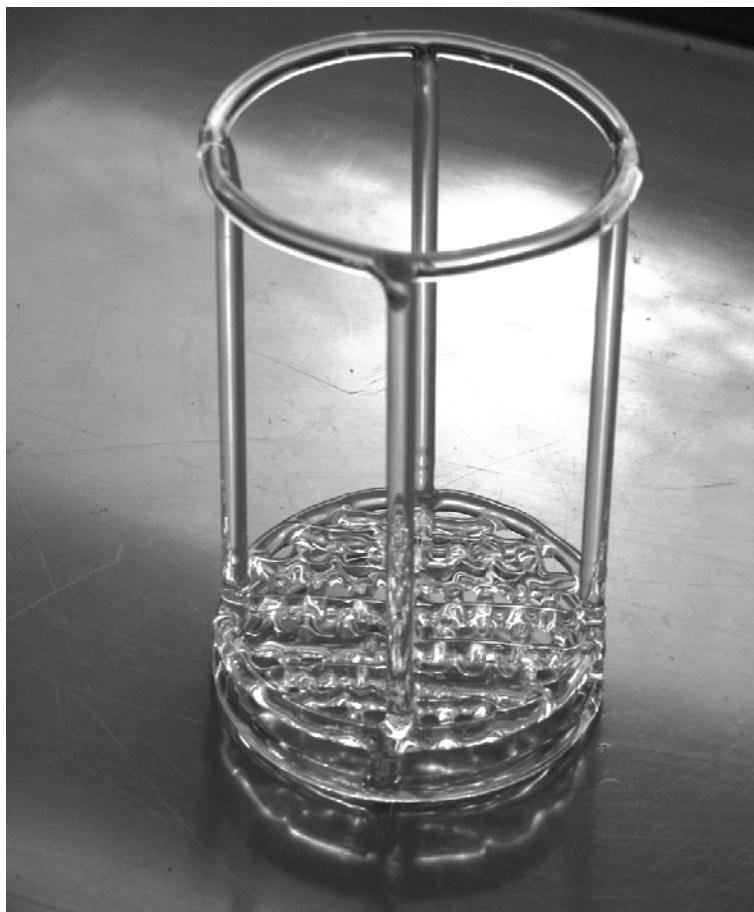


**Figure 22: Dissolver pellet support stand**

It was decided that, to enhance the experiments and allow the collection of more data, an *in situ* or in-line UV-Vis uranium monitor would be used and therefore a Hellma flow-through cell was used. The UV-Vis cell was connected to the vessel using PFA tubing and an FMI Inc. piston pump used to circulate the aqueous dissolver product through the cell. As nitrous acid also absorbs in the UV region, monitoring of the nitrous acid concentration with the UV-Vis flow cell may also be possible. All UV-Vis measurements were made using a Zeiss MCS 501 with deuterium and halogen lamps and 10 m long UV-Vis grade fibre optics and 1 cm path length Hellma flowcell.

A redox monitor was also included, which is based on an electrode system used in recent corrosion studies[169]. This has a platinum wire sheathed in PFA tubing and a salt bridge in the dissolution solution. The salt bridge forms an electrochemical connection to a double junction Ag/AgCl reference electrode, which is situated by the dissolution vessel in a beaker containing 6 mol.l<sup>-1</sup> nitric acid. The salt bridge was made by filling a PFA tube with glass wool strands.

### 4.3.2. Off-line analytical methods

#### 4.3.2.1. Uranium dioxide experiments

In addition to the in-line UV-Vis and *in situ* redox monitor it was also necessary to determine uranium, nitric acid and nitrous acid in the samples taken during the experiments. Due to the low stability of nitrous acid the determination was carried out within a few minutes of sampling. Other analysis was less time-dependent and was performed after completion of each dissolution experiment. A summary of the analytical methods used is given below:

- Uranium analysis was carried out by direct UV-Vis analysis. The extinction coefficients used for the experiments were determined by preparation of a calibration plot in 6 mol.l<sup>-1</sup> nitric acid and preparing solutions at fixed uranium concentration and varying nitric acid concentration. These results are shown in section 9.1.1.
- Four complementary methods have been used to determine HNO<sub>2</sub>:
  - Titration method, which is applicable to higher concentrations. This method has also been used in uranium dioxide dissolution studies [20] and is discussed by Vogel [170]. Some of the calibration results are shown in section 9.1.2.
  - Colorimetric method, which is highly sensitive to nitrous acid and can be used to determine low concentrations. This has been used in uranium oxide dissolution studies by Ikeda *et al.* [48, 49] and is based on modifications of the Greiss method, e.g. [171]. Work for Ikeda has been carried out within a sister laboratory [47] using Ikeda's procedure, so the procedure can be followed quite closely. Some of the calibration results are shown in section 9.1.3.
  - Potentiometric method (using potential measurements with a redox probe), which is applicable over a wide range of concentrations (*e.g.* log<sub>10</sub> scale) but the precision on a linear scale is less good compared to the titration and colorimetric methods. The results of a nitrous acid decomposition experiment, comparing the titration / colourimetric and potentiometric method are shown in section 9.1.4.
- The in-line UV-Vis analysis also yielded nitrous acid spectra. A nitrous acid extinction coefficient was determined from the nitrous acid calibration experiment. A correction for uranyl absorbance was carried out using the

6 mol.l<sup>-1</sup> nitric acid uranyl ion extinction coefficients. The nitrous acid spectra and Beer Lambert plot are shown in section 9.1.5 .

- Analysis of the free acidity in the experiments was carried out by potentiometric titration using standard 0.1 mol.l<sup>-1</sup> sodium hydroxide. Sodium hydroxide was standardised against 1 mol.l<sup>-1</sup> standard HCl. Samples containing uranium were titrated in the presence of potassium fluoride (KF) to suppress hydrolysis. This method is used extensively within the laboratory, so no further testing was not carried out. [172]

#### **4.3.2.2. MOx experiments**

All samples were analysed for:

- Uranium and plutonium concentrations using UV-Vis spectrophotometry in a 1 cm cell without dilution
- The redox titration method for nitrous acid analysis was not carried out as plutonium would interfere with the determination.

#### **4.3.3. Characterisation of materials**

##### **4.3.3.1. Uranium dioxide powders**

Uranium dioxide powders were prepared by NNL Preston laboratory from 3 kg of 10.88 g.cm<sup>-3</sup> R&D uranium dioxide pellets. The pellets were crushed using a jaw crusher and sieved in 200-250 g batches using an Octagon 2000 Sieve shaker with 75, 106, 250, 450, 1000, 1400 µm sieve set. This resulted in batches of powder of varying quantity and particle size range:

- 400g un-sieved powder
- 234 g 1000 – 1400 µm
- 242 g 250 – 450 µm
- 116 g 75 – 106 µm

The porosity of these pellets was not measured; however, as the density of the pellets is 10.88 g.cm<sup>3</sup>, the total porosity is ~0.7 %. Due to the high density the porosity of the pellets will be largely closed [173]. BET specific surface area (SSA) analysis was carried out by NNL Preston laboratory. The

75 – 106 and 250 – 150  $\mu\text{m}$  particle sieve fractions surface areas were reported as  $<0.1 \text{ m}^2.\text{g}^{-1}$ .

The particle size distribution was analysed for the two lower size fractions using a Malvern Mastersizer. The uranium dioxide powder was suspended in water and analysed in duplicate. Figure 23 shows the results of this analysis, the instrument does not analyse particles greater than 550  $\mu\text{m}$  and so the 250 – 450  $\mu\text{m}$  fraction analysis is incomplete. The SSA determined by the BET was 0.0050 and  $0.0015 \text{ m}^2.\text{g}^{-1}$  for 75 – 106 and 250 – 450  $\mu\text{m}$  respectively. The determined SSA are close to the theoretical SSA based on a sphere and assuming particle sizes of 90.5 and 350  $\mu\text{m}$  of  $0.0060$  and  $0.0016 \text{ m}^2.\text{g}^{-1}$  respectively.

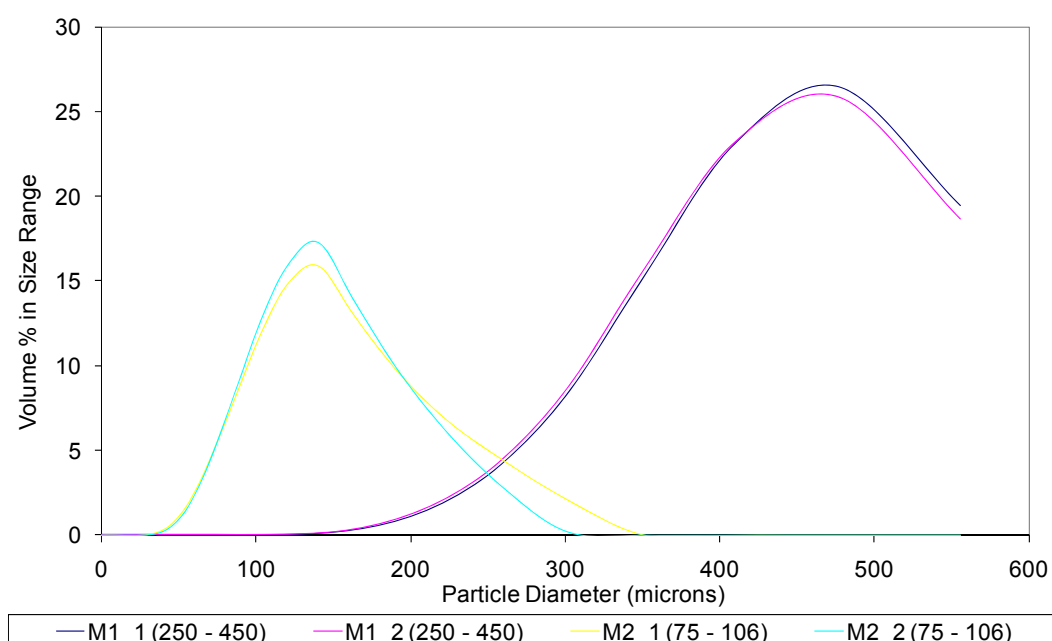


**Figure 23: Particle size distributions for Uranium dioxide powder sieve fractions 75 – 106  $\mu\text{m}$  and 250 – 450  $\mu\text{m}$**

The 250–450  $\mu\text{m}$  uranium dioxide particle size distribution range was found to produce a convenient dissolution time for dissolution in  $6 \text{ mol}.\text{l}^{-1}$  at  $80 \text{ }^\circ\text{C}$ , so this material was used for the uranium dioxide dissolution studies.

#### **4.3.3.2. MOx powder**

MOx powder was supplied by Sellafield MOx Plant (SMP). This powder was prepared by ball milling crushed MOx pellets. This material was not sieved and typically had a SSA of  $1.2 - 1.5 \text{ m}^2.\text{g}^{-1}$ . However, the SSA was not confirmed

by analysis. The particle size distribution is assumed to be 48  $\mu\text{m}$ . The powder had the appearance of a fine black free flowing powder.

#### 4.3.3.3. MOx pellets

MOx pellets supplied by Sellafield MOx Plant (SMP) have been used for these studies. The pellets have been analysed by Sellafield Ltd and the analytical details are listed Table 10.

**Table 10: Summary of MOx pellet analysis details**

<b>Analysis</b>	<b>Results</b>			
Pu	4.38			%
U	83.55			%
Pu/(U+Pu)	4.98			%
Solubility	99.86			% Soluble
Pu239+240	39.9	+/-	3.36	%Alpha/Alpha
Pu238+Am241	59.4	+/-	3.73	%Alpha/Alpha

#### 4.4. *The thermodynamics of actinide dioxide dissolution in nitric acid*

It is planned to submit the following paper to the Journal of Physical Chemistry.

##### 4.4.1. *Introduction*

Uranium dioxide and mixed uranium plutonium dioxide (MOx) are the current commercial nuclear power reactor fuels [65]. Future nuclear fuel cycles may include addition of actinides initially added in the fuel for transmutation, e.g. neptunium and americium. Furthermore, some national programs include thorium, as a potential candidate fuel for future reactors. On this basis it is evident that future fuel cycles may require the reprocessing and recycling of a wider range of actinides than uranium and plutonium, currently achieved using the Purex process. As most current spent fuel processing flowsheets involve dissolution as one of the first steps, it is relevant to continue to develop the understanding of how these materials dissolve. The overall and future aim of this and related work [Section 4.4, 4.6, 4.6.1] will allow improvements in the dissolution step by working towards quantitative

modelling and simulation, thereby also allowing the development of overall mode efficient flowsheets.

The present review focuses on the thermodynamics of the dissolution process. There have been numerous studies considering rates and kinetics of the dissolution process, but relatively little attention has been paid to the thermodynamics governing the dissolution of actinide dioxides in nitric acid. While the presence of a significant thermodynamic driving force indicates a spontaneous reaction it is no guarantee that a reaction or process will actually occur (for example, mass transport and other kinetic barriers may drastically slow down reactions), considering the thermodynamics may allow to rule out reaction paths that are thermodynamically implausible.

This review is limited to the dissolution in nitric acid, as this is the media of choice for industrial spent fuel reprocessing, as it has ideal properties for solvent extraction processes. This paper is divided into three sections, (i) discussion of the methodology, followed by its application to (ii) actinide oxide dissolution in nitric acid, and (iii) to dissolution by use of stronger redox reagents.

#### **4.4.2. Methodology**

The thermodynamic model to be described below is based on the application of Hess' to the standard Gibbs free energy ( $\Delta G_f$ ) of reactions, providing a measure of whether a reaction is spontaneous or not. Values used for thermodynamic quantities have been taken from the literature.[35, 174] For redox dissolutions, if the dissolution reaction is considered as a reversible reaction, the Gibbs free energy can be converted to standard reaction potentials. This is used for a convenient comparison with strong reducing or oxidising agents to assess reaction viability. A limit to the model to be presented here is that we will assume the reactions to proceed at room temperature (25 °C). The reason for this limitation is that heat capacities ( $C_p$ ) are not readily available for all species involved in the reactions, thereby rendering calculations of Gibbs free energies under realistic dissolution conditions (80-120 °C).

The three main chemical processes considered will be dissolution by acid, reduction and oxidation. Published  $\Delta G_{298}^\ominus$  values for  $\text{PuO}_2$  dissolution are compared with our calculated values in Table 11. It can be seen that the

Gibbs free energies calculated in this work are in very good agreement with those published by Berger.[52, 175, 176]

**Table 11: Calculated Gibbs free energy for major dissolution mechanisms of plutonium dioxide**

Reaction	$\Delta G_r$ (kJ.mol <sup>-1</sup> )			
	Berger[52, 175, 176]	Harding[177]	Ryan[178]	This work
$\text{PuO}_{2(s)} \rightarrow \text{Pu}^{4+}_{(aq)} + 2\text{H}_2\text{O}$	32.04 ± 4.0	49.7	41.0	32.4
$\text{PuO}_{2(s)} \rightarrow \text{Pu}^{3+} + 2\text{H}_2\text{O}$	-64.96 ± 4.0	-	-	-64.6
$\text{PuO}_{2(s)} \rightarrow \text{PuO}_2^+$	138.3 ± 9.8	-	-	138.2
$\text{PuO}_{2(s)} \rightarrow \text{PuO}_2^{2+}$	236.2 ± 15.4	-	-	231.1

#### 4.4.3. Dissolution in nitric acid

##### 4.4.3.1. Individual actinide dioxides

Nitric acid is known to contain a wide variety of reduction products during dissolution [26, 48]. During dissolution processes the concentration of reduction products is known to greatly affect dissolution rates, a example is uranium dioxide where the dissolution occurs by a nitric acid initiated nitrous acid autocatalysis mechanism [152]. These reactions are also termed the 'direct' and 'indirect' mechanisms. The 'indirect' route is highly dependent upon the concentrations of nitric acid reduction products highlighted in the dashed box of **Figure 24**. The abilities of the highlighted species to dissolve actinide dioxides are assessed in **Table 12**. This table shows that dissolution by acid is not favourable, except for thorium dioxide, which is not kinetically observed[179]. The table shows that there are several one and two electron oxidation reactions feasible for uranium dioxide and some of these reactions have a high thermodynamic driving force, >-100 kJ.mol<sup>-1</sup>. Neptunium and plutonium oxides can also follow several spontaneous reaction pathways, but the reaction Gibbs energies of is much less favourable when compared to uranium dioxide. Reductive dissolution reactions are favourable for curium dioxide and, interestingly, reduction of plutonium dioxide by nitrogen monoxide is also moderately favoured. There are no neptunium dioxide reactions with a strong thermodynamic driving force.

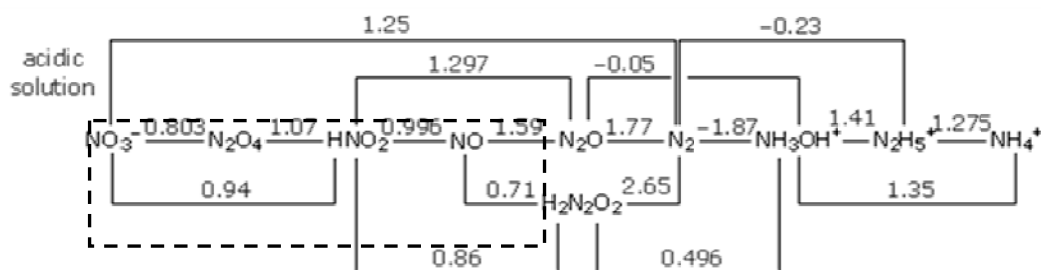


**Figure 24: Standard electrochemical potentials ( $V_{\text{NHE}}$ ) for redox conversions of nitric acid and other nitrogen-containing species [35]**

The results of the calculations clearly that:

1. Uranium dioxide has many more thermodynamically favourable reactions compared to neptunium or plutonium dioxide. The reactions that are favourable for neptunium and plutonium dioxide are also favourable for uranium dioxide.
2. The reactions that are known to cause uranium dioxide to dissolve rapidly, namely nitrate and nitrous acid oxidation are not thermodynamically viable for neptunium and plutonium dioxide.
3. Contrarily to the earlier published calculations that simply consider the dissolution of plutonium dioxide by nitrate[52, 175-178], there are several reactions for plutonium dioxide that are thermodynamically viable; however these reactions are not for the major species present.
4. Neptunium dioxide should be thermodynamically easier to dissolve compared to plutonium dioxide and there are reports that neptunium can be dissolved in nitric acid[180, 181].
5. The calculations suggest americium dioxide does not dissolve in nitric acid, though no data appear to be available in the literature to corroborate this.
6. Curium dioxide undergoes reductive dissolution, where nitrate is not directly involved in the dissolution reactions. However, reactions with nitrogen dioxide and monoxide are viable as nitric acid generally contains nitric acid reduction products, particularly under the intense radiolysis caused by curium. As reactions with nitrogen dioxide and nitrogen monoxide could occur and nitric acid can oxidise the products of these reactions an autocatalytic mechanism could result.

**Table 12: Calculated Gibbs free energies for dissolution of actinide dioxides by various nitric acid reactions**

Reaction type	Reaction	$\Delta G_{298f}^{\ominus}$ (kJ.mol <sup>-1</sup> ) for each actinide dioxide						
		Th	Pa	U	Np	Pu	Am	Cm
Direct	$AnO_2 + 4H^+ \rightarrow An^{4+} + 2H_2O$	-10.1	16.0	26.9	44.9	32.4	348.3	380.0
1e <sup>-</sup> oxidation	$AnO_2 + NO_3^- + 3H^+ \rightarrow AnO_2^+ + NO_2 + H_2O$	n/a	n/d	<b>-11.2</b>	32.4	63.8	64.6	n/a
	$AnO_2 + NO_2 + H^+ \rightarrow AnO_2^+ + HNO_2$	n/a	n/d	<b>-43.7</b>	<b>-0.1</b>	31.3	32.1	n/a
	$AnO_2 + HNO_2 + H^+ \rightarrow AnO_2^+ + NO + H_2O$	n/a	n/d	<b>-31.8</b>	11.8	43.2	44.0	n/a
	$2AnO_2 + 2NO + 2H^+ \rightarrow 2AnO_2^+ + N_2O + H_2O$	n/a	n/d	<b>-89.6</b>	<b>-46.0</b>	<b>-14.6</b>	<b>-13.8</b>	n/a
	$AnO_2 + N_2O_{4(l)} + H^+ \rightarrow AnO_2^+ + HNO_2 + NO_2$	n/a	n/d	<b>-38.5</b>	5.1	36.5	37.3	n/a
	$AnO_2 + N_2O_{3(g)} + H^+ \rightarrow AnO_2^+ + HNO_2 + NO$	n/a	n/d	<b>-45.4</b>	<b>-1.8</b>	29.6	30.4	n/a
	$AnO_2 + N_2O_{3(g)} + H^+ \rightarrow AnO_2^+ + 2NO$	n/a	n/d	96.5	76.8	107.3	108.3	n/a
2e <sup>-</sup> oxidation	$AnO_2 + NO_3^- + 5H^+ \rightarrow AnO_2^{2+} + HNO_2 + H_2O$	n/a	n/d	23.4	644.3	649.4	710.4	n/a
	$AnO_2 + NO_2 + 2H^+ \rightarrow AnO_2^{2+} + NO + H_2O$	n/a	n/d	<b>-122.8</b>	24.1	29.2	90.2	n/a
	$2AnO_2 + 2HNO_2 + 2H^+ \rightarrow 2AnO_2^{2+} + N_2O + 3H_2O$	n/a	n/d	<b>-168.7</b>	<b>-21.8</b>	<b>-16.7</b>	44.3	n/a
	$AnO_2 + N_2O_{4(l)} + 2H^+ \rightarrow AnO_2^{2+} + NO_2 + NO$	n/a	n/d	103.4	147.0	178.4	179.2	n/a
	$AnO_2 + N_2O_{3(l)} + 2H^+ \rightarrow AnO_2^{2+} + 2NO$	n/a	n/d	112.4	259.3	264.4	325.4	n/a
1e <sup>-</sup> reduction	$AnO_2 + 2H^+ + NO_2 \rightarrow An^{3+} + NO_3^- + H_2O$	n/a	n/d	n/a	105.1	9.8	279.4	<b>-141.4</b>
	$AnO_2 + 2H^+ + HNO_2 \rightarrow An^{3+} + NO_2 + H_2O$	n/a	n/d	n/a	374.6	279.3	548.9	128.1
	$AnO_2 + 3H^+ + NO \rightarrow An^{3+} + HNO_2 + H_2O$	n/a	n/d	n/a	125.7	30.4	300.0	<b>-120.8</b>
	$AnO_2 + 2H^+ + N_2O_4 \rightarrow An^{3+} + NO_2 + NO_3^- + H_2O$	n/a	n/d	n/a	291.7	196.4	466.0	45.2
	$AnO_2 + 3H^+ + N_2O_3 \rightarrow An^{3+} + NO_2 + HNO_2 + H_2O$	n/a	n/d	n/a	124.0	28.7	298.3	<b>-122.5</b>
	$AnO_2 + 3H^+ + N_2O_3 \rightarrow An^{3+} + 2NO_2 + H_2O$	n/a	n/d	n/a	230.9	158.8	631.5	215.9

n/a – not applicable, as the oxidation state does not exist, n/d – not determined, **bold** – negative Gibbs free energies, thermodynamically viable reaction

#### 4.4.3.2. Mixed uranium plutonium dioxide

Mixed uranium plutonium oxide (MOx) is currently a commercial reactor fuel. It is of particular relevance to dissolver cycle design because MOx is fabricated by the milling of uranium dioxide and plutonium dioxide[12], which results in plutonium-rich heterogeneities exist. As plutonium and plutonium rich dioxides do not dissolve in nitric acid, dissolution of MOx results in poor dissolution of the plutonium rich heterogeneities[182]. For this result an attempt to use above data to extrapolate the effect of individual oxidation reactions between uranium and plutonium dioxide. These calculations are presented in Figure 25 as standard electrochemical potentials at a temperature of 298 K.

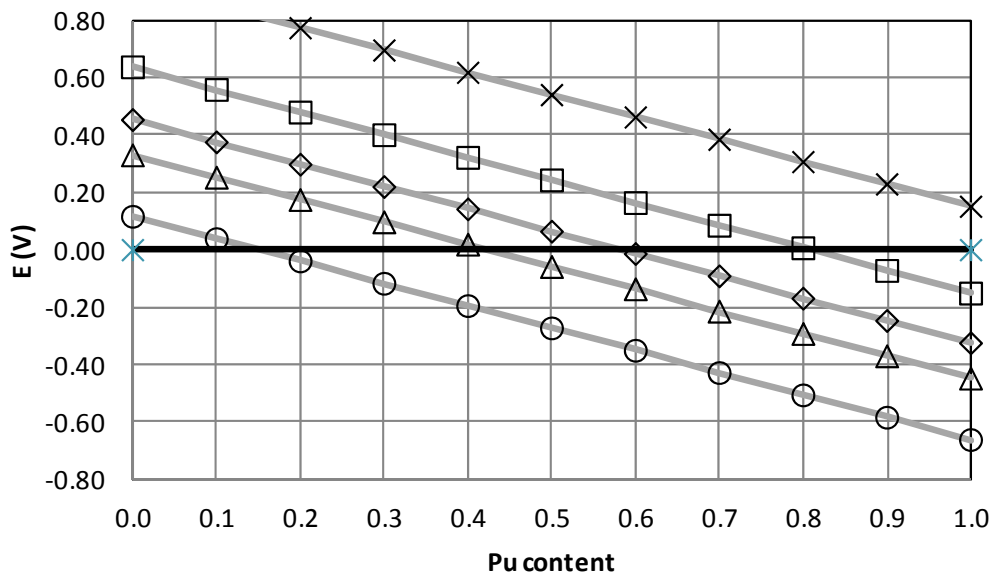


**Figure 25: Thermodynamics of dissolution of mixed uranium plutonium dioxide by favourable nitric acid reduction reactions at 298 K, ○ NO<sub>3</sub><sup>-</sup>/NO<sub>2</sub>, △ HNO<sub>2</sub>/NO, ◇ NO<sub>2</sub>/HNO<sub>2</sub>, □ NO<sub>2</sub>/NO, × NO/N<sub>2</sub>O**

The dissolution of MOx in nitric acid at low plutonium contents can be considered to be similar to that of uranium dioxide, while for higher plutonium contents it can be considered to be similar to plutonium dioxide. The reduction of nitrate (NO<sub>3</sub><sup>-</sup>/NO<sub>2</sub>) is a important reaction in the dissolution of uranium dioxide[48, 49], it is reasonable that this reaction will also be key for the dissolution of low plutonium content MOx and this has been observed for (U<sub>0.95</sub>,Pu<sub>0.05</sub>)O<sub>2</sub> REF-MOx powder, so it is reasonable assume that it proceeds spontaneously for these fuels. However, the reaction becomes unfavourable

above 15 % plutonium content. This suggests that initiation of the dissolution reaction may be more difficult, unless alpha radiolytic generation of nitric acid reduction products becomes significant in the locality of the pellet surface. However, it is known that nitrate concentration remains an important factor in the dissolution of MOx at higher plutonium contents, e.g. 30 % plutonium[183]. As dissolution kinetic experiments for higher plutonium contents MOx attempting to separate relative roles of nitrate and nitric acid reduction products have not been carried out yet. It could therefore be possible that the role of nitrate under these conditions is indirect involvement in an autocatalytic mechanism, rather than directly causing dissolution. That is the nitrate dependence is due to the regeneration of reactants in the 'nitrous acid' reaction route, where nitrate regenerates the reduced species thereby closing the catalytic cycle.

Studies of dissolving MOx at different plutonium contents have shown that the proportion of dissolved MOx declines above 30-40 % plutonium, Figure 26, it is likely that this is because the nitrous acid reduction reaction ( $\text{HNO}_2/\text{NO}$ ) becomes unfavourable. The nitrous acid reaction is known Nitrous acid is known to be a most significant autocatalytic species in uranium dioxide[48, 49] and 5 % plutonium MOx dissolution kinetics REF-Maher. Nitrous acid concentrations are high during dissolution, particularly near the surface of dissolving particles[143], the concentration may become significantly lower through more rapid or other reactions in the presence of higher plutonium contents.

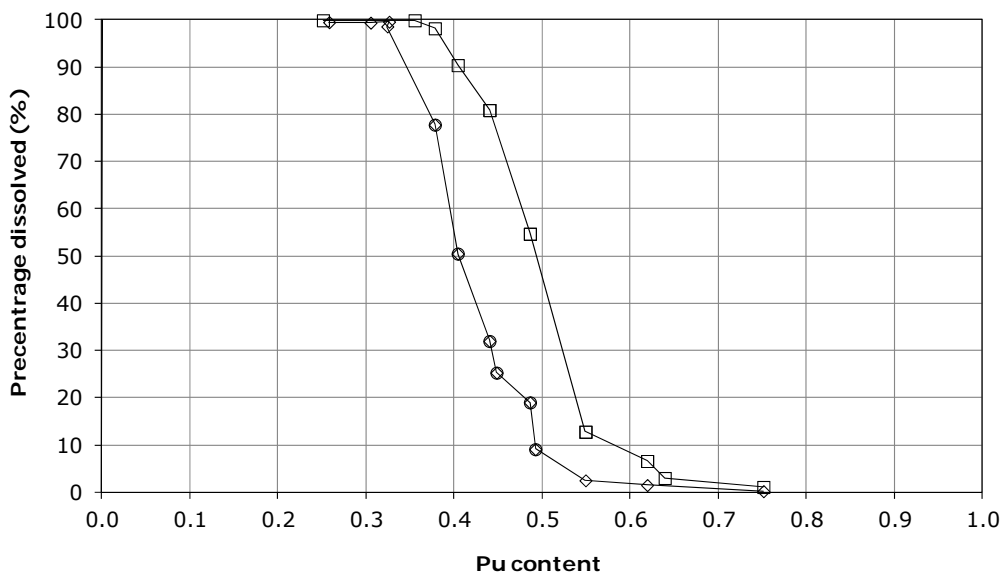


**Figure 26: Percentage MOx dissolved for various Pu contents when  $5 \text{ mol.l}^{-1}$  or  $10 \text{ mol.l}^{-1}$  is used under boiling conditions for 6 hours[53]**

Indeed from **Figure 26** it is clear that dissolution does not stop at 40 % plutonium, but the extent of dissolution becomes low for plutonium content of 60-75 %. This is partially due to morphological reasons, the inhomogeneous plutonium distribution in MOx, which results in regions of high plutonium content. However, another contributing factor for the shallow S-shape extent of dissolution curve could be there are other reactions that contribute to the dissolution mechanism. This reaction could be the reduction of nitrogen dioxide ( $\text{NO}_2/\text{HNO}_2$ ,  $\text{NO}_2/\text{NO}$ ) or nitrogen monoxide ( $\text{NO}/\text{N}_2\text{O}$ ). Low reaction rates can be expected as the concentrations of nitrogen dioxide and nitrogen monoxide under boiling conditions[20]. The nitrogen dioxide reactions become unfavourable at around 60 % and 80 % plutonium (Figure 26), whilst the nitrogen monoxide reaction remains favourable. The extent of dissolution of MOx decreasing to near zero corresponds to region where nitrogen dioxide reactions become unfavourable (Figure 26). This can be surmised from the fact that for the high nitric acid concentrations used in dissolution a high proportion of the nitrogen oxides present will be as nitrogen dioxide[21]. Under these conditions the nitrogen monoxide concentration in the solution will hence be minimised, resulting in low nitrogen monoxide concentrations near the MOx surface.

The above considerations for the overall dissolution reaction do not consider actual rates for the elementary steps involving reaction of the actinide dioxide and the surface-bonded nitrate or reduction products. It could be that the thermodynamics of surface species could change the energetic balance and reduce reaction viability. However, the energetics of the overall reaction are known, and on this basis it is suggested that the three major factors affecting the reduction in MOx dissolution efficiency are (i) the thermodynamics of the nitrous acid and (ii) nitrogen dioxide reduction reactions, and (iii) plutonium heterogeneity in the pellet (the distribution of plutonium content within grains and regions) arising from the MOx manufacture process.

#### **4.4.4. Enhanced dissolution with oxidising and reducing agents**

It is known that actinide dioxides that do not dissolve in nitric acid, can be brought into solution through the use of stronger oxidising or reducing agents. The rationale for these processes has been developed by Madic *et. al.*[52] and examples include the use of chromium(II) or silver(II). The Gibbs free energies for the actinide dioxide reduction and oxidation couples have been

converted to standard electropotentials and are shown **Table 13** with those calculated by Berger.

Actinide dioxide	$E_{298}^{\ominus}$ (V) for half reaction (calculated by Berger[52, 175, 176])		
	$AnO_2 \rightarrow An^{3+} + 2H_2O$	$AnO_2 \rightarrow AnO_2^+$	$AnO_2 \rightarrow AnO_2^{2+}$
UO <sub>2</sub>	-	0.66	0.41
NpO <sub>2</sub>	-0.32	1.11	1.17
PuO <sub>2</sub>	0.67 (0.67±0.04[52, 175, 176])	1.43 (1.43±0.10[52, 175, 176])	1.20 (1.22±0.06[52, 175, 176])
AmO <sub>2</sub>	-2.12	1.44	1.51
CmO <sub>2</sub>	2.24	-	-
For dissolution	A reducing agent with electropotential less than listed	A oxidising agent with electropotential greater than listed	

**Table 13: Electropotentials required for dissolution by oxidation or reduction**

It can be seen from **Table 14** that dissolution of neptunium and plutonium dioxide has been examined. As nitric acid is the preferred dissolution medium for solvent extraction processes, it is a condition for the use of redox reagents that they must be compatible with the nitric acid dissolution process. The reduction potentials for plutonium dioxide dissolution indicate that the reducing agents are in fact capable also of reducing nitric acid. An example of this is  $Fe^{2+}/Fe^{3+}$  standard electropotential is under that required for dissolution of plutonium dioxide, so high  $Fe^{2+}/Fe^{3+}$  ratios are required[184]. The reduction potentials shown for redox couples in Table 14 are also capable of reducing nitric acid, which may mean the dissolution is not possible, as nitric acid is simply reduced. For this reason most reductive dissolution experiments have been carried out in sulphuric or hydrochloric acid. An exception is the reductive dissolution of plutonium dioxide in nitric acid been demonstrated with uranium(IV) in the presence of hydrazine nitrate[117]. The hydrazine acts as a uranium(IV) stabilising agent, due to the rapid reaction between nitrous acid and hydrazine[185]. This may suggest other dissolution couple are possible in nitric acid using nitrous acid scavengers.

**Table 14: List of reducing agents with evidence for plutonium dioxide dissolution**

Reagent		For dissolution		PuO <sub>2</sub> dissolution reaction proceeds
Couple	E <sup>o</sup> (V)	Couple	E <sup>o</sup> (V)	
Fe <sup>3+</sup> /Fe <sup>2+</sup>	+0.77			Yes[184]
		PuO <sub>2</sub> /Pu <sup>3+</sup>	+0.67	
I <sub>2</sub> /I <sup>-</sup>	+0.54			Yes[186]
I <sub>3</sub> <sup>-</sup> /I <sub>2</sub>	+0.53			
VO <sup>2+</sup> /V <sup>3+</sup>	+0.34			Yes[186]
UO <sub>2</sub> <sup>2+</sup> /U <sup>4+</sup>	+0.27			Yes[117]
TiO <sup>2+</sup> /Ti <sup>3+</sup>	+0.19			Yes[186]
Sn <sup>4+</sup> /Sn <sup>2+</sup>	+0.15			N.I.
V <sup>3+</sup> /V <sup>2+</sup>	-0.26			Yes[186]
Eu <sup>3+</sup> /Eu <sup>2+</sup>	-0.35			N.I.
Cr <sup>3+</sup> /Cr <sup>2+</sup>	-0.42			Yes[161, 186, 187]

N.I. No information

**Table 15** shows the oxidising ions that have electrochemical potentials around and above those required for oxidative dissolution of neptunium and plutonium dioxide. An issue with oxidative dissolution is water can be oxidised above 1.23 V<sub>NHE</sub>, so oxidants can be consumed by reacting with water, however as this reaction generally has a high overpotential and so losses to this side reaction can be managed. The majority of studies have focused on plutonium dioxide with relatively few reporting neptunium dioxide dissolution results. Based on the free energies of dissolution by nitric acid (**Table 12**), it is possible that dissolution occurs by oxidation by neptunium(VI) (i.e. Np(VI)/Np(V) ). Unfortunately, no such reports are available in the open literature. If this mechanism is valid, it could explain the conflicting reports between the ease and difficulty of dissolution. As the dissolution rate will be dependent upon the rate of oxidation of neptunium(V) on one hand the neptunium(V):neptunium(VI) ratio (redox potential), which is known to be highly dependent upon the nitrous acid concentration[188]. The situation could then have some similarities with the dissolution of stainless steel highly active evaporators[189].

**Table 15: List of oxidising agents with evidence for neptunium or plutonium dioxide dissolution**

Reagent		For dissolution		Dissolution reaction proceeds	
Couple	E° (V)	Couple	E° (V)	NpO <sub>2</sub>	PuO <sub>2</sub>
		NpO <sub>2</sub> /NpO <sub>2</sub> <sup>+</sup>	+1.11		
NpO <sub>2</sub> <sup>2+</sup> /NpO <sub>2</sub> <sup>+</sup>	+1.14			Possibly [180, 181]	N.I.
		NpO <sub>2</sub> /NpO <sub>2</sub> <sup>2+</sup>	+1.17		
		PuO <sub>2</sub> /PuO <sub>2</sub> <sup>2+</sup>	+1.20		
Cr <sub>2</sub> O <sub>7</sub> <sup>2-</sup> /Cr <sup>3+</sup>	+1.33			N.I.	Not observed[182]
NH <sub>2</sub> OH <sup>+</sup> /N <sub>2</sub> H <sub>5</sub> <sup>+</sup>	+1.42			N.I.	N.I.
		PuO <sub>2</sub> /PuO <sub>2</sub> <sup>+</sup>	+1.43		
Ce <sup>4+</sup> /Ce <sup>3+</sup>	+1.44			Yes [190]	Yes[191]
MnO <sub>4</sub> <sup>-</sup> /Mn <sup>2+</sup>	+1.51			N.I.	
Au <sup>3+</sup> / Au <sub>(s)</sub>	+1.51			N.I.	N.I.
AmO <sub>2</sub> <sup>2+</sup> /AmO <sub>2</sub> <sup>+</sup>	+1.60			N.I.	Yes[182, 192]
MnO <sub>4</sub> <sup>-</sup> /MnO <sub>2</sub> (s)	+1.70			N.I.	Not observed[182]
H <sub>2</sub> O <sub>2</sub> /2H <sub>2</sub> O	+1.78			N.I.	N.I.
Co <sup>3+</sup> /Co <sup>2+</sup>	+1.82			N.I.	N.I.
Au <sup>+</sup> /Au <sub>(s)</sub>	+1.83			N.I.	N.I.
Ag <sup>2+</sup> /Ag <sup>+</sup>	+1.98			N.I.	Yes[118, 160, 161, 182, 193]
O <sub>3</sub> /O <sub>2</sub>	+2.08			N.I.	Yes (slow)[193]

N.I. No information

A much large body of work has been carried out studying the dissolution of plutonium dioxide using oxidising agents. The oxidant with the lowest standard electrochemical potential observed to oxidise plutonium dioxide is cerium(IV). Experiments have shown that a high cerium(IV):cerium(III) ratios are needed to achieve dissolution[194]. To prevent the solution oxidation potential dropping below that required for plutonium dioxide oxidation chemical or electrochemical oxidation has been used to maximise the proportion of cerium as cerium(IV)[195]. The discovery that silver(II) reacts rapidly with plutonium dioxide has led to the application to industrial plutonium dioxide dissolution. The high oxidation potential,  $\sim 1.98 V_{\text{NHE}}$ [195], of silver(II) means that a small silver(II):(I) ratio is required for dissolution to occur. Another useful property of silver(II) is that it is kinetically slow to react with water at near ambient temperatures and in the presence of higher nitric acid concentrations[122], this makes silver(II) an ideal oxidising mediator.

Cerium(IV), cobalt(III) and silver(II) has been used as a mediated[196] for the destruction of organic wastes. Cobalt(III) has advantages over silver(II)

when chloride is present as silver chloride precipitation occurs[197]. Cobalt(III) is known to oxidise plutonium(IV) to plutonium(VI)[198]. Although not demonstrated, the use of cobalt(III) may make a good dissolution mediator for recovery of plutonium dioxide from chloride containing solids.

Bubbling ozone has also been used as oxidant for this dissolution of plutonium dioxide, however dissolution rates are slow due to low solubilities and mass transfer limitations[193]. Ozone has however been used to regenerate silver(II) instead of electrochemical oxidation.

In order to avoid the need for use of large quantities of the oxidising or reducing agents, these mediators are used in catalytic concentrations. Reductive or oxidative dissolution technologies use a method of regenerating active agents to allow a catalytic concentration of the mediator to be used. Regeneration can be carried out using chemical or electrochemical methods, for example persulphate, ozone or electrochemistry, which have been explored in the context of cerium(IV) and silver(II) regeneration. This has led to the development of catalytic or mediated processes, for example catalysed electrochemical plutonium oxide dissolution (CEPOD) and the silver II<sup>TM</sup> process. Oxidative processes have also found spin off applications in areas such as the destruction of organics, e.g. mediated electrochemical oxidation (MEO).

The industrial dissolution of predominately plutonium dioxide for recovery and purification have found use of cerium(IV) and silver(II) oxidation processes [118, 195]. However, one disadvantage of this technique is the mediator adds salts to the waste streams, which often requires additional steps to recover the mediator or adds to wastes for disposal a necessity. This increases process volumes and complicates waste management.

Oxidative dissolution processes have nevertheless been explored for the dissolution of spent fuel, particularly MOx with high plutonium contents or carbides where destruction of organics is necessary[125]. In these cases ruthenium (present as a radioactive fission product) is oxidised to ruthenium tetroxide, which is volatilised[126] increasing complications of dissolver off-gas management. In addition, the mediator increases metal content of the high level waste, thus increasing the volume of final vitrified products. An elegant solution to the dissolution of plutonium-rich residues unirradiated MOx (for recovery/repurification) or irradiated MOx dissolution (for reprocessing) could be the abovementioned reductive dissolution using uranium(IV) in presence of hydrazine. The resulting product would be uranium(IV), plutonium(III) and neptunium(IV) which could be extracted in solvent

developed for grouped actinide extraction (GANEX, e.g. TODGA). The backwashed uranium(IV), plutonium(III), neptunium(IV) and americium(III) could then be finished using a co/gel-precipitation method aimed at producing a homogeneous MOx. This type of approach could also be applied to plutonium dioxide dissolution for fabrication or the direct refabrication into MOx.

#### **4.4.5. Summary**

Thermodynamic considerations for the reactions associated with the dissolution of actinide oxides with nitrate, nitric acid reduction products and other reducing or oxidising agents have been summarised. The calculated Gibbs free energies show that the uranium dioxide – nitric acid dissolution system has multiple reactions that are thermodynamically favoured, whereas there are fewer favourable dissolution reactions for the other actinide oxidations and these are typically less favourable. Applying the results to mixed uranium plutonium dioxide of various proportions suggests the key dissolution reactions become less favourable. The calculated results can be used to rationalise the decline in the extent of dissolution in the region of 35 to 70 % plutonium content, which corresponds to a decline in the dominance of the nitrate reduction, nitrous acid and nitrogen dioxide reactions becoming less favourable.

For the actinide dioxides (except thorium dioxide) the use of enhanced oxidative or reductive dissolution techniques can be employed. For efficient processes, these methods must manage or minimise the side reaction for the reduction of water or nitric acid. The review of reducing and oxidising agents stronger than nitric acid or its reduction products show that the species studied most are cerium(IV) and silver(II). Another interesting method is the reductive dissolution using uranium(IV) in nitric acid stabilised by hydrazine, which could offer simplifications to future unirradiated or irradiated fuel reprocessing flowsheets.

#### ***4.5. The effect of stirring and sparging upon uranium dioxide dissolution in nitric acid***

It is planned to submit the following paper to Hydrometallurgy.

##### ***4.5.1. Introduction***

Current practices for the reprocessing of spent nuclear fuel involve the dissolution in nitric acid as the first chemical treatment [65]. Prior to dissolution spent fuel assemblies are sheared into dissolvers containing a basket [65]. Some of the fuel falls from the hulls and the remainder is trapped in the hulls. This leads to two conditions, the dissolution of fuel powder under chemical control, and the dissolution of fuel from the hulls, which may be under chemical or mass transfer control.

The dissolution of uranium dioxide in nitric acid has previously been studied in detail [19, 20, 30, 34, 45, 46, 48, 49]. The dissolution is known to occur via an autocatalytic mechanism. This process involves the oxidation of the uranium dioxide to uranyl [151] by nitrate or nitric acid reduction products [48, 49]. A slow initiation process of nitrate reduction by reaction with uranium dioxide leads to the formation of nitrous acid, which rapidly reacts further with uranium dioxide forming nitrogen monoxide. The formed nitrogen monoxide reacts further with nitric acid to form nitrous acid, thereby closing the autocatalytic cycle. As the uranium dioxide dissolution is a heterogeneous process this leads to a solution volume close to the surface becoming depleted or elevated in reactants, reaction intermediates and products relative to bulk solution concentrations. The resulting network of reactions is kinetically complex, making it difficult to untangle the reaction rates associated with nitric and nitrous acid; it is known that unless the solution is vigorously stirred nitrous acid builds up close to the surface, leading to rapid autocatalytic dissolution [34]. Careful studies using rapid stirring and controlled addition of nitrous acid (as sodium nitrite) have allowed the derivation of a dissolution rate law based on temperature, nitric acid and nitrous acid concentrations [48, 49]. Variables that effect the rate of decomposition of nitrous acid and loss of nitrogen oxides [19, 20] will therefore affect the dissolution rate.

The roles of nitric acid and its reduction products have previously been examined in the context of other heterogeneous nitric acid chemistry;

examples include applied dissolution experiments [26, 28, 29] and also more fundamental experiments studying the complex reduction chemistry of nitric acid [22-25]. These studies highlighted that the reduction of uranium dioxide occurs *via* a heterogeneous reaction [34], with regeneration of nitrous acid taking place in or with involvement of the boundary layer. It was recently also observed that uranium dioxide dissolution is accompanied with the formation of gas bubbles,[144] which suggests the presence of an additional gas-liquid interface and hence an even more complex heterogeneous reaction involving two interfacial processes, **Figure 27**. Blocking of the volume near the uranium dioxide surface by bubbles could plausibly limit the removal of reaction products and intermediates from the surface, thereby increasing their concentrations dramatically above those in the bulk solution. At the same time, transport of nitric acid to the interface is likely to be limited, and this would likely affect reaction rates further through the known dependence of the nitrogen monoxide and nitric acid reaction on the nitric acid concentration.[19, 21] A dependence of dissolution rates via the 'nitrous acid' route upon nitric acid concentration has indeed been observed [199].

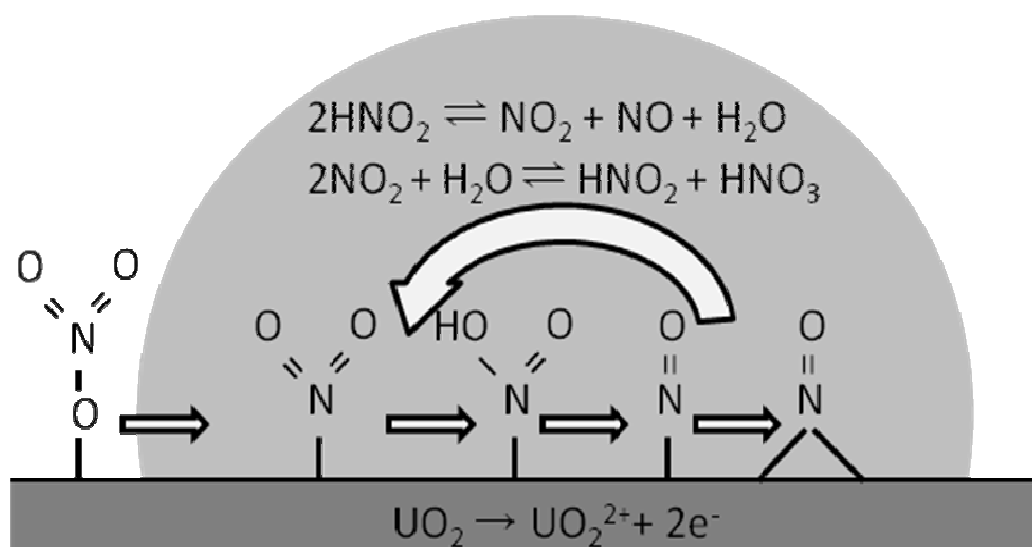


**Figure 27: Surface and near-surface reactions autocatalytic dissolution**

We report here the results of experiments investigating the role of nitrous acid upon the dissolution of uranium dioxide powder. It will become apparent that our findings broadly agree with those of Ikeda [48, 49]. but we find a more complex relationship between the role of nitrous acid and agitation due to the disruption of the autocatalytic dissolution cycle.

## **4.5.2. Experimental**

### **4.5.2.1. Materials**

The uranium dioxide powder used in these experiments were produced from pellets ( $\rho = 10.88 \text{ g.cm}^{-3}$ , 99.2 %T.D.) produced by NNL Preston Laboratory, Springfields. Pellets were jaw crushed and sieved to provide a 250-450  $\mu\text{m}$  sieve fraction. Particle size analysis by a Malvern Mastersizer determined a modal particle size of 460  $\mu\text{m}$ .

### **4.5.2.2. Apparatus and methodology**

A glass flanged 'culture' vessel (Scott Glass Ltd, Stirling) was used with a heater-stirrer plate (IKA RET control) and a Liebig condenser. The vessel lid was fitted with 0.8 mm diameter PFA tubing for sampling by syringe, open circuit (redox) potential measurement and inline UV-Vis analysis. Redox potential measurement measurements were between a Pt wire (in dissolution apparatus) and double junction Ag/AgCl reference electrode (Russell electrodes). A salt bridge made from a PFA tube packed with glass wool was used as an additional junction and all measurements were made with a Hanna HI 4222 pH meter. In-line UV-Vis analysis was carried out using a 0.5 cm quartz flow cell (Hellma), ceramic piston pump (FMI) and fibre-optic spectrometer (Zeiss MCS 501).

Each experiment was carried out by thermostating 250  $\text{cm}^3$  nitric acid to 80  $^\circ\text{C}$  with UV-Vis and potential measurements running, addition of  $\text{UO}_2$  initiated the experiment ( $t = 0$ ). 7.0 or 3.5 g of uranium dioxide powder was used per experiment, resulting in 28 or 14  $\text{g.l}^{-1}$  uranium concentration. For experiments where the variable nitrous acid concentration at fixed stirrer speed, immediately prior to uranium dioxide addition the solution was 'spiked' with 5  $\text{mol.l}^{-1}$  sodium nitrite. Samples were taken periodically for nitrous acid and uranium analysis. Determination of rate constants used a core shrinkage model, used by other workers [48, 49]. For consistency with other published work [48, 49] the mid sieve size, 350  $\mu\text{m}$  has been used for calculation of dissolution rate constants.

#### 4.5.2.3. Analysis methods

Uranium concentrations were determined inline and offline by direct UV-Vis spectroscopy. Example spectra from a dissolution experiment show the uranyl and nitrous acid absorption bands, **Figure 28**. The analysis of the data used baseline corrected absorbance (414 minus 550 nm), **Table 16** shows the molar extinction coefficients used.

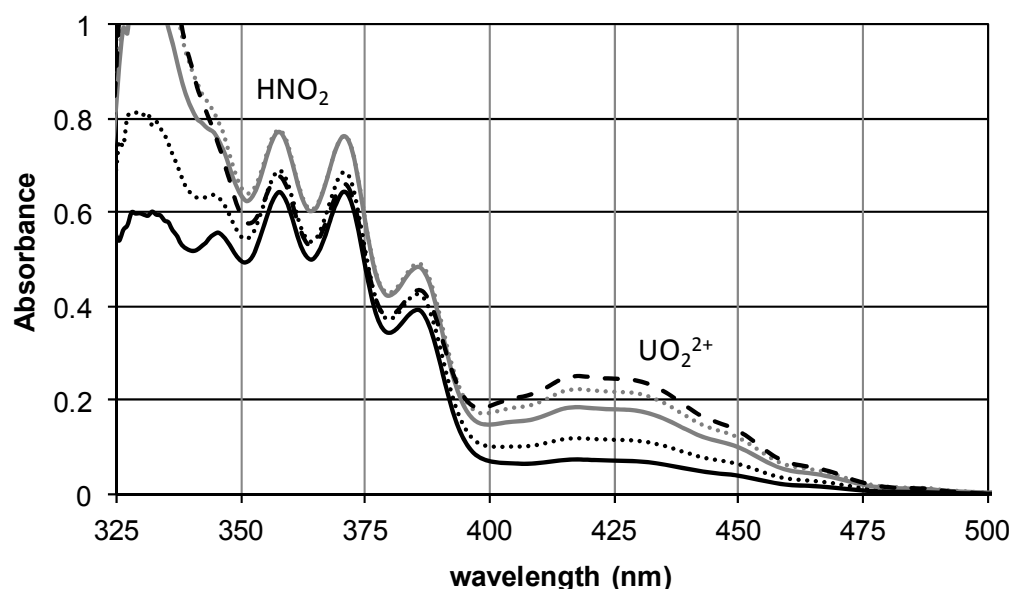


**Figure 28: UV-Vis absorption spectra for the dissolution of 6.9 g  $\text{UO}_2$  in  $6 \text{ mol.l}^{-1} \text{HNO}_3$  at  $80^\circ \text{C}$  with  $25 \text{ mmol.l}^{-1} \text{NaNO}_2$  added, stirring at 500 rpm, 10, 20, 40, 60, 100 minutes**

**Table 16: Molar extinction coefficients for uranium**

$[\text{HNO}_3]$ ( $\text{mol.l}^{-1}$ )	4	5	6	7	8	9	10
$\epsilon_{414-550 \text{ nm}}$ ( $\text{l.cm.l}^{-1}$ )	10.8	12.6	13.0	13.2	13.0	12.9	12.7

Nitrous acid generation was determined quantitatively using a redox titration method; two qualitative methods based on potentiometry and inline UV-Vis spectrometry were also used. The titration method involved the addition of a sample to 10 wt% sulphuric acid containing a known amount of cerium(IV), which was titrated with standardised iron(II) ammonium sulphate[20, 200]. The amount of nitrous acid can principally also be estimated with potentiometry,[21, 26] but due to reference electrode drift this method was used only qualitatively in the present study. An analysis of nitrous acid concentrations from the UV-spectra, using the absorption band around 300-400 nm, was used only qualitatively, as quantitative analysis is complicated due to the presence of uranyl absorption bands in the same region.

### 4.5.3. Results and Discussion

Measured dissolution rates were calculated as the radius of the shrinking particle core as a function of time, assuming the model by Ikeda *et al* [48, 49]. The uranium concentrations at time  $t$  and final ( $[UO_2^{2+}]_t$  and  $[UO_2^{2+}]_\infty$  respectively, mol.l<sup>-1</sup>) to calculate the powder diameter, ( $r$ , cm) equation (1). The gradient of the radius-time ( $dr/dt$ , cm.min<sup>-1</sup>) graph is used to calculate the dissolution rate ( $\phi$ , mol.cm<sup>-2</sup>.min<sup>-1</sup>) (2,3). The measured radius,  $r_0$ , of 0.023 cm (modal particle size 460  $\mu$ m) has been used. An example of this data analysis with nitrous acid trend is shown in Figure 29.

$$r = r_0 \left( 1 - \frac{[UO_2^{2+}]_t}{[UO_2^{2+}]_\infty} \right)^{1/3} \quad (1)$$

$$r = \frac{dr}{dt} t + r_0 \quad (2)$$

$$\phi = - \frac{\rho \left( \frac{dr}{dt} \right)}{M_r} \quad (3)$$

Density of uranium dioxide,  $\rho$  (g.cm<sup>-2</sup>), relative molecular mass,  $M_r$  (g.mol<sup>-1</sup>)

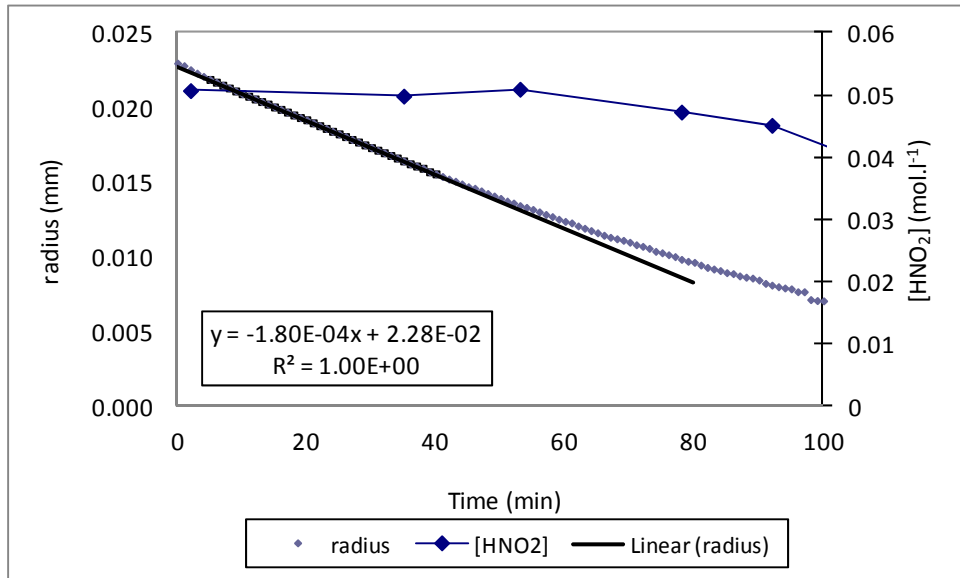


**Figure 29: Dissolution of 6.9 g UO<sub>2</sub> in 6 mol.l<sup>-1</sup> HNO<sub>3</sub> at 80 °C with 25 mmol.l<sup>-1</sup> NaNO<sub>2</sub> added, 6×30 mm follower at 500 rpm, □ [HNO<sub>2</sub>], • radius, — core shrinkage dissolution rate**

Experiments in 6 mol.l<sup>-1</sup> nitric acid at 80°C show a decrease in dissolution rate with increasing stirrer rate (magnetic follower, 6×30 mm), **Figure 30**. This has been observed by other workers [34] and is due to the reduction in the

concentration of nitrous acid at the uranium dioxide surface as the stirrer rate is increased. More vigorous stirring reduces the local concentration of nitrous acid from the reaction of nitrogen monoxide with nitric acid, by transporting nitrous acid into the bulk solution, and thus suppresses the autocatalytic cycle. A linear correlation between uranium dioxide dissolution rate and nitrous acid concentration in the bulk solution is already implicit in the data presented in figure 4, but it is explicitly shown in **Figure 31**. The higher reaction rates observed at low stirring speeds are associated with the formation of higher nitrous acid concentrations through favouring the autocatalytic formation of nitrous acid near the particle surfaces.

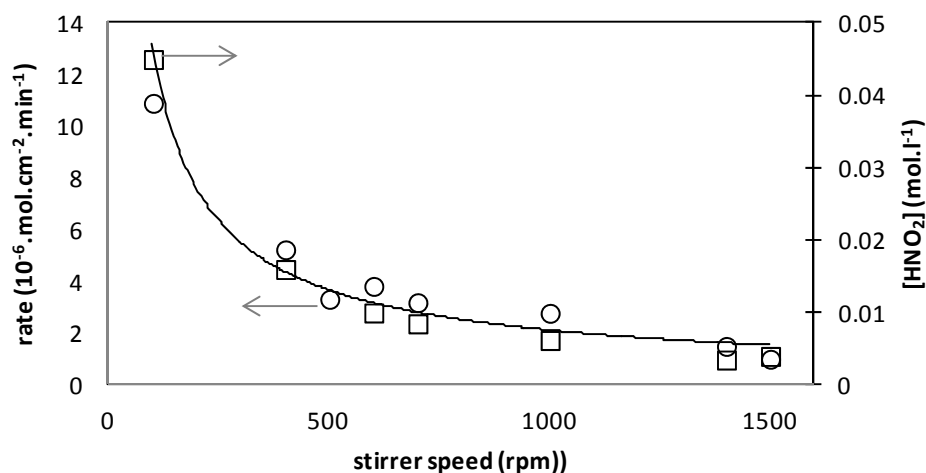


**Figure 30: Effect of stirring (small follower) upon dissolution rate and plateau  $\text{HNO}_2$  concentration, O dissolution rate ( $\mu\text{mol.cm}^{-2}.\text{min}^{-1}$ )**  
**□  $[\text{HNO}_2]$  ( $\text{mol.l}^{-1}$ )**

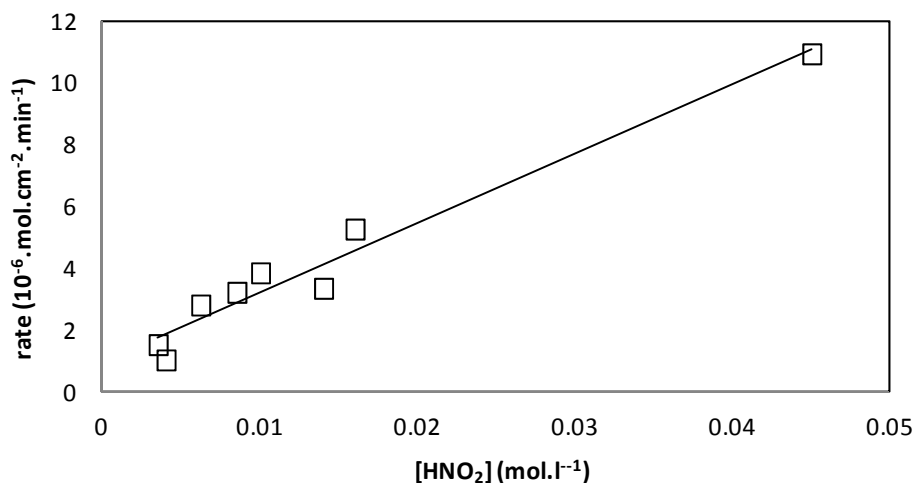


**Figure 31: The effect of plateau  $[\text{HNO}_2]$  (caused by stirring) upon dissolution rate, □ small follower at variable rpm**

In line with these observations, addition of sodium nitrite to the solutions increases the uranium dioxide dissolution rates, **Figure 32**. Nitrite addition was examined using different stirring regimes. First, using a small follower (6×30 mm) stirring at higher rates (1500 compared to 500 rpm) causes a reduction in the dissolution rates and reduction in the effect of nitrous acid (gradient), again this underlines the importance of local build-up of nitrous acid for achieving autocatalytic dissolution. With a larger follower (12×50 mm) stirring at 350 rpm<sup>9</sup> a lower dissolution rate is achieved relative to that observed at 500 rpm with the smaller follower. However, the effect of varying the nitrous acid concentration is greater. On one hand, the larger follower is expected to causes more efficient mixing, suppressing initiation of the autocatalytic dissolution; on the other, the slower stirrer rate employed in this experiment still permits significant acceleration from the autocatalytic reaction caused by nitrite addition.

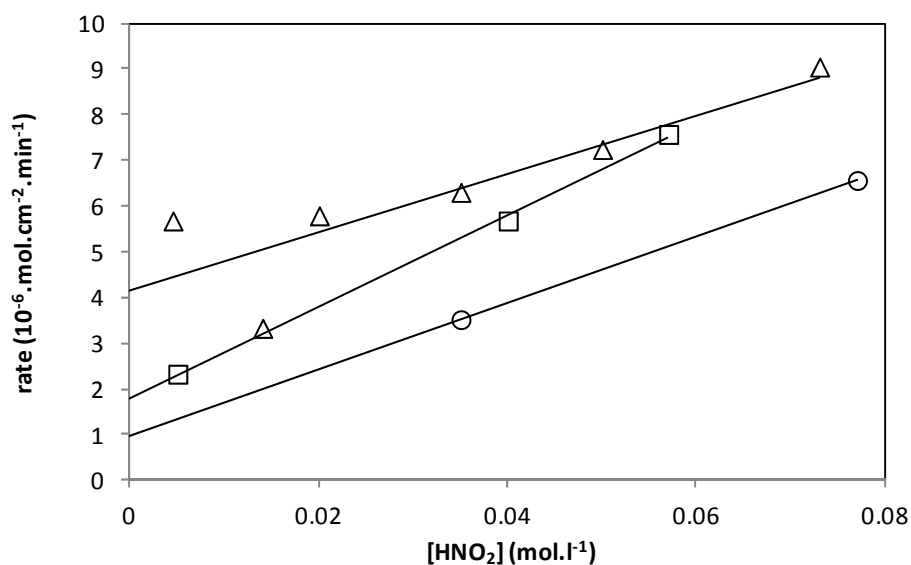


**Figure 32: Effect of increasing [HNO<sub>2</sub>] upon dissolution rate, under three stirring regimes, Δ small follower 500 rpm, ◻ large follower 250 rpm, ○ small follower 1500 rpm**

The effect of stirring can be rationalised if the proposed mechanism, **Figure 27**, is considered; as stirring minimises the potential for bubble formation due to the high turbulence.

---

<sup>9</sup> 350 rpm was the highest achievable stirrer rate for the large magnetic follower.

Sparging solutions with air has been reported to efficiently reduce the nitrous acid concentration in the bulk solution.[21] We found that the uranium dioxide dissolution rate in 6 mol.l<sup>-1</sup> nitric acid stirred at 1500 rpm (1.0 μmol.cm<sup>-2</sup>.min) and at 80 °C was unchanged by sparging the solution at 250 ml.min<sup>-1</sup> with air (0.7 μmol.cm<sup>-2</sup>.min). However, increasing the nitric acid concentration from 4 to 10 mol.l<sup>-1</sup> at 80 °C under stirred and sparged conditions increased the dissolution rate, **Figure 33**. The stirred and sparged systems maintain low nitrous acid concentrations in all, but 10 mol.l<sup>-1</sup> nitric acid. The increased nitrous acid concentration in 10 mol.l<sup>-1</sup> nitric acid is due to the increased stability of nitrous acid [199] combined with its more rapid generation. Comparison of **Figure 32** and **Figure 33** shows that under conditions that minimise the nitrous acid reaction (simultaneous stirring and sparging) the nitric acid concentration significantly increases the dissolution rate, but under unstirred conditions the nitrous acid reaction is more influential. These observations are consistent with the findings of other workers [48, 49].

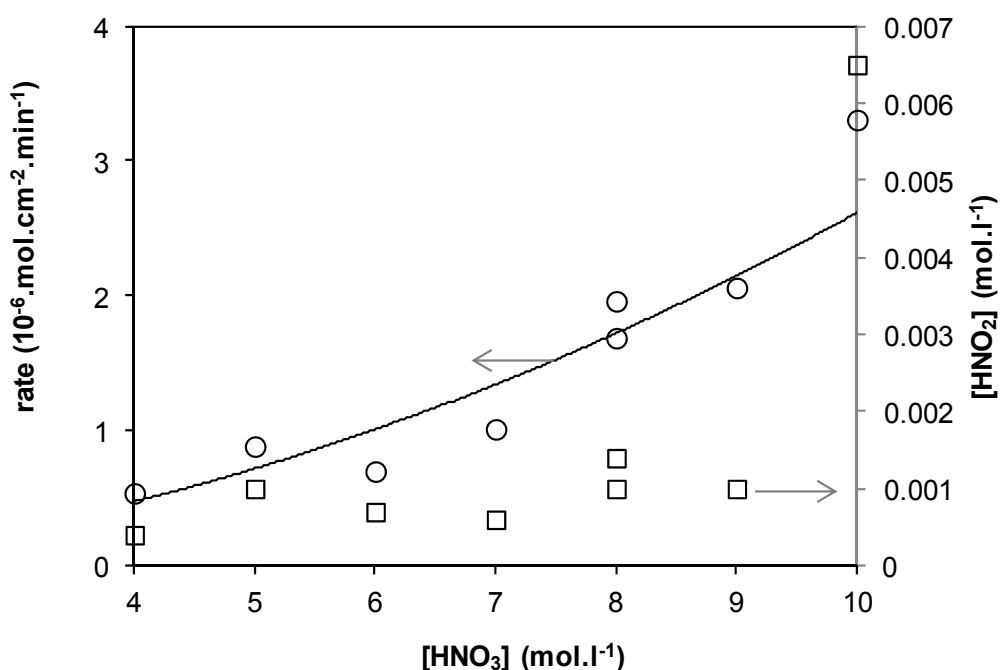


**Figure 33: Effect of nitric acid concentration under air sparge and stirring (1500 rpm small follower), O dissolution rate, □ nitrous acid concentration**

Overall, the effect of nitric acid concentration in the presence of low nitrous acid concentrations is approximately two to three times less than rates calculated from published rate expressions [48], **Figure 34**. However, the

effect of nitrous acid on the dissolution rates, **Figure 35**, is less clear-cut than previously observed. The 250 rpm larger follower gradient is similar to that calculated results, whereas the small follower at 500 rpm has a higher rate and the small follower at 1500 rpm has a slower rate. This suggests that there is a more complex relationship between stirrer rate and nitrous acid concentration the previously suggested.

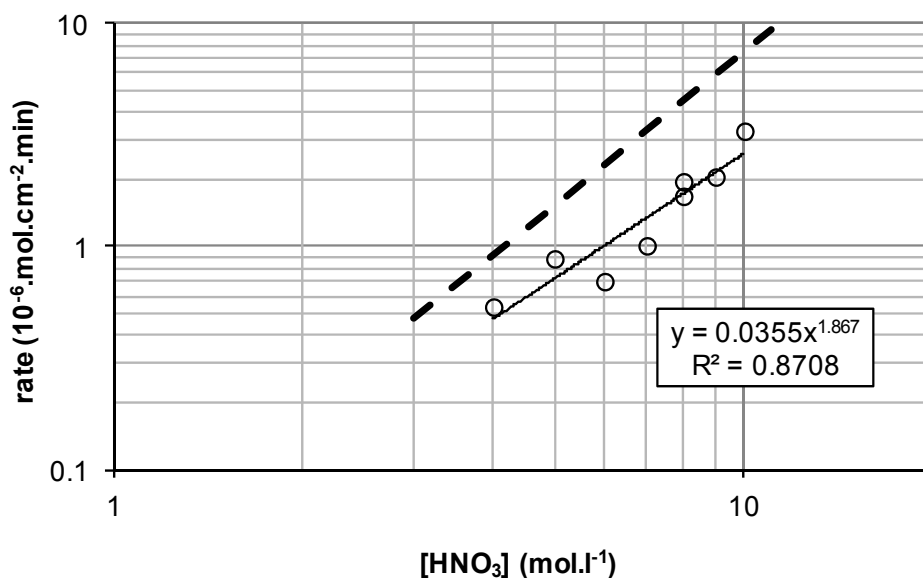


**Figure 34: Comparison of effect of nitric acid (air sparge, small follower, 1500 rpm) with Ikeda *et al.* published kinetic rate law**

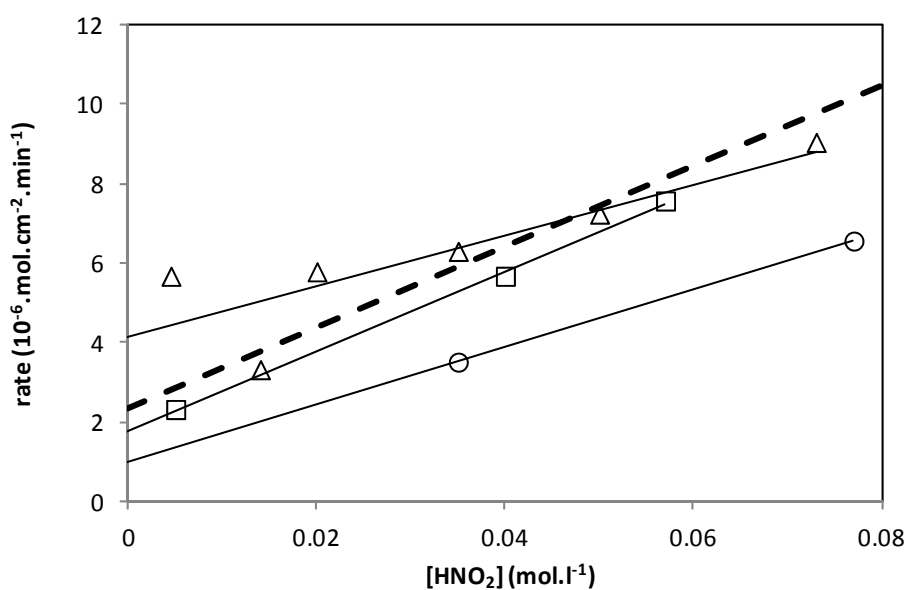


**Figure 35: Comparison of effect of nitrous acid (small follower, 1500 rpm) with Ikeda *et al.* published kinetic rate law**

Nevertheless, overall our results are consistent with previous applied studies of the dissolution of uranium dioxide [19, 20, 30, 34, 45, 46, 48, 49] and other metals [26, 28, 29], as well as of more fundamental studies investigating nitric acid reduction chemistry [22-25]. Our findings support the hypothesis that the key to efficient dissolution of uranium dioxide and other similar materials is the optimisation of bulk and local nitrous acid concentrations, thereby maximising the beneficial effect of the rapid auto-catalytic nitrite cycle.

#### **4.5.4. Summary**

In summary, the influence of nitric acid and nitrous acid on the dissolution rate of uranium dioxide powder confirms the key catalytic role of nitrous acid. Improving the mass transfer from the interface into the bulk solution by varying the stirrer rate and the size of the magnetic follower led to a reduction in dissolution rate. Under conditions that minimise nitrous acid concentration (stirred and sparged) dissolution rate increases with increasing nitric acid concentration; however rates remain low compared to those obtained in the presence of nitrous acid. These results are similar to other published rates.

#### **4.6. *The role of nitrous acid in the dissolution of uranium plutonium mixed oxide powder***

It is planned the following paper will be submitted to Journal of Physical Chemistry A.

##### **4.6.1. Introduction**

Mixed uranium plutonium oxide, (U,Pu)O<sub>2</sub> or MO<sub>x</sub>, uses plutonium recovered by reprocessing spent uranium metal or oxide fuels, allowing the reuse of plutonium in the future cycles. Current practice involves the cutting of bundles of spent fuel rods by shearing in the head end of the reprocessing plant and dissolution of the resulting fragments in nitric acid[65]. Uranium dioxide dissolution has previously been studied in considerable detail [34, 45, 46, 48, 49, 145, 151] and a summary of previous work is provided by Maher[Section 4.4]. MO<sub>x</sub> dissolution is more complex, exhibiting two key differences to

uranium oxide processing, because of its heterogeneous nature. MOx fuel has a higher plutonium content compared with spent uranium dioxide fuel and the bulk of the plutonium dissolves with the uranium. However, interspersed in the bulk phase are plutonium-rich regions, which originate from the manufacturing process and do not dissolve in nitric acid, thus yielding solid plutonium containing residue [51]. As plutonium is fissile the presence of plutonium rich residues poses a criticality risk, these solid residues must be controlled carefully and it is highly desirable to minimise the quantity of the plutonium rich residues.

We have now investigated the dissolution of powdered thermal plutonium MOx and compared the results to uranium dioxide dissolution studies performed under the same conditions. The dissolution of uranium dioxide in nitric acid is known to occur via nitrate reduction and an autocatalytic mechanism with a nitrous acid intermediate [48, 49], Figure 36. This mechanism has similarities to other dissolution reactions in nitric acid [26, 148]. Because nitrous acid is formed autocatalytically during the dissolution process its concentration near the interface can become very high relative to the bulk aqueous phase. As a result, the dissolution reaction proceeds more rapidly when the reaction mixture is left to take place without agitation, while highly agitated or strongly stirred systems exhibit comparatively low dissolution rates.[34][Section 4.4]. For this reason, recent studies[26, 48, 49][Section 4.4] have been carried out under highly stirred conditions in an attempt to prevent the build-up of reduction products close to the material surface, which accelerates dissolution.

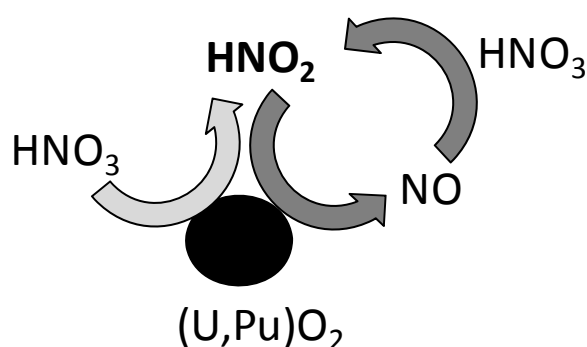


**Figure 36: Nitrous acid autocatalytic cycle**

The aim of this work is to investigate the role of nitrous acid and compare the similarities between the dissolution of thermal plutonium MOx and uranium dioxide powders[201].

## **4.6.2. Experimental**

### **4.6.2.1. Materials**

Mixed uranium plutonium dioxide pellets with 4.1 wt% plutonium (4.7 %HM Pu/U+Pu) prepared using the short binderless route by Sellafield Ltd at the MOx plant (SMP). The SMP process is described in detail elsewhere.[12] Briefly, this process blends uranium dioxide and plutonium dioxide powders by ball milling. The resulting powder product is pressed into pellets, calcined, sintered and finished. For this work the sintered pellets were crushed and ball milled to produce a powder where 95% of the powder was <56  $\mu\text{m}$  sieve, with a surface area of approximately  $1.3 \text{ m}^2.\text{g}^{-1}$ , as determined by BET adsorption measurements.

### **4.6.2.2. Apparatus and methodology**

All experiments were carried out in a shielded high integrity alpha containment glove box. Dissolution experiments were undertaken in a thermostatted (27-70 °C) stirred (1400 rpm) 250 ml solution of AR nitric acid (4-7  $\text{mol.l}^{-1}$ ). The addition of a volume of 5  $\text{mol.l}^{-1}$  AR sodium nitrite (when used) with 1 g MOx powder initiated the experiment (time = 0 min).

The dissolution apparatus used was similar to the equipment used in previous studies [Section 4.4]. Briefly, it includes a flanged culture vessel with Pt-100 thermometer, a Liebig condenser and a magnetic follower (30 × 6 mm). The vessel was fitted with 0.8 mm diameter PFA tubing for sampling, with *in situ* potentiometric as well as inline UV-Vis analysis. Condenser cooling was achieved with a recirculating chilled water supply (Haake) outside of the glove box, with water flowing into and out of the glove box via permanently installed pipework. Potentiometric measurements were made between a platinum wire and gelled double junction Ag/AgCl reference electrode (Sentek Ltd, UK) separated *via* a salt bridge [Section 4.4]. All UV-Vis measurements were carried out via fibre-optics, using custom fibre-optic feedthroughs (Hellma). Inline UV-Vis analysis was carried out with a 2 mm quartz flow cuvette (Hellma), a peristaltic pump (Masterflex), and a fibre-optic spectrometer (Zeiss MCS 501).

#### 4.6.2.3. Analysis methods

Inline and off-line UV-Vis analysis of samples was used to determine the uranium-plutonium dissolution rate. Nitrous acid concentration determination used the Griess colorimetric method e.g.[202], immediately after sampling to minimise decomposition. This method was calibrated using two independent sodium nitrite standards, one prepared in-house and one obtained from Fisher Scientific.

#### 4.6.3. Results and Discussion

Dissolution rates are expressed as the reduction of the particle radius as a function of time ('linear penetration rates'), calculated using a shrinking core model that assumes spherical MOx powder particles [48, 49], thereby allowing to use the uranium (and plutonium) concentration in solution at any time  $t$  ( $[UO_2^{2+}]_t$  and  $[UO_2^{2+}]_\infty$  respectively, mol.l<sup>-1</sup>) to estimate the powder particle diameter ( $r$ , cm), eq. (1). The gradient of the radius-time graph ( $dr/dt$ , cm.min<sup>-1</sup>) is used to calculate the dissolution rates ( $\phi$ , mol.cm<sup>-2</sup>.min<sup>-1</sup>), eqs. (2,3). The initial radius,  $r_0$ , is of 24.3  $\mu\text{m}$  ( $2.43 \times 10^{-3}$  cm), calculated from the surface area ( $1.3 \text{ m}^2.\text{g}^{-1}$ ), which is as expected for particles where 95 % particles pass a 56  $\mu\text{m}$  sieve. It is recognised that there is considerable uncertainty in the assumed particle size and a relatively large particle size distribution may exist. An example of this data analysis with nitrous acid trend showing a 'plateau' region is shown in **Figure 37**. This example shows the induction period where nitrous acid is produced and after dissolution the nitrous acid decomposition due to the relatively high temperature.

$$r = r_0 \left( 1 - \frac{[UO_2^{2+}]_t}{[UO_2^{2+}]_\infty} \right)^{1/3} \quad (1)$$

$$r = \frac{dr}{dt} t + r_0 \quad (2)$$

$$\phi = - \frac{\rho \left( \frac{dr}{dt} \right)}{M_r} \quad (3)$$

Where,  $r$  is the radius (cm),  $r_0$  is the initial radius (cm),  $[UO_2^{2+}]$  is the uranium concentration at time  $t$  (mol.l<sup>-1</sup>) and at the end of the experiment,  $\infty$ .

$\rho$  is the density ( $\rho$ , g.cm<sup>-2</sup>) and  $M_r$  is the relative molecular mass of uranium dioxide (g.mol<sup>-1</sup>),  $\phi$  is the dissolution rate (mol.cm<sup>-2</sup>.min<sup>-1</sup>).

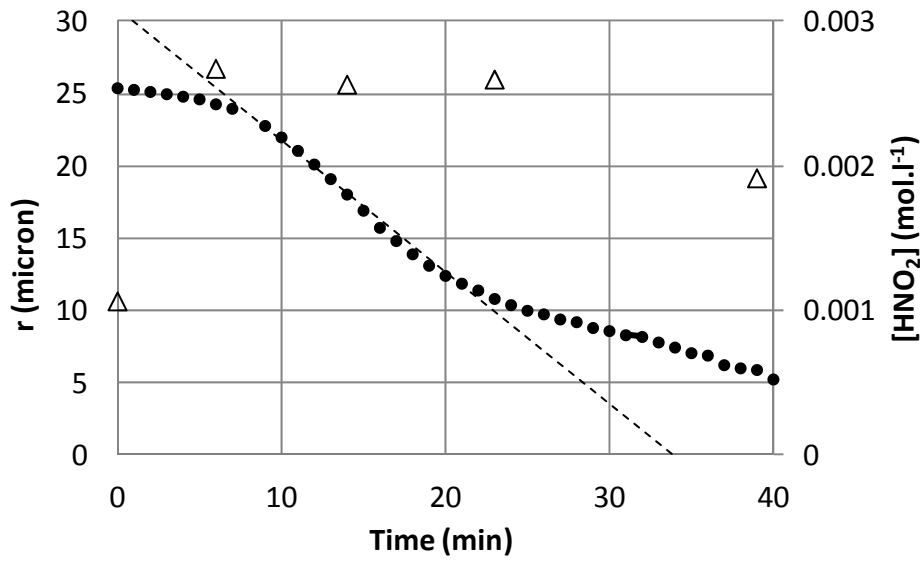


**Figure 37: Dissolution of 1 g MOx powder in 5 mol.l<sup>-1</sup> HNO<sub>3</sub> at 70 °C without added NaNO<sub>2</sub>: ● radius determined by inline analysis and equation (1), Δ [HNO<sub>2</sub>]**

The dissolution rate constant at 40 °C is plotted for increasing nitrous acid concentration for 4 to 7 mol.l<sup>-1</sup> nitric acid (**Figure 35**). This shows that increasing the nitric and nitrous acid at 40 °C increases the rate of dissolution. Using the intercepts (corresponding to the absence of nitrous acid) and the gradients from **Figure 35** for each nitric acid concentration one can determine the rate constants for the nitric acid and the nitrous acid reactions, respectively. It is found that there is a strong relationship between the observed rate constants and nitric acid concentration (**Figure 39**). These data allow the derivation of eq. (4), which shows dissolution of MOx powder follows the same form as uranium dioxide powders[48].

$$\phi = k_1[HNO_3]^{2.3} + k_2[HNO_3]^{2.3}[HNO_2] \quad (4)$$

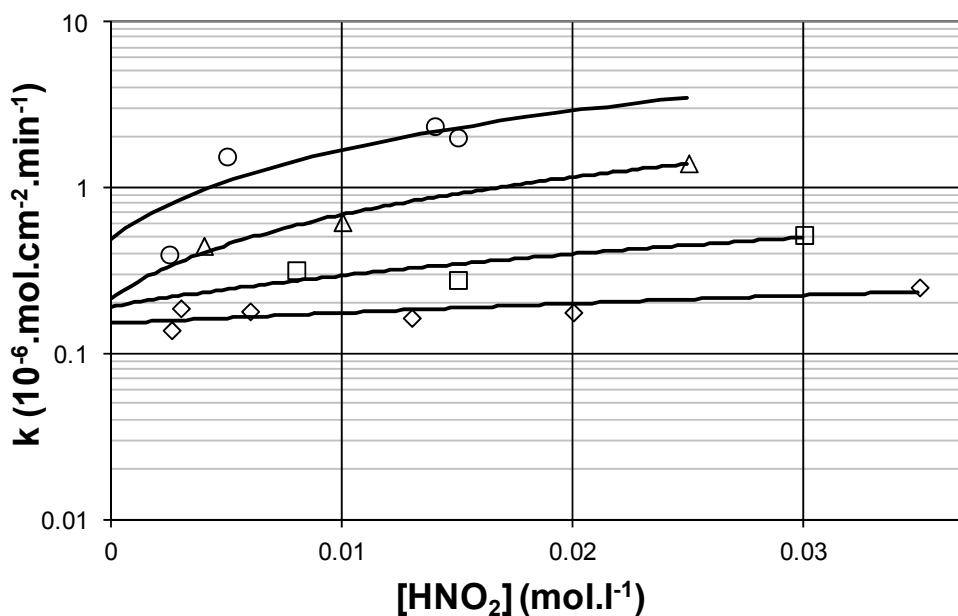


Figure 38: Effect of nitric and nitrous acid upon dissolution rate constant at 40 °C,  $\diamond$  4 mol.l<sup>-1</sup>,  $\square$  5 mol.l<sup>-1</sup>,  $\triangle$  6 mol.l<sup>-1</sup>,  $\circ$  7 mol.l<sup>-1</sup>

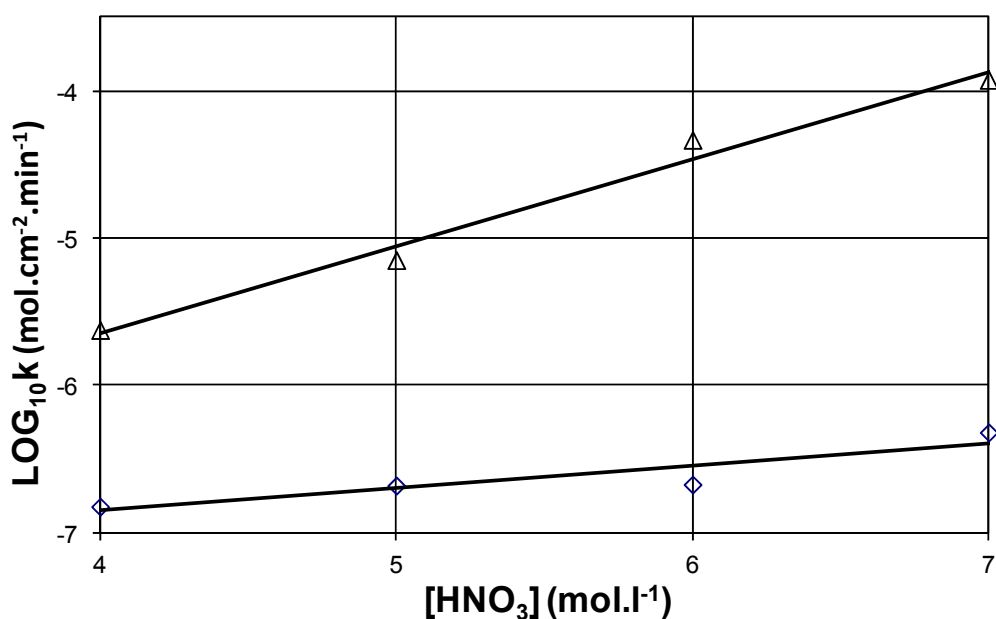
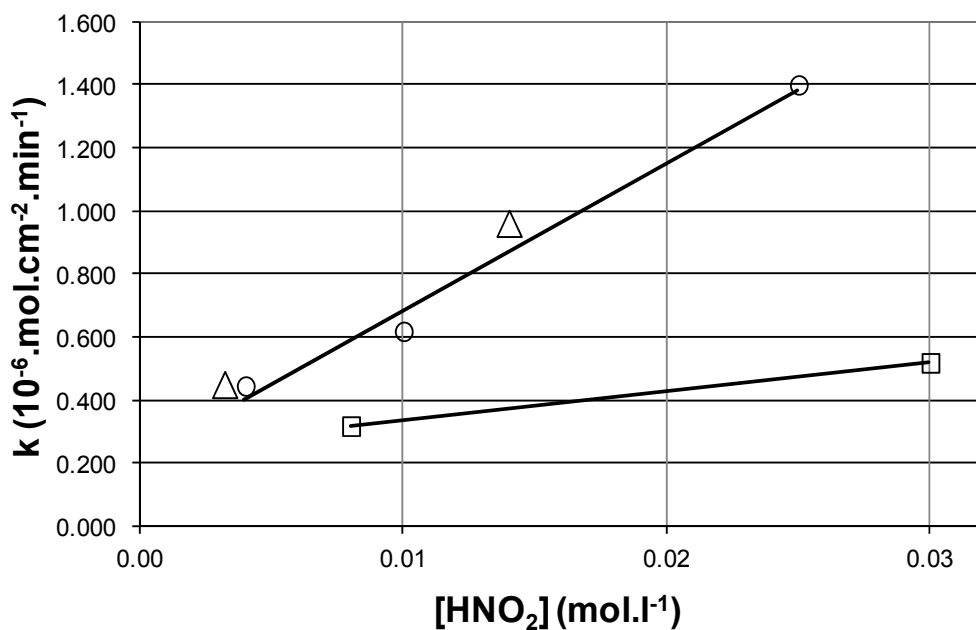


Figure 39: Nitric acid and nitrate dissolution rate constants at 40 °C,  $\triangle$  nitrous acid reaction (gradient),  $\diamond$  nitrate reaction (intercept)

Two additional experiments were undertaken to separate the influences of pH and nitrate concentration. To achieve this the dissolution rates in 5 and 6 mol.l<sup>-1</sup> nitric acid have been compared with 1 mol.l<sup>-1</sup> potassium nitrate in 5 mol.l<sup>-1</sup> nitric acid (6 mol.l<sup>-1</sup> nitrate). It can be seen from the results in **Figure 40** that the overall nitrate concentration determines the rate rather than the nitric acid concentration.



**Figure 40: Effect of added potassium nitrate upon dissolution rate constant at 40 °C, □ 5 mol.l<sup>-1</sup> HNO<sub>3</sub>, ○ 6 mol.l<sup>-1</sup> HNO<sub>3</sub>, △ 5 mol.l<sup>-1</sup> HNO<sub>3</sub>+ 1 mol.l<sup>-1</sup> KNO<sub>3</sub>**

The Arrhenius plot in 5 mol.l<sup>-1</sup> nitric acid (with MOx powder added and no sodium nitrite) indicates an observed activation energy of 74 kJ.mol<sup>-1</sup> above **Figure 41**. The determined activation energy reflects the dissolution phenomena observed, but is due to a composition of both the nitric acid and nitrous acid dissolution reaction routes. Experiments dissolving uranium dioxide pellets in nitric acid have previously reported activation energies of 62±5[34] and 66[45] kJ.mol<sup>-1</sup>. The experiments in this work show a more pronounced effect of temperature.

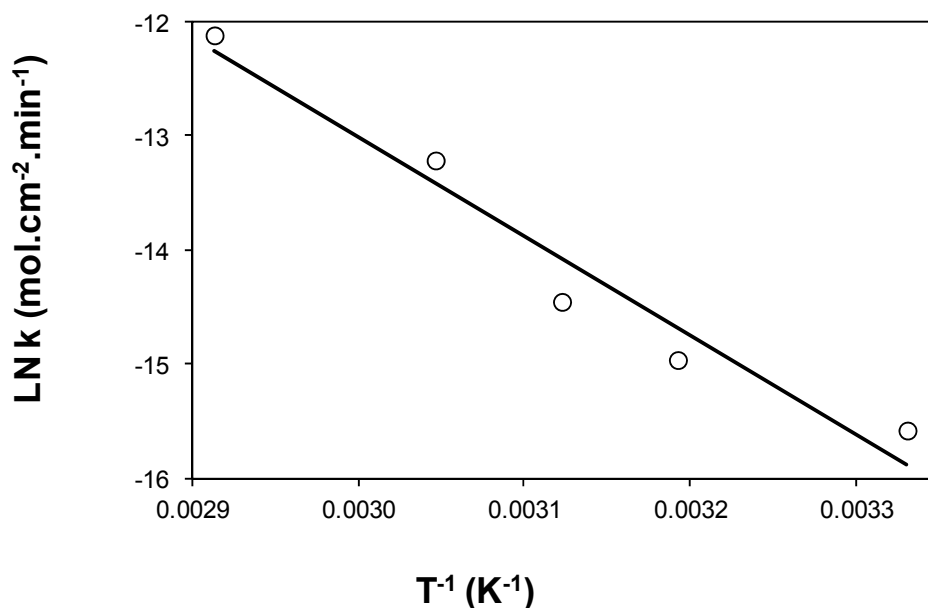


**Figure 41: Arrhenius plots without addition of sodium nitrite in 5 mol.l<sup>-1</sup> HNO<sub>3</sub>**

It is recognised that the temperature dependence is a composite of two reactions with nitrous and nitric acids. For this reason additional experiments in 4 mol.l<sup>-1</sup> nitric acid with varying amounts of sodium nitrite added for temperatures between 27 and 70 °C. These experiments examining the relative rates of the nitric and nitrous acid reactions are shown in **Figure 42**. These experiments show that increasing the nitrous acid concentration increases the dissolution rate for both the nitric and nitrous acid dissolution reactions. There again appears to be no detectable effect of temperature between 27 and 40 °C. Using the intercept and gradients results in Arrhenius plots for the nitric and nitrous acid reactions, **Figure 43**. Above 40 °C the nitrate reaction has an activation energy of 80 kJ.mol<sup>-1</sup>, which is similar to 79.5 kJ.mol<sup>-1</sup> determined for uranium dioxide[48]. The nitrous acid Arrhenius plot has no observable effect between 27-40 °C and a large gradient between 40-70 °C (150 kJ.mol<sup>-1</sup>). The activation energy determined for uranium dioxide powders (70-90 °C) has an activation energy of 36.8 kJ.mol<sup>-1</sup> was previously reported.[48]. The large difference in determined activation energy and that reported for uranium dioxide could be due to different in temperature, which may could be due to (i) the presence of an autocatalytic mechanism or (ii) a reaction rate limit that occurs in the moderate and high temperature regions (not observed in this study). Previous experiments studying the effect of temperature in unstirred systems have shown that

linear Arrhenius plots can be obtained[34]. This could be suggests that under the low temperatures (24 °C) the rate of the nitrous acid autocatalysis reaction is less than the nitric acid reaction route. In the middle temperatures region the activation energy for the autocatalytic nitrous acid dissolution route is observed. At higher temperatures (above those studied in this work) there could be a change in the factor determining the dissolution rate (e.g. mass transfer limitation).

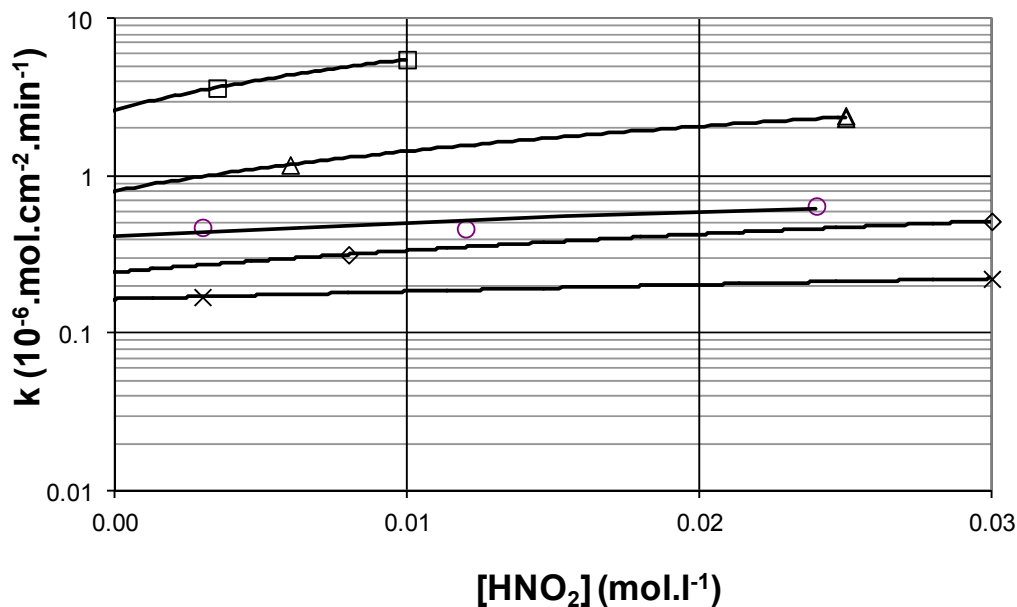
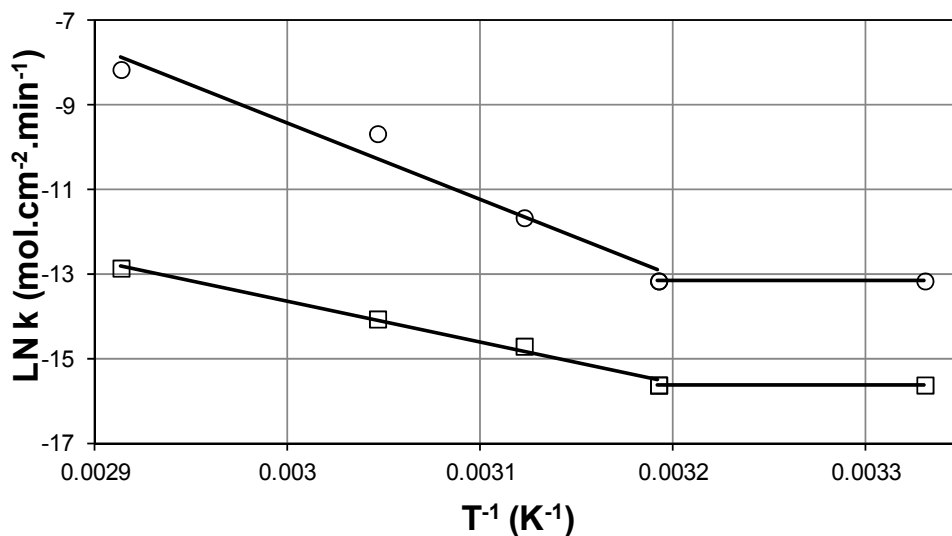
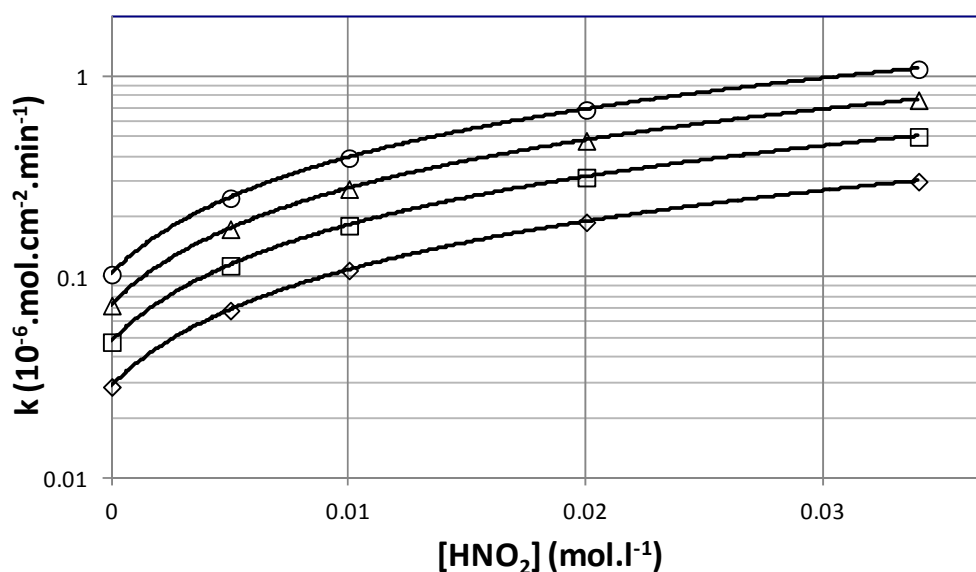


Figure 42: Effect of temperature and nitrous acid upon the dissolution rate constant in 5 mol.l<sup>-1</sup> HNO<sub>3</sub>, x 27 °C , ◇ 40 °C, ○ 47 °C , △ 55 °C, □ 70 °C



**Figure 43: Arrhenius plots for nitrous acid and nitrate reactions in 5 mol.l<sup>-1</sup> HNO<sub>3</sub>, O nitrous acid reaction (slope), □ nitrate reaction (intercept)**

Comparison of the effect of nitric and nitrous acid concentration between this work (Figure 35) and those calculated for uranium dioxide[48] (Figure 44) clearly show the calculated dissolution rates for uranium dioxide are approximately an order of magnitude lower than those determined in this study. The larger effect of nitrous acid may be due to the lower temperature used in this study (40 °C) compared to the earlier uranium dioxide study (80 °C).[48]



**Figure 44: Effect of nitric and nitrous acid upon calculated dissolution rate constant of uranium dioxide at 40 °C, ◇ 4 mol.l<sup>-1</sup>, □ 5 mol.l<sup>-1</sup>, △ 6 mol.l<sup>-1</sup>, ○ 7 mol.l<sup>-1</sup>**

Comparison of the effect of nitrous acid concentration and temperature from this work (**Figure 41**) and that calculated for uranium dioxide[48] (**Figure 45**) shows the dissolution rates approximately one order of magnitude faster compared to those published for uranium dioxide, but the MOx experiments show greater gradients.

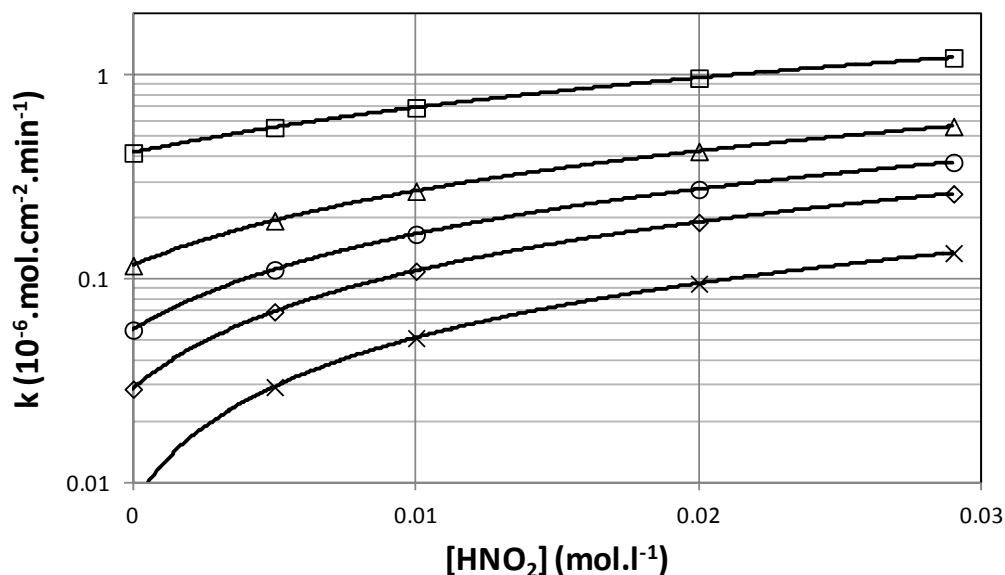


**Figure 45: Effect of temperature and nitrous acid upon the calculated dissolution rate constant of uranium dioxide in 5 mol.l<sup>-1</sup> HNO<sub>3</sub>, × 27 °C , ◇ 40 °C, ○ 47 °C ,△ 55 °C, □ 70 °C**

#### 4.6.4. Summary

Experimental studies investigating the role of nitrous acid in the dissolution of ~5 %Pu thermal MOx reveal similar kinetics compared to that observed for pure uranium dioxide. Experiments with 4-7 mol.l<sup>-1</sup> nitric acid with varying concentration of nitrous acid show there are two reaction routes, one dependent upon nitrate concentration the second dependent upon nitrous acid and nitrate concentrations, (5). The effect of temperature upon the nitrate, nitrous acid reaction indicates an overall activation energy of 80 kJ.mol<sup>-1</sup> for the nitrate reaction, which is similar to that previously observed for the dissolution of pure uranium dioxide (80 kJ.mol<sup>-1</sup>) under higher temperature conditions. There is a more complex temperature dependence of the nitrous acid influence. At low temperatures (27-40 °C) little effect of temperature is observed, at higher temperatures (40-70 °C) a high activation energy (150 kJ.mol<sup>-1</sup>) has been observed, perhaps due to the lower temperature conditions used compared to other studies. The dissolution of uranium dioxide at temperatures greater than used in this study have observed an activation

energy of 37 kJ.mol<sup>-1</sup> [48]. This clearly shows a difference between uranium dioxide (at 80 °C) and MOx at lower temperatures, which could be due to (i) the presence of an autocatalytic mechanism or (ii) a reaction rate limit has occurred in the moderate and high temperature regions for uranium dioxide.

$$\phi = k_1[HNO_3^-]^{2.3} e^{\frac{-80000}{RT}} + k_2[HNO_3]^{2.3}[HNO_2] e^{\frac{-150000}{RT}} \quad (5)$$

#### ***4.7. Dissolution kinetics of 5 % plutonium content mixed oxide pellets in nitric acid***

It is planned that this paper will be submitted to Industrial Engineering Chemistry

##### ***4.7.1. Introduction***

Mixed uranium plutonium oxide (MOx) is a commercial thermal reactor fuel which uses plutonium recovered from the reprocessing of uranium based fuels. After irradiation MOx fuel can be stored for transfer to a geological disposal facility or stored on an interim basis prior to reprocessing. The key difference between the reprocessing of uranium oxide and MOx fuels is the head-end flowsheet. There are two main questions when designing MOx dissolver cycles:

1. How quickly does the bulk of the MOx fuel dissolve?
2. How can the dissolution of plutonium-rich residues be optimised?

The dissolution of uranium dioxide[48, 49] and MOx [Section 4.4 and 4.6] powders and pellets[34, 45, 46] is known to occur via a nitrate-initiated autocatalytic dissolution mechanism involving nitrous acid as the key species. It is also known that as the plutonium content of MOx is increased the dissolution rate decreases[53] [203]. The dissolution rate has been observed to decrease rapidly above 25-40 % Pu/(U+Pu).

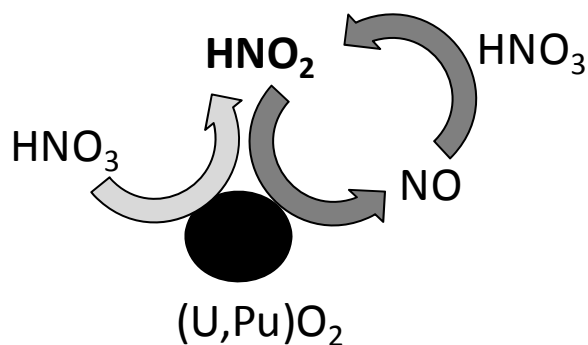


**Figure 46: Nitrous acid auto-catalytic cycle**

The aim of these dissolution tests is to investigate whether nitrous acid also has a dominant role in dissolving MOx pellets, by observing the dissolution rate under defined conditions. To assess the role of nitrous acid, experiments aimed to increase or decrease the nitrous acid concentration, through the addition of sodium nitrite or stirring/sparging the solution will be reported.

#### **4.7.2. Experimental**

##### **4.7.2.1. Materials**

Mixed uranium/plutonium dioxide pellets with 4.4 wt% plutonium content (5.0 % Pu/(U+PU)) prepared using the Short Binderless Route (SBR) by Sellafield Ltd at the Sellafield MOx Plant (SMP) were obtained.[12] The cylindrical pellets had an average diameter of 10.35 mm and 12.60 mm length, mass of 11.02 g corresponding to a density of  $10.4 \text{ g.cm}^{-2}$ , corresponding to 94.7 at% of theoretical density (%T.D.). The pellets were used in dissolution experiments without any further treatment.

##### **4.7.2.2. Apparatus and methodology**

All experiments were carried out in a shielded high-integrity alpha containment glove box. The dissolution apparatus was similar to the setup used in previous studies [Section 4.4 and 4.6]. This included a flanged culture vessel with Pt-100 thermometer, a Liebig condenser and a magnetic follower ( $30 \times 6 \text{ mm}$ ). The condenser cooling circuit was based on a recirculating chilled water supply (Haake) that was placed outside of the glovebox but

connected to the internals via pipework. UV-Vis measurements were carried out with fibre optic system using custom fibre optic feedthroughs (Hellma).

Dissolution experiments were carried out in a thermostatted stirred (200 rpm unless stated) vessel with pellet stand in 350 ml nitric acid, a solution of 5 mol.l<sup>-1</sup> sodium nitrite (when used) and a MOx pellet addition initiated the experiment. 4 ml samples were taken periodically, typically every 30 min.

#### 4.7.2.3. Analysis methods

The determination of the uranium and plutonium concentrations used direct UV-Vis spectroscopy. Preparation of a multi-component UV-Vis calibration used solutions of different nitric acid concentrations for solutions containing a mixed uranium and plutonium solution.

#### 4.7.2.4. Dissolution rate interpretation

The pellet dissolution rates follow an 'S' shaped profile typical for autocatalytic mechanisms, due to generation of the autocatalytic species nitrous acid, which initiates the dissolution,[34] and due to changes in the effective surface area of the pellet.[30, 34] All dissolution curves were fitted using a fragmentation model[31] (1), where  $f$  is the fragmentation constant and  $\lambda$  is the inverse rate constant (min). Dissolution rates ( $k$ , mg.cm<sup>-2</sup>.min<sup>-1</sup>) have been calculated by solving (3) for the dissolution time at 1 % dissolution ( $W_d/W_o = 0.01$ ), this corresponds to a small fraction so a geometric surface area can be assumed and converting the units using the average pellet mass ( $m_{\text{pellet}} = 11.02$  g) and surface area ( $S_a = 5.78$  cm<sup>2</sup>) (2).

$$\frac{W_d}{W_o} = \left( \frac{f}{1-f} \right) \left( \frac{1}{f} - 1 + \exp\left(-\frac{t}{\lambda}\right) \right) - \frac{\exp\left(-\frac{ft}{\lambda}\right)}{f} \quad (1)$$

$$k = \frac{0.882 \frac{W_d}{W_o} m_{\text{pellet}}}{t_{W_d/W_o} S_a} \quad (2)$$

### 4.7.3. Results and Discussion

#### 4.7.3.1. Multi-component UV-Vis calibration

UV-Vis spectra of a solution containing 5.2 g l<sup>-1</sup> uranium and 0.26 g l<sup>-1</sup> plutonium in 6-14 mol l<sup>-1</sup> are shown in **Figure 47**. These spectra show the uranium(VI) and plutonium(IV) absorption spectra changes with nitric acid concentration.[204] However, the absorbance, due to uranium and plutonium, does not change significantly at 440 nm in the range of these experiments, Figure 47. Quantification can therefore be carried out using equation (3). The extinction coefficient for plutonium(IV), however, does change significantly with nitric acid concentration (**Figure 47**), however as as the uranium and plutonium dissolves together no correction of the 440 nm absorbance is needed.

$$A_{440nm} - A_{522nm} = 0.0397l[U + Pu] \quad (3)$$

where A is absorbance at wavelength or baseline (BL) corrected and l is the path length (cm).

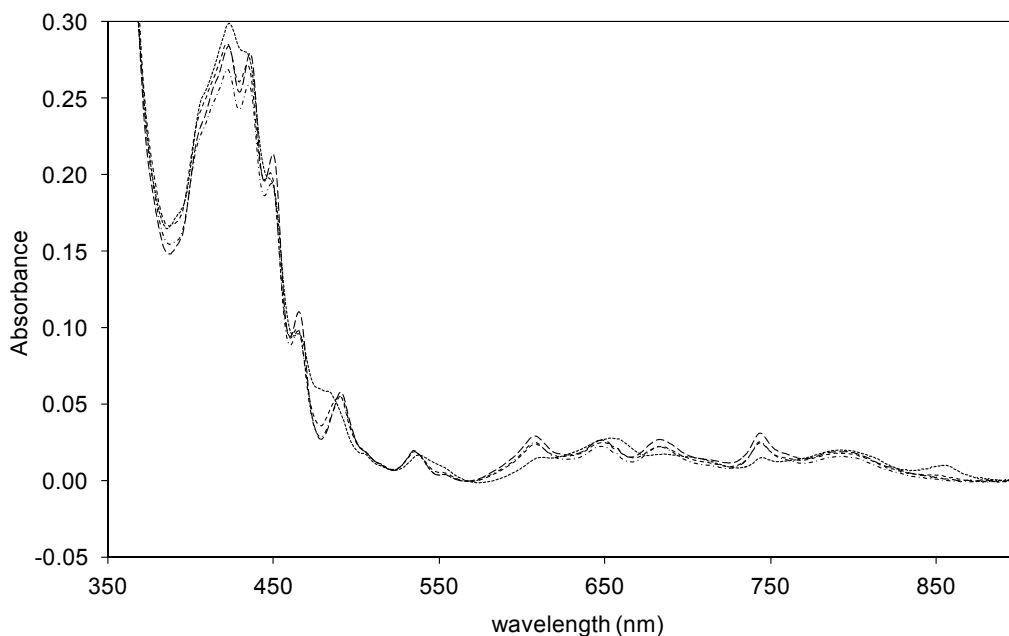


**Figure 47: Baseline corrected absorption spectra for U+Pu solution for --- 8 mol.l<sup>-1</sup>, -- 10 mol.l<sup>-1</sup>, -.- 12 mol.l<sup>-1</sup>, — 14 mol.l<sup>-1</sup> HNO<sub>3</sub>**

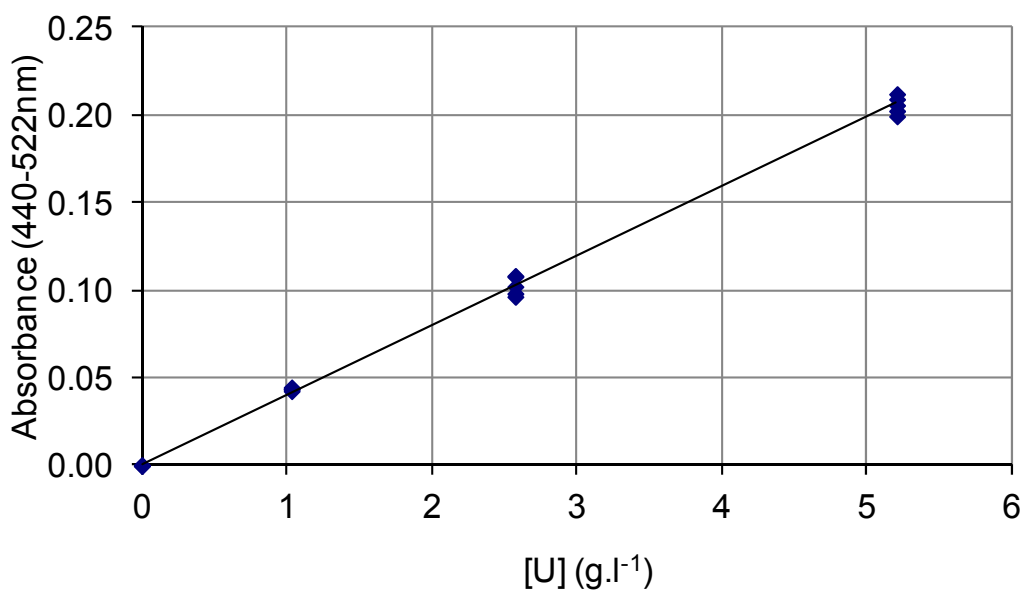


**Figure 48: Beer Lambert plot for uranium in 6-12 mol.l<sup>-1</sup> HNO<sub>3</sub>**

#### **4.7.3.2. Effect of cell conditions**

The effect of cell variations upon the dissolution curves in 10 mol l<sup>-1</sup> at 80 °C is shown in **Figure 37** and **Figure 45**. The dissolution rates are in the following order: no pellet stand > pellet stand ~ 200 rpm with pellet stand > 200 rpm and sparged with pellet stand > 900 rpm with pellet stand. With the pellet stand present the effect of cell conditions is reasonable, as stirring and

sparging are known to decrease the contribution of the 'nitrous acid' reaction route. Stirring at 200 rpm has no apparent effect on dissolution rate, reflecting the rapid rates of 'nitrous acid' autocatalytic reaction under the high nitric acid concentrations and temperature. The dissolution rate of the pellet on the dissolver vessel base (without pellet stand or stirring) may be higher than that observed with a pellet stand because of a higher temperature of the pellet through additional conductive heating. Varying the stirring speed (200 vs 900 rpm) in 10 mol.l<sup>-1</sup> nitric acid at 110 °C has no influence on the observed rate (**Figure 35**). However, it is very different compared to the rate observed at 80 °C (**Figure 45**) and may suggest the role of nitrous acid is much smaller at higher temperatures.

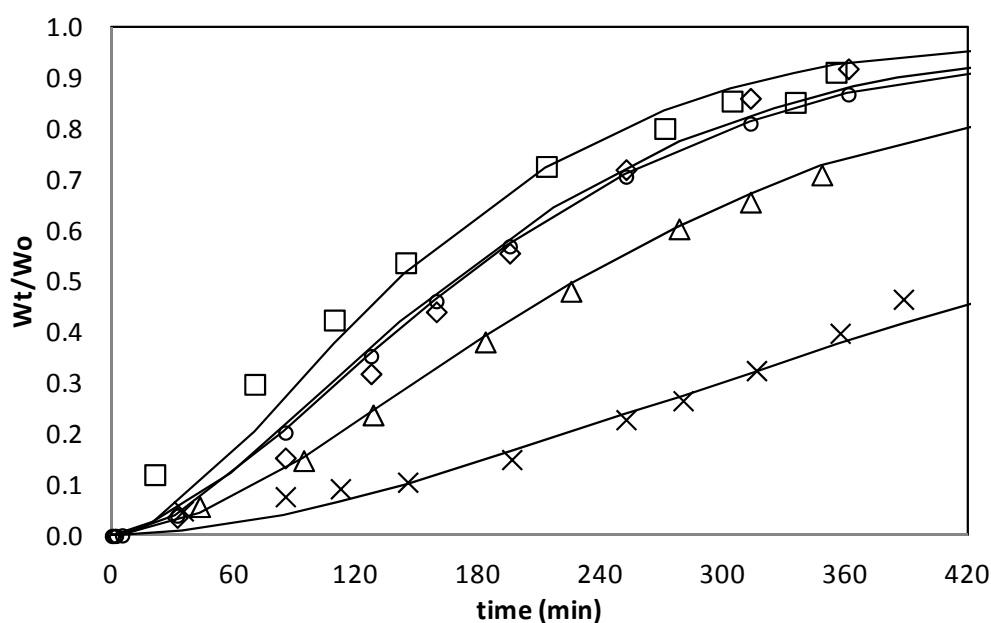


**Figure 49: Effect of dissolver cell conditions, 10 mol.l<sup>-1</sup> HNO<sub>3</sub> 80 °C, □ unstirred no pellet stand ( $f = 1.00$ ,  $\lambda = 83.6$ ), ○ unstirred with pellet stand ( $f = 1.00$ ,  $\lambda = 99.0$ ), ◇ 200 rpm with pellet stand ( $f = 1.00$ ,  $\lambda = 102$ ), △ 200 rpm with pellet stand sparged 250 ml.min<sup>-1</sup> ( $f = 1.00$ ,  $\lambda = 136$ ), × 900 rpm with pellet stand ( $f = 1.00$ ,  $\lambda = 273$ )**

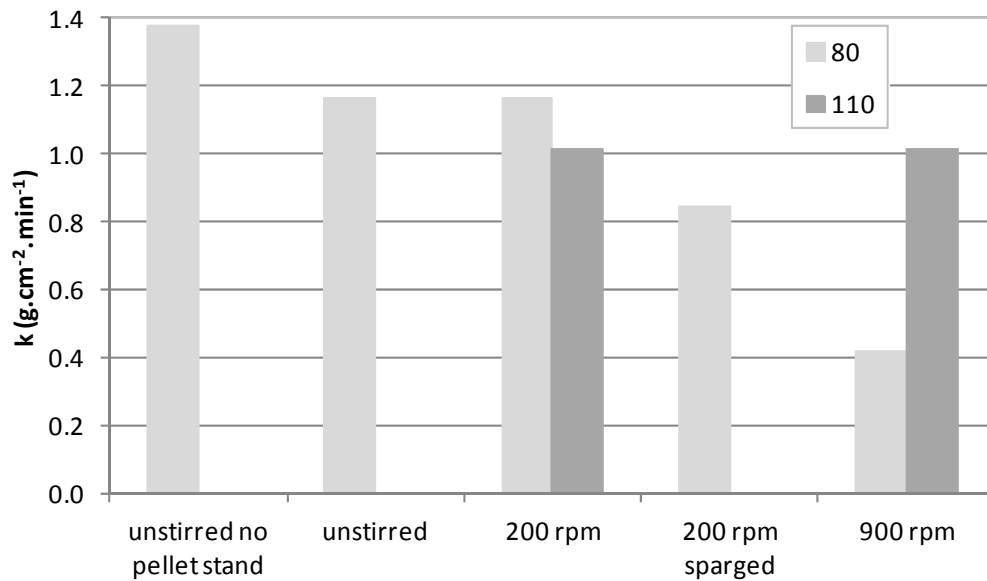


Figure 50: Effect of cell conditions, ■ 80 °C, ■ 110 °C

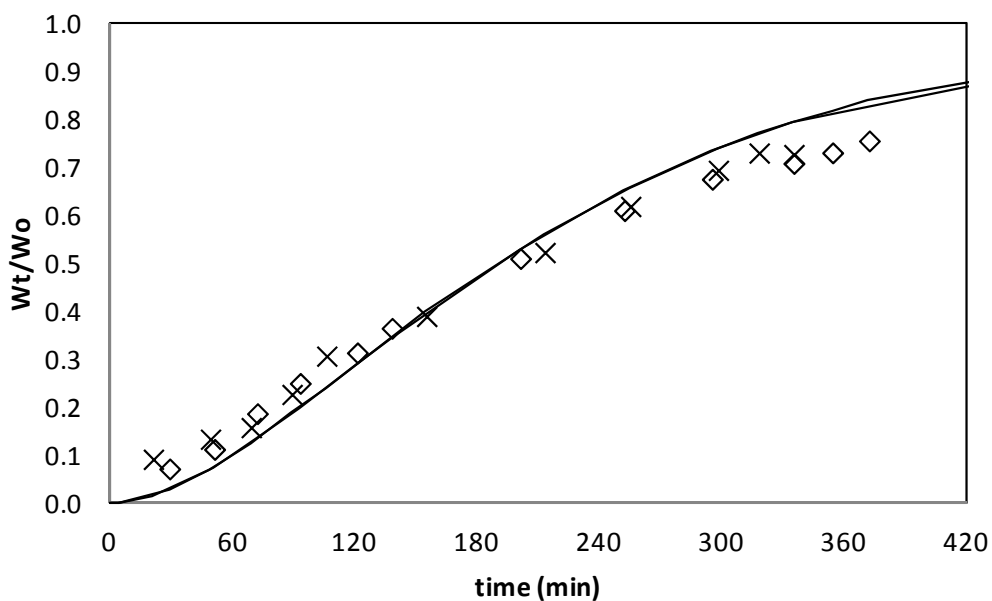
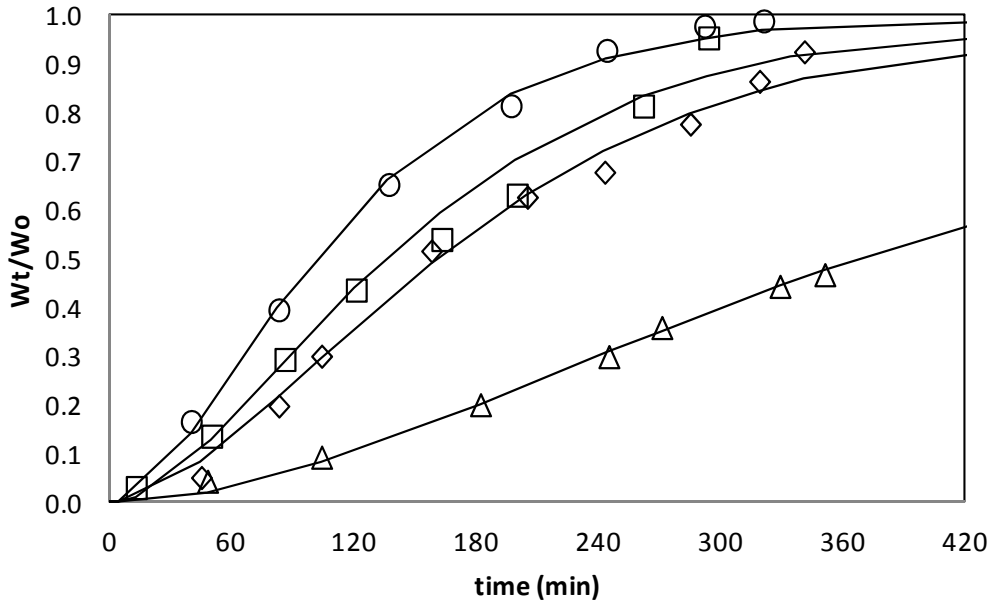


Figure 51: Effect of dissolver cell conditions, 10 mol.l<sup>-1</sup> HNO<sub>3</sub>, 110 °C, ◇ 200 rpm with pellet stand (f = 1.00, λ = 113), × 900 rpm with pellet stand (f = 1.00, λ = 113)

#### 4.7.3.3. Effect of nitric and nitrous acid concentration

The increase of nitric acid concentration (8-14 mol.l<sup>-1</sup>) at 80 °C leads to an increase in dissolution rate, **Figure 39**. Based on these results, it is clear that the fragmentation model provides a good method of simulating the dissolution

curves. The dissolution rate increases between 8 and 12 mol.l<sup>-1</sup> nitric acid for 60, 70 and 80 °C, but there appears to be little increase in dissolution rate between 12 and 14 mol.l<sup>-1</sup> nitric acid, **Figure 53**, which suggests a mass transfer limit may have been reached. The dissolution rate is observed to increase as a function of [HNO<sub>3</sub>]<sup>1.7</sup>, but less than observed for uranium dioxide[48] dependent upon [HNO<sub>3</sub>]<sup>2.3</sup>,, but similar to 30 %Pu/(U+Pu) MOx ([HNO<sub>3</sub>]<sup>1/7</sup>)[183]. The effect of addition of 3.5 ml of 5 mol.l<sup>-1</sup> sodium nitrate, equivalent to 0.05 mol.l<sup>-1</sup> if complete absorption occurs, causes a small increase in dissolution rate, **Figure 53**. Whilst there is a small increase in dissolution rate for 8 and 10 mol.l<sup>-1</sup> nitric acid, however, decreases in dissolution rate are observed at 12 mol.l<sup>-1</sup> nitric acid. This shows that nitrous acid does play a role in determining the 'S' shape dissolution curve. However, it also shows that at higher nitric acid concentration the speciation or autocatalyst role may change.



**Figure 52: Effect of HNO<sub>3</sub> concentration at 80 °C upon dissolution rate, O 14 mol.l<sup>-1</sup> (f = 1.00, λ = 60.5), □ 12 mol.l<sup>-1</sup> (f = 1.00, λ = 81.2), ◇ 10 mol.l<sup>-1</sup> (f = 1.00, λ = 95.9), △ 8 mol.l<sup>-1</sup> (f = 1.00, λ = 219)**

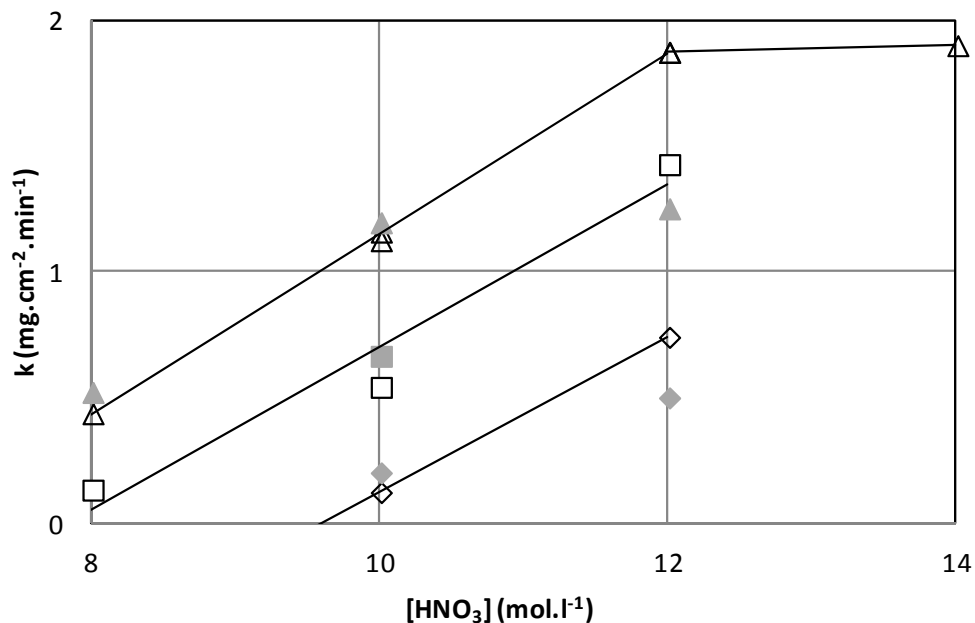


**Figure 53: Effect of HNO<sub>3</sub> concentration at different temperatures:**  
 $\Delta$  80 °C,  $\square$  70 °C,  $\diamond$  60 °C, outline - no NaNO<sub>2</sub> added, shaded - NaNO<sub>2</sub> added,

#### 4.7.3.4. Effect of temperature

Increasing the temperature increases dissolution rate up to 90 °C; higher temperatures result in rates plateauing and decreasing, **Figure 41** and **Figure 42**. The activation energy determined depends upon the temperature region selected, which is known to be due to two mechanisms[48, 49] **REFs-Maher2**,. For the temperature regions shown the activation energies are 78, 50 and 45 kJ.mol<sup>-1</sup> for 8, 10 and 12 mol.l<sup>-1</sup> respectively. Selecting larger temperature regions and excluding data before the plateau results in a high apparent activation energy at higher temperatures, likely reflecting nitrous acid induction periods. In contrast, the apparent small activation energies determined for 10 and 12 mol l<sup>-1</sup> nitric acid are closer to the 38 kJ mol<sup>-1</sup> value determined for uranium dioxide[48]. This suggests that the dominant reaction under these conditions is the autocatalytic nitrous acid mechanism observed for the powders. The reduction in dissolution rate above 90 °C has been observed by other authors[34] and is due to high decomposition rates of nitrous acid[49] and perhaps reduction in apparent surface area due to the formation of bubbles on the pellet surface. The decomposition of nitrous acid also explains the overestimation of the fragmentation model for above 50 % dissolution for the higher temperature, **Figure 41**.

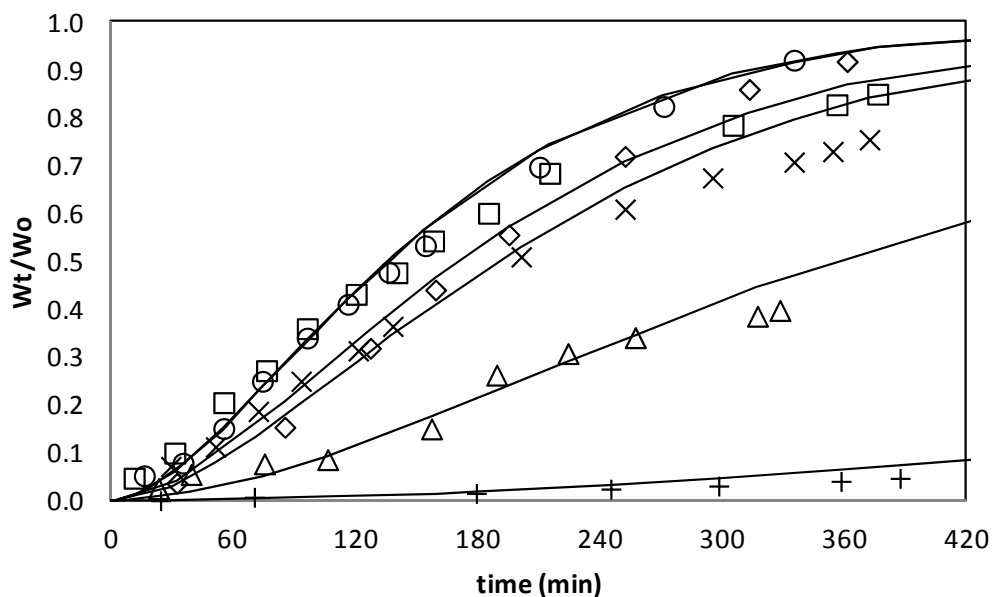


Figure 54: Effect of temperature for 10 mol.l<sup>-1</sup> HNO<sub>3</sub>, ○ 90 °C (f = 1.00, λ = 81.4), □ 100 °C (f = 1.00, λ = 81.0), ◇ 80 °C (f = 1.00, λ = 102), × 110 °C (f = 1.00, λ = 113), △ 70 °C (f = 1.00, λ = 211), + 60 °C (f = 1.00, λ = 902)

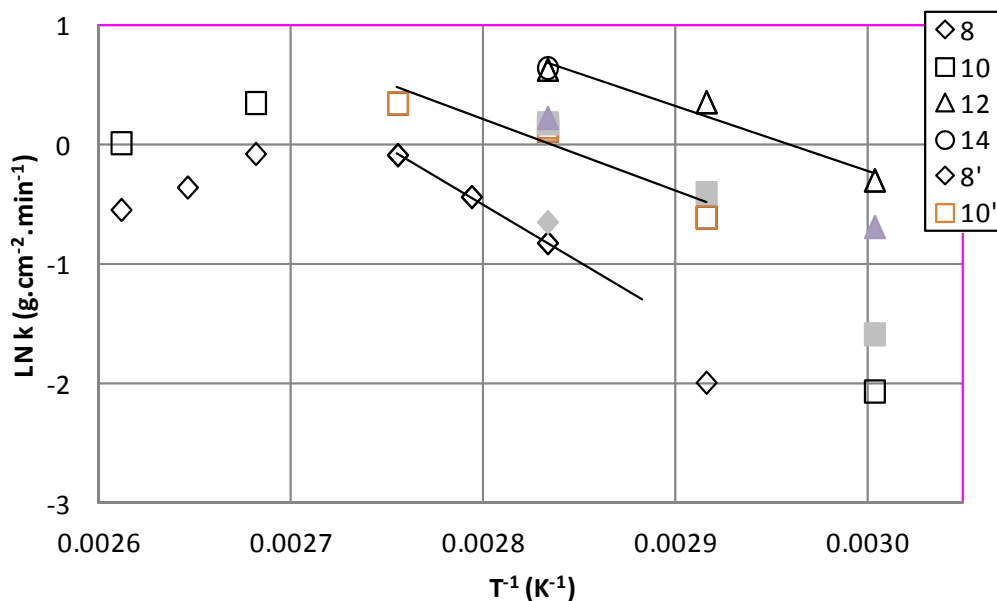


Figure 55: The effect of temperature for different HNO<sub>3</sub> concentrations, ○ 14 mol.l<sup>-1</sup>, △ 12 mol.l<sup>-1</sup>, □ 10 mol.l<sup>-1</sup>, ◇ 8 mol.l<sup>-1</sup>, (grey solid points with NaNO<sub>2</sub> added),

The addition of sodium nitrite, equivalent to 0.05 mol.l<sup>-1</sup> nitrous acid (assuming complete absorption occurs), increases the dissolution rate in 10 mol.l<sup>-1</sup> nitric acid at 60, 70 and 80 °C and is shown in Figure 40 and Figure 42 (solid, grey points addition of nitrite).

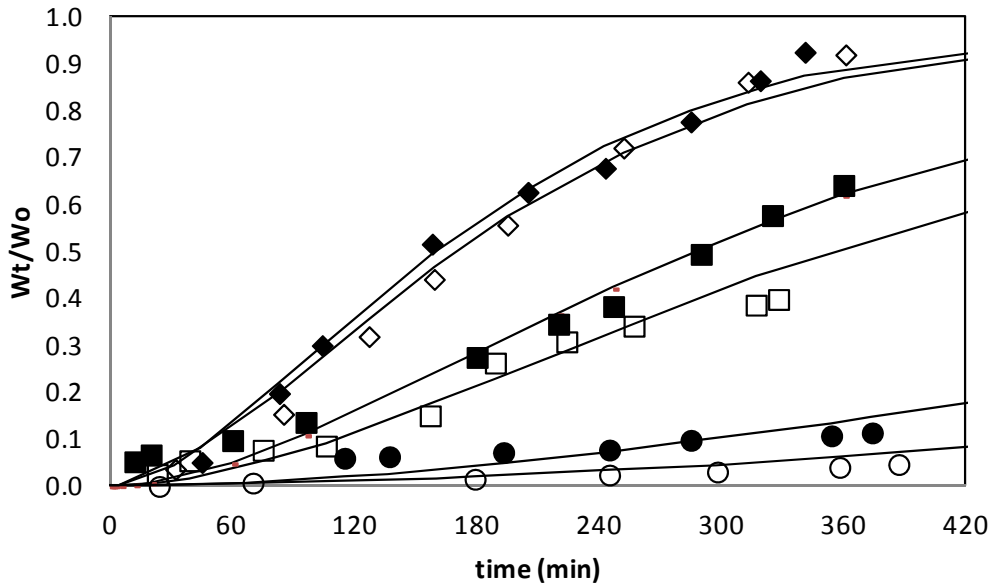
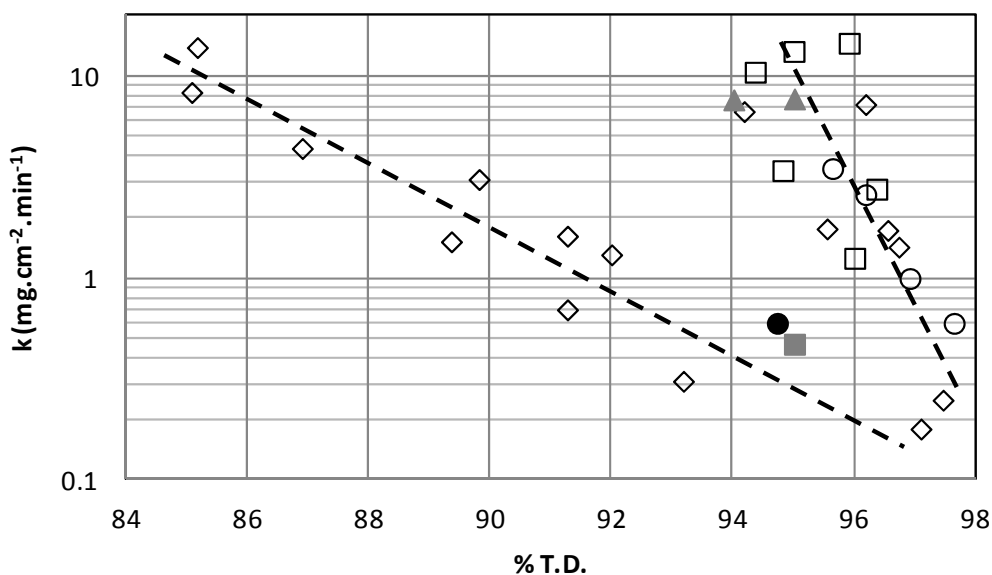


Figure 56: Effect of temperature in 10 mol.l<sup>-1</sup> HNO<sub>3</sub> with (solid filled) and without (outline) added sodium nitrite, ◆ 80 °C (f = 1.00, λ = 95.9), ■ 70 °C (f = 1.00, λ = 172), ● 80 °C (f = 1.00, λ = 560)

#### 4.7.3.5. Comparison of dissolution rates with previously published results

Several workers[34, 74] have recognised that the dissolution rate of uranium dioxide pellets is dependent upon their density (or percentage of theoretical density, %T.D.). This is due to a reduction in the open and closed porosity with increasing density. It can be envisaged that this can reduce the rate of dissolution progression through the pellet structure. Figure 57 compares the dissolution rate for uranium dioxide pellets at 6 mol.l<sup>-1</sup> nitric acid and MOx pellets at 10 mol.l<sup>-1</sup>. The available data for uranium dioxide falls on one of two trend lines. The mechanically blended MOx pellets fit the lower trend and the co-precipitated MOx pellets fit the upper trend. The dissolution rates of this work SBR MOx pellets in 10 mol.l<sup>-1</sup> is similar to uranium dioxide and mechanically blended MOx pellets in 6 mol.l<sup>-1</sup> nitric acid, this suggests 5 %Pu/JM MOx pellets dissolve more slowly compared to uranium dioxide. The explanation for the two separate trend lines is not understood.



**Figure 57: Effect of density upon dissolution rate, O Taylor UO<sub>2</sub>, ◇ Uriarte (ORNL) UO<sub>2</sub>, □ Uriarte (NUMEC) UO<sub>2</sub>, ■ Uriarte 5 % Pu/(U+PU) Mechanical blended MOx ▲ Uriarte 0.5 % and 5 % Pu/(U+PU) Co-precipitated MOx, ● This work 5 % Pu/(U+PU) 110 °C 10 mol.l<sup>-1</sup> HNO<sub>3</sub>**

#### 4.7.4. Summary

The dissolution rate of MOx pellets containing 5 %Pu/(U+PU) in nitric acid under various nitric acid concentrations and temperature with and without added sodium nitrite has been studied. The dissolution rate has been observed to increase between 8 and 12 mol.l<sup>-1</sup> nitric acid, but dissolution rates are similar at 12 and 14 mol l<sup>-1</sup> nitric acid concentrations. The apparent activation energy has been observed to depend on the nitric acid concentration and the temperature range selected. Between 70-90 °C and 10 and 12 mol.l<sup>-1</sup> nitric acid concentrations an apparent activation energy of 45-50 kJ.mol<sup>-1</sup> is observed, which is consistent with the activation energy for the 'nitrous acid' reaction route observed for uranium dioxide[48] and 5 %Pu/(U+PU) MOx [Section 4.6]. These results support the nitrate initiated, nitrous acid catalysed dissolution mechanism. Experiments adding nitrite show an increase in dissolution rate for 8 and 10 mol.l<sup>-1</sup> nitric acid, but a decrease in dissolution rate for 12 mol.l<sup>-1</sup> nitric acid. Experiments stirring and sparging the dissolving solution show that experiments that stirring at 110 °C causes less reduction in dissolution rate compared to 80 °C, consistent with a increasing involvement of mass-transfer control.

#### **4.8. Summary of direct dissolution of oxides in nitric acid**

Uranium dioxide and MOx with low plutonium contents, like many other materials, dissolve in nitric acid via oxidation involving a complex autocatalytic mechanism. The material surface area is a fundamental factor in defining dissolution rate. The dissolution mechanism occurs via nitrate reduction, though both direct and indirect nitrate reaction routes. As in many circumstances the reaction kinetics is dominated by the indirect or autocatalytic mechanism. This makes dissolution susceptible to factors affecting the concentration of nitric acid reduction products (nitrous acid) and the concentration gradient close to the material surface. For this reason the following factors affect the dissolution rate; bulk solution phase nitrous acid, agitation and sweep gases/solution sparging. The relative rates of direct and indirect nitrate reduction are dependent upon the nitrate and nitrous acid concentration, as well as temperature. Temperature also affects the stability of nitrous acid, as at elevated concentrations there is an increase in the decomposition rate. The decomposition is most pronounced around boiling conditions, where the boiling action effectively self-sparges the nitric acid reduction products from the solution and potentially decreases the materials effective surface area.

As the plutonium content of MOx increases the material becomes increasingly plutonium oxide like, which is not oxidised by nitric acid or its reduction products. The results of literature experiments where MOx dissolution tests showing the reduction in the extent of MOx dissolved[53], can be explained by the viability of nitrate and its reduction products towards MOx. At high plutonium contents, which are inevitably present in MOx due to current mechanical manufacturing methods, plutonium oxide rich residues will be produced. To dissolve these the plutonium rich residues literature and thermodynamic calculations studies have shown that reducing or oxidising agents stronger than nitric acid and its reducing products can be used.

These experiments have demonstrated that the dissolution of uranium dioxide and MOx with low plutonium contents,  $\sim 5\% \text{U}/(\text{U}+\text{Pu})$  dissolve using similar chemistry and at similar rates. This is relevant to the design of process for the industrial dissolution of MOx for further reprocessing.

The design of industrial dissolution cycles for MOx can be considered to include two parts, 1) optimisation of the rate and extent of MOx, that can be dissolved in nitric acid and 2) dissolution of plutonium-rich particles. The

current generation of MOx dissolution cycles (e.g. Areva UP2-800 and UP3) uses only method 1. However, increased focus on safety will lead to a requirement to remove the plutonium-rich particle. This will lead to the reconsideration of techniques to dissolve plutonium dioxide, e.g. mediated processing using silver.

## 5. APPLICATION OF MEDIATED ELECTROCHEMICAL OF SILVER(II) FOR FUEL DISSOLUTION

### 5.1. *Summary of literature relating to mediated electrochemical dissolution*

#### 5.1.1. *Review of the development leading MEO dissolution processes for plutonium dioxide*

Plutonium dioxide is notoriously difficult to dissolve in aqueous solutions, particularly low surface area material which has been calcined to high temperatures. The kinetics of dissolution in nitric acid are kinetically slow and plutonium dioxide has limited thermodynamic solubility [178] [Section 4.7.1]. An early common method for the dissolution of this materialised mixed nitric acid – fluoride solutions [196]. This method has the disadvantages that:

- Dissolution is slow, particularly with low specific activity material,
- Plutonium solution concentrations are limited due by the solubility of plutonium(IV) fluoride. This necessitates the use of relatively large volumes of dissolution liquor.
- Fluoride complexation of plutonium and fission products interference with or complicate separation processes, such as solvent extraction.
- Fluoride is corrosive to stainless steel.
- The above factors often necessitate the addition of fluoride complexants such as aluminium nitrate or borate to increase plutonium solubility, allow efficient separation processes and reduce dissolver/downstream corrosion. This increases waste volumes and complicates waste management.

During the development of the nitric acid - fluoride based dissolution method it was recognised that there were many benefits to the oxidation of plutonium(IV) to plutonium(VI) during the dissolution [205]. This increased the free fluoride, i.e. as less is complexed by plutonium(IV), allowing reduced fluoride concentrations to be used that increases the dissolution rate, reducing corrosion and easing separation and waste management issues. However, it was also recognised that the dissolution rate had a dependence upon the cerium(III)/(IV) ratio and above +1.38 V<sub>NHE</sub> dissolution rates increase, which lead to the possibility that it was possible to dissolving plutonium dioxide by

oxidation [206]. This led to experiments using electrochemical re-oxidation of the cerium(IV) and the development of the catalysed electrochemical plutonium oxide dissolution (CEPOD) process [195, 207]. Thermodynamic calculations recognised that a range of oxidants can be used and experiments showed that cerium(IV), cobalt(III) and silver(II) could be used [208, 209]. During these studies it was observed that cerium(IV) allows dissolution on useful timescales at temperatures near boiling, whilst silver(II) could be used at ambient temperatures and slowed at higher temperatures. Other developments in the USSR and France made the same conclusion that mediated dissolution using ether ozone [193] or electrochemically regeneration [118] are good methods for plutonium dioxide dissolution. This has led to the development of industrial processes for dissolution of plutonium dioxide [118] and plutonium from scrap [207].

Although a great deal of development work for cerium catalysed dissolution have been conducted, industrial dissolvers have largely used silver(II) as more rapid dissolution is possible [195]. Applied dissolution studies have shown that the key factors for dissolution revolve around the efficient generation of silver(II). A predominant feature in early dissolution studies shows linear concentration – time graphs [195, 210], as powders can be approximated as spherical dissolving particles, a curved dissolution rate is expected [123]. On this basis it is clear that dissolution rate is limited by the generation rate of silver(II) and/or the plutonium dioxide – silver(II) rate constant is diffusion controlled. However a common feature is the departure from linearity towards the end of the dissolution, which can be rationalised by the presence of a small population of larger particles and the plutonium dioxide – silver(II) rate constant being finite [123]. As most published dissolution experiments were carried out under conditions where there is a large excess of plutonium dioxide compared to silver(II), i.e. under conditions relevant to industrial dissolvers, the plutonium dioxide – silver(II) rate constants could only be estimated. A series of experiments were carried out under conditions where dissolution is slow, e.g. low temperature and low silver concentration, this allowed determination of dissolution rate constant [211]. These experiments have shown that there is a strong dependence upon the plutonium dioxide calcination temperature [212], which is strongly correlated with surface area [138]. In the same series of experiments, investigations into the effect of temperature determined a activation energy of  $25 \text{ kJ.mol}^{-1}$  [120]. As the activation energy of the silver(II) - water reaction is  $100 \text{ kJ.mol}^{-1}$  this provides a kinetic explanation to the observed optimum dissolution temperature of around  $40 \text{ }^\circ\text{C}$ .

Applied experiments studying the dissolution of plutonium dioxide using silver(II) initially used classical bulk electrolysis equipment, e.g. a beaker with porous cup membrane large anode and a smaller cathode or a H-cell [195, 210]. Depending upon the scale of industrial equipment this type of equipment can be scaled up, however most industrial dissolvers designed have tended to use a flow system where the anolyte is recirculated to provide mass transport of the silver(II) and plutonium dioxide, an example is shown in Figure 14 [118]. Mediated electrochemical oxidation has also been developed as a technology for the destruction of organics, and due to the much higher current demands these systems tend to be designed around 'plate and frame' electrolysis cells with separate recirculating anolyte and catholyte, Figure 58. This type of equipment has also been developed for plutonium dioxide dissolution [213]. The advantage of the 'plate and frame' type of electrolyzers are that they are used by other industries, so can be purchased and are readily scaled from laboratory or industrial scale. However they require high fluid flow velocities for efficient operation, and as maintenance is more difficult for plutonium (gloveboxes) or highly-active (shielded) operations, custom dissolver designs typically somewhere between 'classic beaker' and flow-type electrolyzers have been designed, which reduce the reliance of pumps for active liquors [118]. Although historically a great deal of work has been carried out in the UK, MEO type technology has been used to a limited industrial extent.

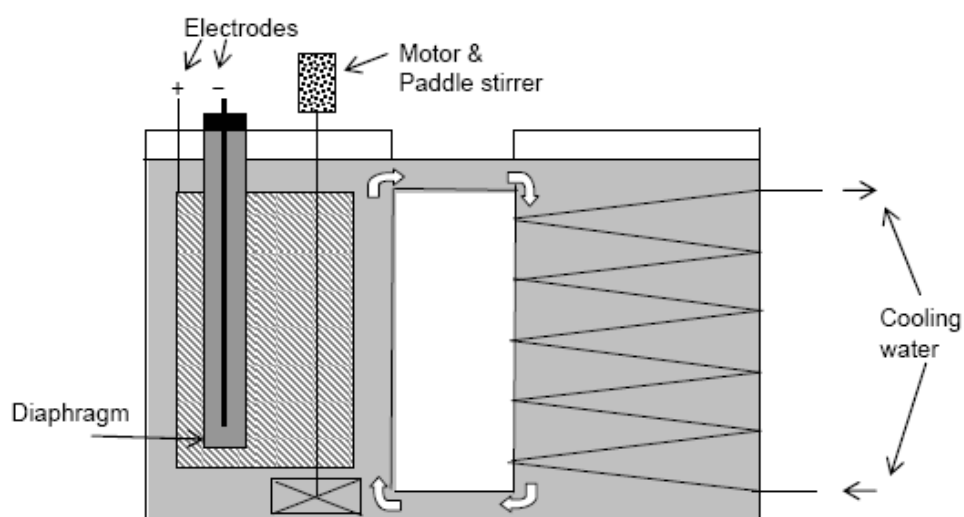


**Figure 14: Industrial plutonium dioxide dissolver [123]**

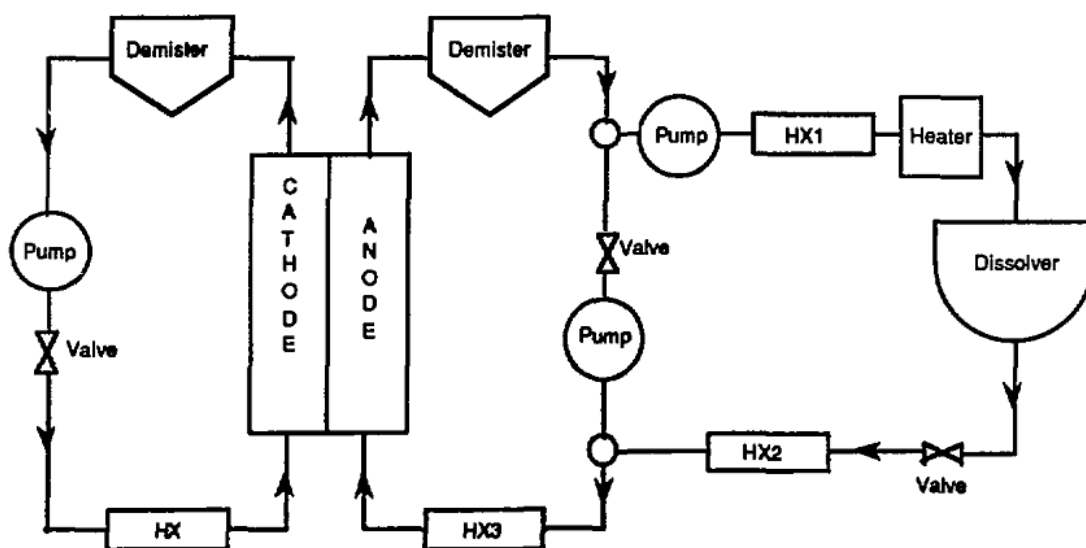
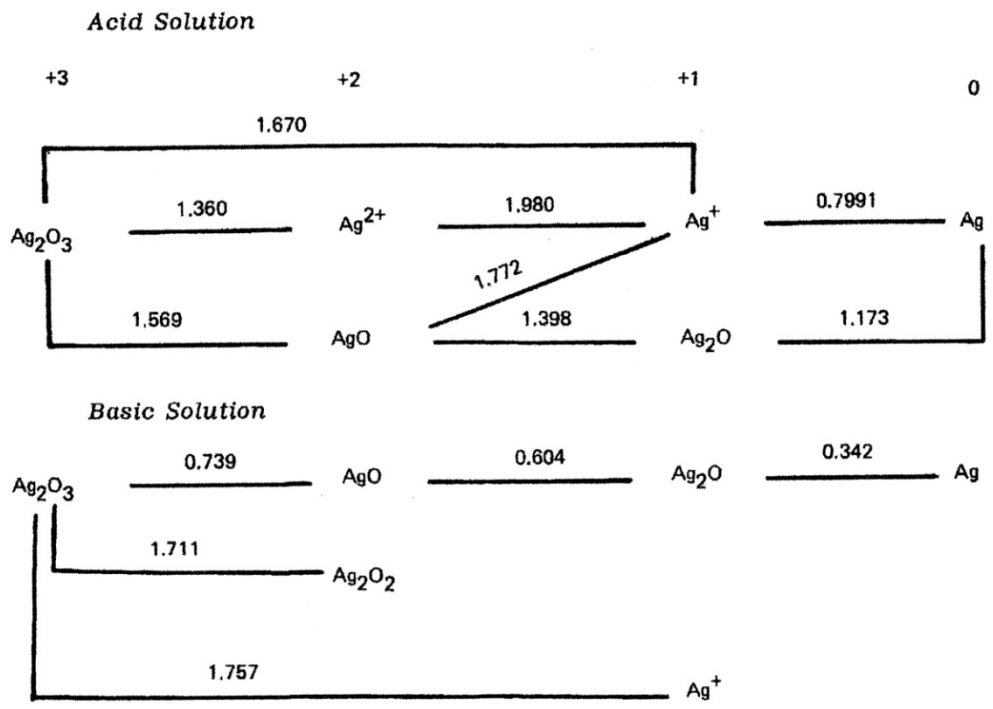


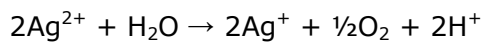
Figure 58: MEO re-circulating dissolver [213]

#### 5.1.1.1. Silver(II) chemistry in nitric acid

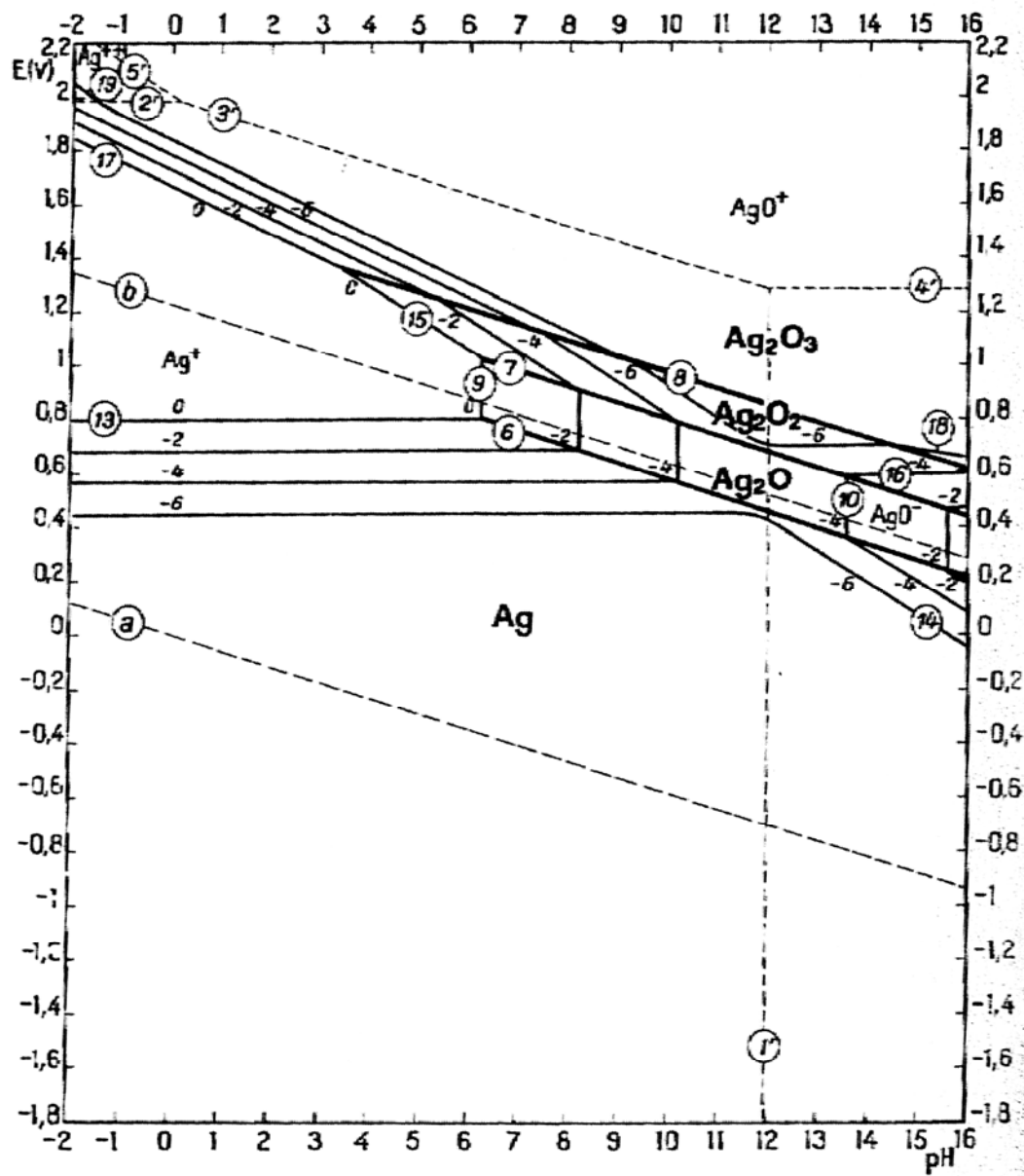
Silver is commonly present as silver metal and silver(I), however under high electropotentials silver may be oxidised to a number of higher oxidation states, silver(II, III, IV, V) [214, 215]. The most notable is silver(II), due to the considerable stability in acidic mildly complexing solutions and so has found some chemical applications. Silver(II) has a high electropotential only surpassed by chemicals such as persulphate, ozone and fluorine. The potential diagrams for silver are shown in Figure 59, it can be seen that many of the higher oxidation states have potentials above that needed to oxidise water, Figure 60. When considering silver(II) chemistry, the oxidation of water, Figure 60, or other oxidisable species is an important consideration.



**Figure 59: Potential diagrams for silver [35]**



**Eq 48**

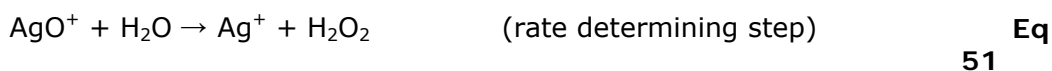


Note line-a reduction of water, line-b oxidation of water  
**Figure 60: Potential-pH equilibrium diagram for silver-water (non-complexing media) [216]**

Higher oxidation states of silver are known to form several compounds such as oxides and fluorides and their structures have been confirmed by crystallography and magnetic studies [215]. Silver(II) oxide is an example and this has been found to be a mix of silver(I, and III) [215]. Solutions of higher silver oxidation states are known to be present nearly exclusively as silver(II), the presence of silver(III) at very low concentrations, Eq 49 and Eq 50, has demonstrated by Silver-110m tracer studies and it support by kinetics [217] and magnetic studies.

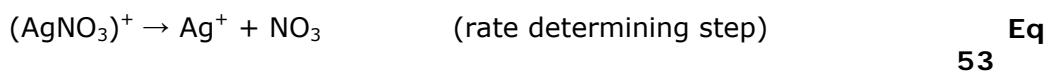


Evaluation of systematic kinetic results in various acidic media have shown that silver(III) is a key intermediate in the silver(II) reduction by water is silver(III), Eq 51 [122]. No evidence has been produced to support hydrogen peroxide as the reaction product, however it is expected that hydrogen peroxide will be rapidly consumed by silver(II), so the steady state hydrogen peroxide concentration would be very low. Kinetics for the decomposition of silver(II) reaction with water show a increase in rate with increase silver(II) concentration and a decrease with increasing silver(I). This 2<sup>nd</sup> order silver(II) dependence is shown in Eq 52 [122, 218, 219].



$$-\frac{d[\text{Ag}^{2+}]}{dt} = \frac{k_a[\text{Ag}^{2+}]^2}{k_b + k_c[\text{Ag}^+][\text{H}^+]^2} \quad \text{Eq 52}$$

Kinetic studies in nitric acid show a strong increase in the silver(II) stability, that is a reduction in the reaction rate with water, with increasing nitric acid concentration. There is also a pronounced change in the silver(II) absorption spectra, these changes can be attributed to the formation of silver(II) nitrate complex(es). These complexes also cause an increase in the observed activation energy for the silver(II) – water reaction from 47 kJ.mol<sup>-1</sup> [220] in non-complexing media to 100-130 kJ.mol<sup>-1</sup> in nitric acid [122, 218]. The decomposition of low concentrations, <1×10<sup>-4</sup> mol.l<sup>-1</sup>, of silver(II) in nitric acid has also been shown to decompose by a second route. This route has a first order silver(II) dependence and is believed to be proceed via nitrate radical mechanism, Eq 53 [122]. For this reason, it is expected that increases in nitrate concentration may increase this route, but there is no evidence for this. Whilst other workers have suggested at high silver(II):(I) ratios there is a additional mechanism that is dependent upon a fourth order of silver(II) [218].



Based on the results of numerous authors, the rate is dependant upon the silver(II):(I) ratio, nitric acid concentration and temperature. One or more of the three mechanisms discussed above could dominate and affect the rate of silver(II) decomposition. These mechanisms can be summarised in Eq 54. The effect of increasing total silver, nitric acid concentrations, decreasing temperature and silver(II):(I) ratio have all been shown to decrease the rate of decomposition of silver(II) with water and thus the stability of silver(II).

$$-\frac{d[\text{Ag}^{2+}]}{dt} = k'[\text{Ag}^{2+}] + k''\frac{[\text{Ag}^{2+}]^2}{[\text{Ag}^+]} + k'''\frac{[\text{Ag}^{2+}]^4}{[\text{Ag}^+]} \quad \text{Eq 54}$$

### 5.1.2. Electrochemical generation of silver(II)

Aqueous solutions of silver(II) can be prepared by dissolution of silver(II) oxide, AgO, in acid, oxidation of silver(I) by strong oxidants such as persulphate or ozone or by bulk electrolysis [214]. Nuclear industrial processes using silver(II) favour the use of ozone [221, 222] or bulk electrolysis [195, 223, 224] as they are low salt methods, which minimises waste volumes. These silver(II) generation methods are discussed in detail in the literature and electrochemical generation will be discussed in detail below.

The electrochemistry of the silver(I, II) couple has been studied in detail using classic electrochemical methods such as linear-sweep or cyclic voltammetry (LSV, CV) at a stationary electrode, rotating disc or ring-disc electrochemistry (RDE or RRDE) and bulk electrolysis (BE). These methods have been used to understand the rate determining steps in the electron transfer process, the number of electrons involved, fundamental constants such as the exchange rate constant, ion diffusion coefficients and electropotential. These methods have also been used to determine more applied information such as current efficiency and mass-transfer limits for various cell parameters. This information is useful to help model the electrochemical process, which can help the experimental optimisation of laboratory or industrial cells.

Most studies have been carried out using platinum as a working electrode, due to the high stability; initially discussions will be limited to this electrode type. Researchers in [121] carried out slow scan rate (steady state) LSV at a disc electrode rotating at 600 rpm, this data shows the cathodic Tafel slopes (LOG current density ( $J$ , A.cm<sup>-2</sup>) versus potential ( $E$ , V)). The linear part of

these plots has been used to calculate a slope of  $60 \text{ mV.decade}^{-1}$ , indicated a one electron transfer occurs ( $\alpha = 0.5$ ) and the standard electrode potential of  $1.95 \text{ V}_{\text{NHE}}$ . It is also noteworthy that Fleischmann ascribes the derivation of current from linearity at above *ca.*  $2.0 \text{ V}_{\text{NHE}}$  due to formation of a solid phase on the working electrode, probably silver oxide film formation and that above this voltage there is minimal silver(II) production. Berg [225] found two different Tafel slopes in the anodic region that were ascribed to a two electron transfer occurring at higher potentials. However, neither author appears to have accounted for the currents from direct oxygen discharge, unlike Arnaud [226]. Arnaud described both the cathodic and anodic Tafel regions accounting for oxygen evolution and found Tafel slopes consist with a one electron transfer ( $\alpha \approx 0.8$ ). Arnaud, like Berg did find a second Tafel region at higher potentials, this could suggested there is a second mechanism at high potentials for the oxidation of silver(I).

Fleischmann carried out experiments at various rotating speeds with  $0.01 - 3 \text{ mol.l}^{-1}$  silver nitrate – nitric acid in  $3 \text{ mol.l}^{-1}$  nitric acid to determine the cathodic kinetic rate constant of  $1.5 \times 10^{-2} \text{ cm.s}^{-1}$  [121], which is rapid and close to the mass transfer limit. As RDE studies have unique mixing conditions that can be modelled Berg's used RDE studies to determine the rotational current limit and diffusion coefficients for silver(I) and silver(II) [225].

Several authors have recorded LSV or CV at small stationary electrodes; these studies have shown the oxidation of silver(I) is not diffusion limited, as the anodic peak current does not shift with scan rate [121]. The reduction peak from cathodic scans shows more complicated behaviour. Depending upon to the final cathodic scan potential, the silver(II) reduction peak, could be broad or absent. This has been attributed to the slow silver(II) reduction rate on the platinum electrode surface, due to the presence of platinum oxide film when the electrode is exposure to higher potentials. When the electrode is polarised to lower potentials the platinum oxide surface is reduced and faster silver(II) reduction can occur.

Many authors have continued their experiments by carrying out bulk electrolysis studies [121, 213, 225]. These studies have either been carried out with constant potential or constant current, both methods have advantages and disadvantages [227]. Constant potential allows electrolysis to be carried out with high selectivity and efficiencies, whilst constant current methods require simpler instrumentation, but selectivity and efficiencies will be reduced towards the end of the electrolysis. Several authors have observed that only a fraction of the silver(I) can be oxidised to silver(II) during

electrolysis, this yields a steady state or plateau silver(II) concentration (or potential). Attempts to achieve higher silver(II:I) ratios result in reduced efficiencies. This is easily understood as there are two competing reactions electrochemical generation of silver(II) and consumption of silver(II) by reaction with water [213], other side or desired reactions also reduce the steady state silver(II) concentration.

Several authors have explored the use of other working electrode materials to reduce the costs, improve efficiencies or explore applications for novel electrodes. Arnaud used LSV RDE in 0.1 mol.l<sup>-1</sup> silver nitrate and 4 to 8 mol.l<sup>-1</sup> nitric acid to compare platinum, platinum-clad titanium (Ti/Pt) dimensionally stable anode (DSA),  $\beta$ -lead dioxide DSA ( $\beta$ -PbO<sub>2</sub>), glassy carbon, non-stoichiometric titanium oxide (TiO<sub>2-x</sub>) [226]. By comparing the oxygen and silver(II) generation, predicted efficiencies were calculated and showed that the yield followed this order:

Platinum > glassy carbon > Ti/Pt DSA >  $\beta$ -PbO<sub>2</sub> DSA

Although the highest efficiencies were observed on platinum, Arnaud concluded that all electrode materials showed acceptable efficiencies. However, parasitic silver oxide formation was observed at high silver(II) and lower nitric acid concentrations; this was particularly observed on glassy carbon and  $\beta$ -PbO<sub>2</sub> DSA. Also, after 24 hours of electrolysis test glassy carbon electrode surface showed pitting and so is an unsuitable electrode type.

Dauids found that gold electrodes can generate silver(II) with higher efficiencies compared to platinum [228]. Berg's experiments agreed with these findings, however research into the use of gold was discontinued when literature research showed that gold suffers from slow dissolution at high applied potentials [225]. However, it is also known that platinum can suffer similar dissolution [229].

Platinum coated titanium DSA's have been tested and found applications in many applications. Indian workers have also manufactured mixed ruthenium, titanium platinum oxide coated titanium DSA's with various compositions for dissolution of uranium and uranium-plutonium carbides [230]. The results detailed analysis of the electrodes and conclude that electrodes with platinum coatings on top of the mixed ruthenium-titanium oxide coating yield higher current densities. Some of the anodes tested have shown no deterioration in that short term (20 hours) tests at up to reflux temperatures (120 °C) with cerium electrocatalyst (instead of silver). A large body of research into DSA's from other applications in other fields may also be relevant.

Two novel electrode types, antimony-doped tin oxide [231] and boron-doped diamond (BDD) [232] electrodes have been found at the small scale to have advantages over platinum and gold. Antimony-doped tin oxide anodes have been used to generate silver(II) at approaching 100 % efficiency in 3-5 mol.l<sup>-1</sup> nitric acid at 0 °C and at less than 5 mA.cm<sup>-2</sup> for the use in analytical coulometric titrations. Whilst BDD electrodes have also been capable of generation of silver(II) at high efficiencies and high potentials, due to the high water oxidation overpotential on BDD.

### **5.1.3. Summary of silver(II) mediated electrochemical processes**

Electrochemically generated silver(II) clearly has many advantages for the dissolution of plutonium dioxide. The dissolution is in competition with other reactions, this includes water, organic species present and catholyte products, if imperfect cell membrane separators are used. As the reaction with water has high activation energy, for high faradaic efficiencies anolyte temperature is a key factor. However, higher nitrate concentrations decrease the rate of reaction with water through stabilisation of silver(II) as a nitrate complex. The generation rate and efficiency of silver(II) is dependent upon the electrode type, surface area and potential. These factors and others need to be taken into account when designing dissolvers, as the dissolver will need to be optimised for faradaic efficiency or time. If optimisation is to be carried out these factors need to be understood. However, as the dissolution rate between silver(II) and plutonium dioxide is known to be rapid, the key factor is optimisation of the generation rate of silver(II).

### **5.2. Aims and objectives**

There are several questions about how mediated electrochemical dissolution can be used for either the dissolution of plutonium dioxide, scrap or plutonium rich undissolved MOx residues. This includes:

- As the rate of reaction between plutonium dioxide and silver(II) is rapid, dissolution is often limited by the generation rate of silver(II). The key factor in determining dissolution rate is the rate of generation of silver(II). For this reason inactive experiments aimed at determining the relative significances of chemical and cell variables have been carried out.

- After understanding factors controlling the generation of silver(II), plutonium dioxide dissolution experiments exploring chemical, cell and material variables were planned and setup. However, only a limited number of these experiments were possible due to a unscheduled outage of the glovebox where the dissolution experiments were setup.

### Inactive experiments

#### Aims:

- Understand the key variables that affect the rate of generation of silver(II)
- Define limits for the generation rate of silver(II)
- Understand the key factors that affect the stability and steady state silver(II) concentration
- Compare experimental results with thermodynamic or kinetic model(s)

#### Approach:

- Use Stirred Linear Staircase Voltammetry (LSCV)[233] to produce I-E curves under a variety of conditions, *e.g.* stirrer rate, concentration of silver(II). During these studies optimised conditions can be defined. Compare results with Tafel's law.
- Carry out bulk electrolysis experiments to observe the generation, steady state and decomposition of silver(II). Use experimental data to determine the efficiency of silver(II) generation and derive kinetic law for silver(II) reduction by water. Simulate experimental data using a standalone model.
- Selected bulk electrolysis experiments will repeat the conditions of the LSCV experiments. Comparison of the LSCV and electrolysis results will show where LSCV is a useful tool for applied optimisation of cell performance.

### Plutonium-active experiments

(Only limited number of these experiments was completed, due to unscheduled outage of the dissolution glovebox)

#### Aims:

- Small scale experiments (using 0.5 g plutonium), aims to:
  - Understand the relative significance of cell variables (nitric acid and silver nitrate concentration, temperature, stirrer rate)

- Provide information to construct and validate a process model for the dissolution kinetics.
  - Compare the dissolution kinetics of fresh, old and low surface area plutonium dioxide (calcined to higher temperatures)
- Large scale experiments (up to 20 g plutonium), aims to:
  - Provide information on the effect of increasing concentration of plutonium (up to 200 g.l<sup>-1</sup> plutonium) upon dissolution rate
- Small scale experiments 2, aims to:
  - Investigate the effect of added inactive metals with an aim to understand the viability or efficiency of a Silver(II) dissolution process for the recovery of plutonium rich residues from an irradiated MOx dissolution sludge.

Approach:

- Carry out a systematic series of batch dissolution experiments

### **5.3. Experimental**

#### **5.3.1. Apparatus and methods**

##### **5.3.1.1. Glassware**

A custom glass divided reaction vessel based upon the original electrochemical cell used for plutonium dioxide dissolution (CEPOD) studies [195] and was constructed by Scott Glass Ltd (Stirling, UK). Two versions of these apparatus have been used in this work. The main features of the vessel are:

- 100 ml anode volume
- Interchangeable cathode compartments
- Gap under cathode compartment to allow space for a magnetic follower
- Side arm for anode vessel to allow an existing platinum gauze electrode to be fitted (as used by Berg [225].)
- Sockets in the anode vessel to allow a thermometer, gas inlet, condenser, salt bridge, sampling and UV-Vis tubes
- Sockets in cathode vessel for electrode, condenser, salt bridge and sampling tubes.

The second version, shown in Figure 61B, of the vessel added:

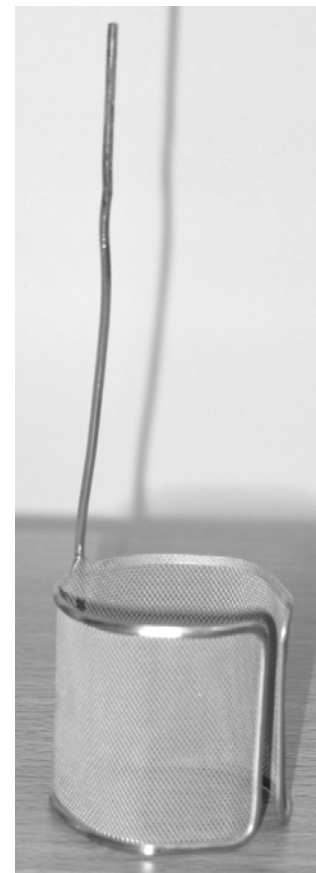
- A jacketed vessel to the anode compartment for thermostating or cooling
- Three additional side arms to the anode compartment to reduce clutter at the top of the vessel.
- The cathode compartment was manufactured to two parts to simplify installation of the electrode.



**A – version 1**



**B – version 2 with jacket, additional inode side fittings and two part cathode**



**C – Platinum electrode**

**Figure 61: Photographs of assembled version 1 and 2 reaction vessel and platinum working electrode**

The use interchangeable cathode compartments permitted simple replacement, if a membrane was broken (which did not occur) and for testing of different membrane types. During the testing five membrane types have been used, see Table 17 and Figure 62. Initially testing used membrane types 1-3, and later types 4 and 5 were constructed and tested. The volume of the cathode cup or thimble can increases greatly from type 3 to 5.

**Table 17: Membrane types tested for divided cell**

#	Manufacturer	Grade	Material	Size	Pore Ø (µm)	Volume (ml) <sup>h</sup>
1	AIMER Ltd	4	Glass frit	25 mm disc	10-15	15 / 20
2	AIMER Ltd	5	Glass frit	25 mm disc	<2	15 / 20
3	ACE Glass Inc (D141352)	E	Glass frit	21.5 mm Ø, 30 mm long, 6 mm wall thickness	4-8	3 / 12
4	ACE Glass Inc (D141352 bored)	E	Glass frit	21.5 mm Ø, 30 mm long, 3 mm wall thickness	4-8	5 / 15
5	CoorsTek Inc (60491)	P-1/2-BC	Aluminium oxide	25 mm Ø, 40 mm long, 3 mm wall thickness	<0.5	15 / 20

---

<sup>h</sup> Approximate volume that the cathode compartment can be filled to so the thimble is full / the liquor level of catholyte and anolyte are equal

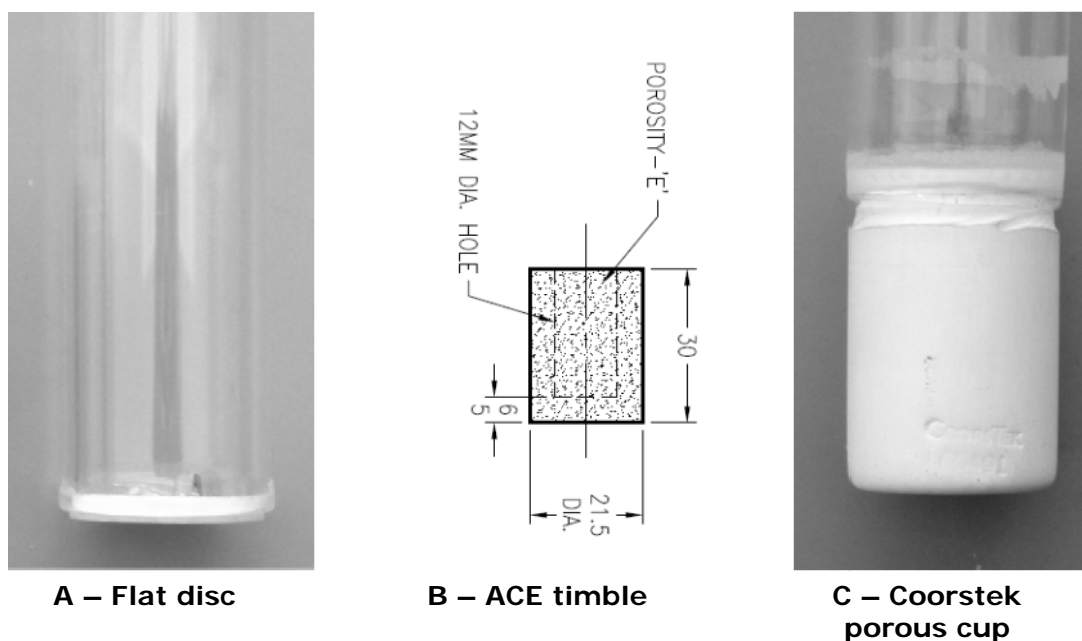


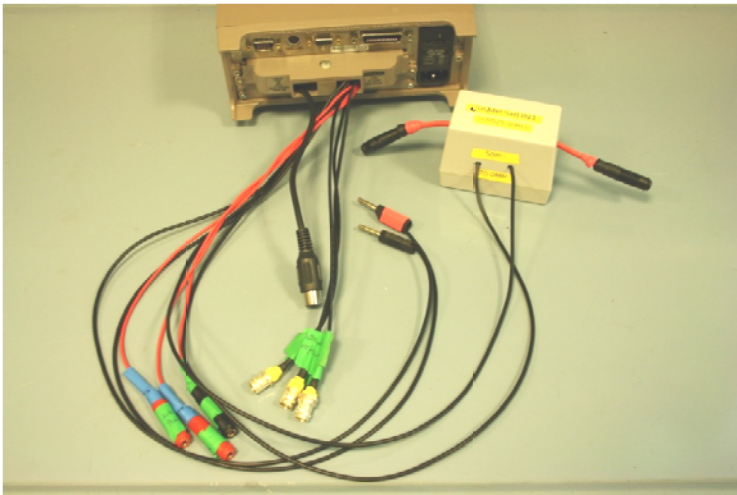
**Figure 62: Photographs and diagrams of membranes**

### ***5.3.1.2. Power supply and voltage meters***

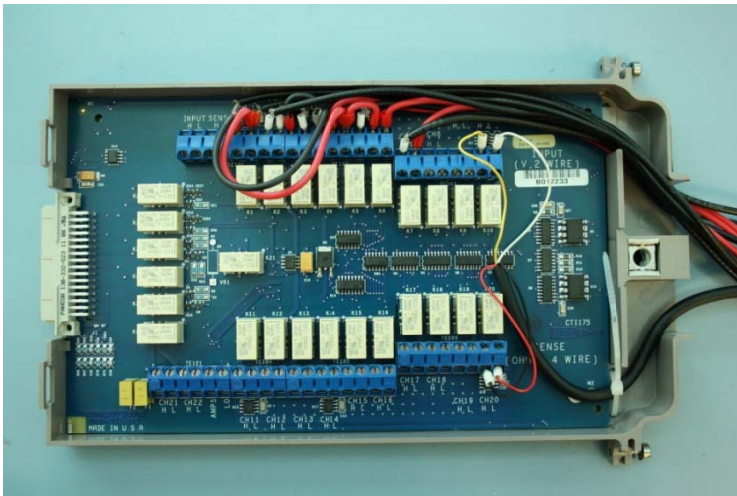
During the testing two different DC power supplies and digital multimeters (DMM) have been used. Initial testing used a DC variable power supply type, Farnell PDD3010A, see Figure 67. The majority of the experiments used an Agilent E3133A programmable DC power supply (PSU) with a dual range 8 V / 20 A and 20 V / 10 A, see Figure 63. The power supply offered the high currents needed for testing, was simple to program and used low voltages to minimise the risk from electric shock. Two types of digital multimeter used are an Agilent 34411A, see Figure 63, and Keighley Instruments 2700/E with 20 channel switching module, model 7700, see Figure 64. Two different types of DMMs were used as the Agilent meter allowed simple programming for LSCV experiments, whilst the Keighley instrument is particularly suited for the bulk electrolysis experiments as multiple channels can be logged simply.



**Figure 63: Photograph of digital multi meters and Agilent DC power supply**



**A – Rear-view of Keighley 2700/E with wiring**



**B – switching model 7700 wired for electrolysis experiment**

**Figure 64: Photograph of Keighley multimeter and switching card**

During LSCV experiments the Agilent E3133A and 34411A were used with Intuilink, which adds options to control both the PSU and DMM in Microsoft Excel. A simple programme in Visual Basic for Applications (VBA) was written to set a applied voltage, measure the voltage, current (PSU) and redox potential (DMM). This programme allowed a potential step to be applied then voltage, current and potential measured. Then after a defined time the next potential step could be continued. This staircase could be carried out over a defined range. A copy of the macro used is shown in Appendix 1. This data was collected in an MS Excel sheet, multiple sheets allowed simple comparison of data from different experiments.

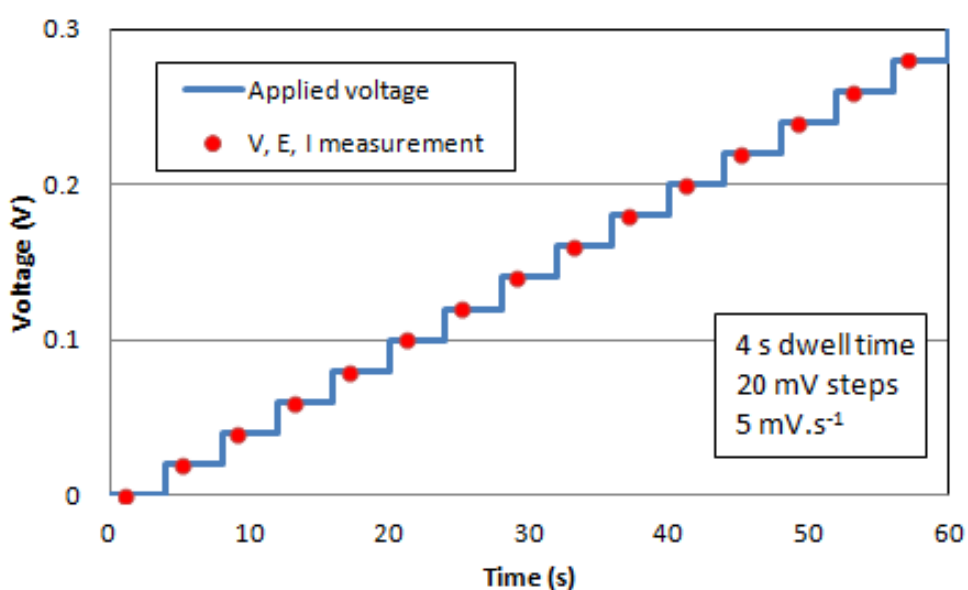


**Figure 65: Example schematic timeline for LSCV experiment measurements**

During bulk electrolysis experiments the Agilent PSU and Keighley DMM were used independently. The Keighley DMM was set to log the data using Keighley ExcelLINUX software. Then at a defined time the Agilent PSU voltage and current limits were set (to start the experiment) using Intuilink in Excel, then voltage and current datalogging was started.

### **5.3.1.3. Electrodes**

All experiments have been performed with a single platinum gauze anode, this electrode was in storage from previous silver(II) experiments [225]. The

electrode was purchased from Johnson Matthey in 2004 and a type 72070 electrode made of 4.5 % ruthenium – platinum, shown in Figure 61C.

During LSCV experiments two designs of cathode were used and all were manufactured in house. Materials were obtained from Advent Research Materials, Oxfordshire, unless specified

- Tantalum pig-tail electrode, made from 50 cm length of 1.7 mm diameter rod (Ta-RD-002, shopmetals.co.uk).
- Stainless steel gauze tube electrode was manufactured from a type 316L stainless steel gauze (FE634117) sewn into a tube. The tube was sewn onto a 3 mm weld rod to provide an electrical contact. The weld rod from in-house stocks.

Pseudo-reference electrodes were manufactured from 0.20 mm platinum (PT541518), 0.20 mm tantalum (TA551811) or 0.25 mm 304L stainless steel wire (FE20218) supplied by Advent research. These were glued into a short length of 1/32" ID PFA tubing with an epoxy adhesive to allow simpler handling and to allow the measurement vessel to be sealed.

#### ***5.3.1.4. Redox potential measurements***

During the LSCV and bulk electrolysis experiments redox potential were made by measuring the potential different between the anode or cathode and 'reference electrodes'. Two types of 'reference electrodes' have been used. LSCV and initial bulk electrolysis experiments used a custom silver/silver chloride with a double junction filled with gelled potassium nitrate manufactured by Sentek Ltd. Bulk electrolysis experiments also used a thin wire of the same metal as the electrode. As this wire was connected to a high resistance voltmeter this wire acts as a 'pseudo reference' and the potential measured represents the degree of polarisation. All measurements have been made in a separate measurement cell connected to the main experimental cell by a salt bridge. The salt bridge was constructed using glass fibre strands and 1/32" ID PFA tubing.

As the resistance of the DMMs used in these experiments are not as high resistance as ideally used in electrochemical measurements, the potentials measured for a series of solutions were compared with a research pH meter (Hanna HI 4222).

### 5.3.1.5. Temperature measurement

Temperature measurements were made with a Pt100 resistance thermometer, this was connected to the IKA RET Control hotplate. The thermometer was sheathed in a custom titanium tube, see Figure 66. This was manufactured in-house using a 6.3 mm titanium tube (Ti-TB-008) and 9.5 mm diameter rod (Ti-RD-007) obtained from shopmetals.co.uk. The rod was drilled to provide an interference fit with the tube. The tube and end-piece were welded by ArcAlloys Ltd (West Midlands, UK).



**Figure 66: Photograph of Titanium thermometer pocket with Pt-100 thermometer**

### 5.3.1.6. Inline UV-Vis spectrometry

During the bulk electrolysis experiments inline UV-Vis spectra were measured. This was desirable due to the low stability of silver(II) at high silver(II)/silver(I) ratios, which allowed more rapid measurements to be made compared to offline analysis. Due to the relatively poor chemical compatibility of Viton with silver(II) a peristaltic pump was not used. A FMI QCVG50 piston pump with ceramic P1 Ceramic head and V300 controller. 1/32" ID PFA tubing with a Hellma 0.5 mm pathlength flowcell (Hellma 170700-0.5-40) was used to provide a low flow-loop hold up volume. The piston pump was run at a high relative flowrate (of *ca.* 13 ml.min<sup>-1</sup>) to allow liquor residence time of less than 10 seconds. All UV-Vis measurements were made with a Zeiss MCS 501 spectrometer with 10 m Hellma fibre optics and WPI 1 cm cell holder.

The narrow pathlength of the necessary due to the high molar extinction coefficients of the silver(II) nitrate complex.

### 5.3.1.7. Silver(II) by sampling

During initial bulk electrolysis experiments samples were taken for analysis of silver(II) concentration by a titration and UV-Vis method. Both of these methods initially allow reaction of a sample of known volume containing

silver(II) with cerium(III). The cerium(IV) generated, which has a higher stability, could be titrated with iron(II) or determined by UV-Vis in 5 cm cell. Titrations were carried out using a Metrohm Titrando autotitrator. UV-Vis measurements were made with a Ocean optics HR4000 CCD spectrometer, WPI D2H combined halogen-deuterium light source with a pair of 10 m Hellma fibre optics and 10 cm WPI cell holder.

### 5.3.2. Initial testing

An initial bulk electrolysis experiment was carried out in an inactive laboratory to provide confidence that the apparatus was functioning prior to transfer to the active laboratory. In this experiment a stirred anolyte of 0.1- 4 mol.l<sup>-1</sup> silver nitrate – nitric acid and 12 mol.l<sup>-1</sup> catholyte were used. An increasing potential was applied until silver(II) was observed coming from the anode. The apparatus with DC power supply are shown in Figure 67, gas feed and off-gas wash bottles not shown for clarity. The rapid increase in black silver(II) provided confidence to transfer the glassware to the active laboratory for further testing.

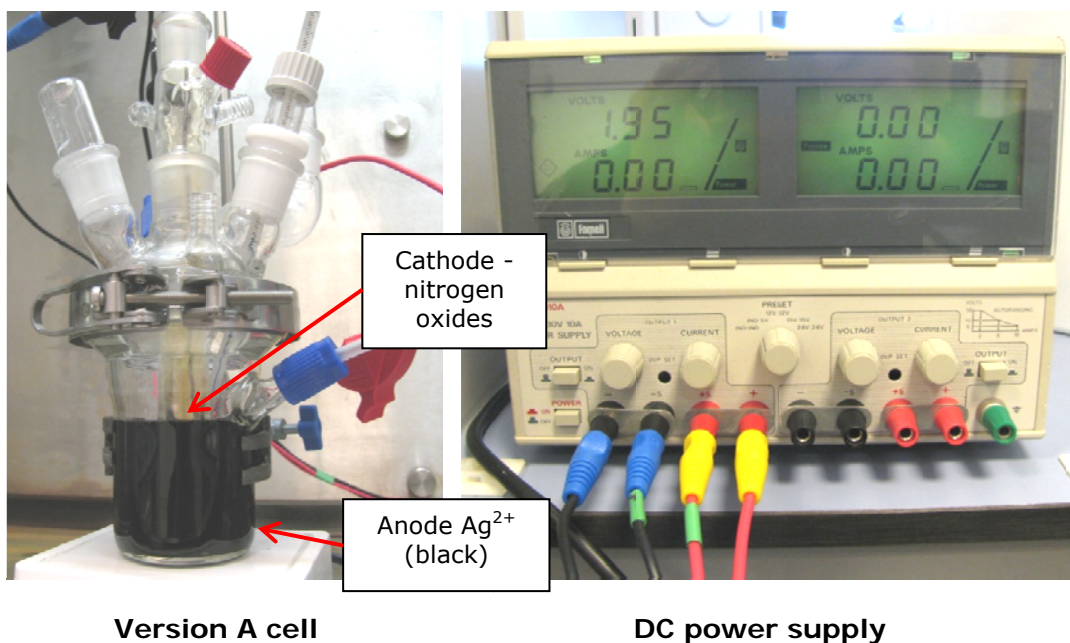


Figure 67: Photograph of 1<sup>st</sup> bulk electrolysis test

### 5.3.3. Linear Staircase Voltammetry

As discussed in section 5.3.1 the Linear Staircase Voltammetry (LSCV) apparatus involved the glass vessel with gas purge and off-gas wash bottles with Agilent PSU and DMM controlled via an MS Excel VBA programme. Early experiments were carried out between 0 -2 V applied, most experiments were carried out between 0 – 4 V applied and several experiments were carried out between 0 – 8 V.

The cathode and anode compartments were purged with 30-80 and 250 ml.min<sup>-1</sup> air respectively from the house low pressure air supply. The experiments were run by setting up the cell for the defined conditions and running the VBA macro to perform the voltammetry experiment. At the end of the experiment the silver(II) generated during the experiment was destroyed by adding several 10 µl aliquots of 5 mol.l<sup>-1</sup> NaNO<sub>2</sub>, each anode solutions was typically used for less than five voltammetry experiments. The catholyte was replaced after each experiment. The anolyte temperature was not controlled over the course of these experiments and during some experiments this led to ohmic heating. The apparatus setup is shown systematically in Figure 68.

The reference electrodes E<sub>0</sub> was compared daily to a reference electrode solely used for this purpose, and all potentials quoted are vs. the silver/silver chloride electrodes. The salt bridges for the anode and cathode were positioned within several millimetres of the electrodes.

The cell configuration was adjusted, one parameter at a time. The conditions for each experiment and were added to explore the following parameters:

- Potential step size and dwell duration
- Stirrer rate 0-1500 rpm with rare earth magnetic follower 25 × 6 mm (Fishers Scientific FB57997).
- Catholyte nitric acid concentration 8 – 16 mol.l<sup>-1</sup> nitric acid
- Membrane type
- Cathode design
- Anolyte silver nitrate concentration 0 – 0.2 mol.l<sup>-1</sup> in 4 mol.l<sup>-1</sup> nitric acid
- Anolyte nitric acid concentration 3-8 mol.l<sup>-1</sup> nitric acid with 0 and 0.05 mol.l<sup>-1</sup> nitric acid concentration

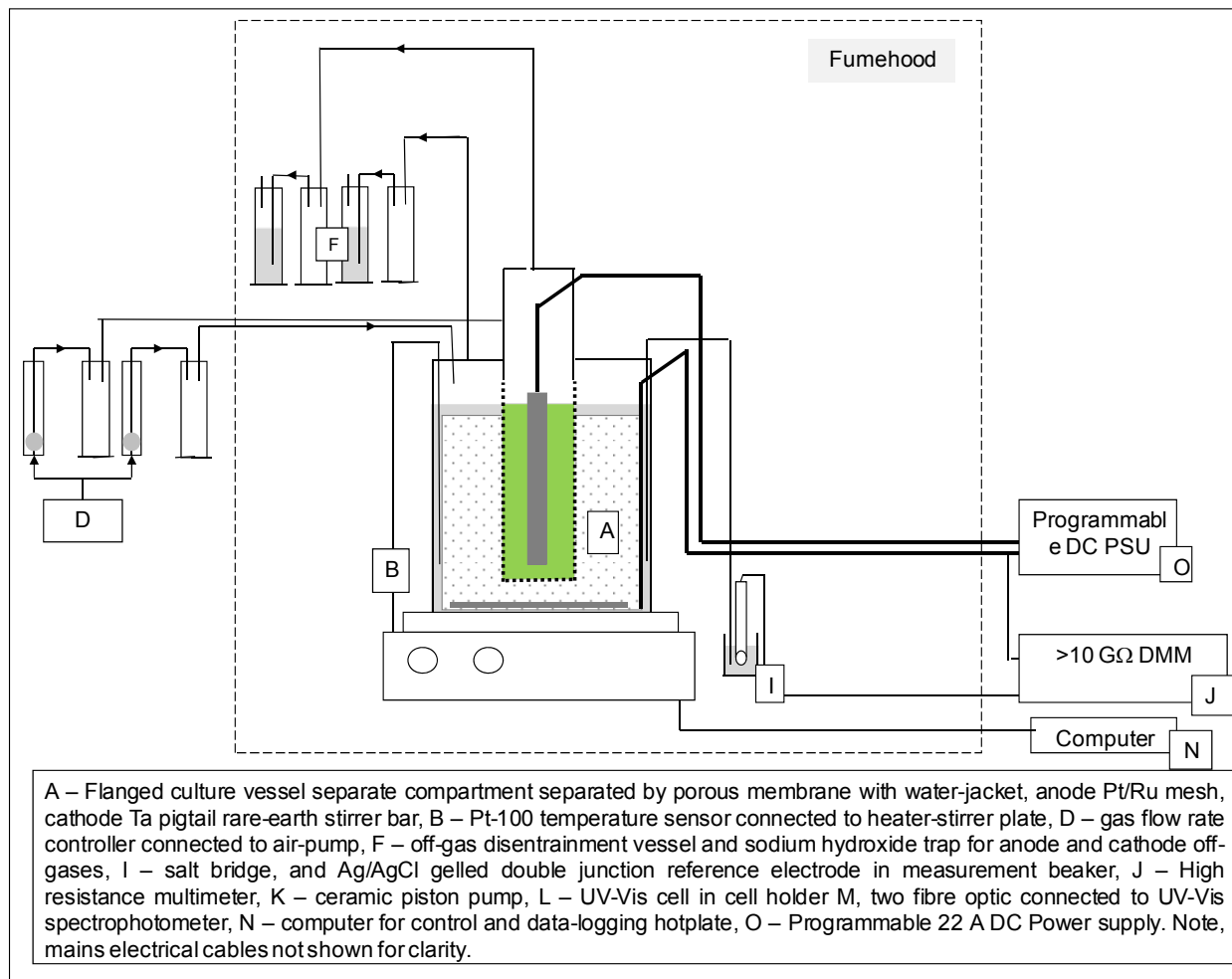


**Figure 68: Schematic diagram of LSV setup (anode monitoring shown)**

#### 5.3.4. Bulk electrolysis

As discussed in section 5.3.1 the bulk electrolysis experiments were carried out using the Agilent DC PSU and Keightley switching DMM. The DC PSU was either run at:

- constant applied voltage by settling the current much higher than required for the set voltage
- or constant applied current by settling the voltage much higher than required for the set current

The apparatus was setup in a similar manor to the LSCV experiments, except the Keighley switching DMM module was wired to allow measurement of applied voltage, redox potential for anode and cathode vs. silver/silver chloride reference electrode and 'pseudo reference'. Current was also measured by measuring the potential across a 20 A shunt (0.025  $\Omega$  calibrated resistor or shunt, to give 50 mV at 20 A). The last channel in the switch data collection sequence was not connected to minimise influence upon the applied voltage circuit during the time between measurements.

In a similar manner to the LSCV experiments, the apparatus was setup using defined experimental conditions. Before the experiment was current was applied datalogging with the Keighley DMM, pump UV-Vis spectrometer was started. The experiment time=0 when the PSU voltage and current was set. The DC PSU applied voltage and current datalogging was then immediately started. The electrolysis was run for a define time, typically 10 or 120 minutes. The DC PSU data logging was stopped and applied voltage turned off. For some experiments the redox potential and UV-Vis measurements was continued to observe the decomposition of the silver(II). The apparatus setup is shown systematically in Figure 70.

In early experiments the periodic analysis of silver(II) concentration using a colourimetric method was carried out. This was not carried out during later experiments due to poor reproducibility between the offline UV-Vis measurements and inline UV-Vis measurements, due to the low stability of silver(II).

To confirm that under normal operating conditions low concentrations of hydrogen were produced six experiments where cathode off-gas samples were collected. These samplers were analysed by gas chromatography (Agilent micro-GC) calibrated for hydrogen determinations.

Later bulk electrolysis experiments used the second version of glassware with a water-jacket and 'Coorstek porous cup' membrane. This apparatus allowed low temperature and improved temperature control over the variable temperature experiments, as cooling water removed heat generated by ohmic heating.

During the electrolysis experiments solution temperature was thermostated using the stirrer-hotplate. The hotplate was used to log the stirrer rate, solution and hotplate temperatures. When the jacketed vessel was used the vessel was thermostated using a Haake recirculating chiller/heater unit.

At the end of the experiment the silver(II) generated during the experiment was destroyed by adding several 10  $\mu\text{l}$  aliquots of 5  $\text{mol.l}^{-1}$   $\text{NaNO}_2$ , each anode solutions was typically used for less than five electrolysis experiments for short experiments, or one a single experiment for longer experiments. The catholyte was replaced after each experiment.

The cell configuration was adjusted, one parameter at a time. The conditions for each experiment and were added to explore the following parameters:

- Current – stirred rate (0, 500, 1000, 1500 rpm)
- Current – silver concentration (0, 0.01, 0.05, 0.1, 0.2  $\text{mol.l}^{-1}$ )
- Temperature (10 - 70  $^{\circ}\text{C}$ )
- Anode nitric acid concentration (3 – 8  $\text{mol.l}^{-1}$ )
- Cathode nitric acid concentration (4 – 16  $\text{mol.l}^{-1}$ )



**Figure 69: Photograph electrolysis testing, apparatus in fumehood only (experiment e83)**

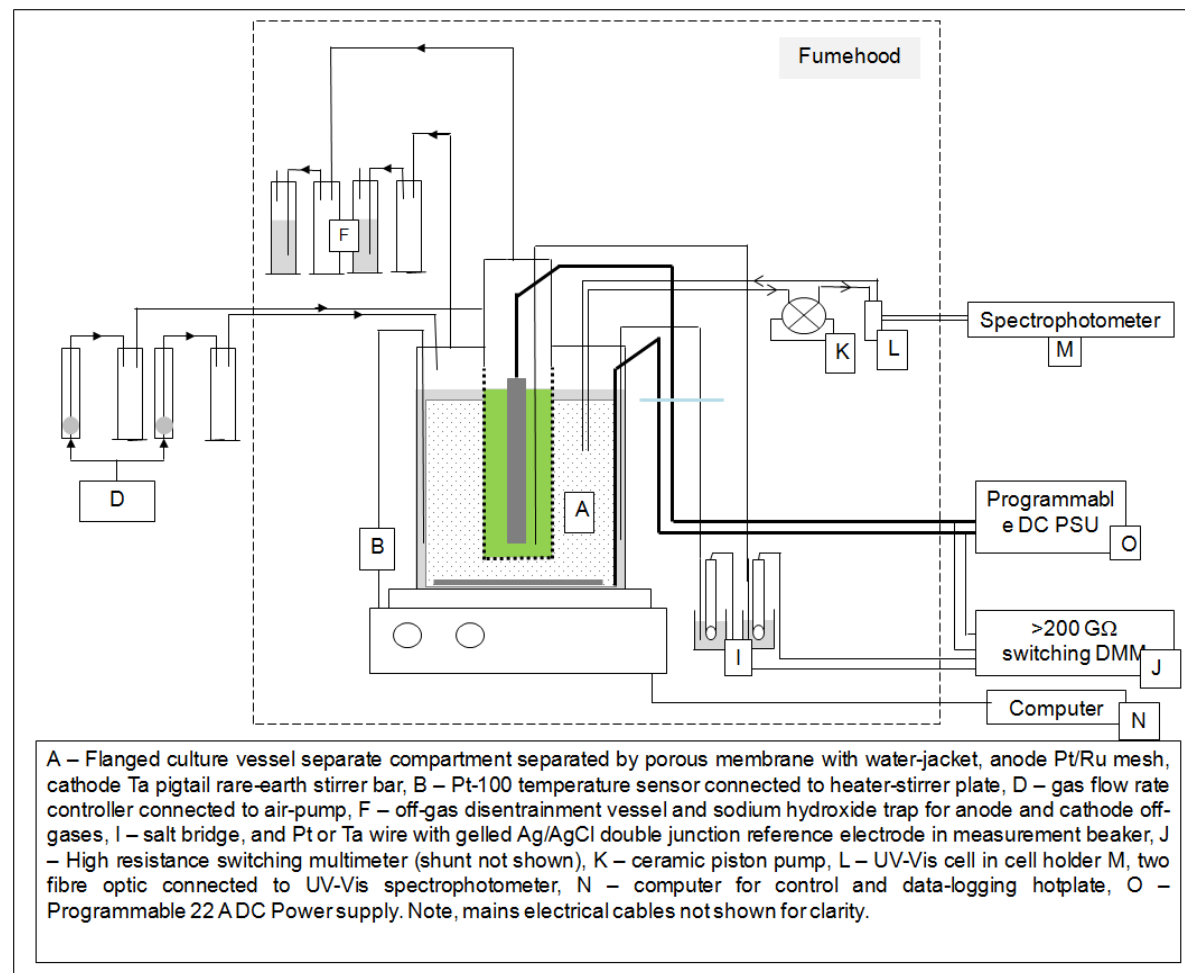


**Figure 70: Schematic diagram of bulk electrolysis setup.**

### **5.3.5. Dissolution apparatus and methodology**

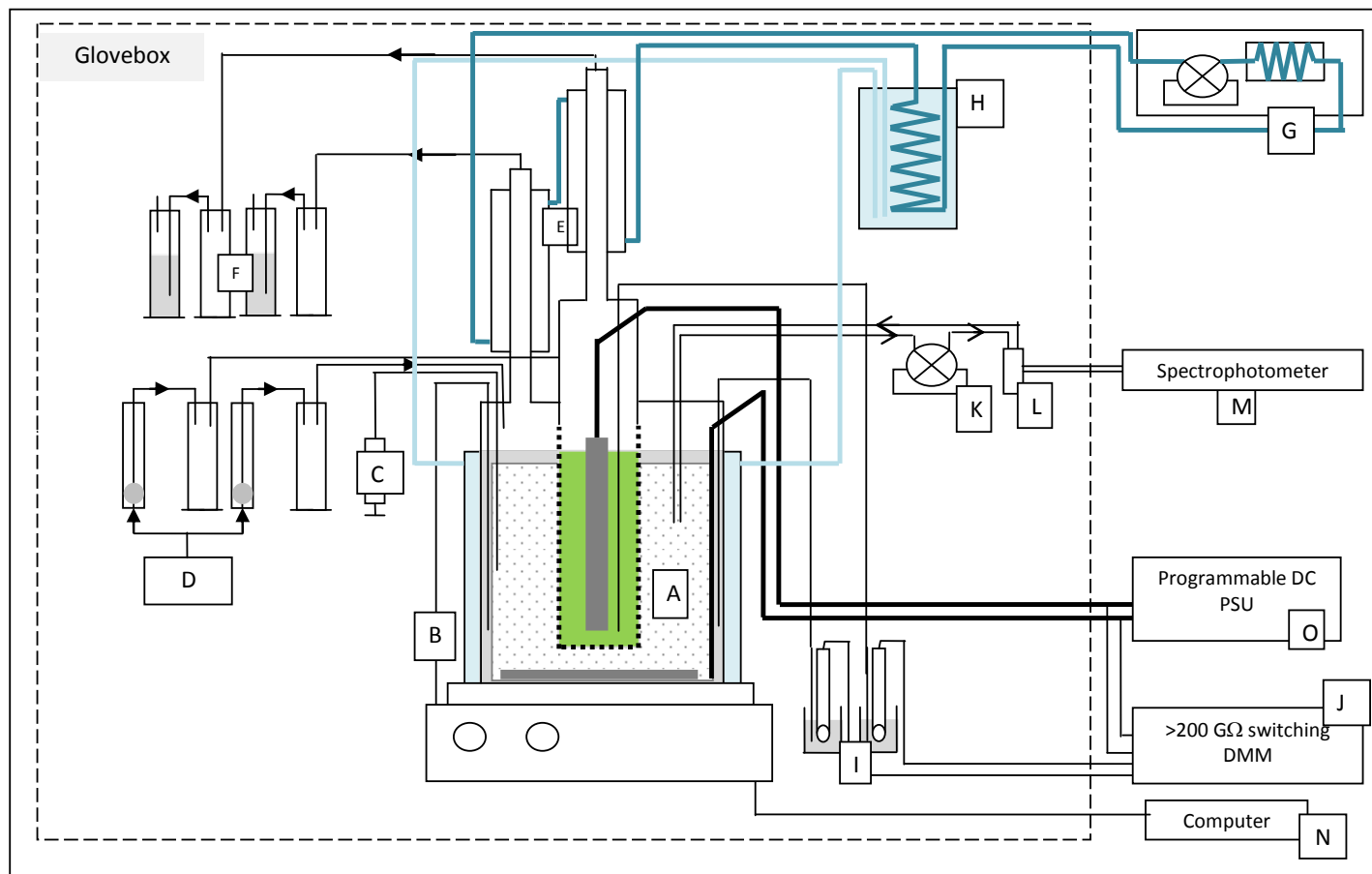
The apparatus is as used in the inactive studies[234], see Figure 71, with the following modifications:

- Glassware from inactive studies was used without modification [234]. Several different lids were used during the experiments due to breakages, the cause of the breakages was traced to stress placed upon the cathode compartment by the temperature sensor. Adjustment of the shape of the temperature sensor resolved this issue.
- An air pump supplied the sweep gas, instead of the house low pressure air
- 'Internal cooling water supply' was used to cool the jacketed dissolution vessel to minimise the consequences of breakage of the dissolution vessel. An 'internal cooling water supply was produced using a heat exchange vessel, which comprised of a 1 litre culture vessel containing water, a stainless steel cooling coil and a Pt100 temperature sensor. The stainless steel cooling coil was cooled, with the condensers, using a chiller-recirculator unit situated in an adjacent fumehood. Water from the heat exchange vessel was transferred to and from the jacketed dissolution vessel using a peristaltic pump.
- Temperature control was achieved setting the temperature on the hotplate and running the cooling water at a rate to remove the excess heat. The rate of cooling was controlled, to a degree, by controlling the peristaltic pump flow rate, and then the hotplate would apply heat to achieve thermostating. Thermostating via the chiller-recirculator unit was not possible as it also applied cooling water to the condensers and the permissioned temperature range of the chiller-recirculator is 5-30 °C.

A summary of the key features of the apparatus is as follows:

- 100 ml anode compartment with high surface area (111 cm<sup>3</sup>) 4 % ruthenium – 96 % platinum mesh anode, as used in earlier studies [225, 234]
- 2.5 cm diameter, 4 cm long Coorstek P-1/2-BC aluminium oxide porous cup cell membrane[234]
- 20 ml cathode compartment with tantalum pig-tail electrode[234]

- Anode vessel contained a Pt-100 temperature sensor placed inside a tantalum sheath [234]
- Anode vessel contained 0.8 mm PFA tube(s) for inline or atline UV-Vis analysis using a Hellma 0.5 mm pathlength flowcell and Zeiss MCS 501 spectrometer[234]
  - In-line analysis - early (low mass plutonium dioxide) experiments used a piston pump to pump the liquor through the flowcell. However later experiments, with larger masses of plutonium dioxide, resulted in problems with tubing connectors popping apart, due to the large amount of suspended particulates increasing pressure. Attempts to resolve this issue using new omnifit cones and later stainless steel Swagelok fittings where unsuccessful.
  - At-line analysis - later (high mass plutonium dioxide) experiments used a syringe to draw a sample through the flowcell. This method meant reduced risk of pumping liquor onto the glovebox base; however the frequent of data point collection was greatly reduced due to manual sampling. There was also a longer and variable time delay between taking the sample and measuring the UV-Vis spectra, this could determine silver(II) concentration at high concentrations, due to decomposition. It was also noted that plutonium dioxide solids collected in the cell and syringe resulting in losses from the experiment.
- The open-redox potential for the anode and cathode compartments was measured using the sample equipment used in earlier studies [234].
- An Agilent E3133A DC power supply was used to supply a fixed current to the cell. Current-voltages were set and trends logged by PC control. A fixed current was used to simplify the analysis of the results.



A – Flanged culture vessel separate compartment separated by porous membrane with water-jacket, anode Pt/Ru mesh, cathode Ta pigtail rare-earth stirrer bar, B – Pt-100 temperature sensor connected to heater-stirrer plate, C – Syringe for sampling, D – gas flow rate controller connected to air-pump, E – separate Leblig condensers for anode and cathode compartments, F – off-gas disentrainment vessel and sodium hydroxide trap for anode and cathode off-gases, G – Chiller recirculator unit, H – Heat exchange vessel for cooling jacketed vessel, I – salt bridge, and Pt or Ta wire electrode in measurement beaker, J – High resistance switching multimeter, K – ceramic piston pump, L – UV-Vis cell in cell holder M, two fibre optic connected to UV-Vis spectrophotometer, N – computer for control and data-logging hotplate, O – Programmable 22 A DC Power supply. Note, mains electrical cables not shown for clarity.

**Figure 71: Systematic diagram of plutonium dioxide dissolution apparatus**

#### ***5.4. Optimisation of a batch electrolysis cell for silver(II) generation to dissolve plutonium dioxide***

It is planned that the following paper will be submitted to the Journal of Industrial Chemical Research.

##### ***5.4.1. Introduction***

The dissolution of plutonium dioxide and mixed uranium plutonium oxide (MOx) with high plutonium contents using silver(II) is of industrial interest in the development of safe and sustainable future nuclear fuel cycles. A key challenge for the recycle of irradiated MOx fuel is to ensure the dissolution of the plutonium is achieved with high efficiency. As fine plutonium-rich heterogeneities from fuel manufacture [142, 235] currently lead small losses to waste streams. To increase head end process safety and minimise the waste long term radiotoxicity and heat output it is desirable to achieve an dissolution with a high recovery. A second example for the use of silver(II) is the purification of plutonium dioxide prior to fuel fabrication or for americium-241 production[236]. The production of americium-241 for use as radioactive power sources, which can be used in the radioactive thermal generators (RTGs) for space exploration is currently under development for the European space agency (ESA)[236].

Mediated oxidative dissolution of plutonium dioxide quickly became the technology of choice for the dissolution of plutonium dioxide [195], as the technology is low salt, thus reducing waste volumes, and avoids the use of highly corrosive fluorides [207]. The technology works by use of a mediator or catalyst to generate of a oxidizing species that has a sufficiently high oxidation potential to dissolve plutonium dioxide [52], after which the species can be regenerated (Figure 72). The use of cerium, cobalt and silver are all suitable, but silver(II) is preferred due to the high oxidation potential, relative high stability in nitric acid and rapid kinetics of reaction with plutonium dioxide [196]. The generation of the oxidising species, silver(II), can be achieved using ozonation or chemical and electrochemical methods[237]. The use of electrochemistry in glovebox environments is often the preferred technique and this work describes optimisation studies aimed at understanding the key parameters in the development of batch industrial

cells. These processes are termed mediated electrochemical oxidation (MEO) [238] or catalysed electrochemical plutonium oxide dissolution (CEPOD) processes [195]. Figure 72 also highlights a counter reaction, the oxidation of water, this reaction is known to occur via two mechanisms, **Eq 55** [122]. In these reactions silver(I) and silver(II) are the dominate solution species and silver(III) has been suggested to be present as a transient species, based on the kinetics of reaction with water[122]. Another example of a side reaction for silver(II) is the migration of catholyte (nitric acid reduction products, e.g. nitrous acid) into the anolyte through the porous membrane.

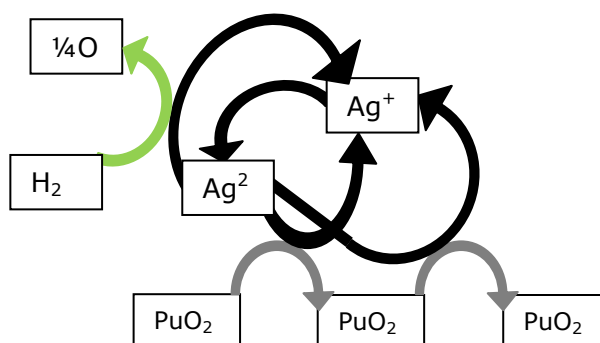


**Figure 72: Dissolution of plutonium dioxide with silver(II)**



**Eq 55**

The experiments described herein use classical electrochemical methods in an applied manor aimed at understanding the factors that control the generation and stability of silver(II). The effect of cell variables are investigated using linear staircase voltammetry (LSCV) and bulk electrolysis (BE). An example to show the effectiveness of plutonium dioxide dissolution is shown as an example, where the rapid dissolution of 11.4 g plutonium dioxide to produce a 100 g.l<sup>-1</sup> product.

#### **5.4.2. Experimental**

All solutions where prepared from AR nitric acid (Fishers), AR NormaPur silver nitrate (VWR) and 18 MΩ water (Elga). A systematic diagram of the apparatus is shown in Figure 73. The cell used in this work is similar to that used in the early US CEPOD development work[195]. Custom glassware was designed with a flat bottomed vessel, a 100 ml working anode compartment, a removable central 25 mm diameter cathode compartments with space under the cathode compartment for a magnetic follower. Several different designs of

cathode compartment where used with 25 mm $\varnothing$  sinter glass disc, glass thimble (ACE grade E) and Alumina porous cup (Corrstek). The cell used a single platinum-4.5 % ruthenium basket anode (Johnson Matthey type 72070) with a surface area of 116 cm<sup>2</sup>. Different cathodes were testing including a tantalum pig-tail and stainless steel mesh fabricated into a basket or folded up. Temperature measurement were made using a Pt-100 thermometer sheathed in a titanium tube with end cap, manufactured in-house and welded by Arc alloys, UK. The cell temperature was controlled using a water jacketed vessel fed from a thermostated water recirculator unit (Haake) and heating from a hotplate (IKA). Air was used to purge the anode and cathode vessel head-spaces and off-gases scrubbed using sodium hydroxide gas wash bottles.

The LSCV experiments were carried out by applying voltage steps and measuring applied voltage, current and potential. Separate experiments where run to measure the anode or cathode potentials, these where made versus a gelled double Junction Ag/AgCl reference electrode (Sentek) separated from the electrochemistry cell by 0.8 mm ID tube packed with glasswool thread. These experiments were run using an 22 A/8 V DC power supply (Agilent E3133A) and digital multimeter, DMM, (Agilent E3133A). Voltage scans and measurements were made using MS excel VBA utilizing Agilent Intuilink add-in.

Bulk electrolysis was carried out at constant current, during the experiments a switching DMM (Keightley 2700/E with 7700 module) was used to measure the voltage, current (via 25m $\Omega$  shunt, Murata Power Solutions), anode and cathode potentials. Potentials were measured against Ag/AgCl reference electrodes and pseudo reference electrodes (platinum, tantalum or stainless steel wire). In-situ silver(II) concentration was measured using a 0.05 cm quartz flow curvette (Hellma), a piston pump with ceramic piston head (FMI) and Zeiss MCS UV-Vis spectrometer. This is shown schematically in Figure 73. The extinction coefficient for silver(II) was determined from the rate of generation of silver(II) (constant current coulometry), results were compared to an off-line UV-Vis method. The off-line method allow the reaction of a small of silver(II) to react with cerium(III) to produce cerium(IV), which was quantified by UV-Vis. Plutonium dioxide dissolution experiments were carried out in a high integrity alpha containment glovebox using the same cell setup.

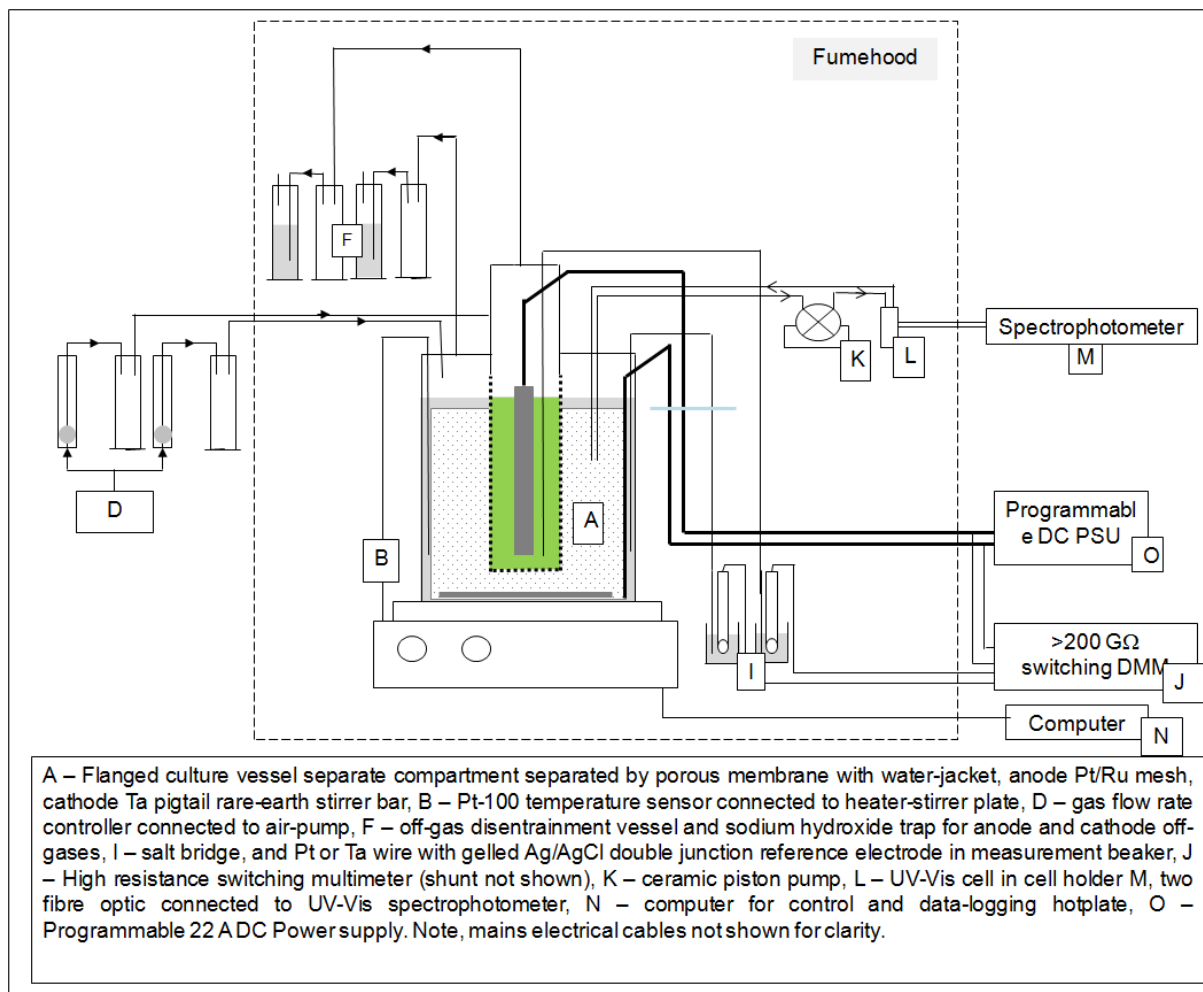


**Figure 73: Schematic diagram of bulk electrolysis experiment**

### 5.4.3. Results and discussion

#### 5.4.3.1. Linear Sweep Staircase Voltammetry

To characterise the potential generation rates of the cell linear staircase voltammetry has been used to characterise the effect of voltage and potential – current ( $V-I$  and  $E-I$ ) plots have been recorded. These have been used to investigate the effect of various cell parameters such as nitric acid and silver nitrate concentration, stirrer rate, membrane and cathode type.

To confirm the non-standard voltammetry setup was functioning adequately a series of experiments in 4 mol.l<sup>-1</sup> nitric acid without and with various silver nitrate concentrations is described here. In this series of experiments the same cathode type and membrane have been used. The results of this series of experiments has been compared with theory by carrying out Tafel analysis, this compares the relationship between potential and electrochemical kinetics (current density,  $J$ , A.m<sup>-2</sup>). Figure 74 shows an example results from this analysis, the  $E-J$  curve for 4 mol.l<sup>-1</sup> electrolyte due to water oxidation has been subtracted from 4 mol.l<sup>-1</sup> nitric acid – 0.1 mol.l<sup>-1</sup> silver nitrate curve and linear regions are used for the Tafel analysis. These plots produce similar transfer coefficients,  $\alpha_{cathodic}=0.82$ ,  $\alpha_{anodic}=0.90$ , to other workers 0.84-0.86[121, 225, 226, 239]. The comparison between the silver concentration and the exchange current density is shown in Figure 75, this shows the current density under these conditions at the standard electropotential is 125 mA.m<sup>-2</sup>.mol.l<sup>-1</sup>. However the determined standard electropotential,  $E_0$ , of 1.85 V<sub>NHE</sub> is lower than other workers 1.90-1.95 V<sub>NHE</sub>, this is easily rationalised as the potential measurement was carried out using a relatively low resistance DMM (>10 GΩ), rather than an electrometer (>1000 GΩ). These observation are supported by the preparation of a Nernst plot with a series of solutions with known cerium(III,IV) ratio. Measurements of the potential of these solutions with a Hanna HI4222 pH meter and the DMMs used in this work show the Agilent DMM showed measurements *ca.* 10 mV lower than the pH meter, Table 18. However despite the potential measurement bias, this does not affect the general applied interpretation in the cell optimization studies. Table 18 also shows the measured potentials with the Keightley DMM (>200 GΩ) used in the bulk electrolysis experiments and this shows similar measured potentials to the Hanna pH meter.

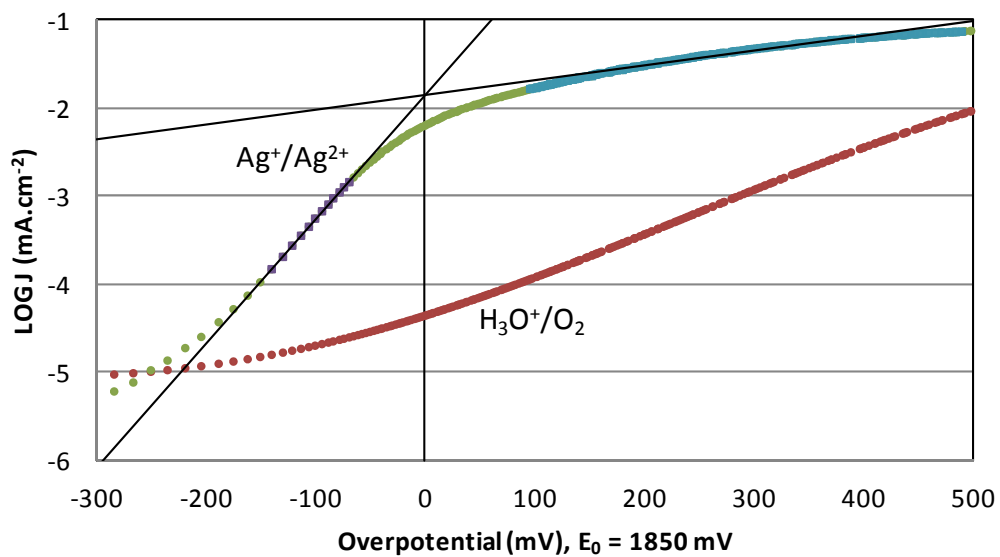


Figure 74: LSCV – Tafel plot, 4 mol.l<sup>-1</sup> with and without 0.1 mol.l<sup>-1</sup> AgNO<sub>3</sub> (E<sub>0</sub>=1.85 V<sub>NHE</sub>)

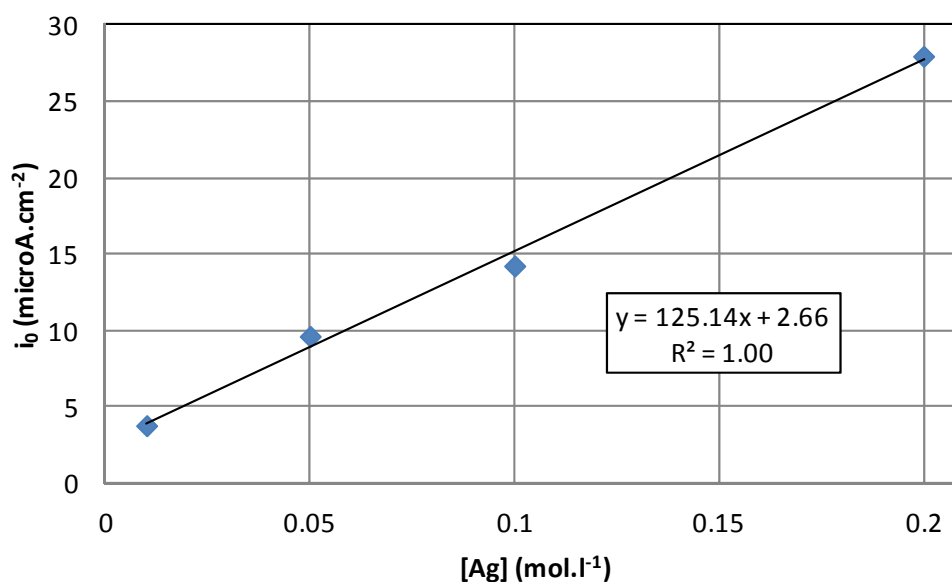


Figure 75: LSCV – effect of [Ag] with exchange current density

**Table 18: Measured potentials over rate of  $[\text{Ce}^{3+}]/[\text{Ce}^{4+}]$** 

$[\text{Ce}^{4+}]/[\text{Ce}^{3+}]$	Hanna HI4222 (V)	Agilent DMM (V)	Keightley DMM (V)
0.122	1.403	1.375	1.394
0.235	1.389	1.372	1.384
1.22	1.350	1.330	1.348
10.1	1.297	1.283	1.297
111	1.206	1.188	1.204

Figure 76 shows the change in current with potential for various silver concentrations. Due to small amount of silver (100 ml 0.01-0.2 mol.l<sup>-1</sup> silver) and high current (up to 10 A) electrolysis occurs during the voltammetry sweep. This can be used to rationales the lack of a 'generation peak', which is typical observed in cyclic voltammetry carried out under un-stirred conditions, where the reduction is current is due to depletion of the reactant concentration with the vicinity of the electrode. This same phenomena can be used to explain the effect of anode nitric acid concentration, Figure 77, as at higher nitric acid concentrations the silver(II) is more stable, so there are lower concentration of silver(I); due to this reduction in silver(I) concentration there is a decrease in rate of oxidation of silver(II) (current at a defined potential). The rate of stirring of the anode solution, Figure 78, clearly increases the silver(II) generation rate by improving mass transfer. Increasing the surface area of the anode – cathode separator membrane also has a pronounced effect upon the generation rate (Figure 79). There silver(II) generation rate increases in the following order sintered glass flat disc < sintered glass thimble < alumina porous cup, this order reflects an increase in the surface area and porosity of the separators. The effect of cathode nitric acid concentration (8-15.8 mol.l<sup>-1</sup>) and type of cathode electrode did not show an observable effect in the *I-E* curves. However, electrode design has a significant effect upon the *V-E* curves at less than 1.5 V voltage (Figure 80) with cell resistance decreasing in this order tantalum pig tail (*ca.* 1.6 cm<sup>2</sup>) > stainless steel gauze basket (*ca.* 7 cm<sup>2</sup>) > stainless steel gauze folded around contact rod (*ca.* 12 cm<sup>2</sup>). The effect of nitric acid concentration is shown in Figure 81, *ca.* 14 mol.l<sup>-1</sup> cathode nitric acid produced the highest current density at a defined potential. Higher and lower concentrations yield lower current densities. This is pronounced for 15.8 mol.l<sup>-1</sup> (concentrated) nitric acid, which shows significantly lower current densities (duplicate experiment shown) compared to even 8 mol.l<sup>-1</sup> nitric acid.

In this type of cell under study the rate of silver(II) generation is defined by the silver concentration, stirrer rate and membrane type or size. The effect of

anode nitric acid upon silver(II) generation rate has not been observed, but it is known that increasing nitric acid concentration decreases the silver(II) decomposition rate. Little effect upon silver(II) generation rate has been observed for cathode type and size and cathode nitric acid concentration have been shown, despite large anode:cathode surface area ratio.

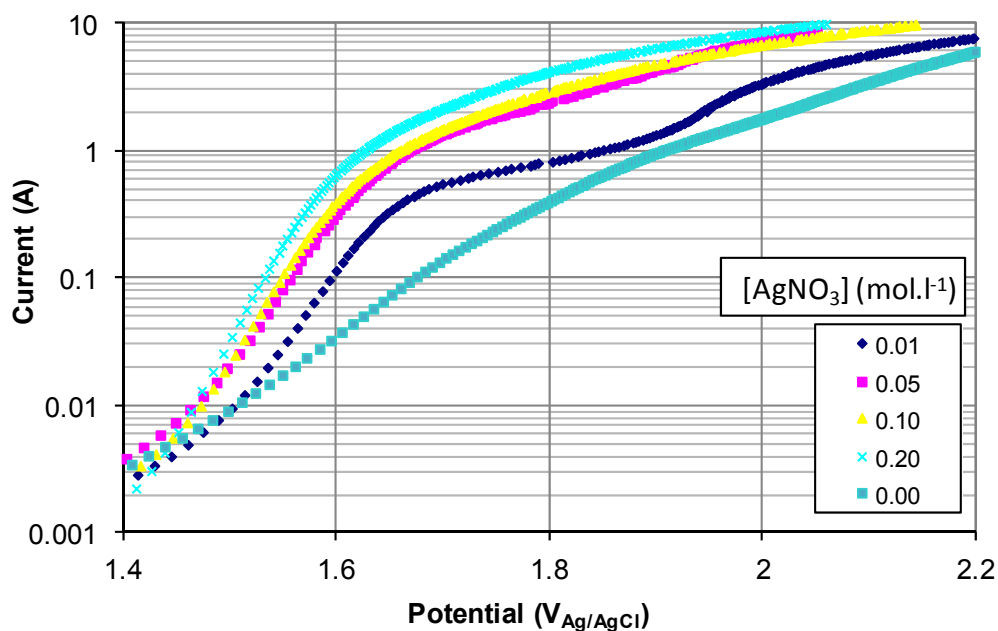


Figure 76: LSCV – Effect of anode [AgNO<sub>3</sub>] in 4 mol.l<sup>-1</sup> HNO<sub>3</sub>, 500 rpm stirring)

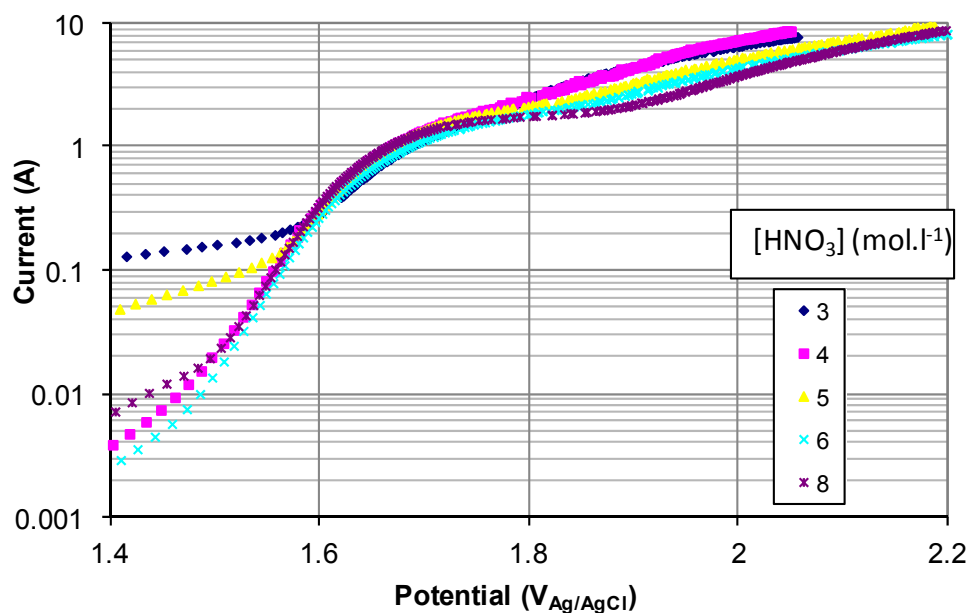


Figure 77: LSCV – Effect of [HNO<sub>3</sub>] for 0.05 mol.l<sup>-1</sup> AgNO<sub>3</sub>, 1500 rpm stirring

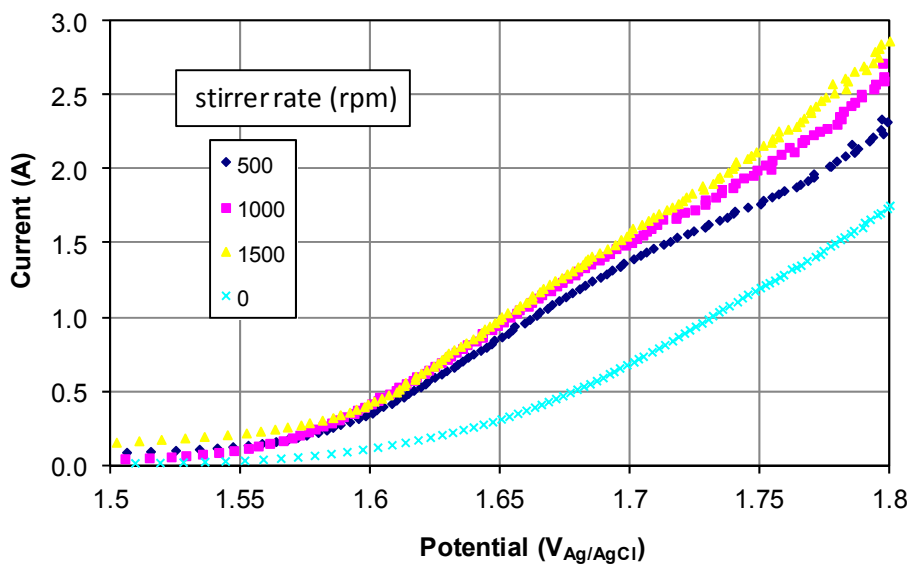


Figure 78: LSCV – Effect of stirring rate for 0.05 mol.l<sup>-1</sup> AgNO<sub>3</sub> – 4 mol.l<sup>-1</sup> HNO<sub>3</sub>, 1500 rpm stirring

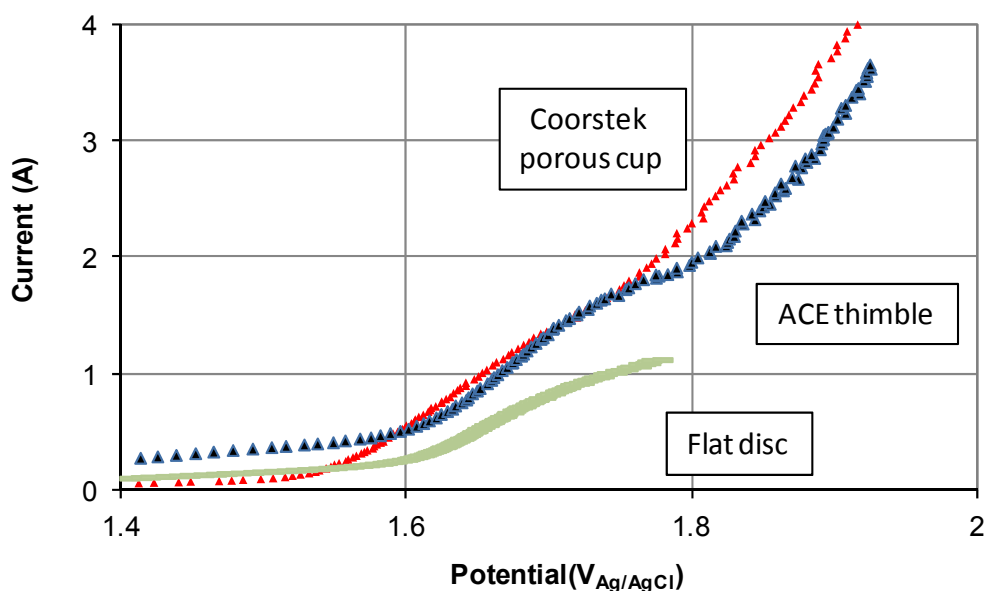


Figure 79: LSCV – Effect of membrane type, 0.05 mol.l<sup>-1</sup> AgNO<sub>3</sub> 4 mol.l<sup>-1</sup> HNO<sub>3</sub>, 500 rpm stirring

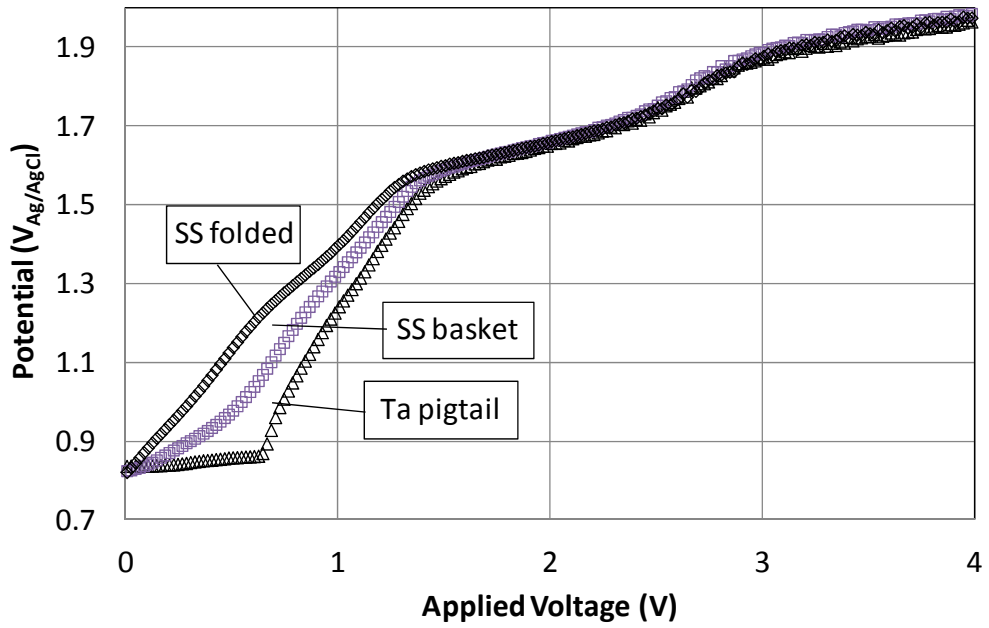


Figure 80: LSCV – Effect of cathode type (ACE thimble,  $0.05 \text{ mol.l}^{-1} \text{ AgNO}_3$   $4 \text{ mol.l}^{-1} \text{ HNO}_3$ )

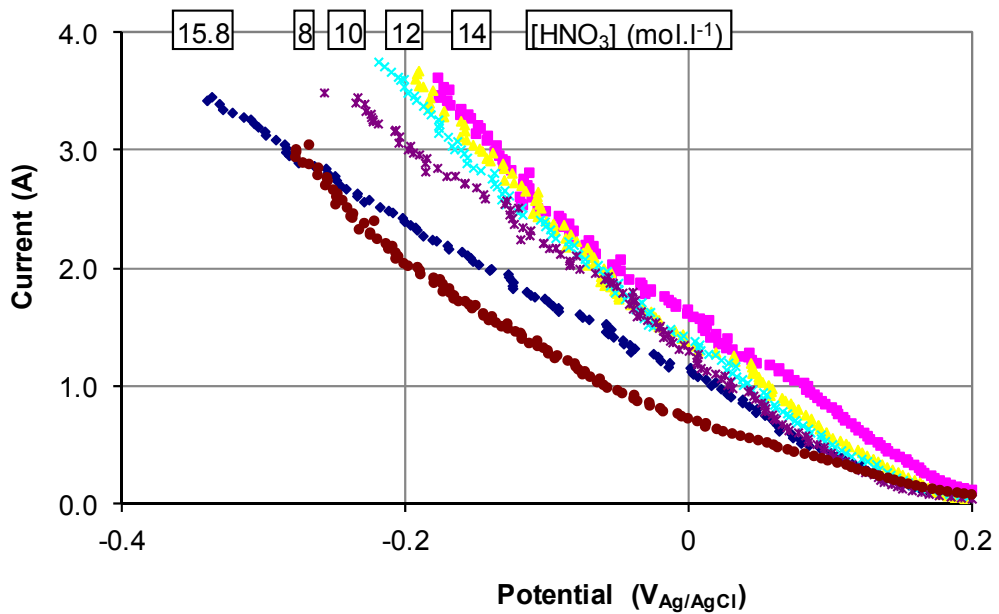


Figure 81: LSCV – Effect of cathode nitric acid concentration (shown in figure) upon cathode potential, Ta pigtail cathode

### 5.4.3.2. Bulk Electrolysis

To verify the LSCV results a series of constant current electrolysis experiments have been carried out. These experiments allowed the measurement of the voltage, current, anode and cathode potential and the silver(II) concentration by UV-Vis spectroscopy. An example inline UV-Vis experiment shows the rapid generation of silver(II) at 550 nm (Figure 82). Potential measurements were made using the Keithley DMM and were not subject to the same bias as LSCV experiments (Table 18). Figure 83 illustrates the results from a typical experiment, with a rapid increase in silver(II) concentration, followed by a steady state concentration, then after the current is switched off the decomposition of silver(II). Two pieces of information can be extracted from this UV-Vis data, i) the initial silver(II) generation rate, which can be used to determine generation efficiency and ii) after the current is switched off the decomposition rate of silver(II) can be determined.

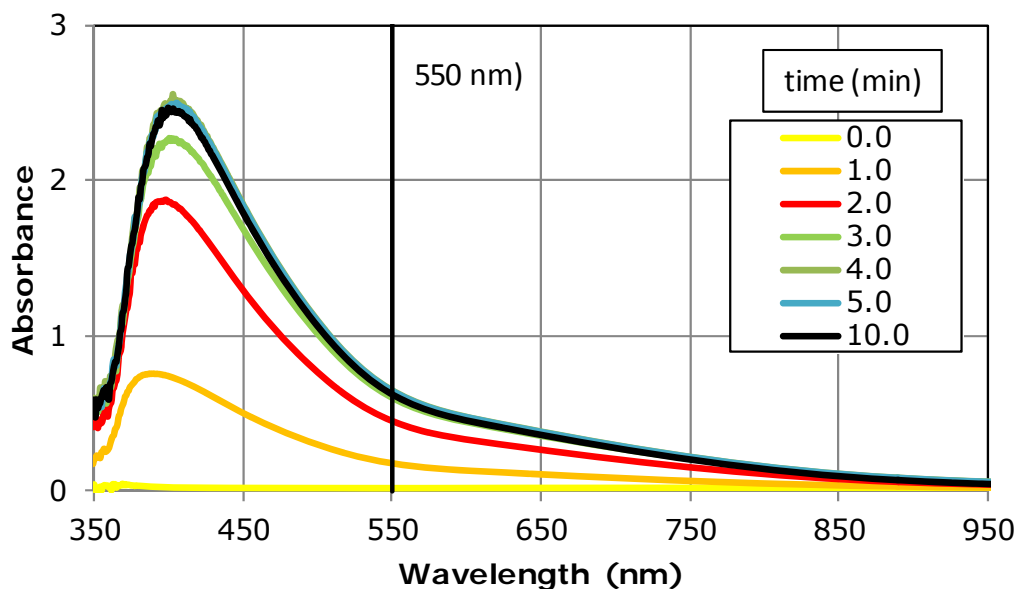
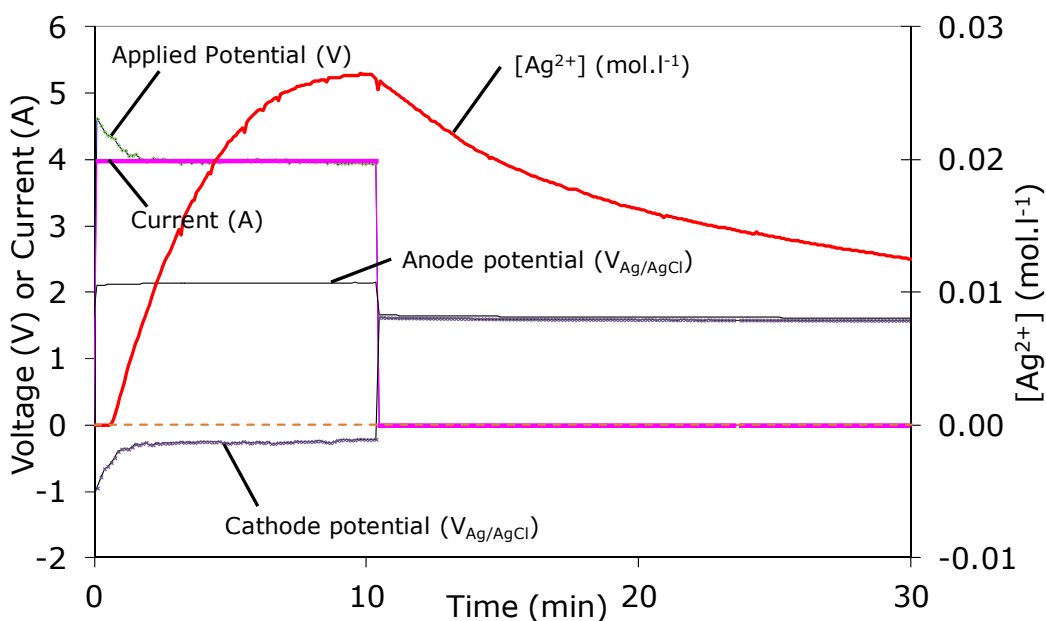


Figure 82: Bulk electrolysis – example UV-Vis spectra



**Figure 83: Bulk electrolysis – Potential, voltage, current (4 A),  $[Ag^{2+}]$  time plots ( $0.05 \text{ mol.l}^{-1} AgNO_3$   $4 \text{ mol.l}^{-1} HNO_3$ ,  $25 \text{ }^\circ\text{C}$ )**

#### 5.4.3.3. Generation of silver(II)

Using the initial rate of silver(II) generation from the inline UV-Vis data the effect of cell parameters have been studied. The results in the following section are compared with the gradient from a series of experiments at low current (0.5 and 1 A), which is assumed to produce silver(II) at a 100 % efficiency, the assumption is valid based on literature studies. Using a assumed electrode surface area of  $116 \text{ cm}^2$ , the results in this section are plot as current density applied ( $J_{\text{applied}}$ ) vs the current density that is used to generate silver(II), i.e. the effective current density ( $J_{\text{effective}}$ ), So when  $J_{\text{effective}}$  deviated from the  $J_{\text{applied}}$ , the system is operating at a current density with a degree of mass transfer control.

These results clearly show that there is an improvement in silver(II) generation with increasing agitation rate between 500 and 1000 rpm, but there is little difference between 1000 and 1500 rpm, Figure 84. Increasing concentration of silver nitrate increases the generation rate of silver(II), Figure 85. There appears to be little effect of temperature on the generation efficiency of silver(II) at 4 A, Figure 86, it is believed the decrease in observed generation rate at higher temperatures is due to the decomposition of silver(II) in the UV-Vis flow loop. This is supported by the observation of a noisy steady state silver(II) profile, which is due to evolution of oxygen from

silver(II) decomposition in the UV-Vis line. The higher surface area and higher porosity of the Corrstek porous cup shows improved generation efficiencies compared to the ACE glass thimble (Figure 87), which is believed to be due to a combination of migration of catholyte into the anolyte consuming silver(II) and the higher surface area of the Corrstek membrane.

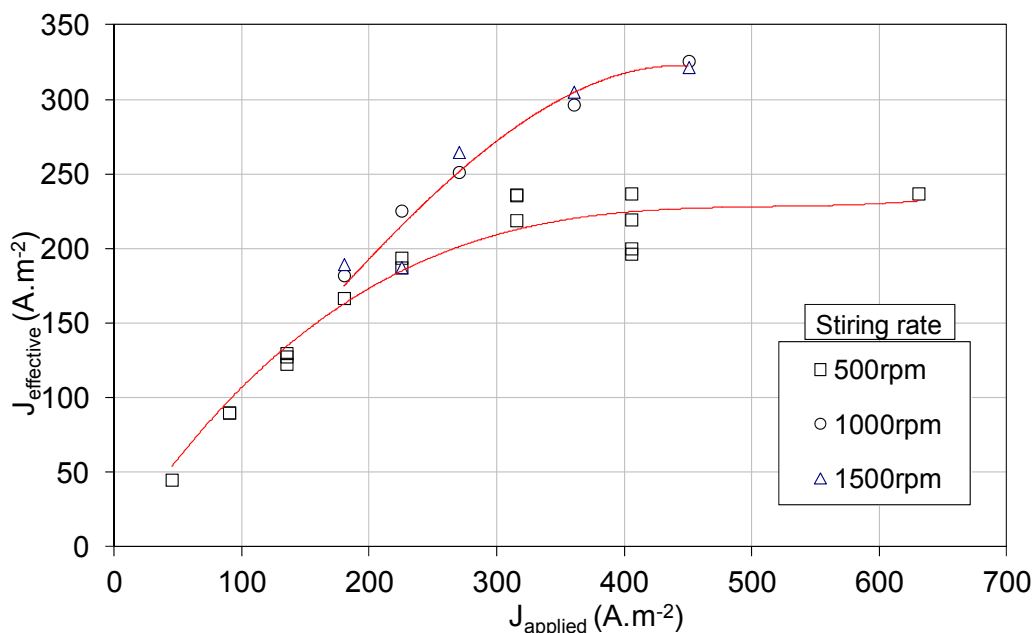


**Figure 84: Bulk electrolysis – Effect of stirrer rate upon  $\text{Ag}^{2+}$  generation efficiency using ACE E membrane ( $0.05 \text{ mol.l}^{-1} \text{ AgNO}_3$   $4 \text{ mol.l}^{-1} \text{ HNO}_3$ ,  $25 \text{ }^\circ\text{C}$ )**

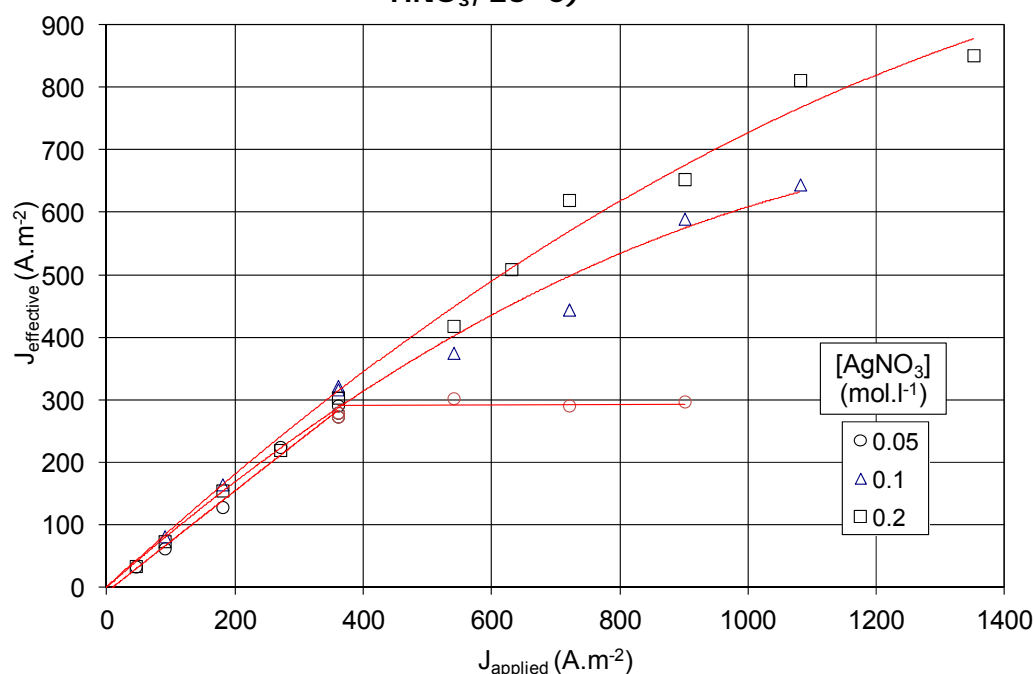


**Figure 85: Bulk electrolysis – Effect of  $[\text{AgNO}_3]$  on  $\text{Ag}^{2+}$  generation efficiency using bored ACE E membrane ( $0.05 \text{ mol.l}^{-1} \text{ AgNO}_3$   $4 \text{ mol.l}^{-1} \text{ HNO}_3$ ,  $25 \text{ }^\circ\text{C}$ )**

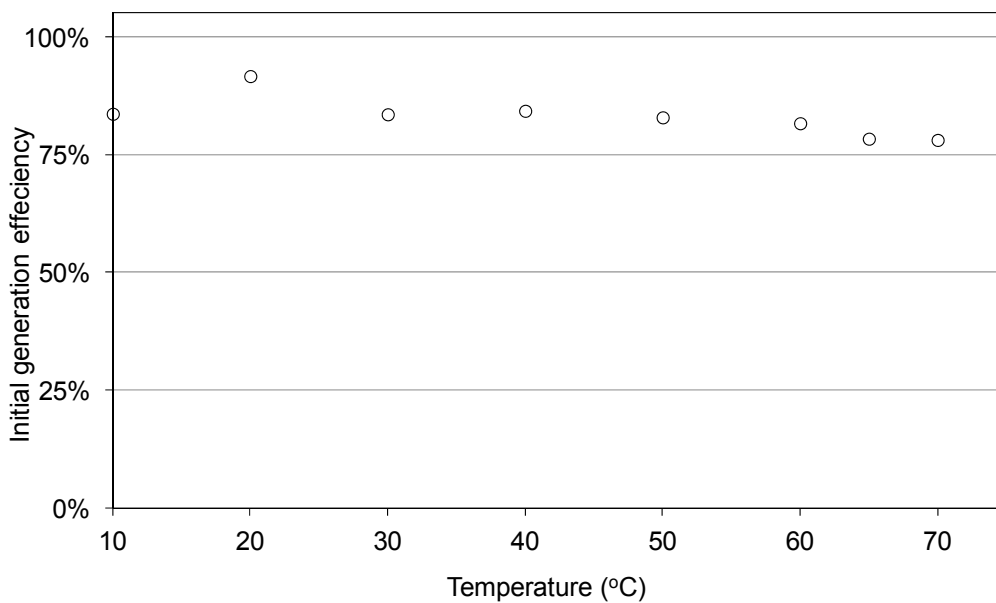


**Figure 86: Bulk electrolysis – Effect of temperature upon  $\text{Ag}^{2+}$  generation efficiency (4A, bored ACE E membrane,  $0.05 \text{ mol.l}^{-1} \text{ AgNO}_3$   $4 \text{ mol.l}^{-1} \text{ HNO}_3$ , 25 °C)**

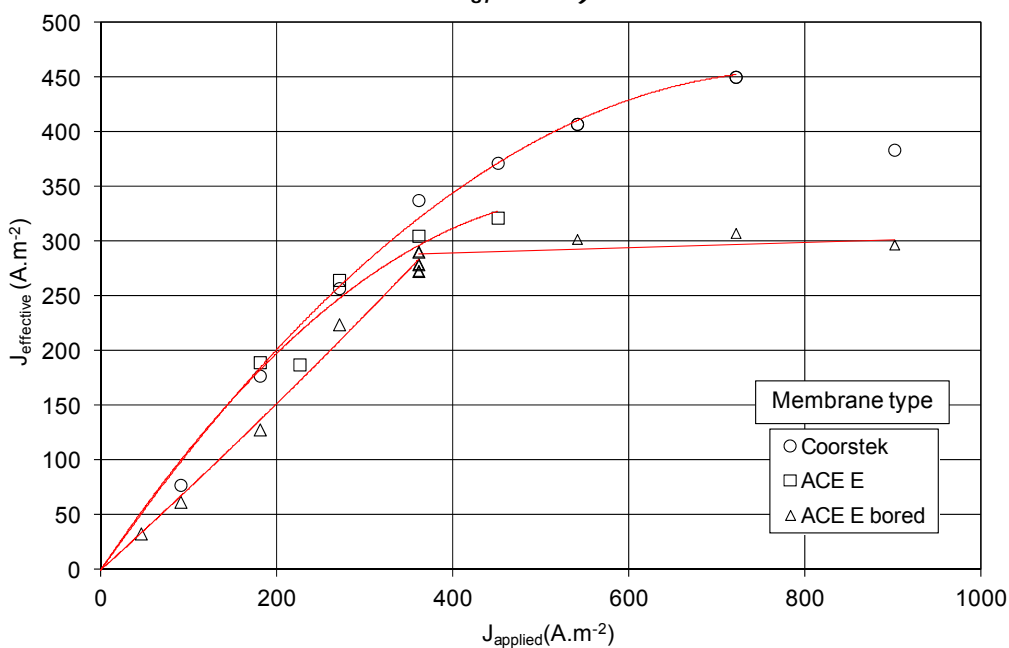


**Figure 87: Bulk electrolysis – Effect of membrane type upon  $\text{Ag}^{2+}$  generation efficiency ( $0.05 \text{ mol.l}^{-1} \text{ AgNO}_3$   $4 \text{ mol.l}^{-1} \text{ HNO}_3$ , 25 °C)**

#### 5.4.3.4. *Dzcomposition of silver(II) and steady state silver(II) concentrations*

A series of the bulk electrolysis experiments measured the silver(II) concentration after the current had been turned off. This allows the determination of the decomposition rate of silver(II). During the electrolysis a steady state silver(II) concentration forms due to the balance of two competing reactions, generation due to electrolysis and decomposition due to reaction of silver(II) with water, this is illustrated mathematically in Eq 56, which is a similar equation to that used by Chiba[213]. The effect of diffusion of cathode reduction products into the anolyte is currently not included in the model and this is a limitation, which will be the subject of future work. The rate constant  $k_1$  and  $k_2$  was determined by the gradient of the inverse silver concentration – time and inverse silver concentration squared – time plots. The effect of each chemical variable for experiments with the bored ACE E membrane where individually compared and then subject to a global analysis. An example of the comparison between the determined and calculated rate constants,  $k_1$ , Eq 57, clearly shows a degree of variation, and Figure 89. It is believed that these variations were due to differences in rate of diffusion of catholyte reduction products into the anolyte (as cathode-anode pressure differential was not controlled or determined) and in some experiments imperfect temperature control due to ohmic heating.

$$\frac{d[Ag^{2+}]}{dt} = \frac{\epsilon I}{FV} - k_1 \frac{[Ag^{2+}]^2}{[Ag^+]} - k_2 \frac{[Ag^{2+}]^4}{[Ag^+]} \quad \text{Eq 56 – } Ag^{2+} \text{ generation and decomposition}$$

Where  $\epsilon$  is efficiency,  $I$  is current (A),  $F$  is faradays constant and  $V$  is volume (l), the concentration of silver(I) and (II) are  $[Ag^+]$  and  $[Ag^{2+}]$  respectively ( $\text{mol.l}^{-1}$ ).

$$k_1 = 1.75 \times 10^{15} \left( \frac{1.22}{[HNO_3]} - 0.338 \right) [Ag] e^{\frac{-80600}{RT}} \quad \text{Eq 57 – } k_1 \text{ and } k_2 \text{ model}$$

$$k_2 = \frac{1.6 \times 10^{24}}{[HNO_3]^4 [Ag]} e^{\frac{-103200}{RT}}$$

Where the total silver and nitric acid concentrations are  $[Ag]$  and  $[HNO_3]$  respectively ( $\text{mol.l}^{-1}$ ),  $R$  is the molar gas constant and temperature is  $T$  (K)

Decreasing temperature, increase silver and nitric acid concentrations and rate of silver(II) generation (current and/or efficiency) increased the steady

state silver concentrations. These findings are inline with the observations of other workers [122, 218].

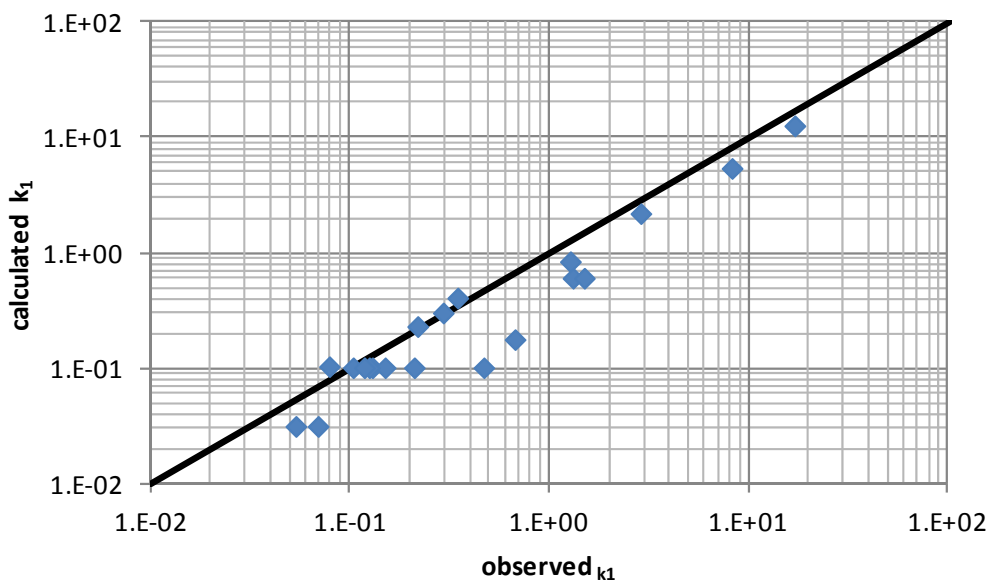


**Figure 88: Bulk electrolysis – Comparison of determined and calculated  $k_1$**

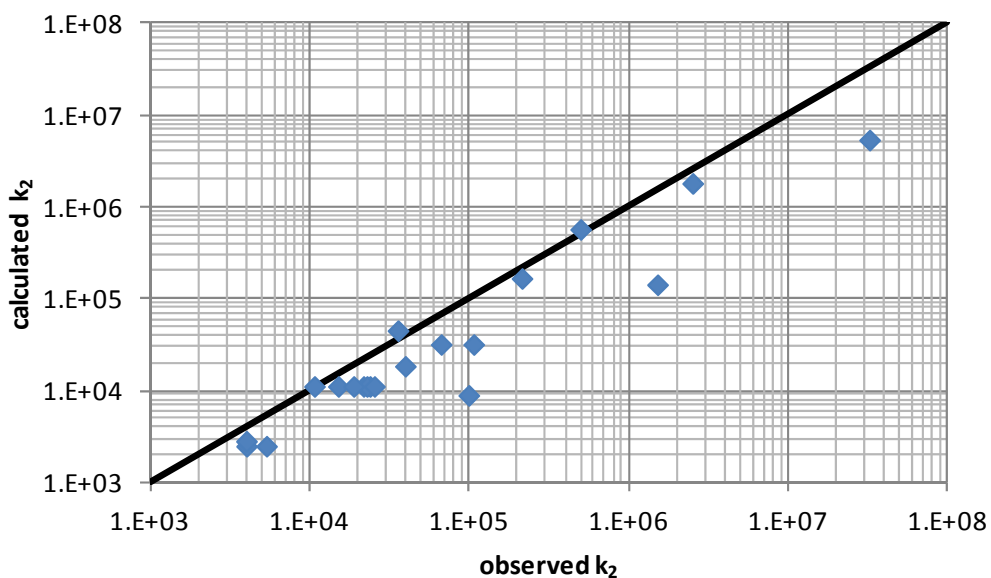


**Figure 89: Bulk electrolysis – Comparison of determined and calculated  $k_2$**

Figure 90-Figure 92 shows the generation, steady state and decomposition of silver(II) for the effect of temperature (bored ACE E membrane), nitric acid

concentration, silver nitrate concentration. Figure 93 and Figure 95 shows the effect of temperature and applied current using the Corrstek membrane.

Figure 90 how the increases the nitric acid concentration decrease the rate of decomposition of silver(II), thereby increasing the steady state silver(II) concentration. These results clearly shown two abnormalities, the 4 mol.l<sup>-1</sup> nitric acid concentration experiment virtually shows identifiable results to the 5 mol.l<sup>-1</sup> results and the 8 mol.l<sup>-1</sup> nitric acid experiment shows lower generation efficiency, which is believed due to an issue with the stirring rate.

Figure 91 shows increasing the silver concentration, increases the steady state silver(II) concentrations, due to higher concentrations of silver(I) at the electrode surface. Analysis of the decomposition rate of silver(II) after electrolysis is complete shows the initial rate ( $k_2$ ) is smaller for higher silver concentrations, however the slower ( $k_1$ ) decomposition rate increases with increasing silver(II) steady state.

Figure 92 shows that increasing the temperature increases the rate of decomposition of silver(II) and decreases the steady state silver(II) concentration. Analysis of the silver(II) decomposition curves allows the determination of activations energies of 80.6 and 103 kJ.mol<sup>-1</sup> for  $k_1$  and  $k_2$  respectively. Po determined values of 93.3±3.7 and 90.2±1.7 kJ.mol<sup>-1</sup> for  $k_1$  and  $k_2$  respectively [122]. Figure 93 shows a repeat experiment showing the effect of temperature using a Corrstek membrane, these results clearly show the higher stability. This is due to (i) the higher rates of generation of silver(II) with the large membrane and (ii) if is also suspected that the finer porosity of the Corrstek membrane compared to the Bored ACE E membrane reduces the diffusion rate of catholyte into the anolyte compartment. Comparison of the modelled experiments (Figure 94) simulate the major fractures of the bored ACE E membrane experiments (Figure 92), but the model over predicts the silver(II) stability. Comparison of the modelled results (Figure 94) with the Corrstek membrane (Figure 93) a larger underestimation of the silver(II) stability, reflecting the higher generation rate and stability of silver(II) using the Coorstek membrane.

Figure 95 shows increasing the applied current increases the generation rate and steady state silver(II) concentrations. The effects of ohmic heating at high currents (8 A) can also be seen; this leads to an increase in solution temperature, which increases the silver(II) decomposition rate and steady state concentration.

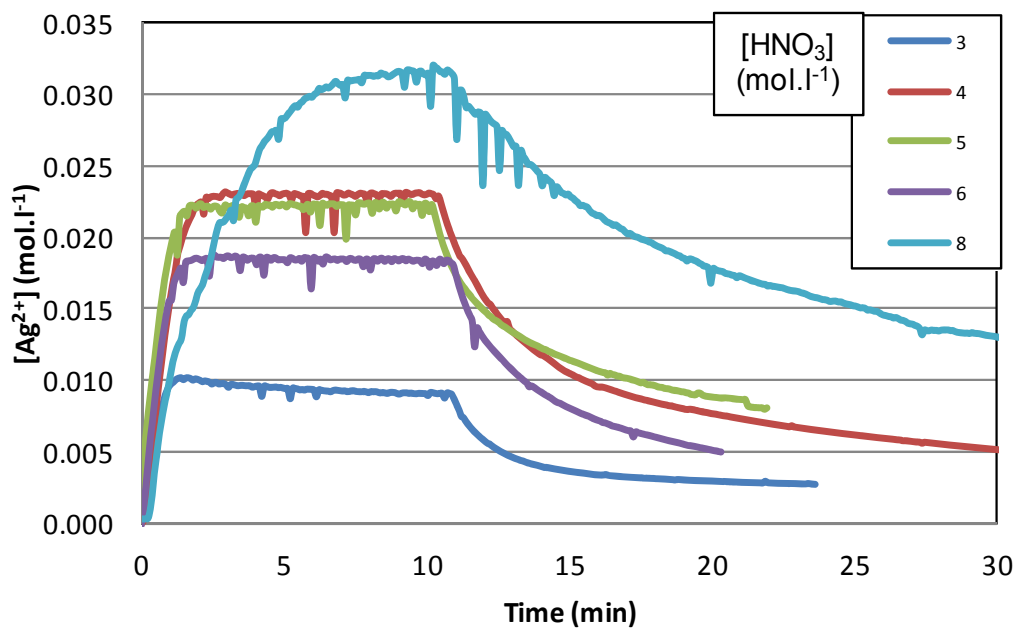


Figure 90: Bulk electrolysis – Effect of  $[\text{HNO}_3]$  (3-8  $\text{mol.l}^{-1}$ ) upon the steady state and decomposition of  $\text{Ag}^{2+}$  (0.05  $\text{mol.l}^{-1}$   $\text{AgNO}_3$  + 30 °C with bored ACE E membrane)

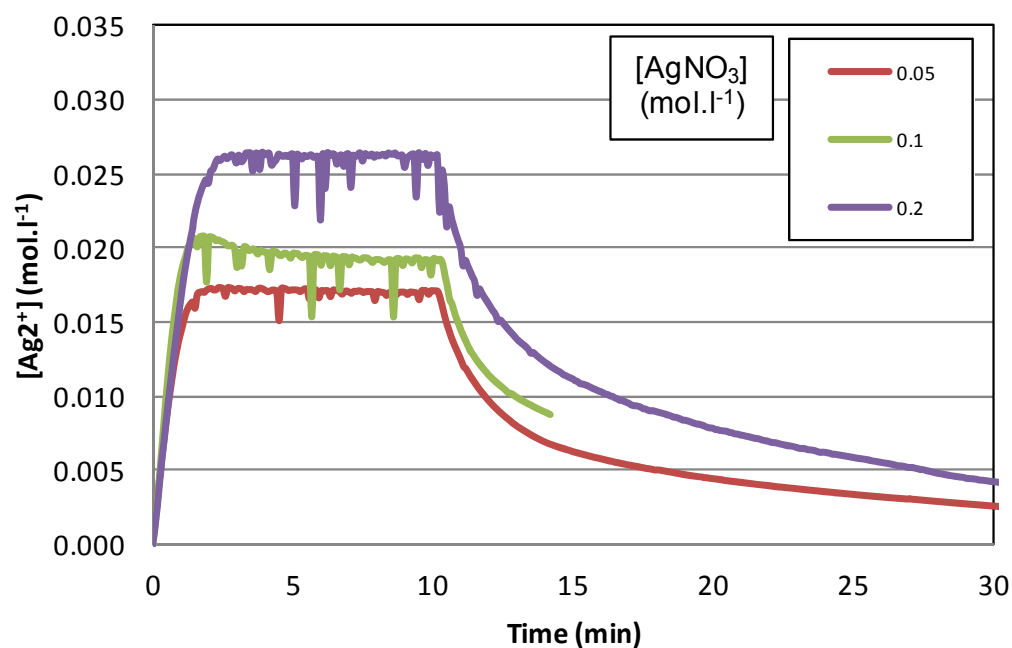
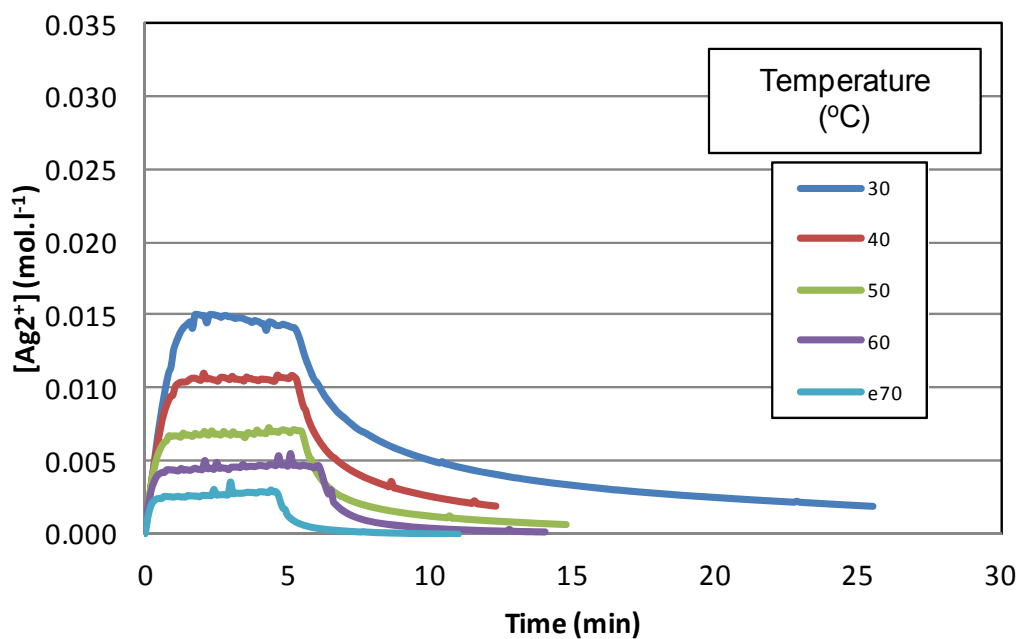
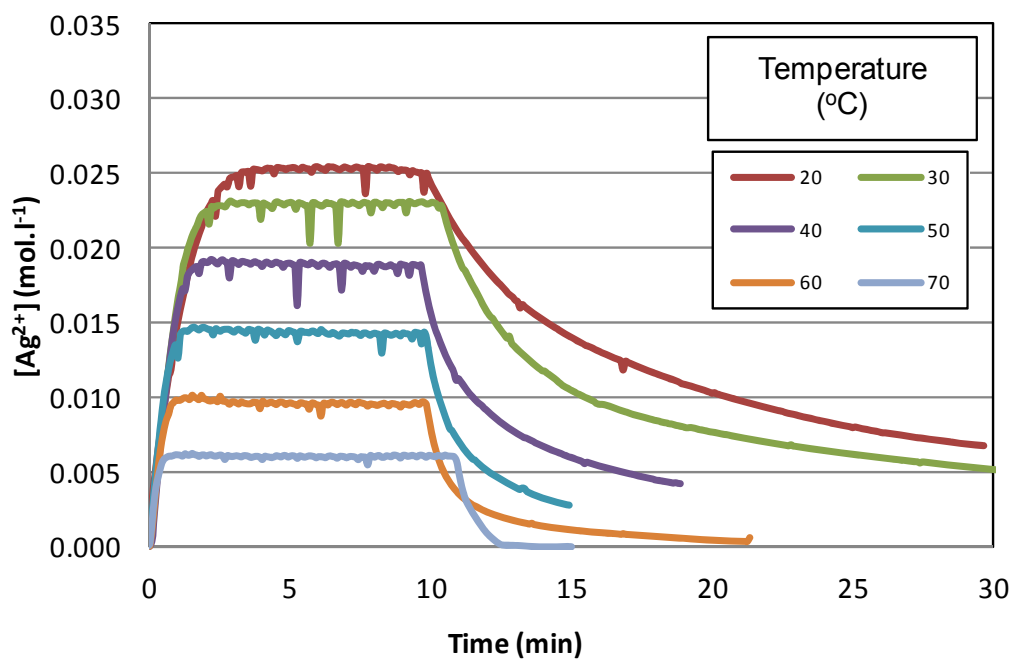


Figure 91: Bulk electrolysis – Effect of  $[\text{AgNO}_3]$  upon the steady state and decomposition of  $\text{Ag}^{2+}$  (4  $\text{mol.l}^{-1}$   $\text{HNO}_3$  ~30 °C with bored ACE E membrane)



**Figure 92: Bulk electrolysis – Effect of temperature (30-70 °C) upon the steady state and decomposition of  $\text{Ag}^{2+}$  ( $0.05 \text{ mol.l}^{-1} \text{ AgNO}_3 - 4 \text{ mol.l}^{-1} \text{ HNO}_3$  with bored ACE E membrane)**



**Figure 93: Bulk electrolysis – Effect of temperature (20-70 °C) upon the steady state and decomposition of  $\text{Ag}^{2+}$  ( $0.05 \text{ mol.l}^{-1} \text{ AgNO}_3 - 4 \text{ mol.l}^{-1} \text{ HNO}_3$  with Coorstek membrane)**

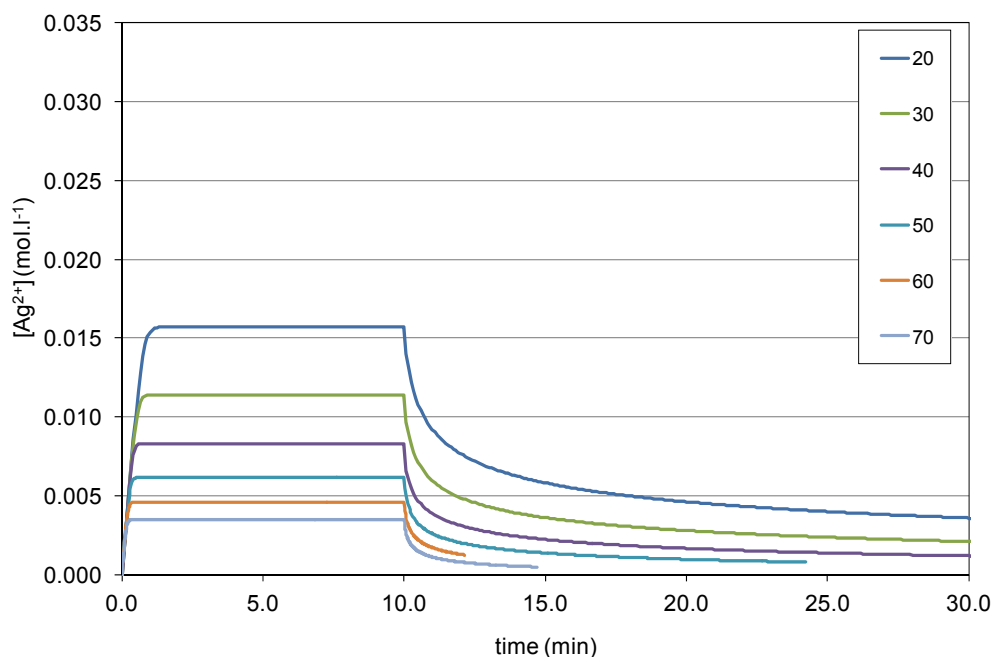


**Figure 94: Bulk electrolysis – Effect of temperature of calculated steady state and decomposition of  $\text{Ag}^{2+}$  (to be compared with Figure 93)**

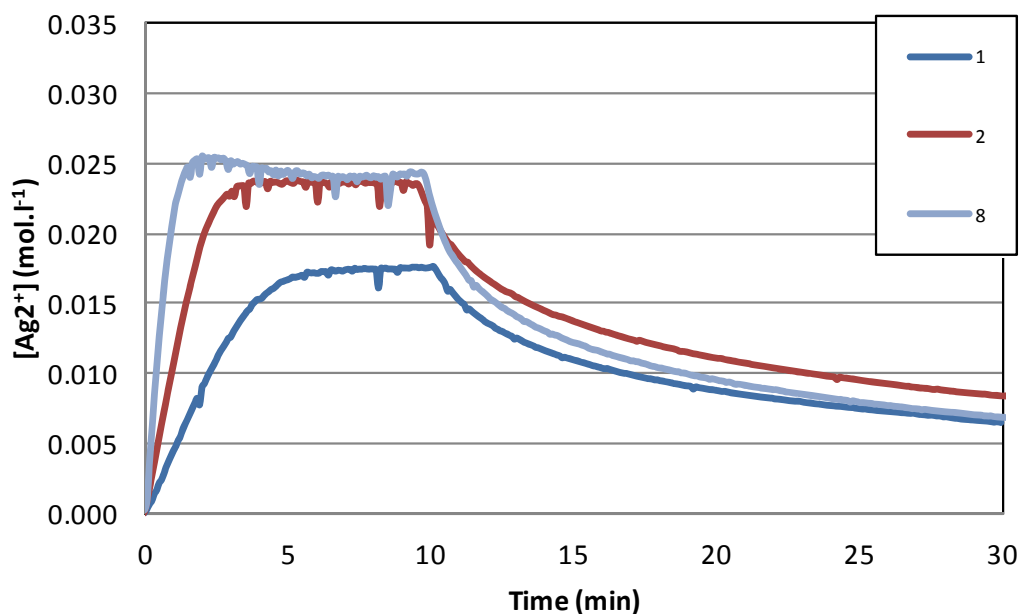


**Figure 95: Bulk electrolysis – Effect on current (1, 2 and 8 A) upon the steady state and decomposition of  $\text{Ag}^{2+}$  ( $0.05 \text{ mol.l}^{-1} \text{ AgNO}_3 - 4 \text{ mol.l}^{-1} \text{ HNO}_3$  with Coorstek membrane)**

#### 5.4.3.5. Plutonium dioxide dissolution

The cell was used to dissolve plutonium dioxide to 50, 100, 150, 200  $\text{g.l}^{-1}$  each experiment was carried out at 4 A for 2 hours with 100 ml of  $4 \text{ mol.l}^{-1}$

nitric acid – 0.1 mol.l<sup>-1</sup> silver nitrate and 20 ml of c. nitric acid (15.8 mol.l<sup>-1</sup>) thermostated to 40 °C. These conditions were chosen to allow complete dissolution within the 2 hours, comparison of the results from each experiment and provide a feed for a solvent extraction flowsheet experiment[236].

Inline UV-Vis analysis was used for the 100 g.l<sup>-1</sup> test, however the increase in pressure of the loop, due to the high solids content result in pumping difficulties, further analysis was carried out by sampling by hand. An experiment with 11.3 g plutonium dioxide, which is equivalent to 100 g.l<sup>-1</sup> plutonium is given here as an illustration. The UV-Vis spectra (Figure 96) shows an increase in the peaks due to plutonium(VI) and as dissolution progresses there is a reduction in the light scattering (due to suspended plutonium dioxide powder), which is the broad feature in the UV-Vis. Plutonium(VI) was quantified using a low extinction coefficient peak at 985 nm as the more intense 830 nm peak quickly becomes highly absorbing, despite the 0.05 cm pathlength cuvette. Two methods of estimating silver(II) concentration were used, based on the 550 nm with and without a slope background correction (BGL), the difference is due to light scattering due to suspended particles. (Figure 97), the completion of bulk dissolution is clearly observed by a rapid increase in silver(II) concentration, which is correlates with the plutonium(VI) concentration plateauing. Two more subtle features are the slow increase in silver(II) concentration after bulk dissolution is complete, suggesting the dissolution of larger particulars or another competing process is occurring slowly. The linear dissolution rate of plutonium dioxide has been observed by others[195, 240] and is due to the dissolution being limited by the generation rate of silver(II)[123]. Based on the current passed and time required for dissolution the calculated efficiency for these dissolutions was *ca.* 80 % and <0.05 % solid residues was observed determined by filtration through pre-weighed 0.1µm PFA membrane filters (Millipore).

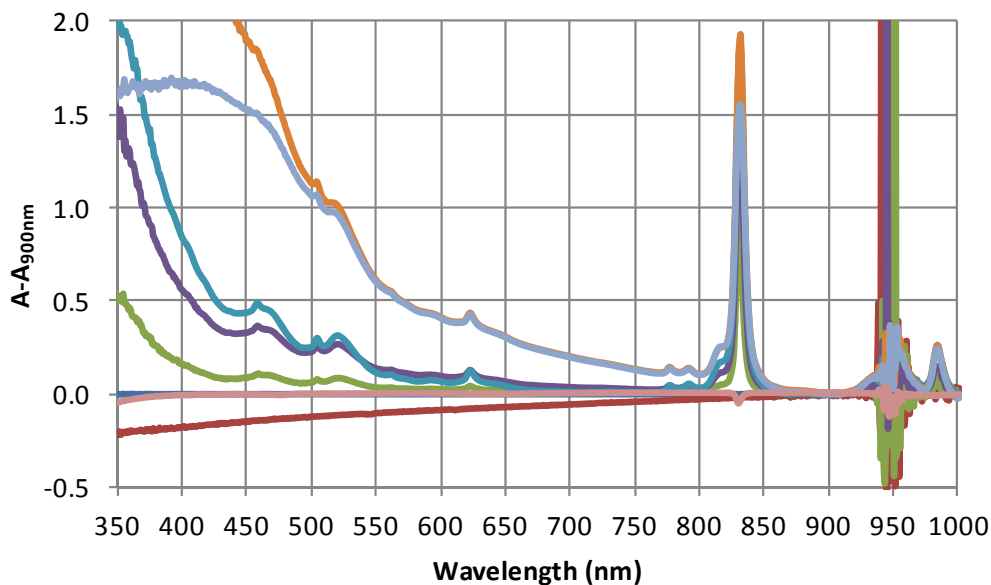


Figure 96: Dissolution – example UV-Vis spectra

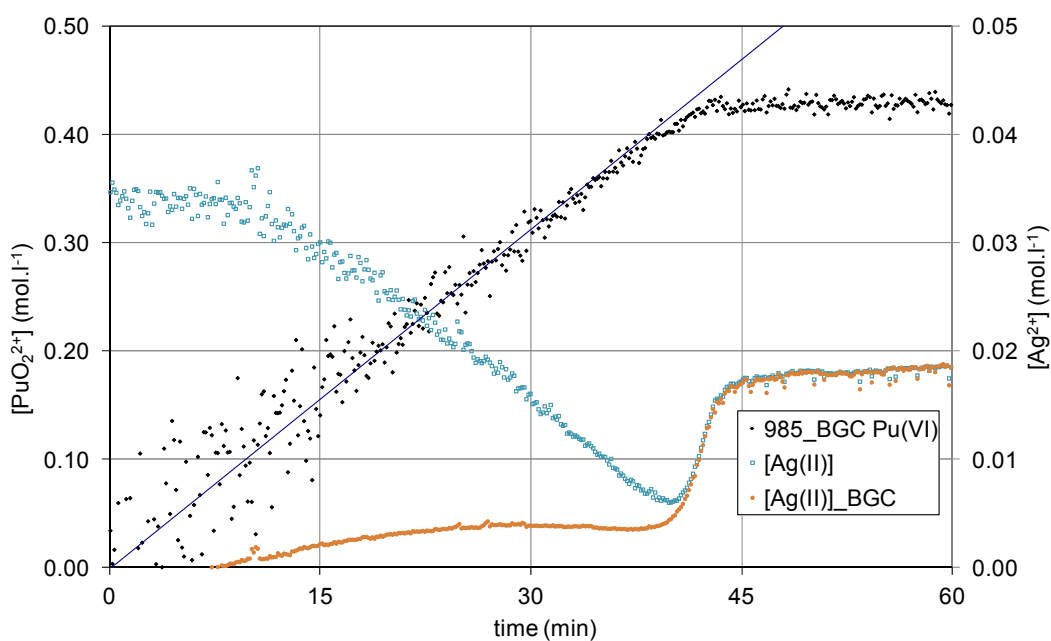


Figure 97: Dissolution –  $[Ag^{2+}]$  time plots (11.4 g  $PuO_2$ ,  $0.05 \text{ mol.l}^{-1}$   $AgNO_3$   $4 \text{ mol.l}^{-1}$   $HNO_3$ ,  $25 \text{ }^\circ\text{C}$ )

#### 5.4.4. Summary

A combination of staircase voltammetry and constant current bulk electrolysis experiments highlight the most significant factors in the generation of silver(II) and highlight the factors affecting the steady state and

decomposition of silver(II) in nitric acid. The same electrochemistry cell provides high efficiency and rapid dissolution of plutonium dioxide.

### **5.5. Summary mediated electrochemical oxidation experiments**

Literature and experimental studies have shown the generation rate of silver(II) is dependent upon the fundamental anode electrochemical processes. These processes can be described using Tafel analysis as two competing reactions direct oxidation of water and oxidation of silver(I) to silver(II). The generation of silver(II) can be optimised for efficiency or rate using this approach. An alternative, applied approach, has also been used, which shows the generation of silver(II) is limited by mass transfer of silver(I) to the electrode. The effect of temperature, cathode type, membrane type/size stirring regime, silver and nitric acid concentration have all been shown to affect the generation rate of silver(II) and its efficiency.

The stability and steady state silver(II) concentration under electrolysis have been shown to dependent upon the electrolysis current, stirring regime, temperature, silver and nitric acid concentration. These process can be described by using Faradays law of electrolysis and the kinetics of silver(II) – water reaction. The cell developed has been demonstrated to be capable of dissolution of plutonium dioxide using silver(II) to 200 g.l<sup>-1</sup> plutonium at high faradaic efficiency.

To maximise the generation rate and stability of silver(II), high rates of stirring, higher silver nitrate and nitric acid concentrations should be used at lower temperatures. Current (or current density) and cell configuration (e.g. increasing the membrane size and porosity) effect cell voltage, which defines the extent of ohmic heating and cooling requirements. Efficient stirring is also an important factor during the dissolution of plutonium dioxide to ensure the powder, which has a high density, is suspended, thereby allowing efficiency reaction between silver(II) and plutonium dioxide. Although this work did not permit the systematic investigation into relatively the rate of reaction of silver(II) with water and plutonium dioxide under various conditions. It is probable that the system can be optimised for rate or efficiency by using the effect of temperature, silver nitrate and nitric acid concentration. However, as the dissolution of plutonium dioxide is aimed at producing a feed for a solvent extraction process, the final acidity is fixed by the requirements of the downstream process. On this basis, the conditions that can be optimised are

silver nitrate concentration and temperature, which is affected by extent of ohmic heating.

## 6. CONCLUSIONS

### 6.1. Literature flowsheet studies

An immense amount of research has been undertaken in the last seven decades on the reprocessing of spent fuel. A fundamental process step in the reprocessing of spent fuel is head-end where dissolution in nitric acid occurs. This will continue to be the key process. The introduction of complementary technology may occur to overcome issues relating to spent fuel treatment. Examples included issues caused by changes in the:

- Fuel type, e.g. carbide or nitrogen-15 nitride
- Overall reprocessing plant specification, such as a requirement for the abatement of tritium, carbon-14 or iodine-129,131.

Legacy and future advanced fuels could include fuels containing uranium, plutonium and the minor actinides (neptunium and americium). Although it is currently not planned to recycle curium, this could be a possibility in the future. Thorium based or containing fuels could also be introduced if uranium continues to increase. Actinides oxides, carbides, nitrides (nitrogen-14 or -15) and alloyed or composite materials could be used. All the potential changes in fuel type will affect head-end.

The two technologies that could overcome the issues caused by changes to the feed stocks (spent fuels) and changes to process specification (isotope end-states) can be overcome by two broad technologies:

- Fuel pre-treatment
- Enhanced dissolution techniques

Fuel pre-treatment could be carried out to allow the improved control of radionuclides in head-end or to overcome difficulties with the dissolution of advanced fuel types. Examples include the abatement of tritium, krypton-85, and conversion of carbides to oxides to overcome the generation of organic at the dissolution step or oxidation of nitride fuel to allow the recovery of nitrogen-15 for reuse.

Enhanced dissolution techniques could be used to overcome difficulties in fuel dissolvability. Examples include the use of:

- Fluoride or metal complexants for thorium or plutonium based fuels.
- Strong reducing agents produced electrochemical process, such as uranium(IV) to dissolve plutonium rich residues.

- Strong oxidants, such as cerium(IV), cobalt(III) or silver(II) generated by electrochemical oxidation or ozonolysis, for the dissolution of plutonium or neptunium oxides or destruction of organics generated from the direct dissolution of carbides.

## **6.2. Direct dissolution in nitric acid**

### **Thermodynamic studies**

Simple thermodynamic considerations for the reactions associated with the dissolution of actinide oxides with nitrate, nitric acid reduction products and other reducing or oxidising agents. The calculated the Gibbs free energies show that the uranium dioxide – nitric acid dissolution system has multiple reactions that are thermodynamically favoured, whereas there are fewer favourable dissolution reactions for the other actinide oxidations and these are typically less favourable. Applying the results to mixed uranium plutonium dioxide of various proportions suggests the key dissolution reactions become less favourable. The calculated results can be used to rationalise the decline in the extent of dissolution in the region of 35 to 70 % plutonium content, which corresponds to a decline in the dominance of the nitrate reduction, nitrous acid and nitrogen dioxide reactions becoming less favourable.

For the actinide dioxides (except thorium dioxide) the use of enhanced oxidative or reductive dissolution techniques can be employed. For efficient processes, these methods must manage or minimise the side reaction for the reduction of water or nitric acid. The review of reducing and oxidising agents stronger than nitric acid or its reduction products show that the species studied most are cerium(IV) and silver(II). Another interesting method is the reductive dissolution using uranium(IV) in nitric acid stabilised by hydrazine, which could offer simplifications to future unirradiated or irradiated fuel reprocessing flowsheets.

### **Uranium dioxide studies**

The influence of nitric acid and nitrous acid on the dissolution rate of uranium dioxide powder confirms the key catalytic role of 'nitrous acid'. Increasing the mass transfer conditions (stirrer rate and size magnetic follower) leads to a reduction in dissolution rate. Under conditions that minimise nitrous acid concentration (stirred and sparged) dissolution rate increases with increasing nitric acid concentration; however rates remain low compared to those

obtained in the presence of nitrous acid. These results are similar to other published rates.

These studies are consistent with other applied studies dissolving uranium dioxide[19, 20, 30, 34, 45, 46, 48, 49], other metals[26, 28, 29] and more fundamental studies investigated nitric acid reduction chemistry[22-25]. These findings support the hypothesis that the key to efficient dissolution of uranium dioxide and other similar materials is through maximisation of the bulk and local nitrous acid concentrations, thereby maximising the rapid autocatalytic mechanism.

The dissolution of uranium dioxide has been shown to be linearly dependent upon nitrous acid concentration, under constant nitric acid, temperature and stirring conditions. Stirring conditions have been shown to have a large effect with high stirring rates causing a slower dissolution rates, due to the minimisation of nitrous acid concentration. These findings show that the mass transfer of dissolution products at the uranium dioxide surface are key to defining the extent of the nitrous acid autocatalytic dissolution. Increases in nitric acid concentration under stirred and air sparged conditions, aim at minimising the nitrous acid concentration, causes an increase in dissolution rate. Increasing the nitric acid concentration from 4 to 10 mol.l<sup>-1</sup> increases the rate by a factor of seven, consistent with published kinetics [48].

### **MOx studies**

Experimental studies investigating the role of nitrous acid in the dissolution of ~5 %Pu/(U+Pu) thermal MOx reveal similar kinetics compared to that observed for pure uranium dioxide. Experiments with 4-7 mol.l<sup>-1</sup> nitric acid with varying concentration of nitrous acid show there are two reaction routes, one dependent upon nitrate concentration the second dependent upon nitrous acid and nitrate concentrations (see rate law, below). Increasing the nitric acid concentration, increases the rate of both the nitrate and nitrous acid reaction routes, however the nitrous acid reaction route increases to a larger extent. Comparing the dissolution rates in 5 and 6 mol.l<sup>-1</sup> nitric acid with 5 mol.l<sup>-1</sup> nitric acid – 1 mol.l<sup>-1</sup> potassium nitrate and the effect of nitrous acid concentration shows that dissolution rate is dependent upon total nitrate. The effect of temperature upon dissolution rate without considering the nitrous reaction has been determined as 74 kJ.mol<sup>-1</sup>, which is higher than that observed by other workers, 62±5[34] and 66[45] kJ.mol<sup>-1</sup>. However, experiments with various concentrations of nitrous acid show that the nitrous acid and nitrate reaction routes have separate activation energies;

- nitrate reaction route has been determined as 80 kJ.mol<sup>-1</sup>, which is similar to that published for uranium dioxide, 79.5 mol.l<sup>-1</sup> [48].
- Nitrous acid reaction route has been determined as ~150 kJ.mol<sup>-1</sup> in 4 mol.l<sup>-1</sup> nitric acid at 40-70 °C, which is much higher than that published for uranium dioxide, 38 kJ.mol<sup>-1</sup> in 8 mol.l<sup>-1</sup> at 70-90 °C. This may suggest there is a change in the rate limiting step at lower nitric acid – temperature conditions.

$$\phi = k_1[HNO_3^-]^{2.3} e^{\frac{-80000}{RT}} + k_2[HNO_3]^{2.3}[HNO_2] e^{\frac{-150000}{RT}}$$

### MOx pellet studies

The dissolution rate of MOx pellets containing 5 %Pu/(U+PU) in nitric acid under various nitric acid concentrations and temperature with and without added sodium nitrite has been studied. The dissolution rate has been observed to increase between 8 and 12 mol.l<sup>-1</sup> nitric acid, but dissolution rates are similar at 12 and 14 mol l<sup>-1</sup> nitric acid concentrations. The apparent activation energy has been observed to depend on the nitric acid concentration and the temperature range selected. Between 70-90 °C and 10 and 12 mol.l<sup>-1</sup> nitric acid concentrations an apparent activation energy of 45-50 kJ.mol<sup>-1</sup> is observed, which is consistent with the activation energy for the 'nitrous acid' reaction route observed for uranium dioxide[48] and 5 %Pu/(U+PU) MOx [Section 4.6]. These results support the nitrate initiated, nitrous acid catalysed dissolution mechanism. Experiments adding nitrite show an increase in dissolution rate for 8 and 10 mol.l<sup>-1</sup> nitric acid, but a decrease in dissolution rate for 12 mol.l<sup>-1</sup> nitric acid. Experiments stirring and sparging the dissolving solution show that experiments that stirring at 110 °C causes less reduction in dissolution rate compared to 80 °C, consistent with an increasing involvement of mass-transfer control.

### General conclusions for oxide dissolution in nitric acid

The dissolution of uranium dioxide and mixed uranium-plutonium dioxide (MOx) with low plutonium contents, ~5 %U/(U+Pu) has been shown to occur via two chemical processes, nitrate and nitrous acid reaction routes. The nitrous acid reaction route is autocatalytic, which means under less agitation higher nitrous acid concentrations develop at the oxide surface, causing more rapid dissolution rates. The nitrous acid reaction route has been shown to be dependent upon nitrate concentration, rather than the nitric acid concentration. This suggests that during industrial dissolution, typically to 1-1.25 mol.l<sup>-1</sup> uranium under isothermal conditions, it is the free nitrate

concentration and local mass transfer conditions that will determine contribution of the nitrous acid reaction route. Studies of uranium dioxide and  $\sim 5\% \text{U}/(\text{U}+\text{Pu})$  show similar rates and dependences of chemical variables, suggesting uranium dioxide and low plutonium content MOx will dissolve at similar rates under industrial conditions.

The key difference between uranium dioxide and MOx manufactured by mechanical methods, is MOx will contain plutonium-rich grains, typically much less than 0.5 wt%. The key issue for designing dissolver cycles for MOx is the minimisation the amount of these plutonium rich particulate, as they posse a criticality hazard if mismanaged. Literature and thermodynamic calculations highlight this issue is thermodynamic, rather than kinetic. However, there are two potential approaches to maximising the extent of plutonium dissolution.

1. Maximising the extent of MOx that can be dissolved in nitric acid, e.g. in the 30-50 %Pu/(U+Pu) region, through the optimisation of nitric acid chemistry.

2. Use reducing or oxidising agents that are stronger than nitric acid to allow reductive or oxidative dissolution of plutonium-rich oxides, which are known to be capable of the dissolution of pure plutonium dioxide.

### ***6.3. Optimisation of a 100 ml electrochemical silver(II) dissolver from plutonium dioxide***

The setup, testing and optimisation of a small 100 ml cell for the electrochemical dissolution of plutonium dioxide has been carried out. Inactive studies have used linear staircase voltammetry (LSCV) and constant current bulk electrolysis to investigate the factors that influence the generation rate, stability and decomposition of silver(II). The major factors that affect the generation rate of silver(II) are stirrer rate, silver nitrate concentration, current and membrane type/size. Chemical variables that affect the stability of silver(II) are nitric acid concentration, temperature and silver nitrate concentration.

Despite the use of non standard electrochemistry equipment the potential – current density curves can be rationalised using Tafel analysis. Bulk electrolysis experiments have been used to confirm the mass transfer (current) limit under different cell conditions. From the bulk electrolysis experiments results from the decomposition rate of silver(II) (reaction with water) have been used to develop a chemical model for the generation,

steady state and decomposition rate of silver(II) (see below). These results are only qualitatively accurate, which is believed to be due to the migration of catholyte into the anolyte and poor temperature control, due to ohmic heating.

$$\frac{d[Ag^{2+}]}{dt} = \frac{\epsilon I}{FV} - k_1 \frac{[Ag^{2+}]^2}{[Ag^+]} - k_2 \frac{[Ag^{2+}]^4}{[Ag^+]}$$

The cell has also been demonstrated to be capable of 22.7 g plutonium dioxide (to 200 g.l<sup>-1</sup> plutonium) in 2 hours with <0.05 % solid residues. The dissolution process operated at a high average faradaic efficiency of approximately 80 %.

To maximise the generation rate and stability of silver(II), high rates of stirring, higher silver nitrate and nitric acid concentrations should be used at lower temperatures. Current (or current density) and cell configuration (e.g. increasing the membrane size and porosity) effect cell voltage, which defines the extent of ohmic heating and cooling requirements. Efficient stirring is also an important factor during the dissolution of plutonium dioxide to ensure the powder, which has a high density, is suspended, thereby allowing efficiency reaction between silver(II) and plutonium dioxide. Although this work did not permit the systematic investigation into relatively the rate of reaction of silver(II) with water and plutonium dioxide under various conditions. It is probable that the system can be optimised for rate or efficiency by using the effect of temperature, silver nitrate and nitric acid concentration. However, as the dissolution of plutonium dioxide is aimed at producing a feed for a solvent extraction process, the final acidity is fixed by the requirements of the downstream process. On this basis, the conditions that can be optimised are silver nitrate concentration and temperature, which is affected by extent of ohmic heating.

## 7. FURTHER WORK

### 7.1. *Technology and flowsheet studies*

The ACSEPT project, which this project is part of, was focused on industrialisation of minor actinide partitioning processes by moving R&D towards pilot plant scale testing. As part of any future programme to further develop pilot plant concepts, the development of baseline process specifications for the advanced reprocessing plant (including minor actinide recycling workshop) are needed. From these specifications key technology gaps can be highlighted and incorporated into the development programmes. Any specifications that are drawn up will become out-dated as further detail and policy develops, and therefore a regular (*e.g.* biannual) review would be necessary. Without the clarity offered from a specification, key technological steps may be missed and technologies may be developed that are misaligned or inadequate.

It is therefore specifically recommended that to support future pilot plant testing of an advanced actinide recycling process(es):

1. National and international strategic aims for and constraints on the advanced nuclear fuel cycle globally are analysed.
2. Detailed specifications for the back-end of the nuclear fuel cycle, with emphasis upon the back-end, should be produced. This will allow key technological gaps to be highlighted and incorporated into the development programmes.
3. Regular reviews are held to ensure the specifications are still valid as further detail and policy develops.

### 7.2. *Direct dissolution in nitric acid*

There are three areas where further work could be undertaken in the direct dissolution of mixed MO<sub>x</sub> in nitric acid.

1. Study the relative roles of nitrate and nitrous acid for MO<sub>x</sub> with a range of plutonium contents. The aim of these studies could be to provide evidence to test the result of the thermodynamic studies and understand the key chemical reactions in the dissolution of MO<sub>x</sub> and plutonium rich residues. The results of these studies can be used to help design optimum dissolver cycles. A key prerequisite for these studies is the availability or production of suitable materials, ideally homogenous co/gel-precipitated MO<sub>x</sub>.

2. Study how nitric acid chemistry can be manipulated to dissolve plutonium rich residues. For example through the use of elevated temperatures, to produce conditions that have a higher oxidation potential than typically observed in dissolution experiments.
3. Using the known differences between unirradiated and spent fuel to improve the understanding of spent fuel dissolution and design of improved spent fuel dissolver cycles. Examples could include use the known differences between unirradiated and spent fuels, which include chemical (presence of fission product and  $\epsilon$ -phase) and physical (fuel restructuring / high burn-up structure) differences.

Use the understanding of the oxide dissolution chemistry and technology to improve the chemical knowledge of future advanced fuels aimed at developing dissolved cycles for future advanced fuels.

### ***7.3. Application of mediated electrochemical oxidation to dissolution***

When future research programmes are designed the following areas should be considered at the planning stage.

Improvements in experimental methodology, apparatus and knowledge in the fundamental chemistry:

1. Increase the size of the cathode compartment to allow large membranes and cathode to be used. It is expected that this will reduce applied voltages for a given potential, reducing ohmic heating, thereby reducing the cooling burden. This will also reduce the potential of the cathode, thus minimising undesirable potential side reactions such as hydrogen evolution or metal electrodeposition.
2. Experimental apparatus should include pressure gauges on the anode and cathode compartments to allow measurement and testing off the effect of the relative pressures of the anode:cathode compartments. These tests could include a series of tests investigating the effect of relative pressure of the anode and cathode compartments on the relative migration rates of acid, silver(I, II) or other metals through the membrane. These tests could include the testing of a variety of separator materials, such as ceramics and polymers.

3. Flow meters on the off-gas outlets (and inlets) will allow more information about gas generation rates. Analysis of off-gases anode (oxygen, nitrogen oxides) and cathode (hydrogen, nitrogen oxides) could also be considered.
4. In-line UV-Vis spectrometry has been demonstrated to be useful for the monitoring of silver(II) concentration. However there is evidence that the delay in the sampling loop leads to an inaccuracy in the determination of the silver(II) concentration, due to the rapid silver(II) decomposition at high concentrations. Difficulties in the use of narrow pathlength with slurries of plutonium dioxide have resulted in pipe/cell blockages and leakages from pipe fittings. Alternative techniques could be considered, included in-situ UV-Vis (*e.g.* transflection or ATR optodes), in-situ electrochemical method (*e.g.* potentiometry, RDE voltammetry).
5. If bulk electrolysis experiments are carried out to monitor the silver(II) decomposition, the decomposition rate should be monitored in-situ and a sample should be removed from the cell and monitored under the same temperature conditions. This will allow any additional cell silver(II) side-reactions *e.g.* catholyte nitric acid reduction products or corrosion to be highlighted. These experiments will both need precise temperature measurements to be made, to allow comparison of temperatures, as temperature has a very large effects.
6. During the experiments periodic off-line analysis of total silver (after filtration), silver(II) and free acidity should be considered. The monitoring of total silver will provide information about i) if silver migration into the cathode compartment occurs or ii), precipitation as silver(II) oxides or another solid (*e.g.* silver chloride). These could be used to improve the map-out regions where silver(II) precipitation occurs.
7. A series of experiments could be carried out to understand the mechanisms governing silver(II) precipitation. These tests could include surface studies of anodes after bulk electrolysis tests or electrochemical tests sensitive to formation of surface films, such as quartz-electrode microbalance studies.
8. Consider the benefits for and demonstrate alternative mediators, such as cerium(IV) or cobalt(III).
9. Develop a mathematical and experimental justification for the kinetic and thermodynamic limits for hydrogen evolution. Understand and demonstrate techniques to minimise hydrogen production.

Further applied and industrialisation studies:

1. Demonstrate the treatment of silver(II) as a technology for the treatment of NDA legacy or orphan wastes and the dissolution of plutonium dioxide.
2. Assess the pros and cons at various scales for simple batch electrochemical cells *versus* the conventional flow reactors, e.g. using plate and frame electrochemical cells.
3. Use the results from these experiments to design a larger scale simple beaker electrochemistry cell (scale up studies).
4. Develop a plutonium dioxide dissolution model using silver(II) chemistry and electrochemistry determined in the inactive studies.
5. Applied and fundamental studies to understand the effect of other competing reactions, aimed at demonstrating the viability of the recovery of plutonium dioxide from more complicated matrices, such as dissolved spent fuel. These could include studies into the presence of organic species from carbide dissolution and fission product metals, e.g. insoluble fission products.

## 8. REFERENCES

1. *Spent Nuclear Fuel Reprocessing Flowsheet*. 2012, NEA/NSC/WPFC/DOC(2012)15.
2. *Status of Developments in the Back End of the Fast Reactor Fuel Cycle*. 2011, IAEA NF-T-4.2.
3. *Implications of Partitioning and Transmutation in Radioactive Waste Management*. 2004, IAEA Technical Reports Series no. 435.
4. *Assessment of Partitioning Processes for Transmutation of Actinides*. 2010, IAEA-TECDOC-1646.
5. Bourg, S., et al., *ACSEPT - Partitioning technologies and actinide science: Towards pilot facilities in Europe*. Nuclear Engineering and Design. **241**(9): p. 3427-3435.
6. Maher, C.J., *ACSEPT Deliverable D1.1.1 Head-end options for legacy and future advanced fuels: An initial appraisal*. 2009, NNL(09)9899 issue 1.
7. Moore, R.G., Shearer, C., Rhoes, C., Zimmerman, C.H., *Post Flowsheeting Workshop Report - Issue*. 2008, NNL, ACSEPT Deliverable D3.1.1, .
8. Emin, J.L., Zimmermann, A., Tribout-Maurizi, A., Dancausse J.P., *MOx reprocessing: The success of the first industrial campaign on UP2-800 COGEMA Plant*. in *Global 2005*. 2005.
9. Dancausse, J.P., et al., *CEA preliminary studies for industrial MOx reprocessing: from laboratory results to successful first industrial campaign on UP2-800 AREVA plant*. Icone16: Proceeding of the 16th International Conference on Nuclear Engineering - 2008, Vol 2. 2008, New York: Amer Soc Mechanical Engineers. 51-54.
10. GIF, *A Technology Roadmap for Generation IV Nuclear Energy Systems*. 2002.
11. NEA, *Spent Nuclear Fuel Reprocessing Flowsheet*. 2012.
12. IAEA, *Status and advances in MOx fuel technology*. 2003.
13. Asquith R W., H., P. J., Astill, M., *Shear elegance in the Thorp head end*. Nuclear Engineering International, 1988(March): p. 37-40.
14. Phillips, C., *The thermal oxide reprocessing plant at Sellafield: four years of successful treatment of irradiated nuclear fuel*, in *Waste Management*. 1999.
15. Bierman, S.R., et al., *Criticality experiments with low enriched UO<sub>2</sub> fuel rods in water containing dissolved gadolinium*. 1984.
16. Groenier, W.S., *Equipment for the dissolution of core material from sheated power reactor fuel*. 1971.
17. Parisot, J.F., *Treatment and recycling of spent nuclear fuel. Actinide partitioning - Application to waste management*. 2008: CEA.
18. Bailey, G.H., *Nitrogen Chemistry*, in *Comprehensive Inorganic Chemistry: Nitrogen, phosphorus, arsenic, antimony, and bismuth, by . Nonaqueous chemistry*. 1928.
19. Sakurai, T., et al., *The composition of NOx generated in the dissolution of uranium dioxide*. Nuclear Technology, 1988. **83**(1): p. 24-30.
20. Fukasawa, T., Y. Ozawa, and F. Kawamura, *Generation and decomposition behavior of nitrous-acid during dissolution of UO<sub>2</sub> pellets by nitric acid*. Nuclear Technology, 1991. **94**(1): p. 108-113.
21. Takeuchi, M. and G.O.H. Whillock, *Effect of NOx gases on corrosion of stainless steel in hot nitric acid solutions*. British Corrosion Journal, 2002. **37**(3): p. 199-205.

22. de Groot, M.T. and M.T.M. Koper, *The influence of nitrate concentration and acidity on the electrocatalytic reduction of nitrate on platinum*. Journal of Electroanalytical Chemistry, 2004. **562**(1): p. 81-94.
23. Nakata, K., et al., *Surface-enhanced infrared absorption spectroscopic studies of adsorbed nitrate, nitric oxide, and related compounds 2: Nitrate ion adsorption at a platinum electrode*. Langmuir, 2008. **24**(8): p. 4358-4363.
24. Nakata, K., et al., *Surface-enhanced infrared absorption spectroscopic studies of adsorbed nitrate, nitric oxide, and related compounds 1: Reduction of adsorbed NO on a platinum electrode*. Langmuir, 2008. **24**(8): p. 4352-4357.
25. Rima, F.R., et al., *Surface-Enhanced Infrared Absorption Spectroscopic Studies of Adsorbed Nitrate, Nitric Oxide, and Related Compounds. 3. Formation and Reduction of Adsorbed Nitrite at a Platinum Electrode*. Journal of Physical Chemistry C. **114**(13): p. 6011-6018.
26. Elcheikh, F.M., et al., *The role of intermediates in the kinetics of copper dissolution in nitric acid*. Annali Di Chimica, 1983. **73**(1-2): p. 75-89.
27. El-Egamy, S.S., K.M. Ismail, and W.A. Badawy, *Corrosion behaviour of copper in acidic nitrate solutions*. Corrosion Prevention & Control, 2004. **51**(3): p. 89-97.
28. Khalil, S.A. and M.A. Elmanguch, *The kinetics of zinc dissolution in nitric acid*. Monatshefte Fur Chemie, 1987. **118**(4): p. 453-462.
29. El Haleem, S.M.A. and E.E.A. El Aal, *Thermometric behaviour of cobalt in HNO<sub>3</sub> solutions*. Journal of Materials Processing Technology, 2008. **204**(1-3): p. 139-146.
30. Fukasawa, T. and Y. Ozawa, *Relationship between dissolution rate of uranium dioxide pellets in nitric acid solutions and their porosity*. Journal of Radioanalytical and Nuclear Chemistry-Letters, 1986. **106**(6): p. 345-356.
31. Hodgson, T.D. *A model for fuel dissolution via fragmentation*. in RECOD. 1994.
32. Davis, W.J., G.A. West, and R.G. Stacy, *Oxide particle size distribution from shearing irradiated and unirradiated LWR fuels in Zircaloy and stainless steel cladding: significance for risk assessment*. 1979.
33. Blanc, M., *Etude La Bibliographique relative A La Cinetique de dissolution de UO<sub>2</sub> dans L-acide nitrique*. 1986.
34. Taylor, R.F., Sharratt E.W., de Chazal, L.E.M., Logsdale, D.H., *Dissolution rates of Uranium dioxide sintered pellets in nitric acid systems*. Journal of Applied Chemistry, 1963. **13**: p. 32-40.
35. Bard, A.J., Parsons, R., Jordan, J., *Standard Potentials in Aqueous Solution (Monographs in Electroanalytical Chemistry & Electrochemistry)* 1985: CRC Press.
36. Gresky, A.T., *Recovery of nitrogen oxides and rate gas fission products from the nitric acid dissolution of irradiated uranium*. 1952.
37. Miles, G.L., *The fumeless dissolving of Uranium*. 1955, UKAEA, AERE C/R 1804.
38. Larsen, R.P., *Dissolution of uranium metal and it's alloys*. Analytical Chemistry, 1959. **31**(4): p. 545-549.
39. Swanson, J.L., et al., *Laboratory studies of shear/leach processing of zircaloy clad metallic uranium reactor fuel*. 1985, PNL-5708.
40. Laue, C.A., D. Gates-Anderson, and T.E. Fitch, *Dissolution of metallic uranium and its alloys - Part 1. Review of analytical and process-scale metallic uranium dissolution*. Journal of Radioanalytical and Nuclear Chemistry, 2004. **261**(3): p. 709-717.

41. Laue, C.A., D. Gates-Anderson, and T.E. Fitch, *Dissolution of metallic uranium and its alloys - Part II: Screening study results: Identification of an effective non-thermal uranium dissolution method*. Journal of Radioanalytical and Nuclear Chemistry, 2004. **262**(2): p. 517-524.
42. Schulz, W.W., R.E. Burns, and E.M. Duke, *Nitric Acid Dissolution of Uranium-Molybdenum Alloy Reactor Fuels*. Industrial & Engineering Chemistry Process Design and Development, 1962. **1**(2): p. 156-160.
43. Oudinet, G., et al., *Characterization of plutonium distribution in MIMAS MOX by image analysis*. Journal of Nuclear Materials, 2008. **375**(1): p. 86-94.
44. Carrott, M.J., et al., *The Chemistry of (U,Pu)O<sub>2</sub> Dissolution in Nitric Acid*. Procedia Chemistry. **7**(0): p. 92-97.
45. Shabbir, M. and R.G. Robins, *Kinetics of dissolution of uranium dioxide in nitric acid 1*. Journal of Applied Chemistry of the USSR, 1968. **18**(5): p. 129-8.
46. Shabbir, M. and R.G. Robins, *Kinetics of dissolution of uranium dioxide in nitric acid 2*. Journal of Applied Chemistry of the USSR, 1969. **19**(2): p. 52-8.
47. Ikeda, Y., et al., *Dissolution behavior of pulverized irradiated fuels in nitric acid solutions*. Journal of Nuclear Science and Technology, 1999. **36**(4): p. 358-363.
48. Ikeda, Y., et al., *Kinetic study on dissolution of UO<sub>2</sub> powders in nitric acid*. Journal of Nuclear Materials, 1995. **224**(3): p. 266-272.
49. Nishimura, K.U., Chikazawa, T., Hasegawa, A., Tanaka, T., Ikeda, U, Yasuike, Y., Takahima, Y., *Effect of nitrous acid on dissolution of UO<sub>2</sub> powders in Nitric acid Optimal conditions for dissolving* Journal of Nuclear Science and Technology, 1995. **32**(2): p. 157-159.
50. Croft, T.L.M., Tonkin, J.H., *The dissolution of uranium in nitric acid. Review of the position in 21<sup>st</sup> June 1950*. 1950.
51. Wurtz, R., *The solubility of irradiated MOx fuel elements in reprocessing*. Atomwirtschaft-Atomtechnik, 1987. **32**(4): p. 190-192.
52. Madic, C., P. Berger, and X. Machuronmandard, *Mechanisms of the rapid dissolution of plutonium dioxide in acidic media under oxidizing or reducing conditions*. Transuranium Elements, 1992: p. 457-468.
53. Vollath, D., et al., *On the dissolution of (U,Pu)O<sub>2</sub> solid-solutions with different plutonium contents in boiling nitric acid*. Nuclear Technology, 1985. **71**(1): p. 240-245.
54. Kleykamp, H., *The chemical state of the fission products in oxide fuels*. Journal of Nuclear Materials, 1985. **131**(2-3): p. 221-246.
55. Sakurai, T., et al., *The interaction of iodine with insoluble residue in the dissolution of simulated spent fuel pellets*. Nuclear Technology, 1991. **94**(1): p. 99-107.
56. Magnaldo, A., M. Masson, and R. Champion, *Nucleation and crystal growth of zirconium molybdate hydrate in nitric acid*. Chemical Engineering Science, 2007. **62**(3): p. 766-774.
57. Doucet, F.J., et al., *The formation of hydrated zirconium molybdate in simulated spent nuclear fuel reprocessing solutions*. Physical Chemistry Chemical Physics, 2002. **4**(14): p. 3491-3499.
58. Usami, T., et al., *Formation of zirconium molybdate sludge from an irradiated fuel and its dissolution into mixture of nitric acid and hydrogen peroxide*. Journal of Nuclear Materials. **402**(2-3): p. 130-135.
59. Rosse, E., et al. *Increase of the performances on the Head Facility*. in *Atalante*. 2012. Montpellier, France.

60. Jiang, J., et al., *A Spectroscopic Study of the Dissolution of Cesium Phosphomolybdate and Zirconium Molybdate by Ammonium Carbamate*. Journal of Solution Chemistry, 2005. **34**(4): p. 443-468.
61. Sakurai, T., et al., *Influence of NO<sub>x</sub> and HNO<sub>2</sub> on iodine quantity in spent-fuel solutions*. Nuclear Technology, 1996. **116**(3): p. 319-326.
62. Sakurai, T., et al., *Thermochemical and experimental considerations of NO<sub>x</sub> composition and iodine species in the dissolution of spent PWR fuel specimens*. Journal of Nuclear Science and Technology, 1993. **30**(6): p. 533-541.
63. Sakurai, T., et al., *The iodine species and their behavior in the dissolution of spent fuel specimens*. Nuclear Technology, 1992. **99**(1): p. 70-79.
64. Boukis, N. and E. Henrich, *2-step procedure for the iodine removal from nuclear fuel solutions*. Radiochimica Acta, 1991. **55**(1): p. 37-42.
65. Wilson, P.D., ed. *The nuclear fuel cycle, from ore to waste*. 1996, Oxford science publications.
66. Cleveland, ed. *The Chemistry of Plutonium*. 1970, Americium Nuclear Society.
67. Coleman, G., H., *The Radiochemistry of plutonium*. 1965, National Academy of Sciences
68. Rance, P.J.W., B.Y. Zilberman, and G.A. Akopov, *Radiolysis of hexavalent plutonium in solutions of uranyl nitrate containing fission product simulants*, in *Plutonium Futures-the Science*, K.K.S. Pillay and K.C. Kim, Editors. 2000, Amer Inst Physics: Melville. p. 56-58.
69. OSPAR. *Radioactive Substances*. Available from: [http://www.ospar.org/content/content.asp?menu=00220306000000\\_000\\_000\\_000000](http://www.ospar.org/content/content.asp?menu=00220306000000_000_000_000000).
70. Collins, E.D., et al., *Process Development Studies for Zirconium Recovery/Recycle from used Nuclear Fuel Cladding*. Procedia Chemistry. **7**(0): p. 72-76.
71. Matzke, H., *Science of Advanced LMFBR Fuels*. 1986: North-Holland, Elsevier Science Publishers.
72. NEA, *Radiological Significance and management of Tritium, carbon-14, krypton-85, iodine-129 arising from the nuclear fuel cycle*. 1980.
73. Lerch, R.E., *Dissolution of unirradiated mechanically blended, sol gel and coprecipitated mixed oxide fuel* 1972.
74. Uriarte, A.L. and R.H. Rainey, *Dissolution of high density UO<sub>2</sub>, PuO<sub>2</sub> and UO<sub>2</sub>-PuO<sub>2</sub> pellets in inorganic acids*. 1965.
75. Wallenius, J., *Transmutation*, in *FIRST ACSEPT INTERNATIONAL WORKSHOP, 31 March - 2 April 2010*. 2010: HOTEL VIP ZURIQUE, LISBON PORTUGAL.
76. Ikeuchi, H., et al., *Dissolution Behavior of Irradiated Mixed-oxide Fuels with Different Plutonium Contents*. Procedia Chemistry. **7**(0): p. 77-83.
77. EC, *ASGARD Deliverable Report 1.3.4 - Annual Public Report 2013*. 2013.
78. Berthinier, C., et al., *Experimental study of uranium carbide pyrophoricity*. Powder Technology. **208**(2): p. 312-317.
79. Berthinier, C., et al., *Experimental kinetic study of oxidation of uranium monocarbide powders under controlled oxygen partial pressures below 230 degrees C*. Journal of Nuclear Materials. **432**(1-3): p. 505-519.
80. Bradley, M.J. and L.M. Ferris, *Hydrolysis of uranium carbides between 25 and 100 °C. 1. Uranium Monocarbide*. Inorganic Chemistry, 1962. **1**(3): p. 683-&.
81. Bradley, M.J. and L.M. Ferris, *Hydrolysis of Uranium Carbides between 25 and 100 °C. 2. Uranium Dicarbide, Uranium Metal-Monocarbide Mixtures*

- and Uranium Monocarbide Dicarbide Mixtures*. Inorganic Chemistry, 1964. **3**(2): p. 189-195.
82. Bradley, M.J. and L.M. Ferris, *Hydrolysis of uranium carbides between 25 and 100 °C. 3. Uranium sesquicarbide and mixtures of sesquicarbide with monocarbide or dicarbide*. Inorganic Chemistry, 1964. **3**(5): p. 730-&.
  83. Ferris, L.M. and M.J. Bradley, *Reactions of uranium carbide with nitric acid*. Journal of the American Chemical Society, 1965. **87**(8): p. 1710-&.
  84. Choppin, G.R., H. Bokelund, and S. Valkiers, *Oxalate complexation in dissolved carbide systems*. Radiochimica Acta, 1983. **33**(4): p. 229-232.
  85. Maslennikov, A., et al., *Electrochemical behavior of UC in acidic media: Preliminary results*. Journal of Alloys and Compounds, 2007. **444**: p. 550-553.
  86. Maslennikov, A., et al., *UC oxidation with HNO<sub>2</sub> in aqueous solutions of HNO<sub>3</sub> and HClO<sub>4</sub>*. Radiochimica Acta, 2009. **97**(10): p. 571-580.
  87. Glatz, J.P., H. Bokelund, and S. Zierfuss, *Analysis of the off-gas from dissolution of nuclear oxide fuels and carbide fuels in nitric acid*. Radiochimica Acta, 1990. **51**(1): p. 17-22.
  88. Ferris, L.M. and M.J. Bradley, *Off-gases from the reactions of uranium carbide with nitric acid at 90°C*. 1964.
  89. Ferris, L.M., *Reactions of uranium mononitride, thorium monocarbide and uranium monocarbide with nitric acid and other aqueous reagents*. Journal of Inorganic and Nuclear Chemistry, 1968. **30**(10): p. 2661-2669.
  90. Sugihara, S. and S. Imoto, *Hydrolysis of Uranium Nitrides*. Journal of Nuclear Science and Technology, 1969. **6**(5): p. 237-242.
  91. Hadibi-Olschewski, N., et al., *The fate of nitrogen upon reprocessing of nitride fuels*. Journal of Nuclear Materials, 1992. **188**(0): p. 244-248.
  92. Gens, T.A., *Explosive reactions during reprocessing of reactor fuels containing uranium and zirconium or niobium*. 1958.
  93. Goode, J.H. and J.R. Flanary, *Hot cell evaluation of the grind-leach processes with irradiated pyrolytic carbon-coated sol-gel thoria-urania particles*. 1967.
  94. Bakker, K., et al., *The use of molybdenum-based ceramic-metal (CerMet) fuel for the actinide management in LWRs*. Nuclear Technology, 2004. **146**(3): p. 325-331.
  95. Schulz, W.W., *Reprocessing uranium-molybdenum alloy fuels - dissolution in concentrated nitric acid*, in *Other Information: Orig. Receipt Date: 31-DEC-60*. 1960. p. Medium: ED; Size: Pages: 17.
  96. Bond, W.D., J.C. Mailen, and G.E. Michaels, *Evaluation of methods for decladding LWR fuel for a pyroprocessing-based reprocessing plant*. 1992. p. .
  97. Goode, J.H., *Voloxidation: removal of volatile fission products from spent LMFBR fuels*. 1973.
  98. Strausberg, S., et al., *Low Decontamination-Processing of Uranium Dioxide by Oxidation-Reduction*. Industrial & Engineering Chemistry, 1960. **52**(1): p. 45-46.
  99. Majumdar, D., et al., *Recycling of nuclear spent fuel with AIROX processing*. 1992: United States.
  100. Lee, J.W., G.I. Park, and Y. Choi, *Fabrication of DUPIC fuel pellets using high burn-up spent PWR fuel*. Journal of Nuclear Science and Technology. **49**(11): p. 1092-1096.
  101. Rance, P.J.W. and B. Beznosynk, *The oxidative pulverisation of mixed oxide fuel*, in *Global 2005*. 2005.

102. Anderson, J.S., et al., *The oxides of uranium. Part IV. The system UO<sub>2</sub>-ThO<sub>2</sub>-O*. Journal of the Chemical Society (Resumed), 1954(0): p. 3324-3331.
103. Kang, K.H., et al., *Oxidation behavior of the simulated fuel with dissolved fission products in air at 573±873K*. Thermochemica Acta, 2007. **455**(1-2): p. 129-133.
104. Thomas, L.E., R.E. Einziger, and H.C. Buchanan, *Effect of fission products on air-oxidation of LWR spent fuel*. Journal of Nuclear Materials, 1993. **201**(0): p. 310-319.
105. McEachern, R.J., D.C. Doern, and D.D. Wood, *The effect of rare-earth fission products on the rate of U<sub>3</sub>O<sub>8</sub> formation on UO<sub>2</sub>*. Journal of Nuclear Materials, 1998. **252**(1-2): p. 145-149.
106. Cobos, J., et al., *Phase characterisation of simulated high burn-up UO<sub>2</sub> fuel*. Journal of Alloys and Compounds, 1998. **271-273**(0): p. 610-615.
107. Cadieux, J.R. and J.A. Stone, *Voloxidation and dissolution of irradiated plutonium recycle fuels*. 1980.
108. Goode, J.H. and R.G. Stacy, *Voloxidation and dissolution of irradiated (Th,U)O<sub>2</sub>*. 1979.
109. Goode, J.H., R.G. Stacy, and V.C.A. Vaughen, *Head-end reprocessing studies of H.B. Robinson-2 fuel: II. Parametric voloxidation studies*, in *Other Information: PBD: May 1980*. 1980.
110. Bateman, K.J., et al., *Effect of Process Variables During the Head-End Treatment of Spent Oxide Fuel*. 2006.
111. Capone, F., et al., *Mass spectrometric measurements of fission product effusion from irradiated light water reactor fuel*. Journal Name: Nuclear Science and Engineering; 124; 3, 1996: p. 436-454.
112. DelCul, G.D. *Advanced head end for the treatment of used LWR fuel*. in *OECD Nuclear Energy Agency, 11<sup>th</sup> Information Exchange Meeting on Actinide and Fission Product Partitioning and Transmutation*. 2010.
113. Murbach, E.W. and W.D. Turner, *Oxidation of uranium carbide by carbon dioxide*. 1962.
114. Flanary, J.R., et al., *Hot-cell studies of aqueous dissolution processes for irradiated carbide reactor fuels*. 1964.
115. Nikitina, G.P., et al., *Existing methods for dissolution of plutonium dioxide .1. Dissolution in mineral acids and their mixtures*. Radiochemistry, 1997. **39**(1): p. 12-25.
116. Seaborg, G.T., *Transuranium elements: A half century*. 1990.
117. Inoue, A., *Enhanced dissolution of PuO<sub>2</sub> in nitric acid using uranium(IV)*. Journal of the Chemical Society-Faraday Transactions I, 1988. **84**: p. 1195-1197.
118. Bourges, J., et al., *Dissolution du bioxyde de plutonium en milieu nitrique par l'argent(II) électro-généré*. Journal of the Less Common Metals, 1986. **122**: p. 303-311.
119. Madic, C., Lecomte, M., Bourges, J., Koehly, G., Moulin, J.P., *Mechanism of the rapid dissolution of PuO<sub>2</sub> under oxidizing conditions, and applications*, in *Proceedings of Recod 1991*, . 1991. p. 715-720.
120. Rance, P.J.W., Nikitina, G.P., Kirshyn, M.G., Koroleve, V.A., *The Effects of Temperature, Surface Area and Interfering Species on the Dissolution Rate of Plutonium Dioxide by Silver(II) in Nitric Acid*, in *GLOBAL 2003*.
121. Fleischmann, M., D. Pletcher, and A. Rafinski, *The kinetics of the silver (I)/silver (II) couple at a platinum electrode in perchloric and nitric acids*. Journal of Applied Electrochemistry, 1971. **1**(1): p. 1-7.

122. Po, H.N., J.H. Swinehart, and T.L. Allen, *Kinetics and mechanism of the oxidation of water by silver(II) in concentrated nitric acid solution*. Inorganic Chemistry, 1968. **7**(2): p. 244-249.
123. Zundelevich, Y., *The Mediated electrochemical dissolution of plutonium oxide - kinetics and mechanism*. Journal of Alloys and Compounds, 1992. **182**(1): p. 115-130.
124. Selbin, J. and M. Usategui, *Higher oxidation states of silver. 1. Reaction of ozone with simple silver salts*. Journal of Inorganic & Nuclear Chemistry, 1961. **20**(1-2): p. 91-99.
125. Palamalai, A., et al., *Development of an electro-oxidative dissolution technique for fast reactor carbide fuels*. Radiochimica Acta, 1991. **55**(1): p. 29-35.
126. Mousset, F., F. Bedioui, and C. Eysseric, *Electroassisted elimination of ruthenium from dissolved RuO<sub>2</sub>.xH<sub>2</sub>O in nitric acid solution by using Ag(II) redox mediator: toward a new insight into the nuclear fuel reprocessing*. Electrochemistry Communications, 2004. **6**(4): p. 351-356.
127. Handley, D., *NOx chemistry and absorption mechanisms*. 1988.
128. Takeuchi, A.W., G. O. H., *Calculation of HNO<sub>2</sub> Concentration from Redox Potential in HNO<sub>3</sub>-H<sub>2</sub>O System as an Aid to Understanding the Cathodic Reaction of Nitric Acid Corrosion*. Corrosion Engineering, 2002. **51**(12): p. 549-554.
129. Hirota, M., et al. *Thermodynamic modelling of the (U, Pu, Np)O<sub>2</sub> +/- x mixed oxide*. in *11th International Symposium on Thermodynamics of Nuclear Materials*. 2004. Karlsruhe, GERMANY: Elsevier Science Bv.
130. Truman, J.E., *Factors affecting the testing of stainless steels inboiling concentrated nitric acid*. Journal of Applied Chemistry, 1954. **4**(5): p. 273-283.
131. McIntosh, A.B.E., T.E. *The Effect of Metal Species Present in Irradiated Fuel Elements on the Corrosion of Stainless Steel in Nitric Acid*. in *Proc. 2nd In. Conf. "Peaceful Use of Atomic Energy"*. 1958.
132. Evans, T.E., *Nitric Acid Corrosion and Polarisation of Austenitic steel - Effect of Added Species*. 1956, UKAEA, IGR-TN/C.419.
133. *The chemistry of the actinide and transactinid elements*. third edition ed, ed. L.R. Morss, Edelstein, N.M., Fuger, J. 2006: Springer.
134. Olsson, M., A.M. Jakobsson, and Y. Albinsson, *Surface charge densities of two actinide(IV) oxides: UO<sub>2</sub> and ThO<sub>2</sub>*. Journal of Colloid and Interface Science, 2002. **256**(2): p. 256-261.
135. Roelofs, F., J. Sonnefeld, and W. Vogelsberger, *Solubility kinetics of a synthetic uranium(VI) oxide at different pH and controlled O<sub>2</sub> partial pressure and evaluation of substantial interface properties*. Radiochimica Acta, 2007. **95**(7): p. 381-389.
136. Stumm, W., *The Inner-Sphere Surface Complex A Key to Understanding Surface Reactivity*, in *Aquatic chemistry, chemical equilibria and rates in natural waters*, W. Stumm, Morgan, J.J, Editor. 1995.
137. Facer, J.F.J. and K.M. Harmon, *Precipitation of plutonium(IV) oxalate*. 1954.
138. MachuronMandard, X. and C. Madic, *Plutonium dioxide particle properties as a function of calcination temperature*. Journal of Alloys and Compounds, 1996. **235**(2): p. 216-224.
139. *NDA Statement on future of the Sellafield Mox Plant*, <http://www.nda.gov.uk/news/smp-future.cfm>. 03 August 2011.
140. Bairot, H., Van Valet, I., Edwards, J., Nagai, S.H., Reshetnikov, F.,, *Overview of MOx fuel fabrication achievements*.

141. Ghosh, J.K., J.P. Panakkal, and P.R. Roy, *Use of autoradiography for checking plutonium enrichment and agglomerates in mixed-oxide fuel pellets inside welded fuel pins*. NDT International, 1984. **17**(5): p. 269-271.
142. Fisher, S.B., et al., *Microstructure of irradiated SBR MOX fuel and its relationship to fission gas release*. Journal of Nuclear Materials, 2002. **306**(2-3): p. 153-172.
143. Delwaudle, C., et al., *Dissolution of solid particles in nitric acid: a new approach to understanding the mechanism*, in *Poster at xx*. 2010.
144. Delwaulle, C.I., et al., *Development of a new method for investigating the mechanisms of solid particle dissolution in nitric acid media: Millifluidic study using fluorescent indicators*. Chemical Engineering Journal, (0).
145. Shabbir, M. and R.G. Robins, *Effect of crystallographic orientation on dissolution of uranium dioxide in nitric acid*. Journal of Nuclear Materials, 1968. **25**(2): p. 236-8.
146. Habashi, F. and G. Thurston, *Kinetics and mechanism of dissolution of uranium dioxide*. Energia Nucleare, 1967. **14**(4): p. 238-8.
147. Garisto, N.C. and F. Garisto, *The dissolution of uranium dioxide: a thermodynamic approach*. Nuclear and Chemical Waste Management, 1986. **6**(3-4): p. 203-212.
148. Yasuike, Y., et al., *Kinetic study on dissolution of U<sub>3</sub>O<sub>8</sub> powders in nitric acid*. Journal of Nuclear Science and Technology, 1995. **32**(6): p. 596-598.
149. Inoue, A. and T. Tsujino, *Dissolution rates of U<sub>3</sub>O<sub>8</sub> powders in nitric acid*. Industrial & Engineering Chemistry Process Design and Development, 1984. **23**(1): p. 122-125.
150. Johnson, D.R. and J.A. Stone, *Light water reactor fuel reprocessing: dissolution studies of voloxidized and nonvoloxidized fuel*. 1980.
151. Ikeda, Y., et al., *O-17 NMR-study on dissolution reactor of UO<sub>2</sub> in nitric acid - mechanism of electron transfer*. Journal of Nuclear Science and Technology, 1993. **30**(9): p. 962-964.
152. Asano, Y., et al., *Kinetic studies on dissolution of UO<sub>2</sub> powders in acid solutions by using cerium(IV) or chlorine dioxide as oxidants*. Journal of Nuclear Science and Technology, 1996. **33**(2): p. 152-156.
153. Inoue, A., *Mechanism of the oxidative dissolution of UO<sub>2</sub> in HNO<sub>3</sub> solution*. Journal of Nuclear Materials, 1986. **138**(1): p. 152-154.
154. Uriarte, A.L. and R.H. Rainey, *DISSOLUTION OF HIGH-DENSITY UO<sub>2</sub>, PuO<sub>2</sub>, AND UO<sub>2</sub>-PuO<sub>2</sub> PELLETS IN INORGANIC ACIDS*, in *Other Information: Orig. Receipt Date: 31-DEC-65*. 1965: United States. p. Size: Pages: 82.
155. Sakurai, T., et al., *THE COMPOSITION OF NOX GENERATED IN THE DISSOLUTION OF URANIUM-DIOXIDE*. Nuclear Technology, 1988. **83**(1): p. 24-30.
156. Ikeda, Y., et al., *KINETIC-STUDY ON DISSOLUTION OF UO<sub>2</sub> POWDERS IN NITRIC-ACID*. Journal of Nuclear Materials, 1995. **224**(3): p. 266-272.
157. Guarro, S. and D. Beruto, *Kinetic model for dissolution processes of powders in liquid-phases*. Materials Chemistry, 1979. **4**(1): p. 31-50.
158. Burrows, J.M., Ockenden, D.W., Foreman, J.K., , *The dissolution of Plutonium oxides of known thermal history*. 1965, UKAEA, P.G. emorandum 1353(W), .
159. Ryan Jack, L. and A. Bray Lane, *Dissolution of Plutonium Dioxide?A Critical Review*, in *Actinide Separations*. 1980, AMERICAN CHEMICAL SOCIETY. p. 499-514.

160. Ryan, J.L., et al., *Catalyzed electrolytical plutonium oxide dissolution - the past 17 years and future potential*. Transuranium Elements - a Half Century, ed. L.R. Morss and J. Fuger. 1992, Washington: Amer Chemical Soc. 288-304.
161. Machuron-Mandard, X. and C. Madic, *Basic studies on the kinetics and mechanism of the rapid dissolution reaction of plutonium dioxide under reducing conditions in acidic media*. Journal of Alloys and Compounds, 1994. **213-214**: p. 100-105.
162. *Reprocessing of irradiated mixed oxide fuel of the first generation*. 1982: Hannover.
163. Standardization, I.O.f., *Determination of solubility in nitric acid of plutonium in unirradiated mixed oxide fuel pellets (U,Pu)O<sub>2</sub>*. 1994.
164. Tsukada, T., Yokoyama, H. , Satmark, B., Glatz, J.-P., Koch, L., Pagliosa, G. ., *Dissolution studies on high burn-up UO<sub>2</sub> and MOx LWR fuel*. in *RECOD 98*. 1998.
165. Hodgson, T.D., Holdroyd, S.D., Barrett, T.R., Coates, D.A.,, *The PFR Dissolver: Results of the First Irradiated FUEL Reprocessing Campaign*. 1984, UKAEA Harwell, AERE-R 10560.
166. Edwards, J., *The solubility of commercial fast reactor fuel*. 1983, UKAEA.
167. O'Boyle, D.R., F.L. Brown, and J.E. Sanecki, *Solid fission product behavior in uranium-plutonium oxide fuel irradiated in a fast neutron flux*. Journal of Nuclear Materials, 1969. **29**(1): p. 27-42.
168. Edwards, J., Batey, W., Phillips, B.A. ., *The solubility of fast reactor fuel during reprocessing*. in *RECOD 87*. 1987.
169. Jackson, A., *Unpublihsed work*.
170. Bassett, J., Denney, R.C., Jeffery, G.H., Mendham, J., *Vogel's textbook of quantitative inorganic analysis including elementary instrumental analysis*. fourth edition ed. 1983: Longman.
171. Rider, B.F. and M.G. Mellon, *COLORIMETRIC DETERMINATION OF NITRITES*. Industrial and Engineering Chemistry-Analytical Edition, 1946. **18**(2): p. 96-99.
172. Maher, C.J., *Unpublihsed results*.
173. Hartley, C., *Presonnel communication*.
174. Guillaumont, R., *Chemical thermodynamics 5: Update on the Chemical Thermodynamics of Uranium, Neptunium, Plutonium, Americium and Technetium*. 2003: North Holland.
175. Berger, P., *Etude Du Mecanisme de la dissolution par oxydoreduction chimique et electrochimique des dioxydes d-actinides (UO<sub>2</sub>, NpO<sub>2</sub>, PuO<sub>2</sub>, AmO<sub>2</sub>) en milieu aqueux acide*. 1990, Institut de rechierche technologique et de developpement industriel.
176. Madic, C., P. Berger, and X. Machuronmandard. *Mechanisms of the rapid dissolution of plutonium dioxide in acidic media under oxidizing and reducing conditions*. in *Symp to Commemorate the 50th Anniversary of the Discovery of Transuranium Elements, at the 200th National Meeting of the American Chemical Soc*. 1990. Washington, DC: Amer Chemical Soc.
177. Harding, J.H., Tasker, P.W.,, *The thermodynamics of the Dissolution of Uranium and Plutonium Oixde*. 1981, UKAEA Harwell, AERE-M 3140.
178. Ryan Jack, L. and A. Bray Lane, *Dissolution of Plutonium Dioxide - A Critical Review*, in *Actinide Separations*. 1980, American Chemical Society. p. 499-514.
179. Akabori, M. and T. Shiratori, *Dissolution of ThO<sub>2</sub>-Based oxides in nitric acid solutions at elevated temperatures*. Journal of Nuclear Science and Technology, 1994. **31**(6): p. 539-545.
180. Rudisill, T.S., *Dissolution of Neptunium Oxide in Unirradiated Mark 53 Targets*. 2002.
181. Kyser, E., *Dissolution of neptunium oxide residues*. 2009. p. Medium: ED.

182. Bray, L.A., Ryan, J.L., *Catalyzed Electrolytic dissolution of plutonium dioxide*, in *Actinide Recovery From Waste and Low Grade Sources* 1982, Routledge.
183. Sanyoshi, H., et al., *Dissolution of mixed oxide spent fuel from FBR*, in *Recod 91*. 1991. p. 710-714.
184. Fife, K.W., *A kinetic study of plutonium dioxide dissolution in hydrochloric acid using iron (II) as an electron transfer catalyst*. 1996.
185. Biddle, P. and J.H. Miles, *Rate of reaction of nitrous acid with hydrazine and with sulphamic acid: Its application to nitrous acid control in two-phase industrial systems*. *Journal of Inorganic and Nuclear Chemistry*, 1968. **30**(5): p. 1291-1297.
186. Agarande, M., *Lixiviation de dechetssolides plutoniferes par des solutions de reducteurs electrogeneres*. 1992, CEA.
187. Machuron-Mandard, Z., *Etude de la cinetique et du mechisme de la reaction de dissolution du dioxyde de plutonium par l'ion Cr (II) en solution acide*. 1991, CEA.
188. Gregson, C., et al., *Neptunium (V) Oxidation by Nitrous Acid in Nitric Acid*. *Procedia Chemistry*. **7**(0): p. 398-403.
189. Fauvet, P., et al., *Corrosion mechanisms of austenitic stainless steels in nitric media used in reprocessing plants*. *Journal of Nuclear Materials*, 2008. **375**(1): p. 52-64.
190. Hylton, T., *Dissolution of Neptunium and Plutonium Oxides Using a Catalyzed Electrolytic Process*, in *Other Information: PBD: 25 Oct 2004*. 2004. p. Medium: ED; Size: 39 pages.
191. Ryan, J.L., Bray, L.A., Boldt A.L., *Dissolution of PuO<sub>2</sub> OR NpO<sub>2</sub> using electrochemically regenerated reagents*, in *United States Patent*, E.R.a. Engineering, Editor. 1987: United States.
192. Gelis, V.M., Shumilova, Yu. B., Ershov, B. G., Maslennikov, A. G., Milyutin, V. V., Kharitonov, O. V., Logunov, M. V., Voroshilov, Yu. A., Bobritskii, A. V. , *Use of ozone for dissolving high-level plutonium dioxide in nitric acid in the presence of Am(V,VI) ions*. *Radiochemistry*, 2011. **53**(6): p. 612-618.
193. Ivanov, Y.E. and G.P. Nikitina, *Oxidative dissolution of plutonium dioxide in nitric acid in the presence of ozone. 1. Reaction of plutonium dioxide with cerium(IV) in nitric acid solutions*. *Radiochemistry*, 1995. **37**(3): p. 197-202.
194. Horner, D.E., et al., *Promotion of PuO<sub>2</sub> dissolution in nitric acid with cerium*. *Journal Name: Trans. Am. Nucl. Soc.*, v. 21, p. 252; Conference: Transactions of the American Nuclear Society 1975 annual meeting, New Orleans, LA, 8 Jun 1975; Other Information: Orig. Receipt Date: 31-DEC-75, 1975: p. Medium: X.
195. Ryan, J.L., et al., *Catalyzed Electrolytic Plutonium Oxide Dissolution (CEPOD): The past seventeen years and future potential*. 1990. Medium: ED; Size: Pages: (37 p).
196. Smith, W.H., G.M. Purdy, and S.D. McKee, *Comparison of silver(II), cobalt(III), and cerium(IV) as electron transfer mediators in the MEO mixed waste treatment process*. 1997.
197. Farmer, J.C., et al., *Destruction of chlorinated organics by cobalt(III) mediated electrochemical oxidation*. *Journal of the Electrochemical Society*, 1992. **139**(11): p. 3025-3029.
198. Gopinath, N. and G. Rao, *Oxidation of plutonium by cobalt(III) green*. *Journal of Radioanalytical and Nuclear Chemistry*, 1986. **104**(1): p. 7-12.

199. Zhu, Z.W., et al., *Generation of HNO<sub>2</sub> by bubbling NO in HNO<sub>3</sub> system and its application in the PUREX process*. Journal of Radioanalytical and Nuclear Chemistry, 2003. **258**(3): p. 557-561.
200. Jeffery, G.H., Bassett, J., Mendham, J., Denney, R.C., *Vogel's Textbook of Quantitative Chemical Analysis, Fifth Edition*. 1989: Longman Scientific & Technical.
201. IAEA, *Experiences and Trends of manufacturing Technology of Advanced Nuclear Fuels*. 2012.
202. Rider, B.F. and M.G. Mellon, *Colorimetric determination of nitrites*. Industrial and Engineering Chemistry-Analytical Edition, 1946. **18**(2): p. 96-99.
203. Ikeuchi, H., et al., *Dissolution behavior of irradiated mixed oxide fuel with short stroke shearing for fast reactor reprocessing*. Journal of Nuclear Science and Technology. **50**(2): p. 169-180.
204. Myers, M.N., *Absorption spectra of plutonium and impurity ions in nitric acid solution*. 1956.
205. Wilson, A.S., *Method of dissolving plutonium dioxide in nitric acid using cerium ions*. 1961.
206. Horner, D.E., D.J. Crouse, and J.C. Mailen, *Cerium-promoted dissolution of PuO<sub>2</sub> and PuO<sub>2</sub>-UO<sub>2</sub> in nitric acid*. 1977.
207. Bray, L.A., J.L. Ryan, and E.J. Wheelwright, *Development of the CEPOD process for dissolving plutonium oxide and leaching plutonium from scrap or wastes*. [Catalyzed Electrochemical Plutonium Oxide Dissolution (CEPOD)]. 1985.
208. Bray, L.A., J.L. Ryan, and E.J. Wheelwright, *Development of the CEPOD process for dissolving plutonium oxide and leaching plutonium from scrap or wastes*. [Catalyzed Electrochemical Plutonium Oxide Dissolution (CEPOD)]. p. Medium: ED; Size: Pages: 19.
209. Ryan, J.L., L.A. Bray, and A.L. Boldt, *Dissolving plutonium or neptunium dioxide in nitric acid - using electrolytic cell and regeneratable cerium copper silver or americium cpd*, Exxon Nuclear Co Inc (Esso). p. 42.
210. Bourges, J., Madic, C., Koehly, G., Lecome, M., *Dissolution Du dioxyde de plutonium en milieu nitrique par La Argent(II) electrogenere*, in Actinides. 1985: Aix-en-Provence, France.
211. Rance, P.J.W., Nikitina, G.P., *On the rate of reaction between Plutonium dioxide and Silver(II)*, in *Proceedings of JAERI 2002*,. 2002. p. 519-525.
212. Rance, P.J.W. and G.P. Nikitina, *An investigation into the effect of specific surface area on the reaction between Silver(II) and plutonium dioxide*, in *Plutonium Futures - the Science*, G.D. Jarvinen, Editor. 2003. p. 314-316.
213. Chiba, Z. and C. Dease, *Modeling of a dissolution system for transuranic compounds*. 1991.
214. Mentasti, E., C. Baiocchi, and J.S. Coe, *Mechanistic aspects of reactions involving Ag(II) as an oxidant*. Coordination Chemistry Reviews, 1984. **54**(FEB): p. 131-157.
215. Levason, W. and M.D. Spicer, *The chemistry of copper and silver in their higher oxidation states*. Coordination Chemistry Reviews, 1987. **76**: p. 45-120.
216. Pourbaix, M., *Atlas of Electrochemical Equilibria in Aqueous Solutions, 2nd Ed*. 1974: National Association of Corrosion Engineers.
217. Gordon, B.M. and A.C. Wahl, *Kinetics of the silver(I)-silver(II) exchange reaction*. Journal of the American Chemical Society, 1958. **80**(2): p. 273-276.
218. Noyes, A.A., et al., *Argentite salts in acid solution. IV. The kinetics of the reduction by water and the formation by ozone of argentite silver in nitric*

- acid solution*. Journal of the American Chemical Society, 1937. **59**: p. 1316-1325.
219. Kirwin, J.B., et al., *A kinetic and spectrophotometric examination of Silver(II) in perchlorate media*. The Journal of Physical Chemistry, 1963. **67**(8): p. 1617-1621.
  220. Rechnitz, G.A. and S.B. Zamochnick, *Behaviour of silver(II) in phosphoric acid media and a general mechanism for solvent oxidation*. Talanta, 1965. **12**(5): p. 479-483.
  221. Noyes, A.A., J.L. Hoard, and K.S. Pitzer, *Argentite salts in acid solution I The oxidation and reduction reactions*. Journal of the American Chemical Society, 1935. **57**: p. 1221-1229.
  222. Ivanov, Y.E. and G.P. Nikitina, *Ozone transfer through the gas-solution interface during oxidative dissolution of plutonium dioxide*. Radiochemistry, 1995. **37**(3): p. 209-212.
  223. Matheswaran, M., et al., *Silver-mediated electrochemical oxidation: Production of silver(II) in nitric acid medium and in situ destruction of phenol in semi-batch process*. Journal of Industrial and Engineering Chemistry, 2007. **13**(2): p. 231-236.
  224. Steele, D.F., *Electrochemistry and waste disposal*. Chemistry in Britain, 1991. **27**(10): p. 915-918.
  225. Berg, K.L., *Studies of the Electrochemical Silver (II) Generation in Nitric acid solutions*. 2005, Nexia Solutions 8384.
  226. Arnaud, O., C. Eysseric, and A. Savall. *Optimising the anode material for electrogeneration of silver (II)*. in *5th European Symposium on Electrochemical Engineering - Daniel Simonson Memorial Symposium*. 1999. Exeter, England: Inst Chemical Engineers.
  227. Petcher, D., ed. *A First Course in Electrode Processes, 2nd Edition*. 2009, RSC Publishing.
  228. Davies, D.R.K., *Active trials to assess the dissolution capabilities of silver II on stainless steel coupons*. 1992.
  229. Beesley, A.M., et al., *Evolution of chemical species during electrodeposition of uranium for alpha spectrometry by the Hallstadius method*. Applied Radiation and Isotopes, 2009. **67**(9): p. 1559-1569.
  230. Mudali, U.K., R.K. Dayal, and J.B. Gnanamoorthy, *Mixed RuO<sub>2</sub>/TiO<sub>2</sub>/PtO<sub>2</sub>-coated titanium anodes for the electrolytic dissolution of nuclear-fuels*. Nuclear Technology, 1992. **100**(3): p. 395-402.
  231. Laitinen, H.A. and J.M. Conley, *Electrolytic generation of silver(II) at antimony-doped tin oxide electrodes*. Analytical Chemistry, 1976. **48**(8): p. 1224-1228.
  232. Panizza, M., et al., *Electrochemical generation of silver (II) at boron-doped diamond electrodes*. Electrochemical and Solid State Letters, 2000. **3**(12): p. 550-551.
  233. Kissinger, P.T.H., W.R., ed. *Laboratory Techniques in Electroanalytical Chemistry*. 1984, Dekker.
  234. Maher, C.J., *Electrochemical dissolution of PuO<sub>2</sub> with Ag<sup>2+</sup> mediator - inactive studies*. 2013, National Nuclear Laboratory.
  235. Oudinet, G., et al., *Characterization of plutonium distribution in MIMAS MOX by image analysis*. Journal of Nuclear Materials, 2008. **375**(1): p. 86-94.
  236. Sarsfield, M.J., Stephenson, K., Bell, K., Brown, J., Carrott, M.J., Gregson, C., Maher, C.J., Mason, C., Taylor, R.J.,. *Americium and Plutonium Purification by Extraction (the AMPPEX process)*. in *Actinides*. 2013. Karlsruhe, Germany.

237. Ivanov, Y.E., et al., *Ozone in aqueous solution .2. Kinetics and mechanism of Cerium(III) and Silver(I) ozone oxidation* Zhurnal Fizicheskoi Khimii, 1972. **46**(8): p. 2149-8.
238. Balaji, S., et al., *Destruction of organic pollutants by cerium(IV) MEO process: A study on the influence of process conditions for EDTA mineralization*. Journal of Hazardous Materials, 2008. **150**(3): p. 596-603.
239. Pasquinini, F., *Etude d'une electrode reticulee tournante et de la preparation electrochimique de l'argent(II)*. 1997, Univeristy of Geneva.
240. Bourges, J., et al., *Dissolution of plutonium dioxide in nitric acid medium by electrogenerated silver(II)*. Journal of the Less-Common Metals, 1986. **122**: p. 303-311.
241. Collins, E.D., Del Cul, G. D., Rushton, J. E., Williams, K. A. , *A Practical Solution to Used Nuclear Fuel Treatment to Enable Sustained Nuclear Energy and Recovery of Vital Materials*. 2010.
242. Energy, U.S.D.o., *Characteristics of Potential Repository Wastes, Office of Civilian Radioactive Waste Management*. 1992.
243. Soelberg, N., Abbott, M., Haefner, D., Jubin, R. T. *Gaseous Fission Product Emissions Control During Spent Nuclear Fuel Recycling*. in *235th ACS National Meeting & Exposition, New Orleans, La*. 2008.
244. Benedict, M., Pigford, T., Levi, H.,, *Nuclear Chemical Engineering 2nd edition*. 1981: McGraw Hill, New York, .
245. Uchiyama, G., *Study on Voloxidation Process for Tritium Control in Reprocessing*. *Waste Manage. Nucl. Fuel Cycle*, , 1992. **17**(1): p. 63-79
246. Iwasaki, M., Sakurai, T., Ishikawa, N., Kobayashi, Y.,, *Oxidation of UO<sub>2</sub> Pellets in Air: Effect of Heat-Treatment of Pellet on Particle Size Distribution of Powders Produced*. Journal of Nuclear Science and Technology, 1968. **5**(12): p. 652-653
247. Peakall, K.A., Antill, J. E.,, *Oxidation of Uranium Dioxide in Air at 350-1000 °C*. Journal Nuclear Materials, 1960. **2**(2): p. 194-195.
248. Kleykamp, H., *The Chemical State of Fission Products in Oxide Fuels at Different Stages of the Nuclear Fuel Cycle*. Nuclear Technology, 1988. **80**: p. 412-422.
249. Brett, N.H. and A.C. Fox, *Oxidation products of plutonium dioxide-uranium dioxide solid solutions in air at 750°C*. Journal of Inorganic and Nuclear Chemistry, 1966. **28**(5): p. 1191-1203.
250. Brown, R.A., *Airborne Radionuclide Waste Management Reference Document*. 1983.
251. Rivera, D.A., Alam, M. K., Martin, L., Brown, J. R.,, *Characterization of Water and CO<sub>2</sub> Adsorption by Stores 3A Desiccant Samples Using Thermal Gravimetric Analysis and Fourier Transform Infrared Spectroscopy*. 2003.
252. Herrmann, F.J. *Minimizing of Iodine-129 Release at the Karlsruhe Reprocessing Plant WAK*. in *Proceedings of the 22nd DOE/NRC Nuclear Air Cleaning Conference*. 1992.
253. McKay, H.A.C. *Management Modes for Iodine-129*. in *proceedings of a meeting organized by the Commission of the European Communities and held in Brussels on September 25*. 1982.
254. IAEA, *Treatment, Conditioning and Disposal of Iodine-129*. 1987.
255. Little, D.K. *Noble Gas Removal and Concentration by Combining Fluorocarbon Absorption and Adsorption Techniques*. in *Proceedings of the 17th DOE Nuclear Air Cleaning Conference, CONF-820833*. 1983.
256. IAEA, , *Storage and Disposal of Krypton-85*. 1980.
257. Henrich, E. *Selective Absorption of Noble Gases in Freon-12 at Low Temperatures and Atmospheric Pressure*. 1985.
258. Leudet, A. *Methods of Krypton-85 Management*. in *proceedings of a meeting organized by the Commission of the European Communities and held in Brussel*. 1983.
259. Pence, D.T., *Critical Review of Noble Gas Recovery and Treatment Systems*. Nuclear Safety, 1981. **22**(6): p. 751-765.

260. Goossens, W.R.A., Eichholz, G. G., Tedder, D. W., *Treatment of Gaseous Effluents at Nuclear Facilities, Radioactive Waste Management Handbook Volume 2*. 1991: Harwood Academic Publishers.
261. Department of Energy, *Nuclear Air Cleaning Handbook*, . 2002.
262. Blanc, E., Pommier, A., Poncelet, F. J. Houdin, P., . *Spent Nuclear Fuel Cladding Management: The La Hague Reprocessing Plant Experience*. in *Proceedings of Global 2003 International Conferenc*. 2003. New Orleans, La.
263. Collins, E.D., DelCul, G. D.. Spencer, B. B., Brunson, R. R.. Johnson, J. A., Terekhov, D. S. Emmanuel, N. V., , *Process Development Studies for Zirconium Recovery/Recycle from Used Nuclear Fuel Cladding*, in *ATALANTE 2012 - Nuclear Chemistry for Sustainable Fuel Cycles*. 2012: Montpellier, France.
264. Federov, Y.S., Saprykin, V. F., Beznosyuk, V. I., Kolyadin, A. B. . *Thermo-Chemical Destruction of Zirconium Cladding of the Spent Fuel Assembly and Oxidation of the Fuel Composition Using Technology of Spent Nuclear Fuel Reprocessing at the Experimental-Demonstration Centre*. in *Proceedings of Global 2009 International Conference*. 2009. Paris, France, .
265. *A Technology Roadmap for Generation IV Nuclear Energy Systems*. 2002.
266. Goode, J.H., *Voloxidation: removal of volatile fission products from spent LMFBR fuels*, in *Other Information: UNCL. Orig. Receipt Date: 30-JUN-73*. 1973. p. Medium: ED; Size: Pages: 137.
267. *Management of Waste Containing Tritium and Carbon-14*. 2004, IAEA Technical Reports Series 421.
268. Clark, A.T., *Electrolytic dissolution of power reactor fuel in nitric acid*. 1961.
269. Ferris, L.M., *Mellitic acid from the oxidation of graphite with 90 % nitric acid*. Journal Name: Journal of Chemical and Engineering Data (U.S.); Journal Volume: Vol: 9; Other Information: ORNL-TM-623. Orig. Receipt Date: 31-DEC-64, 1964.

## 9. APPENDICES

### 9.1. Summary of direct dissolution analytical method calibrations

#### 9.1.1. $UO_2$ studies - UV-Vis Uranyl calibration studies

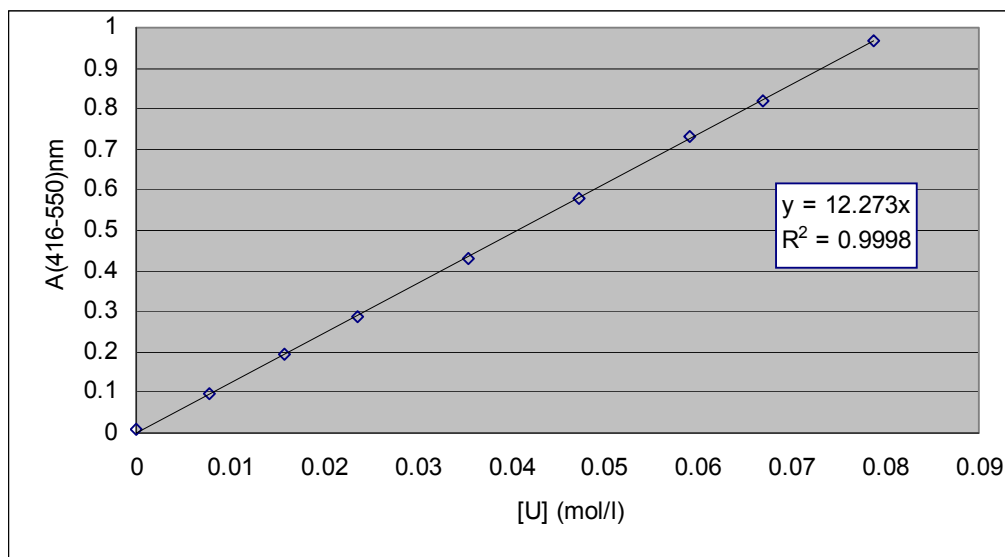


Figure 98: Beer Lambert plot for uranyl in 6 mol.l<sup>-1</sup> nitric acid

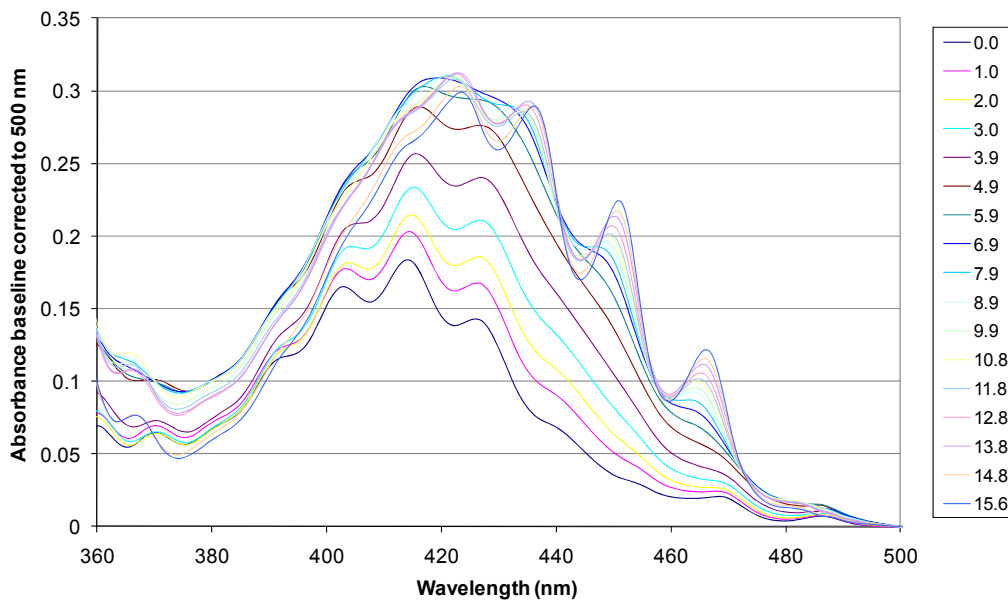
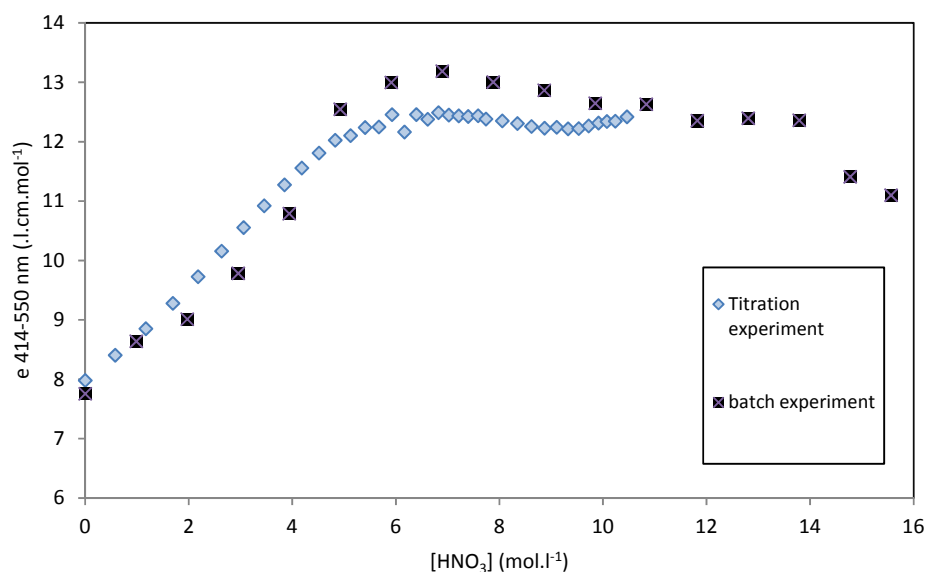


Figure 99: Batch titration - Uranyl nitrate – nitric acid UV-Vis spectra



**Figure 100: Comparison of molar extinction coefficients for titration and batch experiments**

### 9.1.2. $UO_2$ studies - Determination of $HNO_2$ by titration

Sample added to 0.095 mmol  $Ce(IV)$  in 10 v%  $H_2SO_4$ , after 5 minutes the remaining  $Ce(IV)$  by titrated by standardised  $Fe(II)$ .

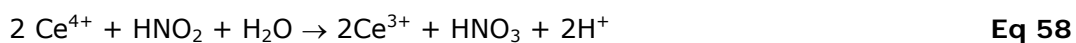


**Table 19: Results of  $HNO_2$  titration method testing**

standard	Volume of standard added (ml)	$Fe^{2+}$ endpoint volume <sup>+</sup> (ml)	Determined $[NaNO_2]$ ( $mol.l^{-1}$ l)
-	0	9.50	-
B	0.45	0.10	0.104
B	0.25	4.27	0.105
B	0.1	7.87	0.082
A	0.4	2.02	0.093
A	0.25	4.04	0.109

Standard A = Fischers  $0.5 mol.l^{-1}$   $NaNO_2$  standard diluted by 5.

Standard B =  $0.1 mol.l^{-1}$  prepared by AR  $NaNO_2$  and deionised water.

### 9.1.3. $UO_2$ studies – Determination of $HNO_2$ by colourimetry

Sulphanilamide in  $0.05 \text{ mol.l}^{-1}$  HCl is reacted with sample containing  $HNO_2$  for 5 minutes. N-(1-naphthyl)-ethylenediamine dihydrochloride (NEDD) is added, and UV-Vis spectra are recorded after 5 minutes. Figure 102 shows the good comparison between colorimetric and titration results from experiment 18.

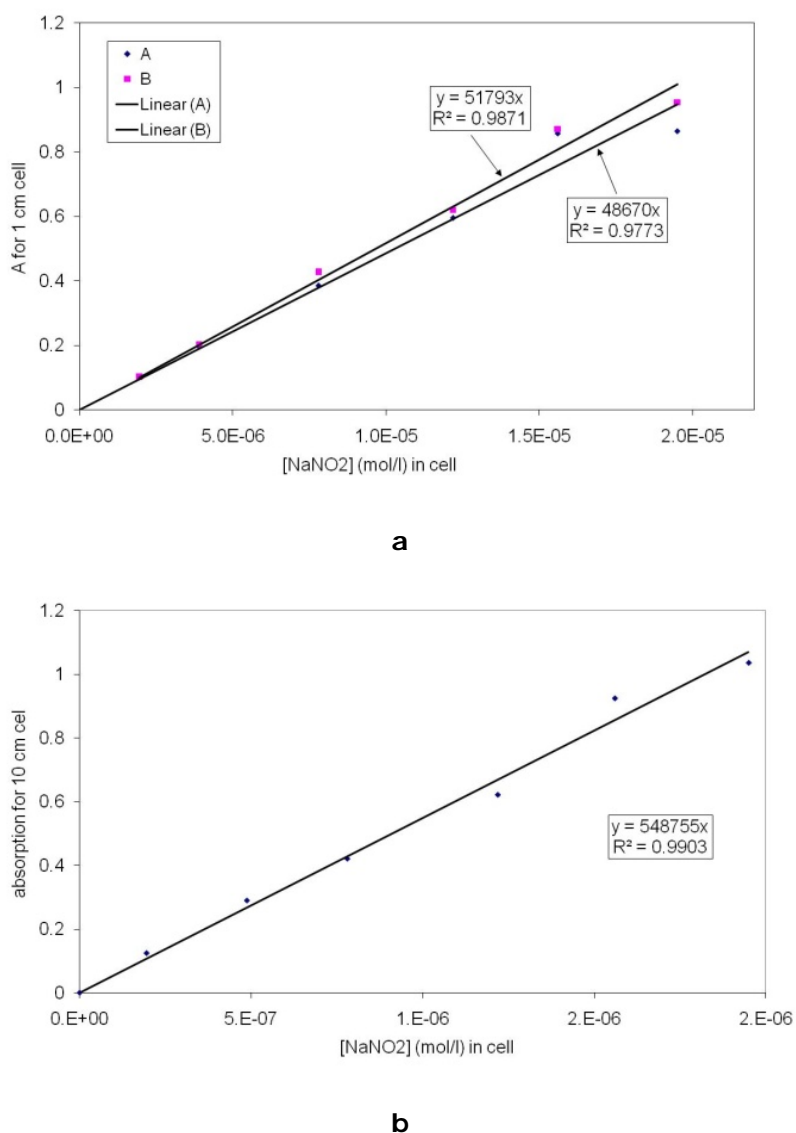


Figure 101: Beer Lambert UV-Vis plots for  $HNO_2$  colorimetric method  
a) 1 cm cuvette, b) 10cm cuvette

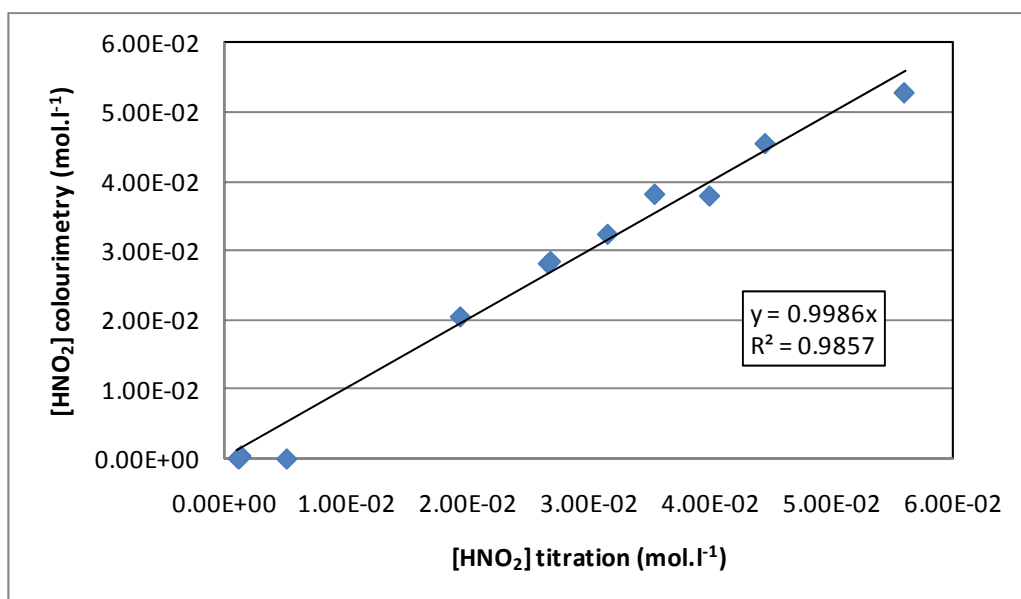


Figure 102: Comparison of colorimetric and titration HNO<sub>2</sub> concentrations

#### 9.1.4. Uranium dioxide studies – Determination of HNO<sub>2</sub> by in-situ potentiometry

Comparison of the colorimetric HNO<sub>2</sub> concentrations and the redox potential was carried out using the Nernst equation, Eq 60.  $E_0$  can be calculated from literature data, knowing the Ag/AgCl reference electrode value and NO<sub>3</sub><sup>-</sup>/HNO<sub>2</sub> couple redox potential as 0.755 V, so the Nernst equation can be solved for [HNO<sub>2</sub>], Eq 61. Figure 103 shows the comparison of the calculated and experimental results and show that the colorimetric method and potentiometry results are in good agreement on a log<sub>10</sub>-log<sub>10</sub> scale. Comparison of the titration and potentiometric methods correlate less well on the log<sub>10</sub>-log<sub>10</sub> scale due to the much shorter range of the method, *ca.*  $>1 \times 10^{-3}$  mol.l<sup>-1</sup>. Comparison of the off-line methods with the potentiometric method on a linear scale shows a large variability, this is a common feature as potentiometry is accurate on the log-scale.

$$E = E_0 + \frac{RT}{2F} \ln \left( \frac{[H^+]^3 [NO_3^-]}{[HNO_2]} \right) \quad \text{Eq 60}$$

$$[HNO_2] = \frac{[H^+]^3 [NO_3^-]}{e^{\left( \frac{2F(E-0.755)}{RT} \right)}} \quad \text{Eq 61}$$

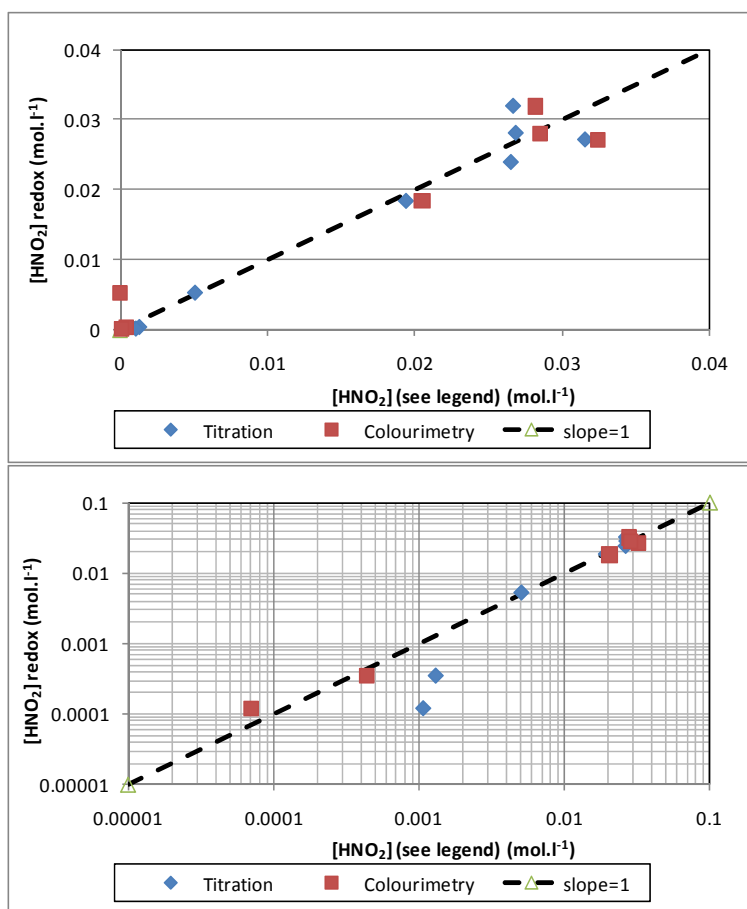


Figure 103: Comparison of off-line  $\text{HNO}_2$  methods with potentiometry method, top linear – linear scale, bottom  $\log_{10}$ - $\log_{10}$  scale

#### 9.1.5. Uranium dioxide powder studies - Determination of $\text{HNO}_2$ by direct UV-Vis

Experiment 18 observed the decomposition of  $\text{HNO}_2$  in  $6 \text{ mol.l}^{-1}$  nitric acid at  $80^\circ\text{C}$  using the four analytical methods. The results from the titration and colorimetric methods were used to calibrate the UV-Vis method. The graphs below show the calculation of the  $\text{HNO}_2$  extinction coefficient as  $14.1 \text{ l.mol}^{-1}$  for the 2 mm cell, Figure 104, or  $70.5 \text{ l.mol}^{-1}\text{.cm}^{-1}$  (for absorbance at 370nm minus baseline absorbance at 550.6 nm). Figure 105 shows the extinction coefficients for uranyl in  $6 \text{ mol.l}^{-1}$  nitric acid. The derivation of the correction for uranyl absorbance from the  $\text{HNO}_2$  absorbance is given below, Eq 62 is the equation used for calculation of  $\text{HNO}_2$  concentrations in the  $\text{UO}_2$  dissolution experiments.

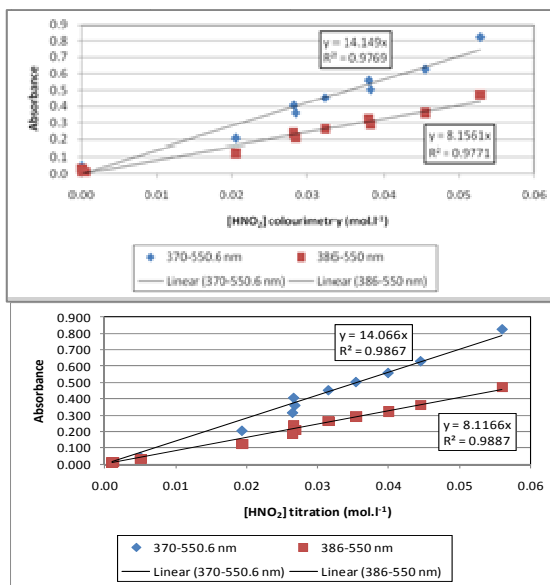


Figure 104: HNO<sub>2</sub> UV-Vis extinction coefficients (0.2 cm flowcell)

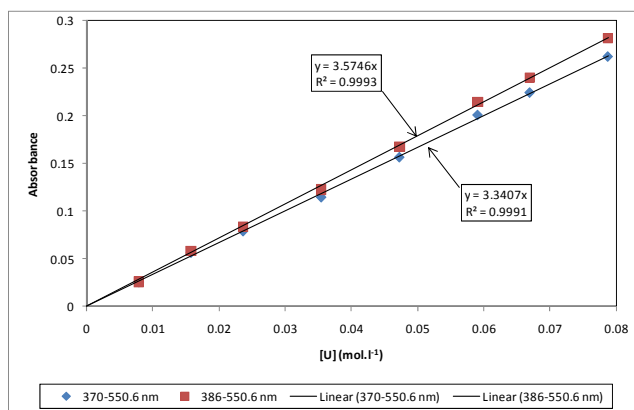


Figure 105: Uranyl in 6 mol.l<sup>-1</sup> nitric acid UV-Vis extinction coefficients at HNO<sub>2</sub> absorption wavelengths (1 cm cell)

### HNO<sub>2</sub> analysis

$$[\text{HNO}_2] = (A_{370} - A_{550.6}) / 70.5$$

### U analysis

$$[\text{U}] = (A_{416} - A_{550.6}) / 12.27$$

$$[\text{U}] = (A_{370} - A_{550.6}) / 3.341$$

### Uranyl corrections for HNO<sub>2</sub> analysis

$$(A_{370} - A_{550.6}) / 3.341 = (A_{416} - A_{550.6}) / 12.27$$

$$(A_{370} - A_{550.6}) = 3.341(A_{416} - A_{550.6}) / 12.27$$

$$(A_{370} - A_{550.6}) = 0.2723(A_{416} - A_{550.6})$$

$$[\text{HNO}_2] = ((A_{370} - A_{550.6}) - 0.2723(A_{416} - A_{550.6})) / 70.5$$

$$[\text{HNO}_2] \text{ (mol.l}^{-1}\text{)} = ((A_{370} - A_{550.6}) - 0.2723(A_{416} - A_{550.6}))/14.1 \text{ (for 2 mm cell)}$$

Eq 62

### 9.1.6. MOx pellet studies – U and Pu UV-Vis-nIR calibration (Off line analysis)

A simple UV-Vis-nIR calibration was carried out by preparation of solutions of three U, Pu concentrations with final HNO<sub>3</sub> concentrations of 6, 8, 10, 12 or 14 mol.l<sup>-1</sup>. All spectra have been baseline corrected using a sloping baseline between 564 and 906 nm. The effect of HNO<sub>3</sub> concentrations upon the highest Pu concentration are shown in Figure 106. To highlight regions in the spectra that change, spectra of the same U, Pu concentrations have been subtracted from the 6 mol.l<sup>-1</sup> spectra and are shown in Figure 107. This allows determination of the wavelengths where there is little or large effects of HNO<sub>3</sub> concentration to be determined. The uranium calibration plot was selected to minimise the effect of HNO<sub>3</sub> concentration and is shown in Figure 108 and Eq 63. The derived calibrations for Pu are affected by nitric acid concentration and so different calibration coefficients are used for different nitric acid concentrations, shown in Figure 109, Eq 64 and Eq 65.

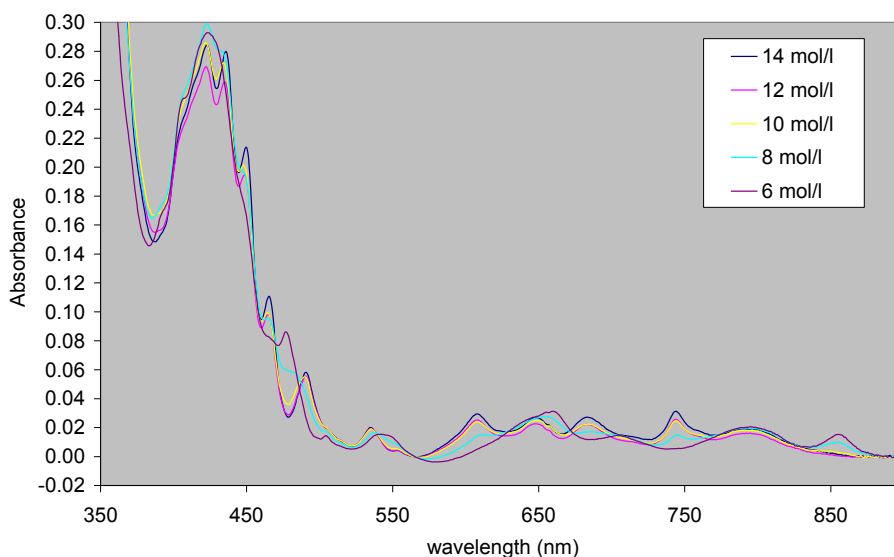
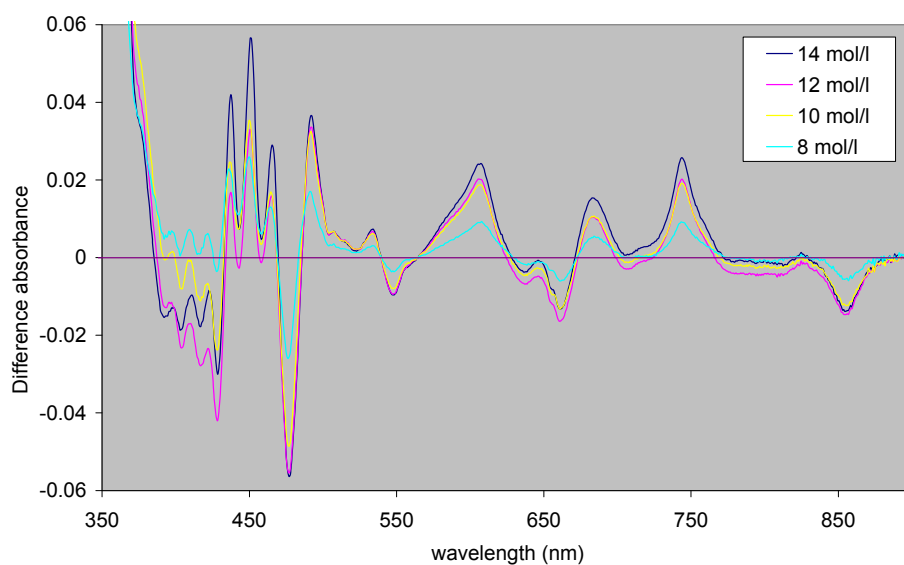
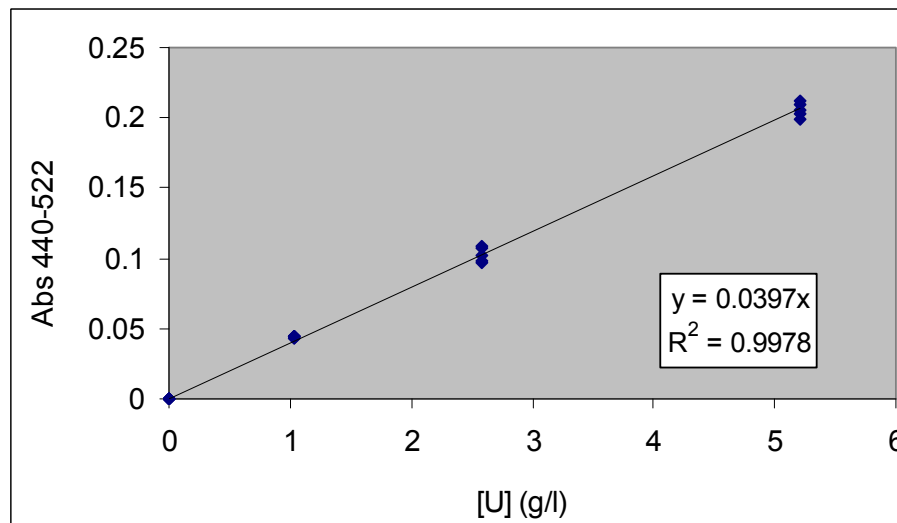


Figure 106: UV-Vis-nIR spectra of 1 ml U,Pu solutions in 6 – 14 mol.l<sup>-1</sup> nitric acid



(Difference spectra are produced by subtracting 1 ml 6 mol.l<sup>-1</sup> nitric acid spectra. These spectra show the differences cause by changing the nitric acid concentration.)

**Figure 107: UV-Vis-nIR difference spectra for U, Pu solutions**



**Figure 108: Uranium Beer Lambert plot**

$$[U] = \frac{A_{440.7} - A_{522}}{0.0397l}$$

**Eq 63**

Where  $l$  is pathlength (cm), and  $[U]$  is uranium concentration (g.l<sup>-1</sup>)

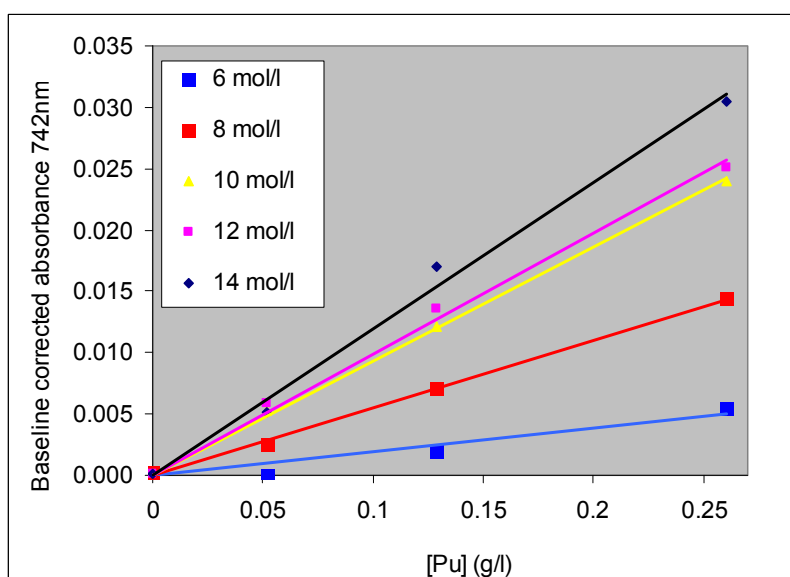


Figure 109: Plutonium Beer Lambert plot for different  $\text{HNO}_3$  concentration

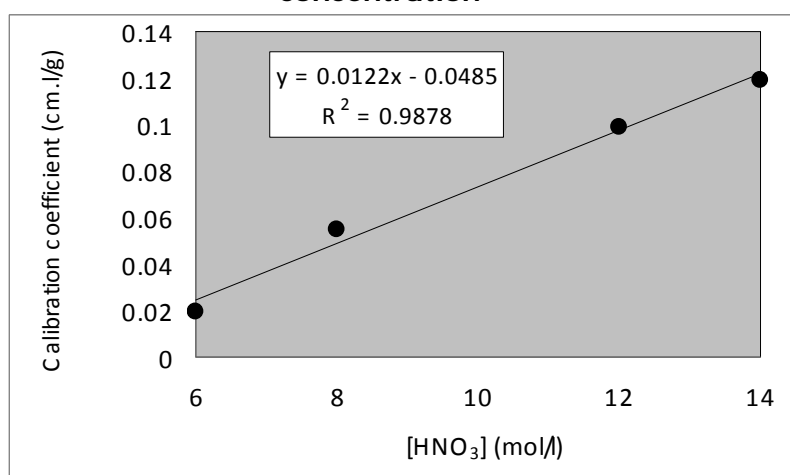


Figure 110: Dependence of Pu calibration coefficient with  $\text{HNO}_3$  concentration

$$[Pu] = \frac{A_{742.5} - A_{742.5\text{baseline}}}{(0.0122[\text{HNO}_3] - 0.0485)l} \quad \text{Eq 64}$$

$$A_{742.5\text{baseline}} = \left( \frac{A_{898.6} - A_{564.6}}{898.6 - 564.6} \right) A_{742.5} + \left( A_{564.6} - 564.6 \left( \frac{A_{898.6} - A_{564.6}}{898.6 - 564.6} \right) \right) \quad \text{Eq 65}$$

Where  $l$  is pathlength (cm),  $[Pu]$  is plutonium concentration ( $\text{g.l}^{-1}$ ) and  $[\text{HNO}_3]$  is nitric acid concentration ( $\text{mol.l}^{-1}$ ).

## 10. SUPPLEMENTARY PUBLISHED MATERIAL

This section details other material prepared solely or in part by the author.

### *10.1. Head-end processing*

The following section details the UK-USA contribution to a forthcoming NEA OECD report on spent fuel reprocessing. This chapter has been written by Barry Spencer, Bob Jubin, Bill DelCul, Emory Collins, Oak Ridge National Laboratory and Chris J. Maher.

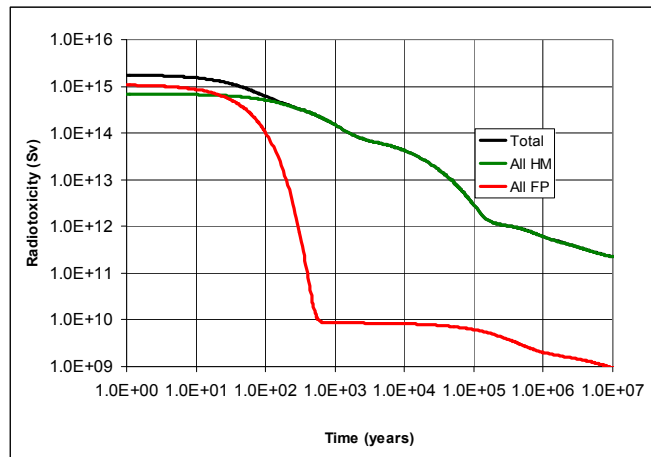
#### *10.1.1. Introduction*

In closed nuclear fuel cycles, the primary role of the used nuclear fuel (UNF) reprocessing plant is to recover the valuable fissile and fertile materials for reuse, thereby improving the sustainability of the nuclear fuel cycle. This also reduces the waste volumes, heat loading and amount of long lived radioactivity consigned to a geological disposal facility (GDF). In designing advanced reprocessing plants for future fuel cycles, it currently seems likely that recovery of uranium, plutonium and the minor actinides (MA), neptunium, americium, and curium, will be required [241]. The recovery of the minor actinides provides potential to reduce the amount of long lived radioactivity consigned to the GDF and allows energy to be generated during the destruction of the MA. To maximise the reduction in radioactivity, a greater value may be placed upon achieving high recoveries; this is illustrated in **Figure 111**.

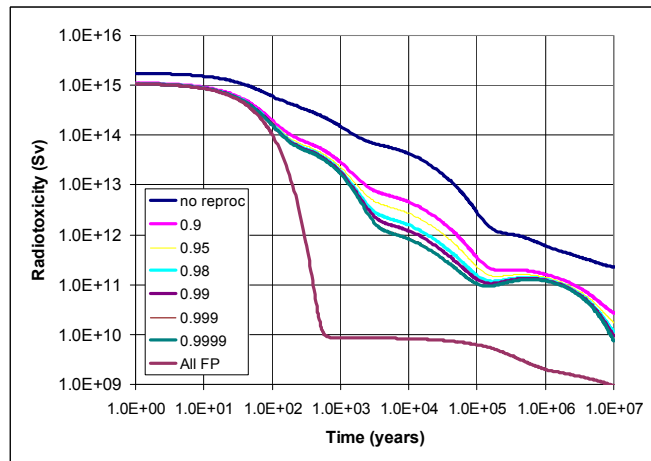
The head-end processes prepare used nuclear fuel (UNF) for chemical separations, electrochemical separations, or combinations of the two types of separations processes. The head-end encompasses disassembly and shearing, an optional voloxidation step, off-gas trapping of volatile used fuel components, potential recovery and recycle of zirconium from Zircaloy® used fuel cladding, and dissolution of the oxide fuel to prepare for subsequent component separations. The head-end processes are coupled with off-gas treatment systems to control the release of radioactive gases arising from the fuel and of harmful chemical vapors arising from the process chemicals.

In comparison with current industrial-scale operations, research, development, and demonstration studies have shown progress in improving the capabilities for volatile component release and trapping by means of the advancements made in the voloxidation process and associated off-gas trapping, as well as in conversion of the ceramic oxide fuel components to a finely divided oxide powder that is amenable to continuous dissolution. Moreover, systems studies have shown the potential benefits of recycling more of the used fuel components, including uranium, all transuranium elements, zirconium from Zircaloy fuel cladding, and several of the valuable fission product components [241].

a) Used fuel and fission products



b) Reprocessing with varying recovery of uranium and plutonium



c) Reprocessing with varying recovery of uranium, plutonium and the minor actinides

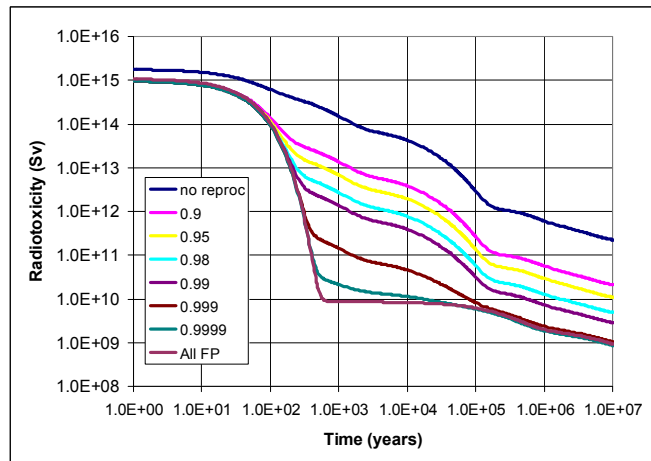


Figure 111: Radioactivity of 4 %  $^{235}\text{U}$  – 40 GWd/tHM, under three scenarios

### 10.2.1.4 Current practices

The UK has operated four reprocessing plants and currently two are undergoing decommissioning and two are operational, Table 20. The Magnox reprocessing plant reprocesses uranium metal fuel from the domestic Generation I Magnox reactors. The Thermal Oxide Reprocessing Plant (THORP) reprocesses domestic and overseas oxide fuel from light water reactors (LWRs).

**Table 20: UK reprocessing plants**

1951 - 1972 <sup>ix</sup>	Windscale	Reprocessing plant for metal fuel, early commercial reactor fuel and decontamination of prototype oxide fuel. Currently undergoing decommissioning.
1960 - 1996 <sup>ix</sup>	Dounreay	Reprocessing of a variety of fuel from the fast reactor development programs. Currently undergoing decommissioning.
1964 -	Magnox	2 <sup>nd</sup> reprocessing plant at Sellafield, reprocesses commercial Magnox clad uranium metal fuel.
1994 -	THORP	3 <sup>rd</sup> reprocessing plant at Sellafield, reprocesses commercial thermal oxide fuel.

#### 10.2.1.1. Disassembly and Fuel Exposure

The different designs of fuel require different fuel preparation. The Magnox uranium metal fuel was declad using a die press, but this was later replaced with a slitter wheel. Dounreay reprocessing plant used and THORP uses a hydraulic cutting blade to chop the fuel into short lengths. Due to the high fissile content and low throughput required, the Dounreay plant used a single pin shear. The higher throughput and lower fissile content of THORP requires the shear of entire pressurized water reactor (PWR) and boiling water reactor (BWR) fuel elements or bundles of advanced gas-cooled reactor (AGR) fuel pins.

Many designs for both PWR and BWR fuel assemblies have evolved over time. A typical Westinghouse PWR fuel assembly is shown in **Figure 112**. This type

---

<sup>ix</sup> *With intermediate refurbishment*

of fuel assembly has a  $17 \times 17$  fuel pin array, of which 264 array positions are occupied by fuel pins and the remaining positions are for control rods. (A BWR fuel assembly typically has an  $8 \times 8$  fuel pin array, of which 63 array positions are occupied by fuel pins.) Eight grid spacers and massive nozzles at the top and bottom of the assembly are clearly visible in the photograph. In terms of mass, one PWR fuel assembly is composed of  $\sim 525$  kg of  $\text{UO}_2$  ( $\sim 461$  kg U metal),  $\sim 108$  kg of Zircaloy, and  $\sim 26$  kg of other steel-based hardware. The nozzles, spider (part holding the control rods), and springs are part of the steel-based hardware. Descriptions of various types of fuel assemblies can be found in DOE/RW-0184 (DOE Rev. 1, 1992) [242].

Because UNF is enclosed in chemically resistant metal cladding, the fuel must be exposed for subsequent chemical treatment. Commercial enterprises for processing and recycling the components of UNF utilize a mechanical shear to cut the fuel pins into segments, although other techniques such as laser cutting have been tested and evaluated. Shearing options range from whole-bundle shearing to single-pin shearing. In both cases, the top and bottom nozzles are usually removed as part of a disassembly operation to eliminate these robust metal components. The non-fuel-bearing plenum areas of the fuel pins may be cropped to eliminate additional metal that does not contain fuel material. In whole-bundle shearing, all the fuel pins are held tightly in a compaction device while they are cut with a shear blade that moves perpendicular to the long axis of the pins. Compaction is necessary to prevent closing the ends of the cladding tube by pinching. The grid spacers remain in place and might hold the group of fuel pin segments together. Compaction can cause significant cladding tube deformation along the entire length of a fuel cladding segment and can result in fracture of the fuel pellets, which is beneficial to fuel dissolution. In single-pin shearing, the individual pins are removed so that the grid spacers are also eliminated from the shearing process. No grid spacer remnants remain to hold groups of sheared pin segments together. The cuts may be smooth and result in little fuel fracturing. Therefore, the difference between whole-bundle and single-pin shearing affects the size of the largest "chunk" of material to be processed and the degree of crushing of the fuel pellets. This variation, in turn, has implications for voloxidizer or dissolution process equipment design.



**Figure 112. Westinghouse PWR fuel assembly. (ORNL Photo 3897-77)**

#### ***10.2.1.2. Dissolution***

All reprocessing plants dissolve oxide fuel in nitric acid, although the dissolver designs differ. The 1<sup>st</sup> Sellafield reprocessing plant dissolved de-clad uranium metal rods in a batch kettle. The sequence of operations was, first, to add the fuel to the dissolver, which was then lidded and heated to temperature. The Magnox dissolver is a large, continuous dissolver where de-clad uranium metal fuel is added continuously and the dissolved fuel liquor is discharged and fed to the reprocessing plant.

The high fissile content of the fast reactor fuel used at Dounreay required a dissolver that was criticality 'eversafe' and for this a thermosyphon dissolver was used. A sheared batch of fuel was placed into a basket which was then inserted into the dissolver vessel. Nitric acid added for fuel dissolution.

THORP uses a similar method to the Dounreay dissolver; however, fuel is sheared and falls directly via a chute into a basket that is contained in the dissolver vessel. Fuel is partially dissolved before more fuel is added. After all of the fuel is dissolved, the chute is removed. The dissolver is lidded and heated to the leaching temperature. The dissolvers are large kettle dissolvers that are not, by geometry, of sub-critical design. Therefore, gadolinium nitrate is added as a neutron absorber to ensure criticality safety. THORP has three dissolvers that operate in sequence. While fuel is added to one, the second is leaching

fuel, and the third dissolver transfers the liquor and hulls to the next processing step and is prepared for the next batch.

Air is added to the reflux condensers of both the Magnox and THORP dissolvers to enable increased conversion of nitrogen oxides (NO<sub>x</sub>), generated from the dissolution of fuel in nitric acid, to the more soluble nitrogen dioxide. This decreases the amount of nitric acid used and the amount of nitrogen oxide released to the dissolver off-gas (DOG) treatment system. This technology is termed 'fumeless' dissolution when operated at high efficiencies.

The Magnox swarf from decanning Magnox elements and THORP leached hulls are encapsulated in cement to form an intermediate level radioactive waste (ILW) waste form.

### ***10.2.2. Potential additional process steps for a future reprocessing plants***

Future reprocessing plants will necessitate the abatement of radionuclides that are currently, currently routed to multiple streams, such as <sup>3</sup>H, <sup>14</sup>C, <sup>36</sup>Cl, <sup>85</sup>Kr, <sup>129</sup>I. To achieve control of these species, additional process steps may be required. Also, the reprocessing of fuels other than standard oxides may also necessitate the use of additional process steps. Two of the major candidate technologies are high temperature pre-treatment (voloxidation) and application of electro-mediated dissolution, *e.g.* using silver(II).

### ***10.2.3. High temperature pre-treatment - Voloxidation***

Voloxidation is a dry head-end method for removing tritium from used reactor fuel prior to aqueous processing. This avoids introducing the tritium into the aqueous systems, where it would accumulate or might be released to the environment with gaseous or liquid water discharges. Recent studies have indicated that tritium removal and retention is necessary to meet exposure limits at the reprocessing site boundary [243]. A general schematic of the process is shown in **Figure 113**.

The voloxidation process usually takes place at 480 to 600°C in the presence of air or oxygen. At these temperatures the reaction of UO<sub>2</sub> with oxygen to form U<sub>3</sub>O<sub>8</sub> is rapid enough to be of practical value. Conversion to the higher oxide results in expansion and restructuring of the grain-level crystallite accompanied by crumbling of the monolithic fuel pellet to a fine powder [150].

Comminution increases the available surface area for reaction and releases the fuel from the segments of cladding. Tritium, which may be present in the fuel in elemental form, diffuses to the surface of the particle, where it reacts with oxygen to form water, which enters the gas stream [244]. A fraction of the tritium is associated with the cladding as zirconium hydride ( $ZrT_x$ ). This fraction has been reported at 40%, and higher [245]. Indications are that voloxidation has little effect on the tritium held in the cladding when processing occurs at a temperature of 480°C for 6 h.

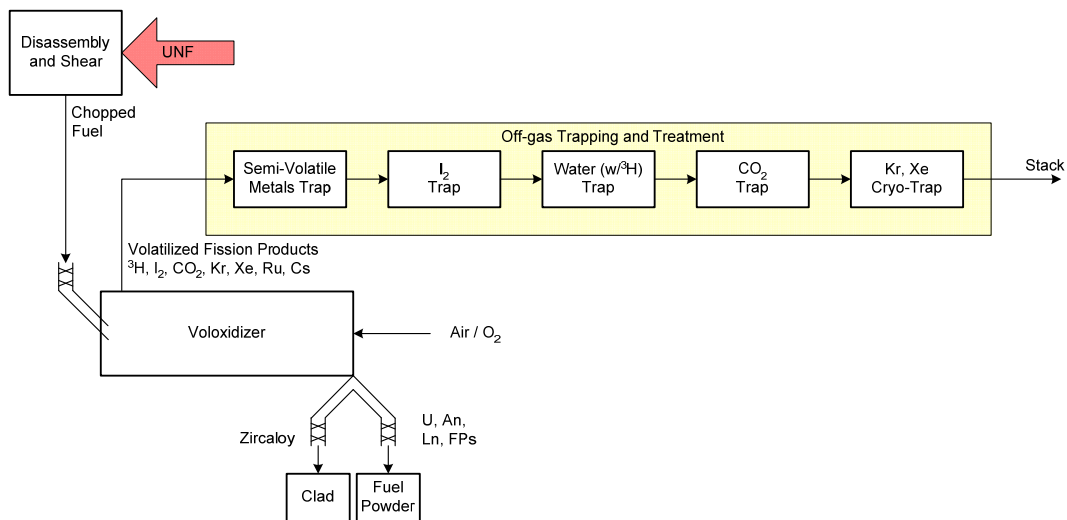


**Figure 113: Standard voloxidation process with off-gas treatment.**

The rate of reaction at 480°C is such that >99.9% of the tritium is released from the fuel in about 4 h. Over 99% of the fuel particles are reduced to <20 µm. Powder size distribution depends on the temperature of the voloxidation process [246-248] and other factors related to the used fuel characteristics. However, nearly all sizes will be <20 µm [245]. Along with the tritium, about half of the  $^{14}C$  and minor fractions of other fission products are volatilized, including ~5% of krypton and xenon; ~1% of iodine and bromine; and <0.2% of the ruthenium, antimony, and cesium. With higher temperatures and longer reaction times, larger fractions of the noble gases may be released.

The conversion to  $U_3O_8$  may also be desirable for other fuel types, such as carbides and nitrides, because:

- During the dissolution of carbides in nitric acid complex organic products are produced that interfere with solvent extraction processes [83, 84].
- The dissolution of nitrides in nitric acid is highly exothermic and conversion to  $U_3O_8$  reduces the reactivity. Also, if  $^{15}N$  containing nitride

fuels are used, the  $^{15}\text{N}$  being a valuable isotope, it may be necessary to recover it for reuse. An oxidation process would release the nitrogen for simple trapping and recovery, whereas, direct dissolution in nitric acid would cause isotopic dilution, complicating  $^{15}\text{N}$  recovery [91].

The large difference in particle sizes between the voloxidized fuel powder and remaining cladding hulls present the option of mechanical separation of the cladding from the fuel. Over 99% of the fuel may be separated from the cladding by screening. Such a separation benefits the dissolution process because a powder dissolver may be much less complex and more compact. Also, the powder dissolves faster and requires less use of nitric acid. However, high fuel recovery will require washing of the cladding hulls to remove the fines that cling to the surfaces.

During voloxidation, partial release of volatiles and trace release of semivolatiles occur at conditions where the tritium is volatilized. This is not problematic. The tritium is easily removed from the voloxidizer off-gas as tritiated water, and the remaining off-gases may be combined with the dissolver off-gas for treatment to sequester iodine,  $^{14}\text{C}$  (as  $^{14}\text{CO}_2$ ), and the radioactive noble gases (krypton, xenon). The partial release of other radioactive fission products indicates the potential to remove other semi-volatiles from the fuel, especially those that complicate downstream processes or their off-gas treatment systems.

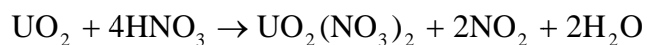
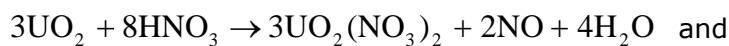
An enhanced voloxidation process is being investigated that utilizes either higher temperatures or alternative reactants (e.g., ozone, steam, nitrogen dioxide) or a combination of both temperature control and alternative reactants to completely remove other volatile or semivolatile fission products. The targeted species depends on the goals of the process, which depend on the trade-offs between benefits obtained for downstream processes and the costs to implement the process. Preliminary results indicate that iodine may be almost completely removed in a voloxidation step using nitrogen dioxide as an oxidant. This possibility would simplify recovery (compared with processing the moisture-laden off-gas from the dissolution step), decrease halogen-enhanced corrosion in downstream processes, and reduce the requirements for iodine emissions controls from multiple points in the plant to a single control point. Similarly,  $^{14}\text{C}$  and the noble gases are more completely removed.

#### ***1.4.3.2 Advanced Dissolution***

Currently dissolved segmented fuel is leached using nitric acid (HNO<sub>3</sub>) to dissolve the fuel while the cladding hulls are separated from the dissolver solution either in batch-wise fashion as described in section 1.4.2.2, or as part of a continuous operation, such as the French rotary wheel-dissolver. In future advanced systems, the voloxidation process can convert a metal fuel or lower oxide fuel (e.g., UO<sub>2</sub>) to the higher oxides and reduce the fuel particle sizes. The reduction in particle size can enable use of a screen to separate the cladding hulls and enable a continuously operated fuel powder dissolution to be used, as illustrated in **Figure 114**.

**Figure 114: Advanced head-end operations.**

The fine powder greatly accelerates the rate of dissolution. Higher oxidation states of the uranium reduce the nitric acid requirement and the amount of NO<sub>x</sub> evolved. For example, dissolution of UO<sub>2</sub> may be described by a combination of two stoichiometries [244].



An empirical approximation for dissolution of U<sub>3</sub>O<sub>8</sub> is:



Strong oxidants used in voloxidation, such as NO<sub>2</sub>, can convert the fuel to the uranium trioxide (UO<sub>3</sub>), which theoretically supports fumeless dissolution:



In practice, small amounts of nitrogen oxides are produced.

Standard voloxidation has been observed to increase the insoluble fraction of the fuel, typically called "undissolved solids" (UDS). The UDS consist primarily of the noble metals, ruthenium, rhodium, palladium, molybdenum,

and technetium, which are found in used fuel as micro-precipitates that are formed from solid solution during irradiation [9]. Fuel burn-up is the major factor that determines the amount of UDS with the greater amounts produced at higher burn-up. Removal of the UDS is normally accomplished by clarification (centrifuging or high efficiency filtration) of the dissolved fuel solution.

Some evidence indicates that very small quantities of plutonium are retained within these undissolved residues. The amount is normally insignificant, but for the higher concentrations of plutonium in MOX fuels, or in cases where the prior fuel fabrication includes milling for homogenization and high temperature treatment, the plutonium is known to be present as plutonium rich inhomogeneities, and may have lower solubility in the acid dissolvent [249].

In such cases, the use of special dissolution technologies to improve the recovery of plutonium may be particularly useful. Such technologies could be carried out upon the as-dissolved liquor or selectively upon the undissolved centrifuge cake. The dissolution of plutonium-containing residues may be carried out using techniques such as mediated electrochemical oxidation, using, for example, electrochemically generated silver(II) [160]. One disadvantage of these processes is that some fission products present in dissolved fuel and UDS are also oxidised and catalyzed by the decomposition of the silver(II).

#### ***1.4.3.3 Off-Gas Treatment***

The processing or treatment of UNF will result in the release of a number of volatile and semivolatile species. Under current US regulations,  $^{129}\text{I}$  and  $^{14}\text{C}$  must be sequestered essentially indefinitely, but tritium, xenon, and krypton (i.e.,  $^{85}\text{Kr}$ ) can be managed in decay storage. Over the past two to three decades, a number of technologies have been developed to various stages of maturity. Off-gas treatment in a fuel reprocessing plant must address three main gaseous streams. The first is the off-gas from the head-end, which includes the shear, the optional voloxidizer, and the dissolver. This collectively is sometimes called the dissolver off-gas (DOG). The second is the vessel off-gas (VOG), which collects in-leakage to all of the process equipment and the instrument air used in bubblers, air sparge discharges, etc. The third is the cell ventilation, which provides confinement to the process cell. Each of these has unique characteristics and processing challenges, although the elements or radionuclides to be captured may be

found in one or more of these streams. For this reason it is convenient to discuss capture technology for each of the targeted species.

### Tritium

Tritium may be removed from the off-gas stream with desiccants or molecular sieves. Anhydrous  $\text{CaSO}_4$  has been reported as a possible desiccant [244]. Molecular sieves exhibit high water capacities: 10 to 20% based on the dry weight of the sorbent [250]. Type 3A desiccants have been shown to also sorb carbon dioxide at temperatures significantly below room temperature [251].

### Iodine

Numerous technologies have been developed for the recovery of airborne  $^{129}\text{I}$  based on scrubbing with caustic or acidic solutions and chemisorption on silver-coated or impregnated adsorbents. However, to achieve the high decontamination factors (DFs) required to meet the regulatory requirement (>500), a critical step is to ensure that the iodine is volatilized into the most concentrated gas stream possible. The distribution of  $^{129}\text{I}$  in gas and liquid process streams has been measured at the Karlsruhe reprocessing plant (WAK) [252] and predicted for the British Nuclear Fuel Processing Plant (BNFP) [253]. These evaluations indicate that about 94 to 99% of the  $^{129}\text{I}$  reports to the DOG, and the remaining is distributed among the high-, medium-, and low-level aqueous waste. While the primary recovery technology is applied to the DOG, the VOG may also require treatment to recover  $^{129}\text{I}$  arising from other processing steps and vessels.

Various types of adsorbents for iodine have been studied and developed over the years. Natural or artificial porous materials such as zeolite, mordenite, alumina, and silica gels have been loaded with metals (e.g., silver, cadmium, and lead) and/or the metal nitrate ( $\text{AgNO}_3$ ) and used in performance studies. Commercially available inorganic sorbent materials include silver-exchanged zeolites (i.e., faujasite, AgX, and mordenite, AgZ) and silver-impregnated silicic acid (AC-6120).

Caustic scrubbing for  $^{129}\text{I}$  recovery has been applied at fuel reprocessing plants in the United Kingdom (at Windscale and the Thermal Oxide Reprocessing Plant [Thorp] at Sellafield), in France (units UP1 and UP2 at La Hague), and in Japan (Power Reactor and Nuclear Fuel Development Corp [PNC] Tokai Reprocessing Plant) [253, 254]. The IODOX (IODine Oxidation) technology was developed for application to liquid metal fast breeder reactor (LMFBR) fuel reprocessing where the used fuel would have been processed

within 180 days of leaving the reactor and would have required high DFs to control  $^{131}\text{I}$  releases ( $>10^4$ ). The Mercurex process was also developed for the treatment of the DOG that evolved during the processing of very short cooled fuels where very high DFs are required ( $>10^5$ ).

### Krypton

Most of the  $^{85}\text{Kr}$  ( $>99\%$ ) remains in the used fuel until it is sheared and dissolved. The  $^{85}\text{Kr}$  is released primarily to the DOG in the range of hundreds of parts per million. Recovery processes are based on physical separation from the off-gas since krypton is chemically inert. The primary technologies for  $^{85}\text{Kr}$  control are cryogenic distillation, fluorocarbon adsorption, and sorption on molecular sieves or charcoal. Xenon is also recovered by these processes. The xenon is present at about 10 times the concentration of krypton in the gas stream.

Cryogenic distillation, a technology to recover rare gases, has been used commercially for many years. The cryogenic distillation process has been successfully used at the Idaho Chemical Processing Plant to recover krypton. Fluorocarbon absorption technology was developed at the Oak Ridge Gaseous Diffusion Plant and at the reprocessing plant located at Karlsruhe, Germany [255-258] [20-23]. This process uses an organic solvent ( $\text{CCl}_2\text{F}_2$ , aka Freon-12 and R-12) to selectively absorb noble gases from air or DOG streams; the noble gases are then stripped from the solvent by boiling.

Both activated carbon and zeolites have been studied for their potential to recover krypton from the DOG stream. One possible system uses a bed of synthetic silver mordenite (AgZ) at ambient temperatures to recover xenon. The "xenon-free" gas is then chilled and passed onto a second hydrogen mordenite (HZ) bed operated at about  $-80^\circ\text{C}$  that absorbs the krypton. Laboratory tests have shown DFs of 400 for krypton and 4000 for xenon [259].

### Carbon-14

The bulk of the  $^{14}\text{C}$  found in the irradiated nuclear fuel is assumed to be evolved as  $\text{CO}_2$  into the DOG during fuel dissolution. If standard voloxidation is used, then approximately 50% of the  $^{14}\text{C}$  will be released in the voloxidizer. A number of technologies have been developed for  $\text{CO}_2$  removal. These include caustic scrubbing, molecular sieve adsorption, adsorbent bed fixation, and co-absorption/concentration in conjunction with  $^{85}\text{Kr}$  recovery followed by fixation.

#### **10.2.4. Recovery of Semivolatile Components and Particulates**

The head-end portion of the fuel reprocessing plant and the waste processing portion presents additional challenges in terms of the composition of the off-gas streams to be treated. In addition to the gaseous species already discussed, a number of "semivolatile" species are released to the off-gas stream. These include oxides of ruthenium, cesium, technetium, tellurium, and antimony. Of these, the most studied are ruthenium and cesium, which also typically require the highest recovery factors. The amount released is highly dependent on the processing conditions. For example, under normal voloxidation conditions, only very limited fractions of krypton, and iodine are released. Work in the United States and Korea has recently shown that, under high temperatures and O<sub>2</sub> or O<sub>3</sub> oxidizing conditions, virtually all of the <sup>3</sup>H, <sup>14</sup>C, <sup>85</sup>Kr, <sup>129</sup>I, <sup>99</sup>Tc, ruthenium, and cesium are released to the off-gas and significant fractions of the tellurium, rhodium, and molybdenum are also volatilized.

In addition, the head-end processes may result in the production of very fine particulates that must also be removed prior to the release of the gas stream to the facility stack. Particulate filtration is for the most part a well-established technology [260, 261].

#### **10.2.5. Recovery and Recycle of Zirconium from Cladding**

An objective of current research is to determine the feasibility of recovery and recycle of zirconium from light water reactor (LWR) used fuel cladding wastes. Zircaloy cladding, which contains 98+% of hafnium-free zirconium, is the second largest mass, on average ~25 wt % of the components in LWR used fuel assemblies [241]. Recovery and recycle of the zirconium would enable a large reduction in geologic waste disposal for advanced fuel cycles. Current practice is to compact [262] or grout the cladding waste and store it for subsequent disposal in a geologic repository.

LWR Zircaloy cladding contains zirconium with natural abundance isotopic composition, and the used fuel cladding contains one radioactive isotope, <sup>93</sup>Zr, formed by neutron capture on natural <sup>92</sup>Zr during irradiation. The recycled zirconium would be radioactive. However, <sup>93</sup>Zr has a low specific activity (half-life is 1.5 million years) and only a weak beta emission, which means that the recycled zirconium would have low radioactivity if it can be decontaminated from other fission and activation product elements.

The zirconium recovery process would be integrated into the advanced fuel cycle head-end process steps for treatment of used fuel assemblies. **Figure 115** illustrates three options where the cladding may be processed to recover the zirconium: (1) following dissolution of the fuel and rinsing of the cladding to remove fuel bearing-solution, (2) following the voloxidation process, where the fuel components are present in the form of finely divided powder that can be separated easily by screening from the empty, sheared cladding hulls, or (3) substituting for shearing where the cladding is removed chemically to volatilize the zirconium [263].

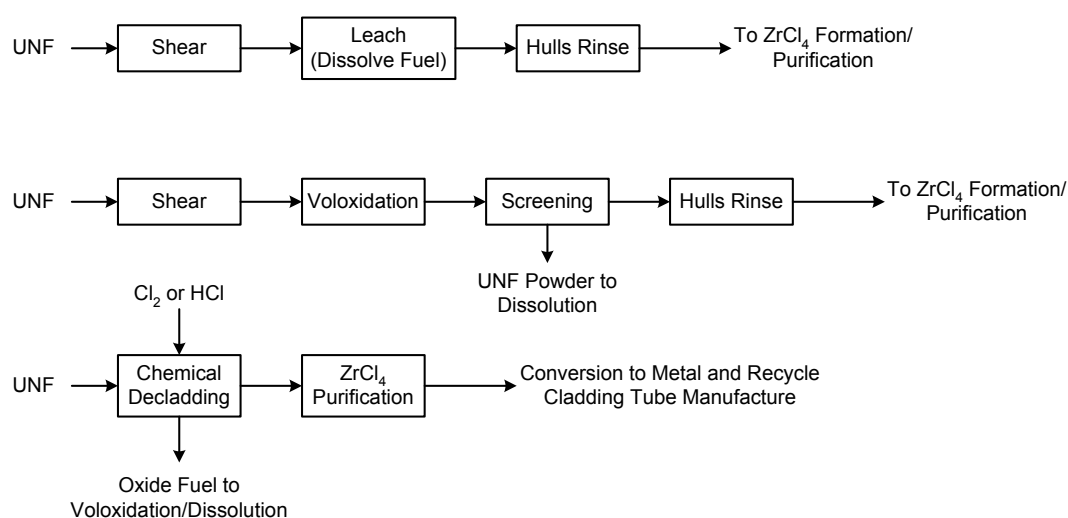


**Figure 115: Typical head-end operations where zirconium recovery may be integrated.**

Recent tests with actual used fuel rods (**Table 21**) have shown that most of the residual fuel powder remaining on the cladding hulls after screening can be removed by hull washing with nitric acid. The washed hulls would nonetheless contain residual contamination sufficient to prevent disposal of the clad as low-level waste. The residual contamination would be removed during the zirconium recovery process along with the alloying constituents and returned to the UNF reprocessing plant for disposal together with other radioactive wastes.

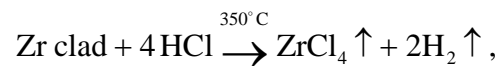
**Table 21: Residual Contamination after UNF Clad Washing.**

Element	Removed by cladding wash (wt % of UNF)	Remaining in washed clad (wt % of UNF)	Reduction factor	Residual clad contamination (ppm)
U	0.6	0.0037	162	100
Pu	0.3	0.013	23	6
Am	0.2	0.013	15	0.6

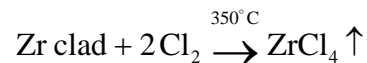
A process step for clad shredding may be needed to increase the surface area and thereby the efficiency of the zirconium recovery step. Previous tests have shown that approximately half of the tritium remains within the cladding hulls [264]. Therefore, removal and capture of residual tritium should be included in any future radioactive process development studies.

Zirconium in the cladding may be converted to volatile  $ZrCl_4$  by reaction with either hydrogen chloride or chlorine. The volatile product can be purified by an additional step of condensation and sublimation. Purified  $ZrCl_4$  may be fed to the metal sponge conversion step of the industrial zirconium metal manufacturing process (**Figure 116**).

An issue for an industrial application of the hydrochlorination process in a radiochemical operation may be the hydrogen generated in the off-gas by the reaction



whereas hydrogen is not generated by reaction with chlorine



Both methods of chlorination are still being considered, and a two-step recovery/purification may provide the best results. Nonvolatile residues, including radioactive contamination, would be returned to the fuel reprocessing plant for disposal with other radioactive wastes.

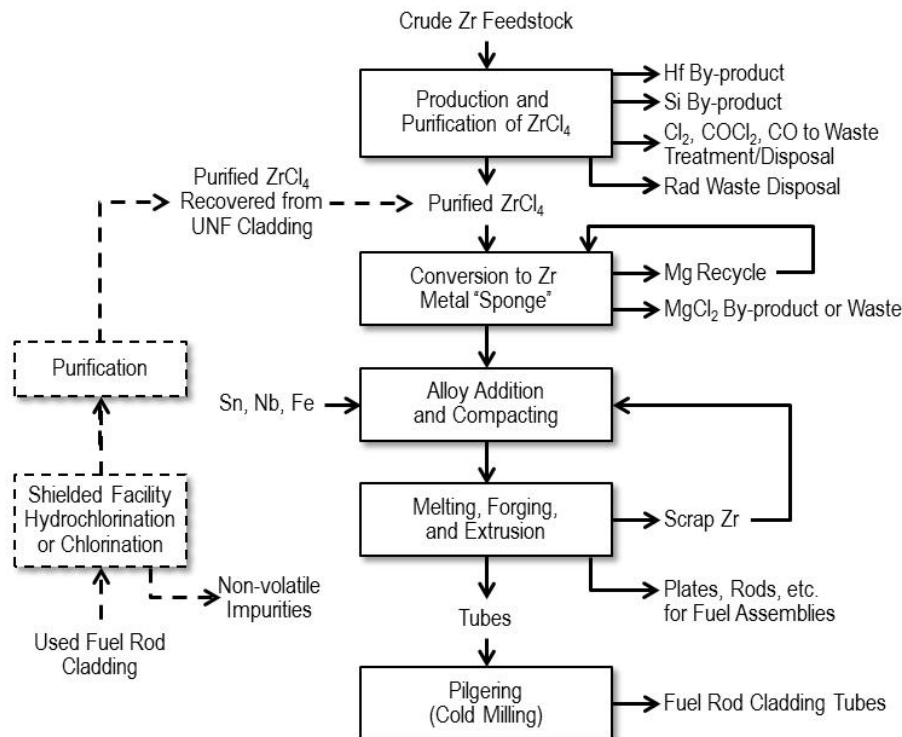


**Figure 116: Interfacing zirconium recovery from cladding with tubing manufacture.**

### 10.2.6. Summary

The discussion of progress in advancements for head-end processing of UNF can apply to any downstream fuel component separations steps that may be selected. In comparison with current industrial-scale operations, research, development, and demonstration studies have shown progress in improving the capabilities for dry volatile component release and emissions control by means of the advancements made in the voloxidation process and associated off-gas trapping methods, as well as in the conversion of the ceramic oxide fuel components to a finely divided oxide powder that is amenable to continuous dissolution in either nitric acid or molten salt. Moreover, systems studies have shown the potential benefits of recycling more of the used fuel components, including uranium, all transuranium elements, zirconium from Zircaloy fuel cladding, and several of the valuable fission product components [241].

### 10.3. Head-end design challenges for minor actinide containing advanced fuels

A chapter written for a book summarising the EU FPVII Farfuels project. This chapter is intended to be one of the introduction chapters to provide a background to the potential future requirements and issues for head-end and provide a background to nuclear fuels and reactor researches. Book edited by Christain Eskberg and Jannes Wallenuis, to be published by Leadcold books and games.

#### 10.3.1. Introduction

Head-end is the first chemical treatment step in the recycle of spent nuclear fuel. Head-end receives decay cooled spent fuel and converts it into an aqueous feed that is conditioned to make it acceptable to the solvent extraction actinide purification process. Upon receipt of the decay cooled fuel it is treated to make it accessible for dissolution whilst allowing segregation of the cladding materials for recycle or disposal. This part of the process often requires heavy engineering steps. In addition, as one of the key steps is the dissolution of the fuel in nitric acid, volatile or insoluble elements must be controlled to minimise their impact on operations and the environment. These steps are summarised in Figure 117 [1].

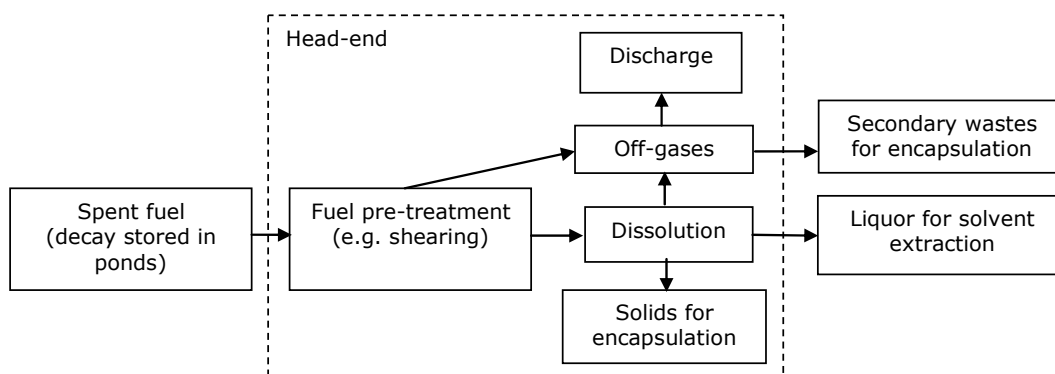


Figure 117: Head-end's position in a reprocessing plant

Another important factor to consider when designing nuclear fuel cycles with alternative fuel types is their compatibility with existing head-end treatment steps otherwise new treatment steps must be developed. Although this means

that alternative fuel types can have a large impact on the head-end process steps they should not greatly affect the later solvent extraction process steps [71].

The nuclear industry is also highly regulated; there are numerous local, national and international regulatory and lobbying groups. The design of future nuclear fuel cycles must take these groups views into account. The decision making processes that shape the requirements for the next generation of nuclear reactors and recycle facilities may place constraints that greatly influence the necessary head-end steps. Some of the possible future requirements and their influence upon head-end will be highlighted in the following chapter.

### ***10.3.2. Potential future minor actinide containing advanced fuels***

There are a large variety of future advanced fuels, which include the Generation IV fuel concepts. These are summarised below in Table 22:

**Table 22: Generation IV Reactor fuels, matrix and cladding description[265]**

Reactor	Fuel				Cladding	Spectrum, Outlet temperature (°C)	Recycle Method			
	Oxide	Metal	Nitride	Carbide			Fuel description	Aqueous process	Pyrochemical process	Once-through
Gas cooled fast reactor (GFR)			Secondary	Primary	Mixed actinide carbide and silicon carbide	Ceramic	Fast 850	Primary	Primary	Not considered
Sodium cooled fast reactor (SFR)		Primary			Mixed U, Pu, Zr alloy	Steel	Fast 520	Primary	Primary	Not considered
	Primary				Mixed actinide oxide	ODS	Fast 550			
Lead cooled fast reactor (LFR)		Secondary	Primary		Mixed actinide nitride	Steel, Ceramic or refractory alloy	Fast 550, and fast 800	Primary		Not considered
Super critical water reactor (SCWR)	Primary				Uranium oxide	Steel	Fast 550	Primary		Secondary
					Mixed actinide oxide	Steel	Thermal 550			
Very high temperature reactor (VHTR)	Primary				TRISO U(OC) in Graphite Compacts; ZrC coating	ZrC coating and surrounding graphite	Thermal 1000	Secondary	Secondary	Primary

### ***10.3.3. Fuel conditioning and pre-treatment steps***

The aim of fuel conditioning is to convert the spent fuel into a form that can be leached whilst allowing:

- the abatement of the key radionuclides and elements within head-end
  - the dissolver product to meet the requirements for solvent extraction
- Separation of the cladding or inert matrix from the fuel matrix can be carried out in this part of the process.[266]

#### ***10.3.3.1. Current practices***

There are several common methods employed for separating the fuel and cladding. Early metals fuels used aluminium or magnesium alloy cladding, which was removed by selective dissolution or mechanical decladding prior to dissolution. Fast and thermal reactor oxides fuel rods or assemblies tend to be cut into short lengths, the fuel leached from the cladding pieces and then the hulls are separated from the dissolver liquor.

The chemical decladding of magnesium or aluminium alloys has been carried out using dilute nitric acid and sodium hydroxide solutions respectively. These processes lead to an aqueous product that has large concentrations of metal salts with small quantities of fission products and actinides. This stream must be dewatered and immobilised or decontaminated and discharged to sea. The alternative approach used for magnesium alloy cladding is to mechanically remove the cladding. This has been achieved either by ramming the fuel rod through a die to produce a cladding puck and bare metal fuel rod or peeling the cladding away from the fuel rod using a cutting method.

Oxide fuels from thermal and fast reactors are conventionally cut into short lengths using a hydraulic shear. Shearing has been carried out upon single fast reactor pins and in small reprocessing facilities. Whilst larger reprocessing plants shear the entire fuel assembly. The sheared hulls then fall via a chute into the dissolver where dissolution can occur. Smaller, lower throughput reprocessing plants have also sheared fuel into a transfer container, which is then transferred into the dissolver. Dissolvers where fuel is leached from cladding use a basket to facilitate removal of the hulls from the dissolver product after dissolution is complete.

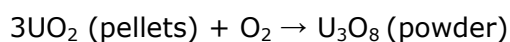
### ***10.3.3.2. Issues and areas for development for fuel pre-treatment***

Depending upon the fuel type and aims of the reprocessing plant there are several issues that may affect the fuel pre-treatment step:

- Size and cost; head-end is a highly active (HA) plant so size greatly affects building and maintenance costs. For these reasons a drive to reduce the size and requirement for maintenance is desirable.
- Dismantling or decladding to expose the fuel matrix; a key step prior to dissolution is the treatment of the spent fuel assembly into a form that can be added to the dissolver, e.g. shear for conventional oxide fuel assemblies. How to condition some of the advanced fuel types, such as CerCers for the GCFR or Triso for VHTR, is a challenge.
- Recovery of tritium, other (semi-) volatile radionuclides [266] or valuable elements (e.g. nitrogen-15) [91]; if fuel is directly dissolved in nitric acid it is not possible to control and efficiently recover tritium or nitrogen-15 so a chemical pre-treatment will be necessary. This chemical pre-treatment step could also be designed to remove other semi-volatile radionuclides, e.g. carbon-14, iodine-129,131 or the noble gases. The off-gases from a pre-treatment process would have higher concentrations of fission products, which simplify the design and efficiency of abatement processes.
- Conversion of advanced fuel materials; advanced fuels may not be soluble in the dissolution step, may be encased in a refractory matrix or may produce solids or soluble species that make conditioning problematic. In these cases conversion of the fuel into another chemical or physical form maybe necessary.

A relative small fraction of the total triium is released into the dissolver off-gases while the remainder is in the dissolver solution. For zircaloy clad fuel up to 60 % of the tritium can be present in the cladding[267]. Any tritium that is not-present in cladding is distributed throughout the reprocessing plant and ultimately discharged into the environment. A high temperature pre-treatment (Voloxidation) technology has been developed to address this issue [150]. This process pulverises the fuel, Eq 66, and a high proportion of the tritium can be driven into the off-gas system where efficient abatement is possible. The fuel powder and fuel cladding hulls can be separated, Figure 118. High-temperature pre-treatment processes are also capable of removing smaller proportions of carbon-14, iodine and the noble gases into the off-gas stream where abatement can be carried out. A disadvantage of this process is

that highly radiotoxic semi-volatile radionuclides, such as caesium and ruthenium, can also be driven into the off-gas system. Work continues on this technology to maximise the removal of the volatile radionuclides but minimising the evolution of the highly radiotoxic semi-volatiles, this could achieve the added benefit of reducing the demands upon the dissolver off-gas treatment system.



Eq  
66

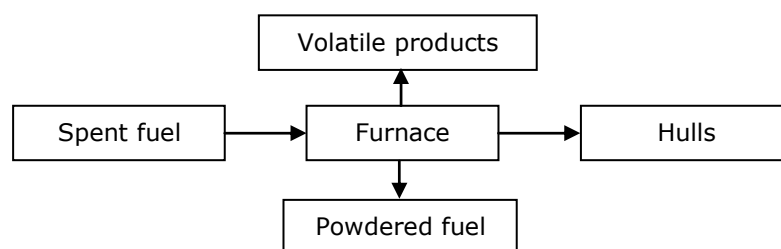


**Figure 118: Systematic diagram of a high-temperature pre-treatment process**

Similar technology could also be used to oxidise carbides or nitride based-fuels and fuels containing Triso particles. This has the added benefits of:

- Carbides – reducing the potential for the formation of organic compounds, which may be detrimental to the chemical separation process, during dissolution.
- Nitrides – allows the possibility for efficient evolution of nitrogen-15 for recovery and reuse.
- Triso – oxidation of the carbon surrounding the Triso spheres has been considered to aid recovery of the fuel.

An alternative fuel conditioning step for Triso based fuels is to grind the fuel prior to leaching, Figure 119 [1]. Current thinking is that the grinding option is the favoured option over oxidation, as oxidation will lead to large quantities of secondary wastes produced from capture of carbon-14.

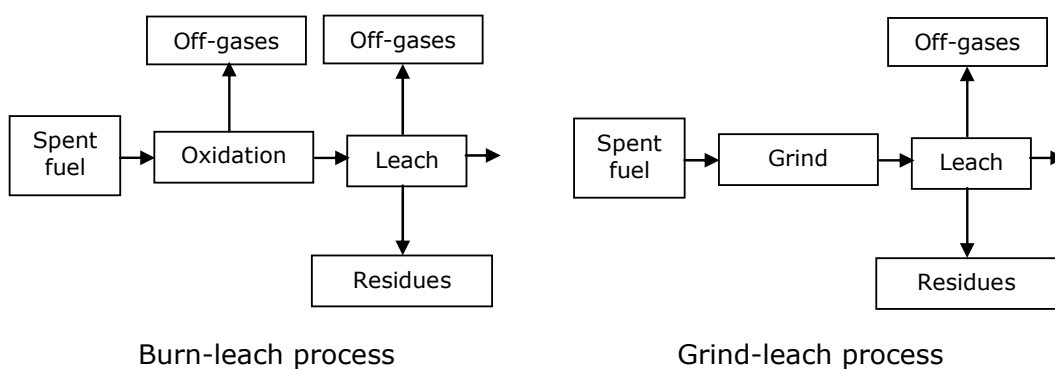


**Figure 119: Flowcharts for Triso head-end processes [1]**

Preconditioning of other fuel types such as refractory alloys, CerMets or CerCers could also be an option to allow dissolution of the fuel or leaching of the fuel from crushed or powdered materials. The details of such schemes have not been published to date.

#### **10.3.4. Dissolution**

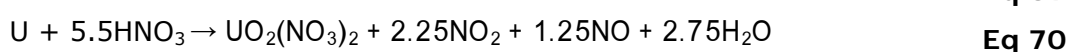
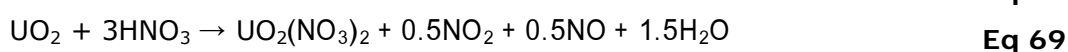
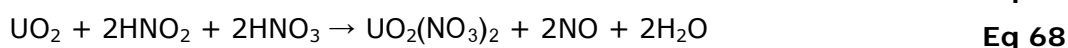
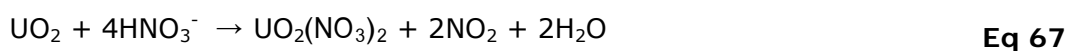
The aim of the dissolver cycle is to dissolve the fuel with a suitably high actinide recovery. Any large cladding components added to the dissolver must also be removed in this step.

##### **10.3.4.1. Current practices**

A key part of the dissolver cycle design is whether to employ batch or continuous dissolvers and where fuel cladding is added and how to remove it. Currently continuous dissolvers are used for the dissolution of declad uranium metal rods while batch or continuous dissolvers are used for the dissolution of sheared oxide fuel. The oxide fuel dissolvers are fitted with a basket to allow removal of the leached hulls. Dissolvers must also be designed to be criticality safe, so dissolvers for fast reactor fuels tend to be smaller, or small quantities of fast reactor fuels are dissolved with larger quantities of thermal reactor fuels.

The dissolution of spent metal [36] and oxide fuels [74, 152] is conventionally carried out in heated nitric acid, as this is the preferred media for solvent extraction processes. Dissolution occurs through a number of reaction steps involving nitric acid and its reduction products. This means that a variable amount of nitric acid can be consumed. This is illustrated with Eq 67-Eq 69 for

oxide fuel [152] and Eq 70 metal fuel. Technologies have also been developed to minimise the amount of nitric acid required during dissolution, this is achieved by conversion of the nitrogen oxides back into nitric acid, resulting in a 'fumeless dissolution', Eq 71 [37]. If a high temperature pre-treatment process is used prior to dissolution higher uranium oxides, such as U<sub>3</sub>O<sub>8</sub> or UO<sub>3</sub>, are produced. As these materials will be finely divided, dissolution will be carried out under mild conditions to allow control.



During the dissolution of uranium oxides slow dissolving or insoluble particulates remain and secondary precipitates can also form. An example of undissolved particulates that remain during dissolution of oxide fuel are the slow dissolving 'insoluble' fission product (IFPs) alloys containing technetium, molybdenum, ruthenium, rhenium and palladium[1]. These IFPs originate from the metal alloy inclusions formed during irradiation. Another common dissolver solid for higher burn-up fuels is zirconium molybdate, this forms at higher temperatures such as those in the dissolver[57]. Minimising the effect that these solids can have can influence the design of a dissolver cycle.

During the dissolution of oxide fuel there are small losses of fuel with the hulls and off-gases. When mixed uranium plutonium oxide (MOx) fuels are dissolved incomplete dissolution, due to plutonium rich regions, also has the potential to allow actinides to be route to the waste streams. These losses are typically 0.05-0.5 % for thermal or fast reactor MOx, although the actual amount depends upon the manufacturing method, irradiation history and dissolution conditions. The presence of plutonium rich particles represents a potential criticality hazard if they were allowed to accumulate in a small area, so these particulates must be closely controlled within head-end and prevented from entering the chemical separation plant.

#### ***10.3.4.2. Issues and areas for development for dissolution***

Issues that may face the dissolution step in the future are largely associated with fuel type. Examples are:

- The fuel material does not dissolve or only partially dissolves in nitric acid, e.g. plutonium rich oxides, refractory alloys metals or ceramics.
- The presence of high concentrations of fission products or metals used in the fuel alloying cause precipitation of secondary solids, e.g. processing of molybdenum alloys.

Issues relating to slow dissolution rates, poor solubility or presence of organics may make the application of enhanced dissolution technologies necessary. These methods would ideally not add a large concentration of metal ions to the dissolver product, as these will increase the amount of high level waste produced. An example method that may be considered is electrochemical mediated oxidation. These processes use a metal ion with a higher oxidation potential than nitric acid, for example cerium(IV) or silver(II). These ions are produced electrochemically and used as a catalyst, thereby minimising the burden upon high level waste. As plutonium dioxide does not dissolve in nitric acid, silver(II) can be used to mediate the dissolution Eq 72-Eq 73. Similar types of processes may be applicable to plutonium rich residues from high plutonium content MOx fuels that do not dissolve readily in nitric acid [53, 71].



Alternative dissolution media could also be considered in the future, such as other mineral acids. The use of alternative mineral acids has been considered in the past but issues such as corrosion, reduced solvent-extraction performance and increased high level waste production has not led to wide spread use.

The dissolution of metal alloy fuels such as molybdenum or electrochemical dissolution of zirconium alloy fuel can lead to the formation of secondary solids such as oxides that can contain a significant actinide content [95, 268]. The formation of large quantities of solids in the dissolver may lead to difficulties in their removal. The risk due to these solids may be high if they contain actinides as they may present a criticality hazard. If any of the future fuels do produce secondary solids or leave residues then strategies to minimise their formation and reduce their impact must be developed.

### **10.3.5. Dissolver solution conditioning**

After dissolution is complete the dissolver product may not be in an ideal form for a solvent extraction process, so it is necessary to treat the liquor to improve the quality. It is current practice to:

- Remove iodine to minimise discharges from downstream process steps and minimise iodine accumulation in the solvent.
- Condition the plutonium(VI) to plutonium(IV) for optimal extraction in current solvent extraction processes.
- Remove suspended solids, e.g. IFPs, to minimise the accumulation in downstream process steps and minimise the formation of solvent extraction cruds.

Other examples are:

- Recover cladding or alloying materials that are for recycle or for diversion to a separate waste route.
- Destroy organic species, e.g. from actinide carbide dissolution[125] or leaching graphite-based fuels[269], to minimise impact on the solvent extraction process.

#### **10.3.5.1. Current practices**

Current head-end reprocessing plants carry out three key conditioning steps, removal of iodine, plutonium oxidation state conditioning and solids removal.

Depending on the type of dissolver used different methods for removal of iodine and plutonium oxidation state adjustment are used. For batch dissolvers it is usual after dissolution is complete and while the liquor is in the dissolver to use an air sparge to remove iodine and then a nitrogen oxide sparge to condition the plutonium. Continuous dissolvers do not need plutonium oxidation state adjustment due to the differences in the nitric acid chemistry within the dissolver. Efficient iodine removal from continuous dissolvers is not possible and so a separate iodine removal step is needed. This can be achieved by passing the dissolver liquor through a bubbler column counter current to the bubble stream.

Early reprocessing plants did not include a step to remove fine suspended solids, however, more modern oxide reprocessing plants use a centrifuge and then send the centrifuge cake for encapsulation.

#### ***10.3.5.2. Issues and areas for development for dissolver product conditioning***

It is expected that the removal of iodine and oxidation state conditioning will continue to be required in the future. Further developments may also be necessary.

As burn-up is expected to increase for future fuels there is expected to be an increase in primary and secondary dissolver solids. In addition, if the fuels are short cooled, then the solids may be more radioactive and have a higher heat output. Also, if the fuels do not completely dissolve then the solids may also contain a fissile component and as the fuels are expected to have a high plutonium and/or minor actinide content, the solids also pose a radiation and criticality hazard. These factors combined with the increased rigour required for safety cases will place an increased demand on the control to minimise the potential of the accumulation of solids.

If cladding materials or fuel alloy materials are dissolved as part of the head-end step a process may be required to recover these materials for re-use.

The dissolution of carbide fuel or fuel leached from graphite may lead to a dissolver product containing dissolved organics that interfere with the solvent extraction process. A step to destroy the organics will therefore be necessary. There are many potential methods for organics destruction but electrochemical mediated catalytic oxidation is considered most favourable, as it has been demonstrated for fast reactor fuels [125]. This process could also be considered for dissolution of difficult to dissolve fuels and the process could be deployed in-dissolver or as a separate step either after dissolution or clarification.

#### ***10.3.6. Off-gas treatment***

Off-gas treatment processes aim to decontaminate gaseous effluent streams from pre-treatment, dissolution, conditioning processes and cave ventilation to a suitably high degree to allow discharge into the environment. These streams can contain both chemical and radioactive species including solids (dusts), gases and liquids (vapours or aerosols). The overall aims of the reprocessing plant will be defined at the design stage and these will dictate what and to what degree these chemical and radioactive species are abated.

#### ***10.3.6.1. Current practices***

Current practices aim to minimise aerial discharge of tritium (hydrogen-3), carbon-14, iodine-129 and particulates by using sodium hydroxide scrubbers and high-efficiency particulate (HEPA) filtration. The need for iodine-131 abatement is avoided by decay storing the fuel. The sodium hydroxide scrubbers allow abatement of tritiated water, carbon-14 (present as carbon dioxide) as a carbonate and iodine-129. Chemical precipitation methods can be used to decontaminate these scrubber solutions and a range of methods have been developed depending on the decontamination factor required. It is common practice to abate carbon-14 by precipitation as a metal carbonate. However, different nations have different views on the best environmental method for iodine-129 control. Iodine-129 can be concentrated and immobilised or disposed of by infinite dispersion in the sea. The long half-life ( $1.6 \times 10^7$  years), low radiotoxicity ( $\beta_{\text{MAX}} = 154$  keV) and potential mobility in deep geological disposal facilities post-closure can make this a complicated decision. However, technology to abate iodine-129, such as silver-impregnated zeolites, has been deployed on some sites. Due to its much higher radiotoxicity high efficiency iodine-131 abatement techniques have been used for the reprocessing of short-cooled fast-reactor fuels using chemical precipitation methods. After these radionuclides have been abated the compounds are incorporated into a waste form with a suitable longevity. An example of this is the precipitation of carbon-14 as barium carbonate followed by incorporation into a cement waste form.

Currently the abatement technologies deployed do not abate the noble gaseous, (e.g. krypton-85). The relatively short half life (10.7 years) and inert chemical nature result in a low radiotoxicity and minimal local or global impact. A tall factory chimney allows efficient dispersion to minimise the local impact.

#### ***10.3.6.2. Issues and areas for development for off-gas treatment***

The decision whether or not to abate a particular radionuclide and to what efficiency is complicated and based on highly political socio-economic studies. The amount, concentration and chemical form can also vary greatly depending upon the process type and, notably, the amount of radioactive species will increase with burn-up. The consequences of the decision to abate the various major radionuclides include:

- Iodine-129,131 – can be achieved with current technologies but there is uncertainty over what is a suitable waste form. If short-cooled fuels are reprocessed then a highly efficiency process will be necessary.
- Carbon-14 – can be achieved with current technologies. However, future fuels such as carbides or nitride (containing nitrogen-14) will greatly increase the quantities and concentration of carbon-14, Table 23. This will mean a large improvement in the decontamination factors will be needed to prevent increases in discharges. This may mean that new technologies are required.
- Noble gases are currently not abated as there is not an efficient method to provide a passively safe waste form for storage.
- Tritium cannot be abated if direct dissolution is carried out but abatement is possible if a pre-treatment process is used.
- Nitrogen-15 is a valuable isotope that could be used for production of nitride fuels and may necessitate recovery for reuse. As nitrogen-15 cannot be recovered if the fuel is dissolved directly in nitric acid[91], then a pre-treatment step will be required.

**Table 23: Carbon-14 contents of different fuel types [71]**

Fuel type	Fuel <sup>14</sup> N content (%)	<sup>14</sup> C (GBq.tHM <sup>-1</sup> @ 30 GWdt)
Oxide	0.02	4.8
Carbide	1.7	273
Nitride	99.6	15630
Nitride	1	156

### **10.3.7. Summary**

Head-end is the first chemical treatment step in the reprocessing of spent nuclear fuel. The fundamental step in head-end is the dissolution of spent fuel but other process steps are needed to achieve the process aims. This makes the build of head-end into a complicated and expensive part of the reprocessing plant. The current major steps are summarised in Figure 120.

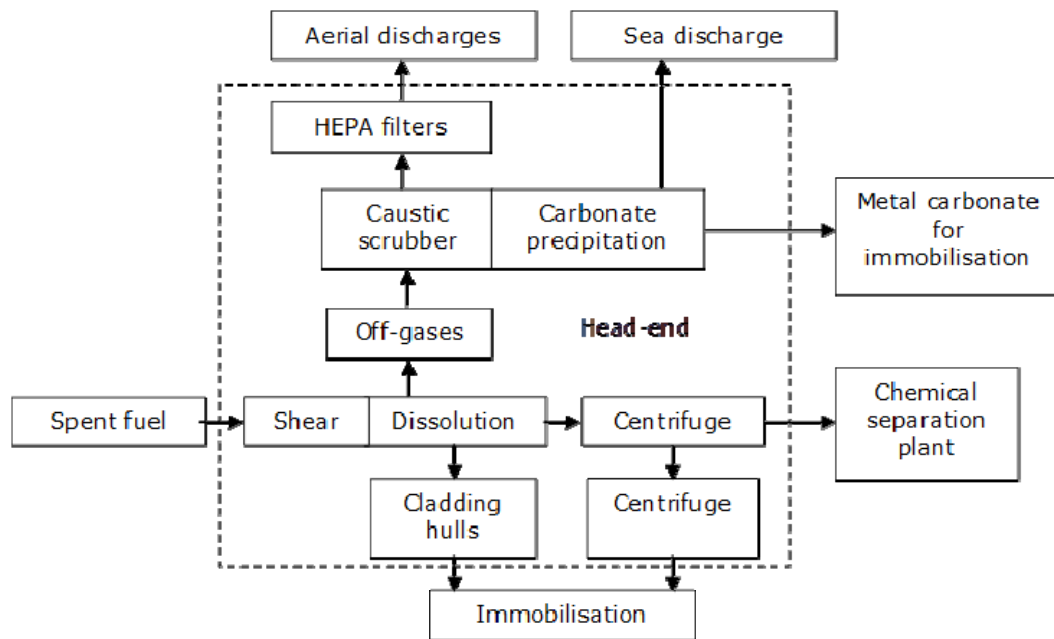


**Figure 120: Outline of steps involved in current head-end plant**

As head-end receives spent fuel, changes in the fuel type and construction affect head-end to the largest extent. Future fuels may require the addition of extra stages that may include:

- Fuel pre-treatment or conditioning to overcome chemical or radionuclide abatement issues.
- Enhanced dissolution and conditioning to aid dissolution, achieve the desired fuel recovery efficiencies or destroy organic contaminants.
- Off-gas treatment to meet the future demands for discharges into the environment, this may include iodine, tritium and the noble gases.

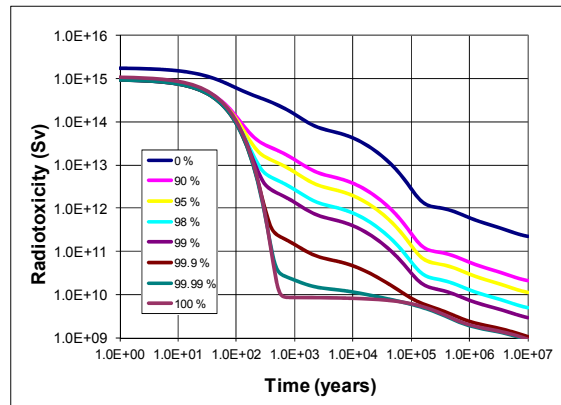
#### **10.4. The chemistry of (U,Pu)O<sub>2</sub> dissolution in nitric acid**

The following summarises a presentation at Atalanta 2012, Montpellier, France and is published as [44]

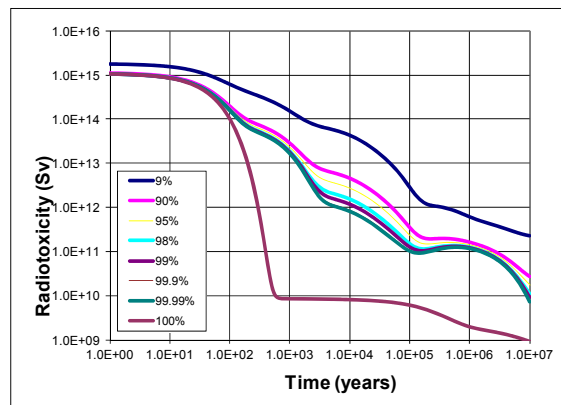
##### **10.4.1. Introduction**

The head-end of a reprocessing plant is the first step to the reprocessing of spent nuclear fuel and has two key steps, shearing and dissolution. The shearing helps to determine how the nitric acid can access the fuel and the degree of pulverization. The sheared fuel is dissolved in nitric acid followed by conditioning prior to the chemical separation process, which purifies the actinides of interest. As fuel is converted from the solid fuel matrix into solution form, any undissolved fuel is lost from the nuclear fuel cycle, increasing the long term radioactivity and radiotoxicity of the reprocessing wastes. Both the shearing and dissolution process steps are important in terms of minimizing fuel losses in head-end. Improvements in the understanding of MOx dissolution chemistry with optimization of the shearing step will allow the maximum recovery of fuel. The focus of this paper is to summarize the chemistry of MOx dissolution.

Figure 1 shows calculated waste radiotoxicity for various percentage recoveries of U, Pu and U, Np, Pu, Am, Cm compared with spent fuel (0 % recovery) and fission products (FP). The graphs clearly show that to maximize the benefits of future reprocessing schemes, where the minor actinides are recycled, high recoveries become increasingly important.



a



b

**Figure 1. Effect upon radiotoxicity of waste per tonne spent  $UO_2$  for various recoveries of a) U, Pu and b) U, Np, Pu, Am, Cm**

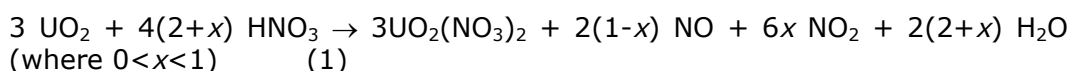
As part of the EU FPVII ACSEPT project, the UK National Nuclear Laboratory (NNL) has undertaken chemical studies in the area of head-end chemistry. These studies are relevant to the design of head-end processes for UK legacy non-standard fuels, support to current operations and future fuels. These studies have focused on:

- conceptual studies considering reprocessing of a variety of fuel types,
- practical studies investigating mixed uranium plutonium oxide dissolution in nitric acid
- practical studies investigating the dissolution of plutonium dioxide (simulated plutonium rich MOx residues) in the presence and absence of simulated insoluble fission products.

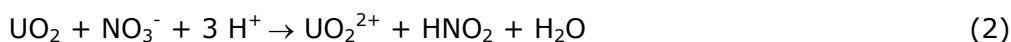
#### **10.4.2. Background chemistry**

Uranium dioxide ( $UO_2$ ) and mixed uranium plutonium dioxide ( $MOx$ ,  $(U,Pu)O_2$ ) are important reactor fuels. During the reprocessing of these materials they are dissolved in nitric acid to produce a dissolver product containing typically

ca. 3 mol.l<sup>-1</sup> nitric acid and 1.0-1.3 mol.l<sup>-1</sup> uranium and plutonium. This product must be suitable for the solvent extraction chemical separation process. The dissolution, is typically carried out at elevated temperature, 70-110 °C, to allow dissolution on a short timescale. During dissolution the uranium is oxidised to uranyl and nitrogen oxides (Equation 1 below) where *x* depends on the nitric acid concentration[19]. Depending upon the dissolver conditions the plutonium can be present in the tetravalent state or the hexavalent state.

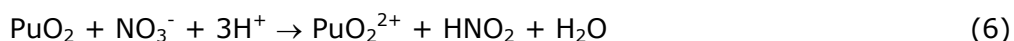
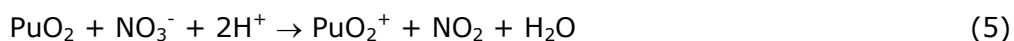


During dissolution isotopic labelling studies have shown that the oxidation of the uranium dioxide is carried out as a solid state reaction[52, 151]. The surface oxidation and dissolution process proceeds via an autocatalytic mechanism; that is, after a slow induction period dissolution occurs more rapidly. Early studies correlated the increase in dissolution rate with temperature and nitric acid concentration in an attempt to interpret and model the mechanism [34, 45, 46, 74]. Due to the autocatalytic nature of the dissolution reaction the dissolution models often had gaps. A careful set of experiments studying the effect of nitric and nitrous acid (a nitric acid reduction product) showed that dissolution is dependent upon nitric and nitrous acid concentrations [49, 152]. Also, under typical dissolver conditions the nitrous acid oxidation step is much more rapid than that with nitric acid, thus providing evidence that explains the induction periods (Equation 2) and more rapid autocatalytic mechanism (Equation 3). The significance of nitrous acid in the rapid reactions and slower nitric acid reactions is supported by fundamental studies of nitric acid, *e.g.* [22], and the dissolution of other materials, *e.g.* copper metal [26].



Unlike uranium dioxide, plutonium dioxide does not dissolve in nitric acid to an appreciable degree [52, 160]. Thermodynamic calculations have shown that the dissolution of plutonium dioxide either by reaction with acid (Equation 4) or by oxidation (Equations 5 and 6) are thermodynamically unfavourable [52]. Despite this, in MOx fuel, when the microscopic plutonium concentration is a small fraction of the uranium, the plutonium does dissolve in nitric acid

[53]. The decrease in the extent of MOx dissolution for increasing plutonium content is clearly shown in Figure 2 [53]. A sharp decrease in the extent of dissolution is observed for >35% Pu (as calculated according to  $[Pu]/([U]+[Pu])$ ) and little dissolution is observed for > 55–65 %Pu.



It was suggested [53] that the reduction in the extent of dissolution of MOx is due to the plutonium solubility saturation being reached. However, an alternative explanation is that at higher plutonium contents one of the reactions becomes thermodynamically unfavourable. Thermodynamic calculations in this work have shown that the nitrous acid reaction becomes unfavourable at *ca.* 40 %Pu. Although this result does not provide proof, it does provide an explanation based on both thermodynamics and kinetics.

Current commercial MOx manufacturing processes are based on the mechanical blending of separate pure uranium and plutonium dioxides, followed by pressing and sintering into pellets. As the starting materials are pure uranium and plutonium dioxides, the final products are not homogeneous on an atomic scale but have microscopic heterogeneities. Based on Figure 2, any plutonium rich regions will result in undissolved residues.

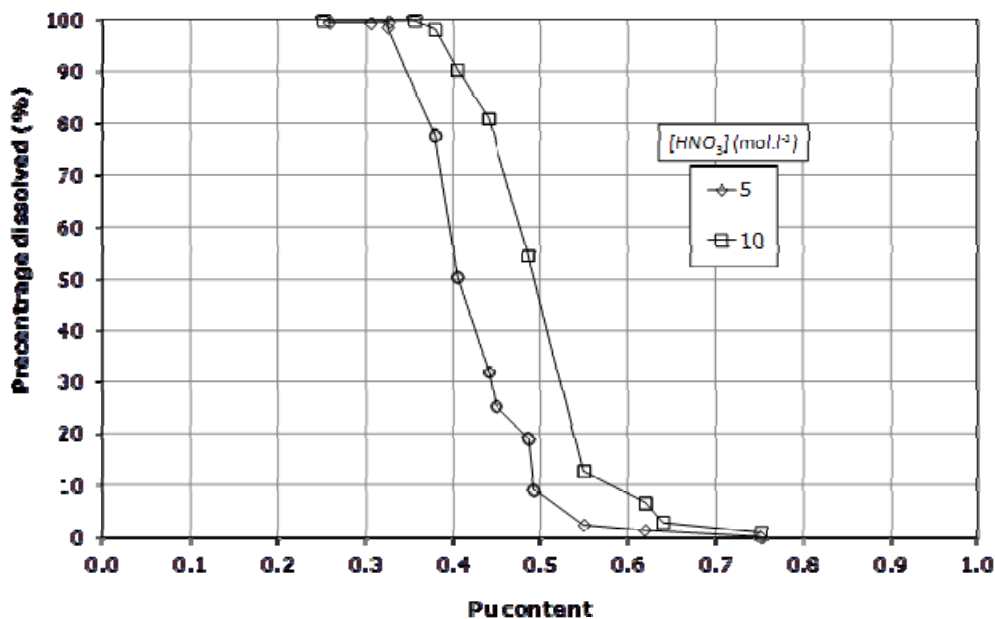


Figure 2. The percentage MOx dissolved with different plutonium contents in 5 or 10 mol.l<sup>-1</sup> nitric acid at reflux for 8 hours [53]

#### 10.4.3. Experimental studies

Batch dissolution experiments were carried out aimed at understanding the factors that affect the dissolution of uranium dioxide and thermal reactor MOx (ca. 5% Pu). The dissolution experiments have been carried out by thermostating a volume of nitric acid, then adding the material and in some experiments sodium nitrite as a nitrous acid source. Most experiments were stirred in an attempt to minimise surface autocatalytic reactions, thereby minimising the difference between the surface and bulk solution composition. The uranium, plutonium and nitrous acid concentrations were determined by in-line and off-line UV-Vis spectrometry, either by direct measurements or by colourimetry. The solution open redox potential was also monitored using a platinum wire and Ag/AgCl reference electrode separated by a salt bridge. Analysis of powder dissolution experiments was carried out by fitting the initial linear dissolution rate to a spherical core shrinkage model, as used by other authors [152]. The results of pellet dissolution experiments will be expressed as an average dissolution rate at 30 % dissolution.

### 10.4.3.1. MOx powder dissolution studies

Dissolution experiments with 4.7 %Pu MOx powder (*ca.* 1.3 m<sup>2</sup>.g<sup>-1</sup>) have been used to study the effect of various nitric and nitrous acid concentrations at 40 °C. The effect of temperature and nitrous acid concentration in 4 mol.l<sup>-1</sup> nitric acid have also been examined. An example of the results is shown in Figure 3.

The results were used to develop a kinetic model (Equation 6), which has a similar form to the results for uranium dioxide[152].

$$\frac{d[U]}{dt} = k_1[NO_3^-]^x + k_2[NO_3^-]^y[HNO_2]^z \quad (6)$$

These experiments confirm that the uranium dioxide and low plutonium content MOx dissolve via a similar mechanism and suggest that the wealth of dissolution literature available for uranium dioxide [34, 45, 46, 74, 152] is relevant to the dissolution of bulk phase MOx.

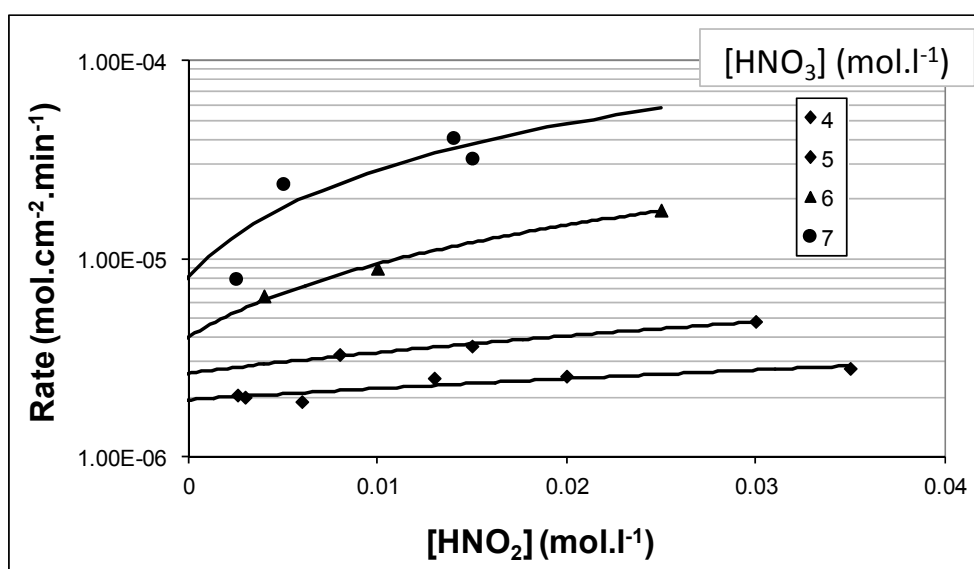


Figure 3. Effect of nitrous acid concentrations in 4-7 mol.l<sup>-1</sup> nitric acid at 40 °C upon dissolution rate of 4.7 %Pu MOx powder

### 10.4.3.2. MOx pellet dissolution studies

Dissolution experiments with 5.0 %Pu MOx pellets, each with a mass of *ca.* 10 g, have been used to study the effect of:

- nitric acid in the absence and presence of added nitrous acid at 80 °C
- temperature

- nitric acid concentration.

An example of the effect of temperature and nitric acid concentration upon the dissolution rate is shown in Figure 4. In contrast to the results of the powder dissolution experiments at high temperature and high nitric acid concentrations, the dissolution rate becomes less sensitive to the effect of nitric and nitrous acid concentrations. Under these conditions bubbles stream from the pellet surface at a high rate and it is believed that the dissolution rate becomes mass transfer limited. Similar observations for uranium dioxide pellets have been made[34].

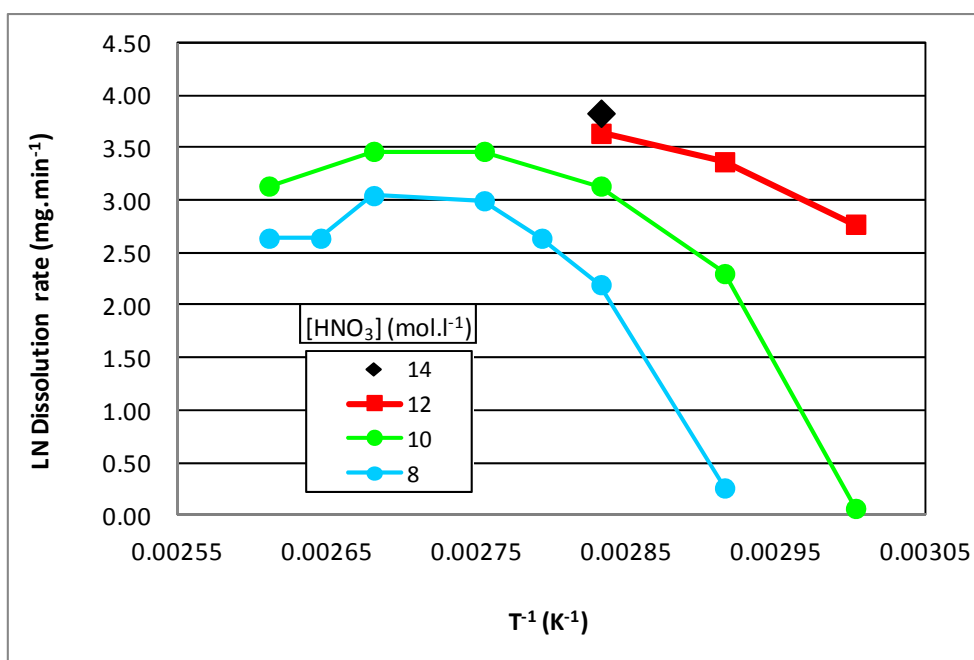


Figure 4. Effect of nitric acid concentration and temperature upon the dissolution rate of MOx pellets at 30 % dissolution

#### 10.4.4. Discussion

The results of this work will allow quantitative predictions to be made about the dissolution of unirradiated MOx. This information is useful for the design of dissolver cycles. It is also important to maximize the extent of dissolution of any plutonium rich particles in MOx, as even small amounts of plutonium insoluble residues must undergo careful criticality safety case analysis. Future work to improve the understanding of the mechanism of high plutonium content MOx is needed, as this will allow the design of time efficient dissolver cycles that maximize plutonium recovery. In the dissolution of irradiated MOx the role of the fission products, in terms of the effect of solid state structure and their interaction with the dissolution mechanism, is topic for further

research... This study therefore helps improve the knowledge of the dissolution of MOx by minimizing plutonium losses in the head-end dissolution step. This type of development is important to aid safety case development for U, Pu recycle schemes and to achieve the waste radiotoxicity reductions in future Np, Am, Cm recycle schemes (Figure 1).